ALTERATIONS OF MITOCHONDRIAL FORM AND FUNCTION CAUSED BY RESISTANCE AGAINST OXIDATIVE STRESS AND CYTOPROTECTIVE, MITOCHONDRIAL PROTEINS

Dissertation

zur Erlangung des Grades
“Doktor der Naturwissenschaften”
am Fachbereich Biologie
der Johannes Gutenberg-Universität in Mainz

Annika I. Pfeiffer
geboren in Steinfurt

Mainz, 2015

Dekan:

1. Berichterstatter:

2. Berichterstatter:

Tag der mündlichen Prüfung: 25.01.2016

Content

List of Figures

List of Tables

Abbreviations

6PGDH	6-Phosphogluconate dehydrogenase
12/15-LOX	12/15-Lipoxygenase
ActA	Listerial actin assembly-inducing protein
ADP	Adenosine 5'-diphosphate
AIF	Apoptosis-inducing factor
Ama	Antimycin A
ANOVA	Analysis of variance
ARE	Antioxidant response element
ATF4	Activating transcriptional factor-4
att	Attachment
ATP	Adenosine 5'-triphosphate
a.u.	Airy unit
Bax	Bcl-2-associated x protein
Bcl-2/BCL-2	B-cell lymphoma protein 2
Bcl-$x_{S/L}$	Bcl-2-related protein, short/long isoform
BH	Bcl-2 homology
Bid/ tBid	BH3-interacting domain death agonist/ truncated Bid
bp	Base pairs
BSA	Bovine serum albumin
°C	Degree Celsius
c	Cytochrome c
$CaCl_2$	Calcium chloride
cDNA	Complementary DNA
cGMP	Cyclic guanosine monophosphate
CMT	Charcot-Marie-Tooth disease
CTB	CellTiter-Blue
$\Delta\psi$	Electrical potential or membrane potential
$\Delta\mu_H^+$	Chemical potential or proton gradient
DAPI	4',6-Diamidino-2-phenylindole, dilactate
dig	Digitonin
dl	Decilitre (10^{-2} litre)
DMEM	Dulbecco's modified eagle medium
DMSO	Dimethyl sulfoxide
DNA	Deoxyribonucleic acid
DNAse	Deoxyribonuclease
DOA	Dominant optic atrophy
D-PBS	Dulbecco's phosphate-buffered saline
Drp1/DRP1	Dynamin-related protein 1
DTNB	5,5'-Dithiobis-(2-nitrobenzoic-acid)
E	Electron transfer system capacity
EA	Ethacrynic acid
EAAT	Excitatory amino acid transporter
EDTA	Ethylenediaminetetraacetic acid
ER	Endoplasmic reticulum
et al.	*et alterii*, and others

ETC	Electron transfer chain
ETS	Electron transfer system
EV	Empty vector
$FADH_2$	Flavin adenine dinucleotide
FBS	Foetal bovine serum
FCCP	Carbonyl cyanide 4-(trifluoromethoxy) phenylhydrazone
Fis1	Fission 1
Fum	Fumarate
g	Gram
G	Glutamate
GDAP1	Ganglioside-induced differentiation associated protein 1
GFP/eGFP	Green fluorescent protein/enhanced GFP
Glu	Glutamate
GSH	Glutathione, γ-L-glutamyl-L-cysteineglycine
GSSG	GSH disulfide
GST	Glutathione transferase
GST-C/N	Glutathione transferase, carboxy-/amino-terminal domain
GTP	Guanosine tri-phosphate
GTPase	Guanosine tri-phosphatase
G6PD	Glucose-6-phosphate dehydrogenase
h	Hour(s)
HA	Hemagglutinin
H_2O_2	Hydrogen peroxide
HCl	Hydrochloric acid
HD	Hydrophobic domain
HO•	Hydroxyl radical
IB	Immunoblotting
ICC	Immunocytochemistry
IL-3	Interleukin-3
IMM	Inner mitochondrial membrane
$InsP_3(R)$	Inositol 1,4,5-trisphosphate (receptor)
IRES	Internal ribosomal entry site
ITR	Inverted terminal repeat
KD	Knockdown
kb	Kilo base pairs
kDa	Kilo Dalton
KO	Knockout
l	Litre
L	Leak respiration
LB	Luria-Bertani
M	Malate
MEF(s)	Mouse embryonic fibroblast(s)
Mff	Mitochondrial fission factor
Mfn	Mitofusin
mg	Milligram (10^{-3} gram)
$MgCl_2$	Potassium chloride
MiD49/51	Mitochondrial dynamics proteins of 49/51 kDa
min	Minute(s)
ml	Millilitre (10^{-3} litre)

mM	Millimolar (10^{-3} moles per litre)
MOM(P)	Mitochondrial outer membrane (permeabilization)
MQ	Menadione
mRNA	Messenger RNA
MRP	Multiple resistance proteins
mt	Mitochondrial
mTOR	Mammalian target of rapamycin complex
N	No adenylates added
NaCl	Sodium chloride
NAD(P)	$NAD(P)^+$ and NAD(P)H
NAD(P)H	Reduced nicotinamide adenine dinucleotide (phosphate)
NaOH	Sodium hydroxide
nm	Nanometre (10^{-9} metre)
nM	Nanomolar (10^{-9} moles per litre)
NO	Nitric oxide
Nrf2	Nuclear factor erythroid 2-related factor 2
n.s.	Not significant
OD_x	Optical density at a wavelength x
OMM	Outer mitochondrial membrane
Omy	Oligomycin
Opa1/OPA1	Optic atrophy 1
ORAI1	Calcium release-activated calcium channel protein 1
OXPHOS	Oxidative phosphorylation
O_2^-	Superoxide anion
P	OXPHOS capacity state
PAGE	Polyacrylamide gel electrophoresis
PB	*Piggy*Bac
PBase	*Piggy*Bac transposase
PBS	Phosphate-buffered saline
PCD	Programmed cell death
PCP	Phosphorylation-control protocol
PCR	Polymerase chain reaction
pH	Potential of hydrogen
pmol	Picomol (10^{-12} mol)
PNS	Peripheral nervous system
Q	Coenzyme Q
QH_2	Ubiquinol
R	Routine respiration
R•	Free radicals
RCR	Respiratory control ratio
RIP	Receptor-interacting protein
RLU	Relative light units
RNA	Ribonucleic acid
ROI	Region of interest
ROOH	Peroxides
ROS	Reactive oxygen species
ROX	Residual oxygen consumption
rpm	Rounds per minute
RT	Reverse transcriptase

S	Succinate
S.D.	Standard deviation
SDS	Sodium dodecyl sulfate
sec	Second(s)
sGC	Soluble guanylyl cyclase
S.O.C.	Super optimal broth with catabolic repressor
SOCE	Store-operated calcium entry
SOD	Superoxide dismutase
SUIT	Substrate-uncoupler-inhibitor titration
TAE	Tris-acetate-EDTA
TBE	Tris-borate-EDTA
TCA cycle	Tricarboxylic acid cycle
TMD	Transmembrane domain
TNB	5′-Thio-2-nitrobenzoic acid
TPR	Tetratrico-peptide repeats
U	Enzyme unit
UV	Ultraviolet
VDAC	Voltage-dependent anion channel
v/v	Volume per volume
WT	Wild type
w/v	Weight per volume
x_c^-	Cystine/glutamate antiporter system
µg	Microgram (10^{-6} gram)
µl	Microlitre (10^{-6} litre)
µm	Micrometre (10^{-6} metre)
µM	Micromolar (10^{-6} moles per litre)

Abbreviations for Amino Acids

A	Alanine	M	Methionine
C	Cysteine	N	Asparagine
D	Aspartic acid	P	Proline
E	Glutamic acid	Q	Glutamine
F	Phenylalanine	R	Arginine
G	Glycine	S	Serine
H	Histidine	T	Threonine
I	Isoleucine	V	Valine
K	Lysine	W	Tryptophan
L	Leucine	Y	Tyrosine

ABSTRACT

Mitochondria are crucial for cellular metabolism, a major source for reactive oxygen species production and play a central role during cell death. This study showed that acute oxidative stress directly influences mitochondria whereby changes in mitochondrial form and functions are dependent on the used oxidative stress-inducing reagent. In mouse hippocampal HT22S cells glutamate increased mitochondrial respiration, however, did not change mitochondrial morphology. In contrast, glutathione-depleting ethacrynic acid (EA) and menadione (MQ) reduced mitochondrial respiration in neuroblastoma SH-SY5Y cells, although EA caused extensive mitochondrial elongation, while MQ induced mitochondrial fragmentation.

Analysis of the glutamate-resistant HT22R cells showed that adaptations against chronic oxidative stress included a less fragmented mitochondrial shape, a reduced mitochondrial respiration and a reduced lactate production. Decreasing energy production in mitochondria seems to be compensated by a shift towards the pentose phosphate pathway for NADPH production used for recovery of the important antioxidant glutathione. Furthermore, two mitochondrial and cytoprotective proteins seem to have a physiological effect to influence mitochondrial form and function. In SH-SY5Y cells, over-expression of oxidative stress-protecting, mitochondrial GDAP1 induced mitochondrial fission. But Charcot-Marie-Tooth disease-causing mutated GDAP1 R310Q did not change mitochondrial shape, whereas GDAP1 S34A with mutation of the predicted amino acid for potential glutathione transferase activity triggered strongly mitochondrial elongation. Even silencing of *GDAP1* influenced mitochondrial morphology, increased total NAD and NADP, and strongly elevated mitochondrial respiration, while wild type and mutated GDAP1 reduced mitochondrial respiratory capacity with the strongest effect through GDAP1 R310Q. Thus, GDAP1 knockdown increased energy production through mitochondria. GDAP1 also prevented EA-induced mitochondrial fusion and a relative reduction in respiratory activity, but could similar to mutated GDAP1 not avoid MQ-induced changes in mitochondria. Additionally, the analysis of cytoprotective Bcl-x_L, which is well-known for its anti-apoptotic function, demonstrated that mitochondrial Bcl-x_L is important for mitochondrial form and function, and to avoid changes in energy metabolism. Deficiency of Bcl-x_L induced mitochondrial fragmentation and reduced mitochondrial respiratory capacity in mouse embryonic fibroblasts. An enhanced susceptibility to two mitochondrial toxins together with an unchanged glycolytic activity, however, elevated total glutathione content, up-regulated glucose-6-phosphate dehydrogenase (G6PD) protein and increased total NADP suggest an increase in pentose phosphate pathway activity under Bcl-x_L deficiency. But re-expression of mitochondrial Bcl-x_L can prevent these changes because it reduced elevated G6PD, total glutathione, total NADP and rescued the observed changes in mitochondrial form and function under Bcl-x_L deficiency.

These results indicate that mitochondrial form and function are affected by acute oxidative stress. Mechanisms against stress including a glutamate resistant phenotype as well as the cytoprotective, mitochondrial proteins GDAP1 and Bcl-x_L induce mitochondrial alterations and if necessary metabolic adaptations in which a shift towards or additional increase in pentose phosphate pathway activity seems to compensate decreasing respiratory function.

ZUSAMMENFASSUNG

Mitochondrien sind ausschlaggebend für den zellulären Stoffwechsel, eine bedeutende Quelle für die Produktion von reaktiven Sauerstoffspezies und spielen eine zentrale Rolle während des Zelltods. Diese Studie zeigte, dass akuter oxidativer Stress direkt die Mitochondrien beeinflusst, wobei Veränderungen in der mitochondrialen Form und Funktion abhängig von der verwendeten oxidativen Stress-induzierenden Substanz sind. In hippokampalen HT22S Zellen erhöhte Glutamat die mitochondriale Respiration, beeinflusste aber nicht die mitochondriale Morphologie. Im Gegensatz dazu verringerte Glutathion-reduzierende Ethacrynsäure (engl. *ethacrynic acid*, EA) und Menadion (MQ) die mitochondriale Respiration in humanen neuroblastoma SH-SY5Y Zellen, obwohl EA eine erhebliche mitochondriale Elongation auslöste, während MQ eine mitochondriale Fragmentierung bewirkte.

Untersuchung der Glutamat-resistenten HT22R Zellen zeigte, dass Anpassungen gegen chronischen oxidativen Stress eine geringere fragmentierte mitochondriale Form, eine reduzierte mitochondriale Respiration und eine verringerte Laktatproduktion beinhalteten. Eine erniedrigte Energiegewinnung in Mitochondrien scheint durch eine Verschiebung in Richtung des Pentosephosphatwegs zur NADPH Produktion für die Rückgewinnung des wichtigen Antioxidans Glutathion kompensiert zu werden. Des Weiteren scheinen zwei mitochondriale und zytoprotektive Proteine eine physiologische Wirkung auf die mitochondriale Form und Funktion aufzuweisen. In SH-SY5Y Zellen bewirkte die Überexpression von vor oxidativen Stress-schützendem GDAP1 mitochondriales Fission. Jedoch beeinflusste Charcot-Marie-Tooth-Erkrankung auslösendes, mutiertes GDAP1 R310Q nicht die mitochondriale Form, wohingegen GDAP1 S34A mit Mutation der prognostizierten Aminosäure für die potentielle Glutathiontransferaseaktivität eine starke mitochondriale Elongation verursachte. Selbst eine Herunterregulierung von *GDAP1* beeinflusste die mitochondriale Morphologie, steigerte totales NAD und NADP und erhöhte gravierend die mitochondriale Respiration, wobei die Überexpression von wildtyp und mutiertem *Gdap1* die mitochondriale respiratorische Kapazität mit dem stärksten Effekt durch GDAP1 R310Q reduzierte. Demnach erhöhte *GDAP1* Knockdown die Energiegewinnung durch Mitochondrien. GDAP1 verhinderte ebenso eine durch EA-induzierte mitochondriale

Elongation und eine relative Reduktion der Atmungsaktivität, aber konnte ähnlich wie mutiertes GDAP1 nicht die MQ-induzierte Veränderungen der Mitochondrien vermeiden. Darüber hinaus zeigte die Analyse von zytroprotektiven Bcl-x_L, welches bekannt für seine anti-apoptotische Funktion ist, dass mitochondriales Bcl-x_L wichtig für die mitochondriale Form und Funktion ist und um Veränderungen im Energiemetabolismus zu verhindern. Ein Mangel an Bcl-x_L löste mitochondriale Fragmentierung aus und verringerte die mitochondriale respiratorische Kapazität in murinen embryonalen Fibroblasten. Eine erhöhte Empfindlichkeit gegen zwei mitochondriale Toxine zusammen mit einer unveränderten glykolytischen Aktivität, aber erhöhten totalen Glutathiongehalt, hochreguliertem Glukose-6-phosphat-Dehydrogenase (G6PD) Protein und erhöhtes totales NADP deuteten auf eine gesteigerte Aktivität des Pentosephosphatwegs unter Bcl-x_L Mangel hin. Allerdings kann die Expression von mitochondrial lokalisierten Bcl-x_L im Bcl-x_L Knockout Hintergrund diese Veränderungen verhindern weil es erhöhtes G6PD, totales NADP und totales Glutathion verringerte und die beobachteten Veränderungen der Mitochondrien korrigierte.

Diese Ergebnisse zeigen, dass die mitochondriale Form und Funktion durch akuten oxidativen Stress beeinflusst werden. Mechanismen gegen Stress, wie ein Glutamat-resistenter Phänotyp sowie die zwei mitochondrialen, zytoprotektiven Proteine GDAP1 und Bcl-x_L, verursachen mitochondriale Veränderungen und gegebenenfalls Anpassungen im Energiemetabolismus, wobei eine Verlagerung in Richtung oder eine zusätzliche Erhöhung in der Aktivität des Pentosephosphatwegs eine erniedrigte respiratorische Funktion kompensiert.

1 INTRODUCTION

1.1 Mitochondria

1.1.1 Mitochondria, Cellular Power Plants

Mitochondria are often described as subcellular, semi-autonomous and double-membrane-bound organelles with highly particular function and morphology (Okamoto and Shaw, 2005; Westermann, 2010; Youle and van der Bliek, 2012). Their discovery goes back to the 19th century (Ernster and Schatz, 1981). Richard Altmann described the ubiquitous occurrence of these intracellular structures in the cytosol and named these structures “bioblasts” (Ernster and Schatz, 1981). He even came to the conclusion that these structures are “elementary organisms” living inside cells (Ernster and Schatz, 1981) and laid the foundation of the still preferred endosymbiosis theory for an explanation of the origin of mitochondria as direct descendants of a bacterial endosymbiont (Gray et al., 1999). In 1898 the term mitochondrion, originating from the Greek words *mitos* (meaning thread) and *chondros* (meaning granules), was introduced by Carl Benda to describe their emergence during spermatogenesis (Ernster and Schatz, 1981).

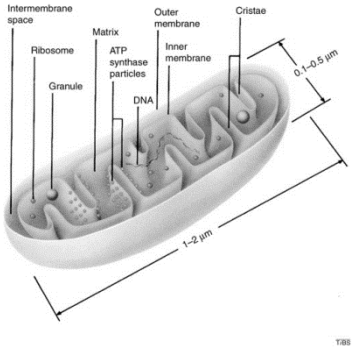

Figure 1: The mitochondrial structure.
Displayed is the mitochondrial structure with the outer membrane, inner membrane, the intermembrane space, the cristae and the matrix. The location of the ribosomes, granule the mitochondrial DNA and the ATP synthase particles is illustrated. This model shows the baffle model based mainly on the observations by Palade,1952 (adapted from Frey and Mannella, 2000).

As observed by electron microscopy, the double-membrane-bound architecture of mitochondria contain an outer membrane, an inner membrane with its convolutions the cristae, an intermembrane space and as innermost a matrix (Figure 1; Palade, 1952, 1953; reviewed in Benard and Rossignol, 2008). Further investigations advanced this model and split the inner membrane into two components, the inner boundary membrane adjacent to the outer membrane and the cristae membrane which reaches into the matrix compartment (Frey and Mannella, 2000; Frey et al., 2002). The newly identified crista junctions connect both components (Frey and Mannella, 2000; Frey et al., 2002).

Mitochondria count as semi-autonomous organelles because these organelles contain their own autonomously replicating circular DNA genomes and comprise a transcription, translation and a protein assembly system, however, most of the mitochondrial proteins are encoded by the nuclear genome and are transferred post-translationally into the organelle (Attardi and Schatz, 1988; Kelly and Scarpulla, 2004; Wallace, 1999). In humans the circular mitochondrial DNA genome comprises about 16,569 base pairs (bp) encoding genes such as the 12S and 16S ribosomal RNAs, 22 transfer RNAs and further enzymes for replication,

transcription and translation beside the 13 protein-encoding genes for subunits of the respiratory enzymes complex I, complex III, complex IV and complex V (Anderson et al., 1981; Kelly and Scarpulla, 2004). Complex II is the only completely nuclear-encoded respiratory enzyme complex (Benard and Rossignol, 2008).

The generation of cellular energy in form of adenosine 5'-triphosphate (ATP) during oxidative phosphorylation (OXPHOS) gets often mentioned as an important function of mitochondria which are even designated as the primary energy source in most eukaryotic cells (Benard and Rossignol, 2008; Chan, 2006; Saraste, 1999). Because of this, they are also referred to as the powerhouse or power plant of the cell (Benard and Rossignol, 2008; Bolisetty and Jaimes, 2013). They take action in the final phase of cellular catabolism (Benard and Rossignol, 2008). After enzymatic degradation of carbohydrates, fats and proteins into smaller molecules like pyruvate, fatty acid and amino acids, these energetic elements are further converted during β-oxidation and the tricarboxylic acid (TCA) cycle (also named citric acid cycle or Krebs cycle) into NADH (reduced nicotinamide adenine dinucleotide) and/or $FADH_2$ (flavin adenine dinucleotide) in mitochondria (Benard and Rossignol, 2008). NADH and $FADH_2$ are then used as electron donors during OXPHOS (Benard and Rossignol, 2008). The NADH dehydrogenase (complex I or NADH:ubiquinone oxidoreductase), the succinate dehydrogenase (complex II or succinate:ubiquinone reductase), cytochrome bc_1 (complex III) and the cytochrome oxidase (complex IV) including two additional mobile electron carriers (coenzyme Q or ubiquinone and cytochrome c) are all part of the so-called respiratory chain or electron transport chain (ETC; Benard and Rossignol, 2008; Saraste, 1999) which are localized with accumulation in the cristae membrane of the inner mitochondrial membrane system (Gilkerson et al., 2003). During OXPHOS electrons are passed along the ETC and are finally transferred to molecular oxygen (O_2; Saraste, 1999). The energy, which is released during this process, is used to transport protons at complex I, III and IV across the inner mitochondrial membrane from the matrix to the intermembrane space (Benard and Rossignol, 2008). Thereby an electrochemical proton gradient (proton motive force) is created consisting of an electrical potential ($\Delta\psi$) and a chemical potential ($\Delta\mu_H^+$) or pH gradient (ΔpH; Benard and Rossignol, 2008). Electrons originating from the energy substrate NADH are transported from complex I, the largest respiratory enzyme complex, via coenzyme Q to complex III (Saraste, 1999). Complex II, which is an element of the TCA cycle, additionally feeds electrons from succinate to the coenzyme Q (ubiquinone) pool (Saraste, 1999). The reduced form of coenzyme Q, ubiquinol (QH_2), can move within the membrane because of its lipid-soluble character (Saraste, 1999). At complex III electrons from ubiquinol are transferred to cytochrome c, a water-soluble hemoprotein, at the cytoplasmic side of the inner mitochondrial membrane (Saraste, 1999). During this process ubiquinol is subjected to two consecutive one-electron reductions which are linked to the

translocation of protons across the inner membrane in a mechanism known as the Q cycle (Finkel and Holbrook, 2000; Saraste, 1999). Electrons from cytochrome c are further passed to complex IV, where they reduce molecular oxygen at the matrix side, water (H_2O) is formed and the released energy is used for the translocation of protons (Saraste, 1999). In the end, the created electrochemical proton gradient is utilized by complex V, the F_1F_0 ATP synthase, for the synthesis of ATP from adenosine 5'-diphosphate (ADP) and phosphate (Saraste, 1999). Because of a convergent electron transfer from complex I and II to the Q-junction, it is more precise to specify the ETC as an electron transfer system (Figure 2; Gnaiger, 2009, 2012). Particularly, ADP-stimulated mitochondrial respiration is maximally stimulated with a convergent complex I and II linked electron flow (Gnaiger, 2009, 2012).

The function of mitochondria is not only restricted to the production of energy. Mitochondria are also important for buffering cytosolic calcium and are essential for the assembly of iron-sulphur clusters. They participate in the biosynthesis of haem, pyrimidins, phospholipids, amino acids and many other metabolites (Attardi and Schatz, 1988; MacAskill and Kittler, 2010; Westermann, 2010). In addition, they play a significant role during apoptosis and in the production of reactive oxygen species (ROS) as well as mitochondrial defects are even associated with degenerative diseases, aging and cancer (Wallace, 1999).

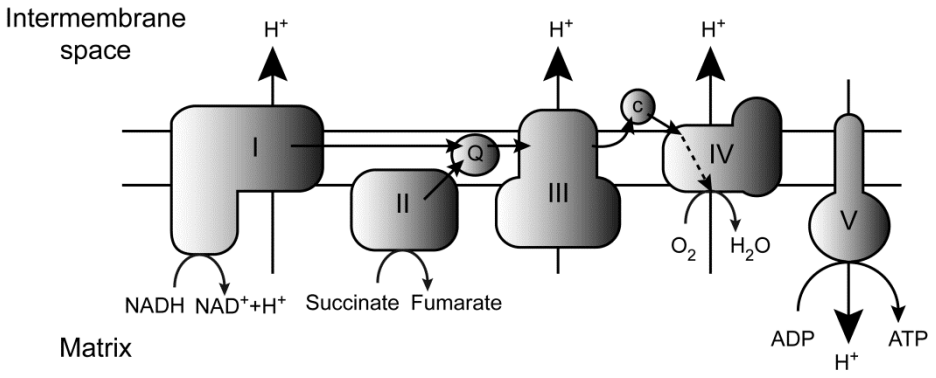

Figure 2: The mitochondrial respiratory system.
The enzyme complexes of the mitochondrial respiratory system are located in the mitochondrial inner membrane and are responsible for generation of ATP during oxidative phosphorylation. NADH-dehydrogenase (complex I, I), the succinate dehydrogenase (complex II, II), cytochrome bc_1 (complex III, III), the cytochrome oxidase (complex IV, IV) and the two mobile electron carriers, coenzyme Q (Q) and cytochrome c (c), are part of the electron transfer system (ETS). Electrons, originating from NADH and succinate are passed as illustrated along the ETS and are finally transferred to molecular oxygen. During this process, released energy is used to translocate protons at complex I, III and IV from the matrix to the intermembrane space, which builds up an electrochemical proton gradient. In the end, the electrochemical proton gradient is used by the F_1F_0 ATP synthase (complex V, V) to generate ATP.

1.1.2 Mitochondrial Dynamics: Fission and Fusion

Mitochondria are very dynamic organelles (Chan, 2012; Westermann, 2010). Their morphology can range from small fragmented distinct organelles to large tubular interconnected networks because of two continuous, but opposing processes, fission and fusion (illustrated in Figure 3; Benard and Rossignol, 2008; Chan, 2012; Westermann, 2010). The balance between fission and fusion events determines the mitochondrial appearance, size, amount of mitochondria, and their physiological function and is dependent on the cell type and physiological conditions (Benard and Rossignol, 2008; Chan, 2012; Kuznetsov et al., 2009). The original term mitochondrion reflects more the single section of a mitochondrial tubule (Benard and Rossignol, 2008). Because of this, the term mitochondrial network or mitochondrial reticulum is often used by researchers to describe the three-dimensional architecture of mitochondria in cells today (Benard and Rossignol, 2008; McBride et al., 2006).

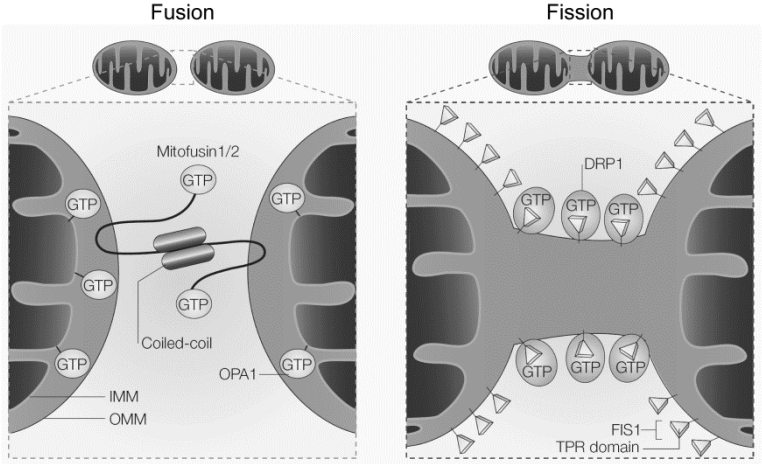

Figure 3: Mitochondrial fission and fusion in mammalian cells. Mitochondrial fusion of the outer mitochondrial membrane (OMM) is mediated by mitofusin1 and 2. Mitofusins, interacting in *trans* on adjacent opposing mitochondrial membranes, cause membrane tethering and fusion. OPA1 (optic atrophy 1) is responsible for fusion of the inner mitochondrial membrane (IMM). The dynamin-related protein 1 (DRP1) is recruited by fission 1 (FIS1) through its tetratrico-peptide repeats (TPR) domain to mitochondrial fission sites and is responsible for mitochondrial fission. The activity of mitofusins, OPA1 and DRP1 are dependent on GTP hydrolysis. (adapted by permission from Macmillan Publisher Ltd: Nature Reviews Molecular Cell Biology, Youle and Karbowski, 2005, © 2005)

The key players for mitochondrial fusion and fission are large and conserved dynamin-related guanosine tri-phosphatases (GTPases; reviewed in Chan, 2012; Hoppins et al., 2007; Okamoto and Shaw, 2005; Westermann, 2010). In mammals mitochondrial fusion is mediated by the two transmembrane GTPases mitofusins, Mfn1 and 2, which are located in the outer mitochondrial membrane (Rojo et al., 2002; Santel and Fuller, 2001), besides the mitochondrial optic atrophy 1 (Opa1) protein which is connected with the inner mitochondrial membrane or the intermembrane space (Cipolat et al., 2004; Delettre et al., 2000; Griparic et al., 2004; Olichon et al., 2002; Satoh et al., 2003). Mitochondrial fusion seems to be achieved in sequential steps by mitofusins and Opa1 (Song et al., 2009). Fusion of the outer mitochondrial membrane is mediated by mitofusins, while Opa1 coordinates the fusion of the inner membrane (reviewed in Chan, 2012). Mfn1 and 2 can form hetero-oligomeric and homo-oligomeric complexes (Chen et al., 2005; Chen et al., 2003). The interaction of mitofusins on adjacent opposing mitochondrial membranes acting in *trans* results in membrane tethering depending on GTP hydrolysis (Ishihara et al., 2004; Koshiba et al., 2004). Cells expressing only *Mfn1* or *Mfn2* show

reduced mitochondrial fusion activity without severe cellular dysfunction, whereas mitochondrial fusion is completely inhibited in cells lacking both mitofusins (Chen et al., 2005; Chen et al., 2003). These cells have additionally major cellular defects including a reduced mitochondrial respiration, an affected mitochondrial membrane potential and reduced growth rate (Chen et al., 2005). Opa1 exists in a long membrane-anchored isoform and a membrane interacting short isoform without a membrane anchor. Both isoforms are essential for inner membrane fusion (Song et al., 2007). Downregulation of Opa1 by RNA interference inhibits mitochondrial fusion leading to mitochondrial fragmentation (Chen et al., 2005; Cipolat et al., 2004; Griparic et al., 2004; Olichon et al., 2003) and similar cellular defects as observed by the lost of mitofusins (Chen et al., 2005). The lost of Opa1 even results in the disorganization of the cristae structure (Olichon et al., 2003).

The key regulator of mitochondrial fission is the dynamin-related protein 1 (Drp1) in mammals which is mainly localized in the cytosol and is possibly recruited to mitochondria by the outer membrane protein fission 1 (Fis1), mitochondrial fission factor (Mff), mitochondrial dynamics proteins of 49 kDa and 51 kDa (MiD49 and MiD51), respectively (Chan, 2012; Palmer et al., 2011). When Drp1 localizes to mitochondria, it oligomerizes and forms a ring-like structure at sites of mitochondrial fission resulting in division of the double membrane by GTP hydrolysis and constriction (Frank et al., 2001; Palmer et al., 2011; Smirnova et al., 2001; Yoon et al., 2001). An additional and non-classical mitochondrial fission factor is the mitochondrial protein ganglioside-induced differentiation associated protein 1 (GDAP1; Niemann et al., 2005).

Mitochondrial dynamics is very important because it is linked to changes in cell metabolism as well as it is associated with mitochondrial inheritance, mitochondrial DNA stability, apoptosis, mitochondrial respiratory function, adaptation to cellular stress and removal of especially damaged mitochondria through mitophagy (Chan, 2012; Westermann, 2010). Mitochondrial dynamics is also referred to as a constituent of a cellular quality control mechanism because it allows content mixing between mitochondria, which supports a uniformly and functional mitochondrial pool (Chan, 2012; Westermann, 2010; Youle and van der Bliek, 2012). Mitochondrial fusion leading to content mixing and extended mitochondrial network is beneficial under situations of high energy demand, whereas resting cells

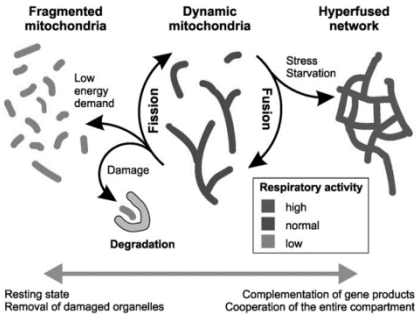

Figure 4: Changes in mitochondrial morphology to respiratory activity. Illustrated is a model of adjustments in the mitochondrial morphology induced by changes in the respiratory activity. Mitochondria favor a fragmented morphology under low energy demand when the respiratory activity is low. Mitochondrial fragmentation is needed to remove damaged mitochondria by mitophagy. In comparison, continuous fission and fusion allows content mixing and supports a uniformly and healthy mitochondrial population. A highly hyperfused mitochondrial network is induced by cellular stress caused by for example UV irradiation or starvation, which increases respiratory activity and thus, optimize mitochondrial function. (adapted from Westermann, 2012, copyright 2012, with permission from Elsevier)

often show fragmented mitochondria (Figure 4; Westermann, 2012). Tondera and colleagues recognized that cellular stress induced by apoptotic stimuli like ultraviolet (UV) irradiation and cycloheximide results in a drastically increased mitochondrial network and described this process as stress-induced mitochondrial hyperfusion, which was accompanied by enhanced ATP production to allow a compensation of cellular stress under such circumstances (Tondera et al., 2009). In neurons, migrating lymphocytes and especially in muscle cells with high energy demand, mitochondria are positioned at sites where ATP is directly needed (Westermann, 2012).

Changes and defects in mitochondrial dynamics have a role in the pathogenesis of human neurodegenerative diseases like Alzheimer's, Parkinson's and Huntington's disease (Itoh et al., 2013). In addition, mutations of genes encoding enzymes of the mitochondrial dynamics machinery cause directly human diseases. Mutations in *OPA1* result in the most common form of autosomal dominant optic atrophy (DOA), a disease leading to degeneration of retinal ganglion cells and atrophy of the optic nerve (Alexander et al., 2000; Delettre et al., 2000). Mutated *MFN2* results in the axonal neuropathy Charcot-Marie-Tooth (CMT) disease 2A (Zuchner et al., 2004). Even mutations in the non-classical fission factor GDAP1 induce in humans various types of CMT disease (Baxter et al., 2002; Chung et al., 2008; Claramunt et al., 2005; Cuesta et al., 2002; Senderek et al., 2003). Thus, mitochondrial dynamics affects mitochondrial bioenergetics and has a role in various human diseases.

1.2 Oxidative Stress

1.2.1 Oxidative Stress, Glutathione Synthesis and Glutathione Metabolism

Oxidative stress is the result from an imbalance between the production of ROS and antioxidants defences (Dringen, 2000). A situation in which the production of ROS like hydrogen peroxide (H_2O_2), hydroxyl radical (HO•) and superoxide anion (O_2^-) is favoured (Dringen, 2000). Although an increase of ROS leads to oxidative stress, ROS are as well specific signalling molecules to maintain physiological homeostasis (reviewed in Finkel and Holbrook, 2000). Oxidative stress can be induced by exogenous sources like ionizing radiation, ultraviolet light, chemotherapeutics, toxins from the environment as well as inflammatory cytokines, but ROS are also by-products of normal intracellular processes (Finkel and Holbrook, 2000). The activity of cytosolic NADPH oxidases and lipoxygenases contribute to the production of ROS as well as peroxisomes and mitochondria (Finkel and Holbrook, 2000). In many subcellular compartments further enzymes are causative to the production of ROS. These are peroxidases, oxidases, monoamine oxidases as well as mono- and di-oxygenases (Novo and Parola, 2008; Tan et al., 2001). Especially mitochondria seem to be the major source of ROS (Finkel and Holbrook, 2000). During

mitochondrial oxygen consumption superoxide radicals can be produced at complex I, but to a higher degree at complex III in the respiratory system (Finkel and Holbrook, 2000). Under normal physiological conditions, a cell has a number of defence mechanisms to prevent oxidative stress and to maintain physiological homeostasis (Finkel and Holbrook, 2000). These defence mechanisms split into an enzymatic system and a non-enzymatic system of small molecules (Finkel and Holbrook, 2000). Part of the enzymatic system is superoxide dismutase (SOD), catalase and glutathione peroxidase (Coyle and Puttfarcken, 1993; Finkel and Holbrook, 2000). Eukaryotic cells express three SODs, a cytosolic copper-zinc SOD, a mitochondrial manganese-containing SOD and an extracellular form of copper-zinc SOD (Coyle and Puttfarcken, 1993). SODs are responsible for the conversion of O_2^- to H_2O_2, which reduces the risk of HO• formation (Coyle and Puttfarcken, 1993; Finkel and Holbrook, 2000). H_2O_2 can further be converted by catalase and glutathione peroxidase to H_2O and O_2 (Coyle and Puttfarcken, 1993; Finkel and Holbrook, 2000). Part of the non-enzymatic system is the thiol glutathione (GSH, γ-L-glutamyl-L-cysteineglycine; Finkel and Holbrook, 2000) which is an important antioxidant in the brain and is present up to 12 mM in mammalian cells (reviewed in Dringen, 2000; Dringen and Hirrlinger, 2003). With the enzymatic and non-enzymatic system a cell has multiple defence mechanisms against oxidative stress and thereby prevents random cellular damages including protein modification, lipid peroxidation and DNA damage caused by ROS (Dringen, 2000).

Glutathione is a tripeptide synthesized from the amino acids glutamate, cysteine and glycine by two ATP-consuming enzymes, γ-glutamylcysteine synthase and glutathione synthase (Figure 5; Dringen, 2000; Dringen and Hirrlinger, 2003). In the first and rate-limiting reaction catalysed by γ-glutamylcysteine synthetase, the dipeptide γ-glutamylcysteine is formed from glutamate and cysteine which is then combined with glycine to form GSH by the activity of the glutathione synthase in the cytosol (Dringen, 2000; Dringen and Hirrlinger, 2003; Lewerenz and Maher, 2011; Maher, 2005). The end product GSH can regulate in a feedback inhibition of the γ-glutamyl-cysteine synthase GSH synthesis, and in that way, regulates the cellular level of GSH (Richman and Meister, 1975). Although GSH is synthesized in the cytosol and most of the GSH is located here, GSH is also found in separate pools in both mitochondria and nuclei (Maher, 2005). The cystine/glutamate antiporter system x_c^- is responsible for the transport of cystine in exchange for the neurotransmitter L-glutamate (1:1 ratio) into the cell which is driven by the transmembrane concentration gradient of glutamate (Bannai, 1986; Bannai and Kitamura, 1980). The x_c^- system is composed of two subunits, the light chain xCT and the heavy chain 4F2hc (Sato et al., 1999). After transport of cystine into the cell, it gets reduced to cysteine (Albrecht et al., 2010). Within the cell, GSH can react non-enzymatically with free radicals like hydroxyl radicals, superoxide anions as well as nitric oxides (Dringen, 2000). The effect of GSH on hydroxyl radicals is tremendously important

because there are no known enzymatic defence mechanisms (Maher, 2005) and hydroxyl radicals are the most reactive species (Dringen, 2000). In addition, glutathione peroxidase can catalyze the reduction of H_2O_2 and organic peroxides (for example lipid peroxides), whereby GSH is oxidized to GSH disulfide (GSSG) and H_2O and alcohol is released (Griffith, 1999; Hayes and McLellan, 1999). Glutathione reductase can regenerate GSH from GSSG under NADPH consumption and according to this, glutathione is not consumed (Dringen, 2000; Dringen and Hirrlinger, 2003). GSH conjugates can also be formed with electrophiles and xenobiotics by the activity of glutathione transferases (former known as glutathione S-transferases; GSTs; Hayes et al., 2005; Hayes and McLellan, 1999; Maher, 2005). GSH does not only offer multiple defence mechanisms against ROS. It is also important to maintain proteins' sulfhydryl groups in a reduced state whereby it protects the thiol redox potential (Dringen, 2000). Some proteins even possess glutathionylation as a post-translational modification (Maher, 2005).

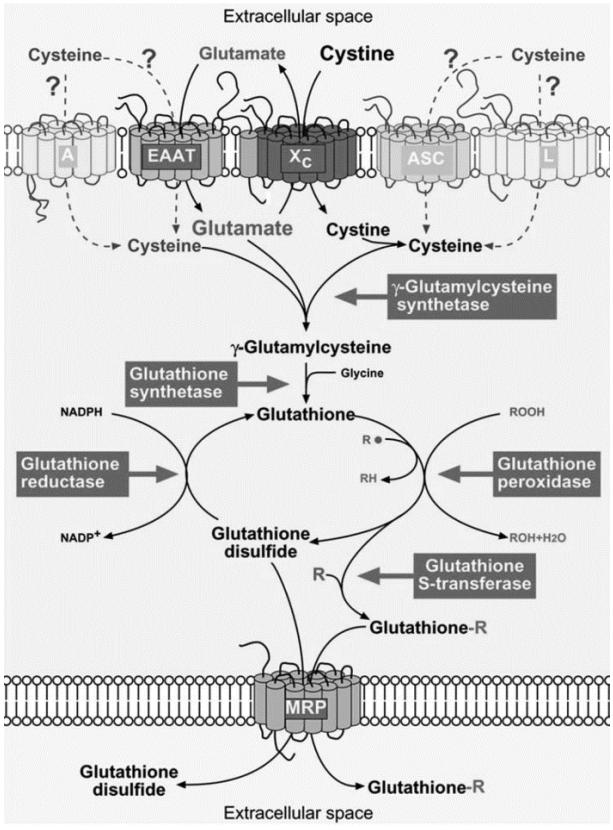

Figure 5: GSH metabolism.
The excitatory amino acid transporters (EAAT) import glutamate into the cell, thereby support the glutamate/cystine exchange by the glutamate/cystine antiporter system x_c^- which is depending on the transmembrane gradient of glutamate. After rapid reduction of cystine to cysteine, glutathione (GSH) is synthesized from cysteine, glutamate and glycine in two ATP-dependent reactions by γ-glutamylcysteine synthetase and glutathione synthase. GSH can non-enzymatically reduces free radicals (R•) or enzymatically by the activity of glutathione peroxidase reduces peroxides (ROOH), whereby it is oxidized to glutathione disulfide (GSSG). GSSG can either be recycled to GSH by glutathione reductase in an NADPH dependent process or is exported from the cell. Glutathione transferases can detoxify electrophilic compounds and xenobiotics (R), which are exported as well as GSSG by multiple resistance proteins (MRP)-transporters to the extracellular space. It is unclear whether the transporter protein A, ASC, L or EAAT can import cysteine from the cellular surrounding. (adapted from Albrecht et al., 2010)

Besides the GSH/glutathione peroxidase system, the thioredoxin/peroxiredoxin system has an important role in the removal of H_2O_2 in brain mitochondria (Drechsel and Patel, 2010; Kudin et al., 2012). These systems and their redox couples, GSH/GSSG and reduced thioredoxin/oxidized thioredoxin, together with NADPH/$NADP^+$ are the most important redox couples in cells and both the GSH and thioredoxin system are dependent on NADPH as a reducing equivalent for recovery (Lewerenz and Maher, 2011; Schafer and Buettner, 2001). Thus, NADPH is helpful by maintaining redox homeostasis. NADPH is produced mainly in the pentose phosphate pathway by the first enzyme glucose-6-phosphate dehydrogenase

(G6PD) and the 6-phosphogluconate dehydrogenase (6PGDH; Stincone et al., 2014). An increasing glucose consumption through both the glycolysis and the pentose phosphate pathway and coupled enhanced production of NADH as well as NADPH results in a neuroprotective effect against oxidative stress (Soucek et al., 2003). An increase in the pentose phosphate pathway seems to be neuroprotective because a higher rate of glycolysis combined with a decrease in the pentose phosphate pathway induced oxidative damage and apoptotic neuronal cell death (Rodriguez-Rodriguez et al., 2012).

The defence mechanisms against oxidative stress are very important because oxidative stress is associated with ageing, numerous human diseases as well as an increase in ROS and an impaired defence mechanism, such as a disturbed glutathione metabolism, can result in damages of DNA, proteins and lipids leading to interfered physiological functions (Dringen, 2000; Dringen and Hirrlinger, 2003; Finkel and Holbrook, 2000).

1.2.2 The Role of Oxidative Stress in Neurodegenerative Diseases and Neurological Disorders

In the last decade more and more evidences showed that oxidative stress and a linked increase in ROS are involved in neuronal loss in neurodegenerative diseases, like Amyotrophic Lateral Sclerosis, Alzheimer's disease, Parkinson's disease and Huntington's disease, as well as in brain trauma, stroke and seizures (Andersen, 2004; Barnham et al., 2004; Coyle and Puttfarcken, 1993; Dringen, 2000; Dringen and Hirrlinger, 2003; Mariani et al., 2005; Melo et al., 2011). Specific brain regions with neurodegenerative signs in post-mortem tissue of Parkinson's disease, Alzheimer's disease and Amyotrophic Lateral Sclerosis patients displayed diverse indices of damages by ROS (Andersen, 2004). The brain is particularly sensitive to damaging effects of ROS in comparison to other tissues in the body because of a high metabolic rate and linked high O_2 consumption beside a relatively low level of antioxidants and a relatively low cellular regenerative capacity (Andersen, 2004; Barnham et al., 2004). The brain accounts for 2 % of the body weight, however, a fifth of the oxygen consumption of the whole body is used by the brain (Dringen, 2000; Dringen and Hirrlinger, 2003). Especially in the brain, which displays high oxygen consumption, ROS will be generated in high quantities during OXPHOS in mitochondria (Dringen, 2000; Dringen and Hirrlinger, 2003). Thus, an imbalance in the antioxidants defence and in ROS is especially vulnerable for neurons. In the substantia nigra, the influenced brain area in Parkinson's disease, GSH levels are decreased and show altered distribution of GSH as well as surviving nigral neurons displayed a reduced GSH content (Pearce et al., 1997; Perry et al., 1982; Perry and Yong, 1986; Sofic et al., 1992) and even the activity of catalases and perhaps glutathione peroxidases are altered (Ambani et al., 1975; Kish et al., 1985; Sian et al., 1994). In affected brain areas of Alzheimer's disease a lowered activity of catalases,

SODs, glutathione peroxidases and reductases have been detected (Pappolla et al., 1992; Zemlan et al., 1989). Thus, a balance between the production of ROS and antioxidant defences is especially important in neurons to avoid damages by oxidative stress.

1.2.3 Mechanism of Oxidative Glutamate Toxicity and Mouse Hippocampal HT22S Cells as a Model System

Instead of inducing neuronal cell death by excitotoxicity through an overstimulation of ionotropic glutamate receptors (Choi, 1988), the neurotransmitter glutamate can cause oxidative glutamate toxicity, a form of programmed cell death which is distinguishable from, but even shares characteristics of both apoptosis and necrosis (reviewed in Albrecht et al., 2010; Tan et al., 2001). Oxidative glutamate toxicity induces cell death via a series of distinct events (illustrated in Figure 6; reviewed in Albrecht et al., 2010; Tan et al., 2001). High concentrations of extracellular glutamate inhibits the gradient-driven cystine/glutamate antiporter x_c^- leading to a shortness of cystine necessary for glutathione synthesis, which results in GSH depletion, increase in ROS and finally cell death (Murphy et al., 1989). Oxidative glutamate toxicity has been studied and described in neuronal cell lines (Davis and Maher, 1994; Maher and Davis, 1996; Miyamoto et al., 1989; Murphy et al., 1989), in primary immature neuronal cultures (Davis and Maher, 1994; Maher and Davis, 1996; Murphy et al., 1990) and in oligodendrocytes (Oka et al., 1993). But in a lot of studies the immortalized mouse hippocampal HT22 cell line (further referred to as HT22S) was used to study the events leading to oxidative glutamate-induced cell death (Davis and Maher, 1994; Landshamer et al., 2008; Li et al., 1997a, b; Maher and Davis, 1996; Pallast et al., 2009; Tan et al., 1998a; Tan et al., 1998b). HT22S cells are a great model system because they are missing functional ionotropic glutamate receptors and consequently glutamate-induced excitotoxicity can be excluded (Maher and Davis, 1996). By the inhibition of the cystine/glutamate antiporter x_c^- through glutamate, it comes to GSH depletion and ROS production (Murphy et al., 1989). After a linear increase of ROS for about 6 h, the cellular GSH level drops below

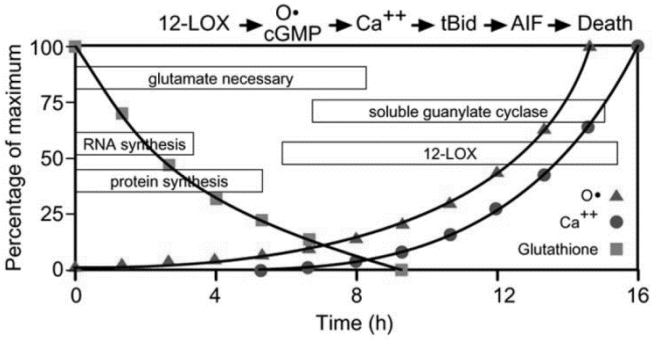

Figure 6: Chronological sequence of oxidative glutamate toxicity.
Illustrated is the approximate time course leading to cell death caused by oxidative glutamate toxicity. Glutamate mediates a decrease in intracellular glutathione. In the beginning necessary RNA and protein synthesis is induced. Decreased glutathione levels below 20 % lead to an exponential increase in reactive oxygen species (O•). The activation of 12-lipoxygenase (12-LOX) as well as soluble guanylyl cyclase results in an accumulation of reactive oxygen species and cause influx of calcium (Ca^{++}). The translocation of Bid (BH3-interacting domain death agonist) to mitochondria is induced, where truncated Bid (tBid) activates apoptosis-inducing factor (AIF) which results in the translocation of AIF from mitochondria to the nucleus and induces cell death. (adapted from Albrecht et al., 2010)

approximately 20 % and ROS production, predominantly by mitochondria, increases exponentially (Tan et al., 1998a). The decrease in GSH activates 12/15-lipoxygenase (12/15-LOX), a lipid-oxidizing enzyme which gives rise to 12/15-hydroxyeicosatetraenoic acid (Li et al., 1997b; Pallast et al., 2009) and can directly damage mitochondria by decreasing the mitochondrial membrane potential, increasing mitochondrial permeability and enhancing ROS production (Pallast et al., 2009). The activation of 12/15-LOX leads to the activity of soluble guanylyl cyclase (sGC) and production of intracellular cyclic guanosine monophosphate (cGMP), which increases 6 h after the beginning of the glutamate exposure (Li et al., 1997a). An enhancement in intracellular cGMP causes an elevation of intracellular calcium by the influx of calcium (Li et al., 1997a) through the cGMP-modulated and plasma membrane-localized calcium channel ORAI1 (Calcium release-activated calcium channel protein 1; Henke et al., 2013). The influx of calcium is essential to induce cell death, because blocking calcium influx in calcium free medium or with cobalt(II) chloride prevents cell death (Davis and Maher, 1994; Li et al., 1997a; Murphy et al., 1989). In the last phase of oxidative glutamate toxicity the pro-apoptotic Bcl-2 family member Bid (Bcl-2 homology 3 (BH3)-interacting domain death agonist) translocates to mitochondria, where it leads to the rapid translocation of the apoptosis-inducing factor (AIF) from mitochondria to the nucleus resulting in nuclear fragmentation (Landshamer et al., 2008). Translocation of Bid to mitochondria causes a perinuclear accumulation of Bid-loaded mitochondria (Landshamer et al., 2008) and is accompanied by a collapse of the mitochondrial membrane potential (Landshamer et al., 2008; Noack et al., 2012; Pallast et al., 2009). All these events lead finally to cell death.

By the repetitive exposure of HT22S cells to high concentrations of glutamate and proliferation of the surviving cells, we have generated a glutamate-resistant cell line, called HT22R (Lewerenz et al., 2006). These cells are protected against glutamate-induced cell death as well as oxidative stress provoked directly by H_2O_2 (Lewerenz et al., 2006). In addition, HT22R cells are resistant to the n-glycosylation inhibitor tunicamycin inducing endoplasmic reticulum (ER) stress or can cope with the over-expression of the pro-apoptotic mitochondrial protein Bcl-2-associated x protein (Bax; Dittmer et al., 2008). As a result, they are not only protected against oxidative stress, but also against other cellular stressors. They are protected against oxidative glutamate toxicity because of an up-regulation of the light chain xCT subunit in the cystine/glutamate antiporter triggering an increase in cystine uptake and intracellular glutathione (Lewerenz et al., 2006). In HT22R cells a glutamate exposure even induces a reduced glutathione depletion compared to glutamate-sensitive HT22S cells (Lewerenz et al., 2006). The increased cystine uptake is probably supported by transport of glutamate into the cell through the excitatory amino acid transporter 3 (EAAT3), which seems to be increased in HT22R cells as well (Lewerenz et al., 2006). This hypothesis was supported by the over-expression of xCT as well as EAAT3 protein in sensitive HT22S cells,

which reduced the susceptibility to glutamate and H_2O_2 (Lewerenz et al., 2006). But the co-expression of both xCT and EAAT3 most prominent increased protection (Lewerenz et al., 2006). The analysis of glutamate-resistant HT22R cells revealed a reduction in the store-operated calcium entry (SOCE) induced by depletion of the main cellular calcium store the ER (Henke et al., 2013). The reduced SOCE is caused by a decreased protein expression of ORAI1, the main calcium entry channel during oxidative glutamate toxicity (Henke et al., 2013).

Mitochondria seem to have a central role in the sensitivity against endogenous oxidative stress because glutamate-induced cell death induces a breakdown of the mitochondrial membrane potential (Landshamer et al., 2008; Noack et al., 2012; Pallast et al., 2009), 12/15-LOX activity directly damages mitochondria (Pallast et al., 2009) as well as the mitochondrial protein GDAP1 is up-regulated in glutamate-resistant HT22R cells (Noack et al., 2012). This mitochondrial protein and its function get introduced in detail in following paragraphs because GDAP1 is a protein that protects against oxidative stress and particularly against oxidative glutamate toxicity (Noack et al., 2012). According to these observations, we suppose an adaptation in the mitochondrial form and function in the glutamate resistant phenotype of HT22R cells.

1.2.4 Effects of the Oxidative Stress-Inducing Reagents Ethacrynic Acid and Menadione

Oxidative stress can be induced by various other reagents whereby ethacrynic acid (EA) and menadione (MQ) induce oxidative stress through a glutathione depleting activity (Chiou and Tzeng, 2000; Kim et al., 2014; Seyfried et al., 1999; Wullner et al., 1999). EA has an inhibitory effect on rat and human GST activity (Ahokas et al., 1985; Ploemen et al., 1990), alkylates cystine residues, is a substrate for GSTs and can form spontaneously or mediated by GSTs a conjugate with glutathione (Awasthi et al., 1993; Habig et al., 1974). Thus, it can induce a complete loss of total glutathione in both cytosol and mitochondria (Seyfried et al., 1999; Wullner et al., 1999). The EA-glutathione conjugate can even inhibit human lung GST more effective than EA alone (Awasthi et al., 1993). In comparison to EA, MQ can redox cycle, which is mediated in part by mitochondrial proteins (Iyanagi and Yamazaki, 1970; Lind et al., 1982; Powis and Appel, 1980), can form a conjugate with GSH and can arylate protein thiols in cells (Di Monte et al., 1984). MQ causes oxidative stress by inducing ROS production through redox cycling and GSH depletion (Chiou and Tzeng, 2000; Criddle et al., 2006; Kim et al., 2014; Loor et al., 2010). Recent publications demonstrated an effect of both EA and MQ on mitochondria because both reagents influenced mitochondrial dynamics (Bowes and Gupta, 2005; Loor et al., 2010; Soltys and Gupta, 1994) as well as they induced glutathione depletion (Chiou and Tzeng, 2000; Kim et al., 2014; Seyfried et al., 1999; Wullner

et al., 1999). But the effects on mitochondrial form are contrary. Whereas EA induces mitochondrial fusion and the formation of a mitochondrial reticulum within a short time in human fibroblasts and BSC-1 cells (Bowes and Gupta, 2005; Soltys and Gupta, 1994), a treatment of cardiomyocytes with MQ results in mitochondrial fission (Loor et al., 2010).
The observations of EA and MQ on mitochondrial dynamics confirmed that mitochondria are directly affected by oxidative stress. Additionally, EA even impairs mitochondrial enzyme activity and decreases the activity of mitochondrial complexes in isolated mitochondria of EA-treated cells (Seyfried et al., 1999; Wullner et al., 1999). These observations suggest that EA and probably MQ as well directly affect mitochondrial function and in particular mitochondrial energy production.

1.3 GDAP1 and Charcot-Marie-Tooth Disease

1.3.1 The Mitochondrial Protein GDAP1: Gene, Structure and Localization

The gene of human *GDAP1* is located on chromosome 8 (8q21.11; Baxter et al., 2002; http://www.ncbi.nlm.nih.gov/gene/54332, 2014), consists of 23,728 base pairs (bp; Cassereau et al., 2011b) and contains six exons and five introns (Baxter et al., 2002). The open reading frame includes 1,077 nucleotides which encodes a protein of 358 amino acids (Liu et al., 1999) that was later denominated as isoform a (Cassereau et al., 2011b). A shorter transcript variant, isoform b, contains only 290 amino acids and shows a shorter N (amino)-terminus (Cassereau et al., 2011b). This transcript variant includes an alternate in-frame exon and the usage of an alternative splice site in the 5' coding region accompanied by a downstream start codon results in the transcription of a shorter transcript (Cassereau et al., 2011b; http://www.ncbi.nlm.nih.gov/gene/54332, 2014). The GDAP1 protein has sequence similarities with GSTs (Cuesta et al., 2002; Marco et al., 2004; Shield et al., 2006), which are mainly cytosolic enzymes catalyzing the detoxification of various compounds like

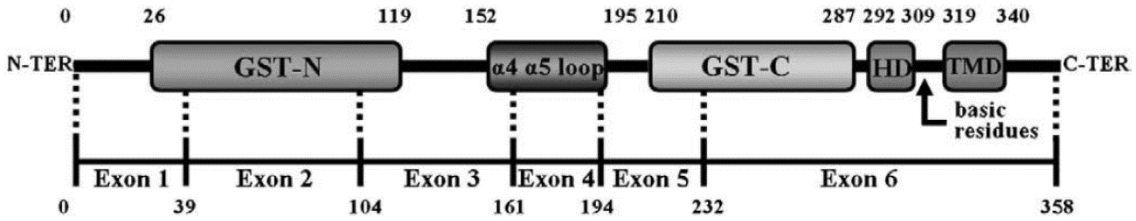

Figure 7: GDAP1 protein and its predicted domains.
Displayed is the GDAP1 protein (isoform a with 358 amino acids) and its various domains including the N-terminal glutathione transferase domain (GST-N) close to the N-terminus (N-TER), the α4-α5 loop, the C-terminal GST domain, the hydrophobic domain (HD) followed by the C-terminal transmembrane domain (TMD) near the C-terminus (C-TER). The amino acids positions of the different domains is given in the top, while the genomic organization with specified amino acids position of the exon boundaries is shown in the bottom. (adapted from Cassereau et al., 2011b, copyright 2012, with permission from Elsevier)

xenobiotics by the conjugation to GSH (Hayes et al., 2005; Sheehan et al., 2001). GDAP1 has two GST domains: domain I, an N-terminal thioredoxin fold domain (GST-N), and domain II, an α-helical C (carboxy)-terminal domain (GST-C; Cuesta et al., 2002; Marco et al., 2004; Shield et al., 2006). The domain I displays conserved active site residues (Cuesta et al., 2002; Marco et al., 2004; Shield et al., 2006). The binding site to GSH, lying within domain I and domain II, was predicted to recognize xenobiotics (Cuesta et al., 2002). In comparison to other canonical cytosolic GSTs, GDAP1 contains a long extended amino acid sequence with two additional alpha helices (named α4-α5 loop) within the GST domain II (Marco et al., 2004). The amino acid serine at position 34 in the GST-N domain was predicted to be the active site for its catalytic activity (Shield et al., 2006). GDAP1 has most similarities to cytosolic GSTs, but does not fit in any known class of the GST family and rather belongs to a novel GST class of GST-like proteins (Marco et al., 2004). This is also due to a transmembrane domain (TMD) in the C-terminal region of the protein besides an additional hydrophobic domain (HD; Marco et al., 2004; Wagner et al., 2009). The overall structure of GDAP1 protein is shown in Figure 7.

GDAP1 protein was shown to be a tail-anchored protein of the outer mitochondrial membrane with a single TMD (Niemann et al., 2005; Wagner et al., 2009). The C-terminus is facing the mitochondrial intermembrane space, while the N-terminal part is located in the cytosol (Wagner et al., 2009). The TMD and its flanking basic amino acids are important for mitochondrial localization because truncated GDAP1 proteins missing the TMD (Niemann et al., 2005; Pedrola et al., 2005) as well as GDAP1 protein with three exchanged basic amino acids in the N-terminal region of the TMD, or two exchanged basic amino acids in the C-terminal region of both the HD or the TMD (Wagner et al., 2009) are losing its mitochondrial localization. But it is unclear, whether the HD is located in the cytosol or integrated in the membrane, however, it seems to be not spanning the mitochondrial outer membrane (Figure 8; Wagner et al., 2009).

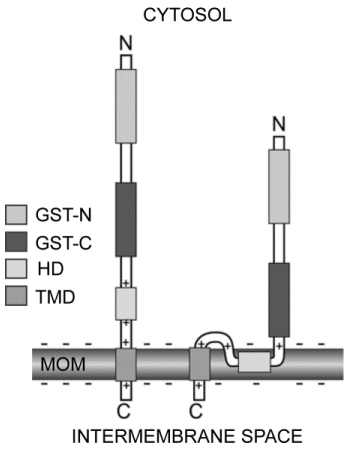

Figure 8: GDAP1's membrane topology.
GDAP1 is located in the mitochondrial outer membrane (MOM) spanning it with a single transmembrane domain (TMD), while the N-terminus (N) and both glutathione transferase domains (GST-N and GST-C) are located in the cytosol as well as the C-terminus (C) is reaching in the intermembrane space. However, the localization of the hydrophobic domain is unclear and two possible localizations are displayed. (adapted from Wagner et al., 2009)

1.3.2 Charcot-Marie-Tooth Disease

GDAP1 belongs to the class of mutated proteins leading to different forms of CMT disease (Baxter et al., 2002; Chung et al., 2008; Claramunt et al., 2005; Cuesta et al., 2002; Senderek et al., 2003). CMT disease, also referred to as hereditary motor and sensory polyneuropathy, was first described by the three neurologists Jean Martin Charcot, Pierre Marie and Howard Henry Tooth in 1886 (reviewed in Bucci et al., 2012; Kazamel and Boes, 2014). It is affecting both motor and sensory nerves of the peripheral nervous system (PNS; Bucci et al., 2012) and is one of the most common inherited peripheral neuropathy in humans (Berger et al., 2002; Cassereau et al., 2011b). Depending on the country of origin the prevalence concludes to about 10-30:100,000 (Emery, 1991). The different subtypes are clinically and genetically heterogeneous syndromes (Berger et al., 2002). Up to now, more than 78 subtypes have been described caused by mutations in more than 40 genes (Jerath and Shy, 2014). Neurons and/or Schwann cells, the myelinating glias of the PNS, are being affected (Niemann et al., 2006). Based on the patterns of inheritance and electrophysiological studies, CMT can be classified, while the inheritance pattern can be autosomal recessive, autosomal dominant as well as X-linked resulting in an axonal, demyelinating or intermediate form (Jerath and Shy, 2014). For example, mutations in *GDAP1* lead to the most frequent autosomal recessively inherited demyelinating subtype CMT4A (Baxter et al., 2002). Consistent clinical symptoms of different subtypes include progressive symmetric distal polyneuropathy, muscle atrophy, deformities of the feet,

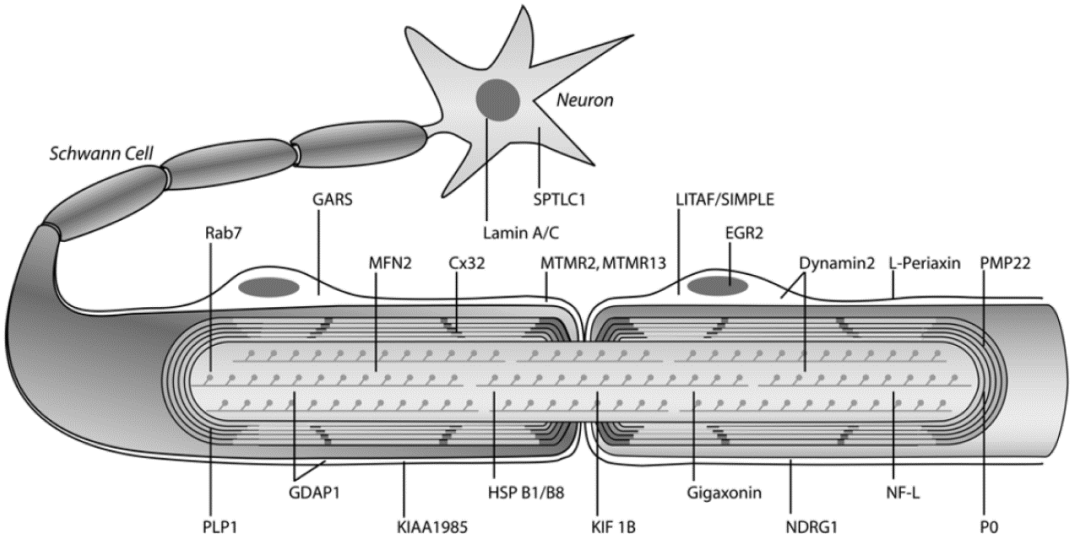

Figure 9: Schematic drawing of mutated proteins in CMT disease in a peripheral neuron and Schwann cells.
Proteins are shown in their regular localization in neurons and/or Schwann cells according to their expression and the observed CMT form. (adapted from Niemann et al., 2006, Copyright © 2006 Humana Press Inc. with permission of Springer)
SPTLC1, serine palmitoyltransferase, long chain base subunit 1; Rab7, ras-related protein 7; GARS, glycyl-tRNA synthetase; MFN2, mitofusin 2; Cx32, connexin 32; MTMR2/13, myotubularin-related protein 2; LITAF/SIMPLE, lipopolysaccharide-induced tumor necrosis factor-alpha factor/ small integral membrane protein of lysosome/late endosome ; EGR2, early growth response 2; PMP22, peripheral myelin protein 22; PLP1, proteolipid protein 1; GDAP1, ganglioside-induced differentiation-associated protein 1; HSP B1/B8, KIF 1B, kinesin-like protein 1B; heat-shock proteins B1/B8; NF-L, NDRG1, N-myc downstream-regulated gene 1;neurofilament light chain; P0, protein zero

steppage gait, weakness, distal sensory loss as well as decreased or absent deep tendon reflexes (Cassereau et al., 2011a; Harel and Lupski, 2014). Depending on the CMT subtypes, the disease can cause hearing loss, cognitive impairment, learning difficulties, optic atrophy, vocal cord and diaphragmatic paresis, respectively (Harel and Lupski, 2014). Mutated proteins causing disease are involved in cellular processes like cytoskeleton/axonal transport, endosomal sorting, myelin assembly, mRNA processing/transcription, protein aggregation, channel abnormalities and mitochondrial function (Figure 9; Jerath and Shy, 2014).

1.3.3 Function of GDAP1 and its Role in Charcot-Marie-Tooth Disease

The function of GDAP1 is still not fully understood. *Gdap1* was first recognized in mouse Neuro2a cells after ganglioside-induced neuronal differentiation triggered by transfection with GD3 synthase (α-2, 8-sialyltransferase) cDNA (complementary DNA) as well as after retinoic acid-induced neuronal differentiation of mouse PC12 cells (Liu et al., 1999). During development of the mouse brain *Gdap1* expression increases with differentiation, but shows the highest expression in the adult brain (Liu et al., 1999). The ubiquitous expression of *Gdap1*/*GDAP1* mRNA was proved in various tissues of mouse and human, whereas the highest expression was detected in the whole brain and spinal cord of the nervous system (Cuesta et al., 2002). GDAP1 displays a higher expression in neurons of the nervous system than in the myelinating Schwann cells (Noack et al., 2012; Pedrola et al., 2008; Pedrola et al., 2005), while others detected its expression in Schwann cells and neurons (Niemann et al., 2005).

Mutations in *GDAP1* lead in humans to the already mentioned autosomal recessively inherited demyelinating subtype CMT4A (Baxter et al., 2002), axonal recessive (AR)-CMT2 subtype (Cuesta et al., 2002), intermediate recessive subtype CMTRIA (Senderek et al., 2003) and the less often dominant subtype CMT2K (Cassereau et al., 2009; Chung et al., 2008; Claramunt et al., 2005). Thus, mutations in *GDAP1* are affecting neurons as well as Schwann cells or even both types of cells. Until now 53 mutations have been identified causing disease (Cassereau et al., 2011a). Most of these mutations are inducing missense mutations (64 %) followed by nonsense mutations (17 %) giving rise to truncated proteins, mutations inducing frameshifts and the smallest group of mutations results in splicing defects (6 %; Cassereau et al., 2011a). The subtypes CMT4A and AR-CMT2 are characterized by an early onset of disease and a more rapid progression resulting in earlier walking disabilities (Cassereau et al., 2011a). More than half of the mutations are located within the GST domains of the protein (56 %; Cassereau et al., 2011a). Both the TMD and HD are rarely influenced with only 2 % (Cassereau et al., 2011a), but this part of the protein is necessary

for proper mitochondrial localization (Niemann et al., 2005; Pedrola et al., 2005; Wagner et al., 2009). Even though the GST domain is affected in most cases, a GST activity or glutathione binding activity was not proved with bacterial expressed recombinant protein missing the transmembrane domain (Pedrola et al., 2005; Shield et al., 2006). But recently, GST enzyme activity was detected with an insect cell-expressed recombinant GDAP1 protein lacking the HD1 and TMD domain (Wagner, 2009).

It is still unclear how mutations in *GDAP1* cause disease. GDAP1 seems to influence mitochondrial dynamics. Over-expression of GDAP1 protein in monkey COS-7 cells as well as HT22S cells induces mitochondrial fission (Niemann et al., 2005; Noack et al., 2012) and a similar effect has been detected in drosophila (Lopez Del Amo et al., 2014). In comparison, the over-expression of recessively-inherited disease-causing mutation like the point mutation R310Q cannot induce mitochondrial fragmentation (Niemann et al., 2005; Niemann et al., 2009; Noack et al., 2012). The effect of GDAP1 on mitochondrial dynamics does neither enhance the sensitivity to apoptosis nor does it compromise mitochondrial fusion (Niemann et al., 2005). In contrast, dominantly inherited mutations increase the sensitivity to apoptosis, affect the mitochondrial membrane potential, impair mitochondrial fusion and enhance the production of ROS and thereby induce mitochondrial damage (Niemann et al., 2009). Thus, the effect of GDAP1 protein on mitochondria and mitochondrial dynamics is dependent on the inheritance pattern. Silencing of *Gdap1* in the mouse neuroblastoma cell line N1E-115 reduces the number of cells with fragmented mitochondria and triggers a tubular mitochondrial morphology (Niemann et al., 2005), while re-expression of wild type (WT) *Gdap1* increases the number of cells with fragmented mitochondria, however, re-expression of the recessively inherited disease-associated mutation R310Q induces only minor changes in *Gdap1* silenced cells (Niemann et al., 2009). The stable knockdown (KD) of *GDAP1* in the human neuroblastoma cell line SH-SY5Y does not induce mitochondrial elongation (Pla-Martin et al., 2013). *GDAP1* KD and control SH-SY5Y cells have a comparable mitochondrial elongation index, whereas an abnormal distribution of mitochondria and a reduced contact between mitochondria and the ER is detectable in *GDAP1* KD cells (Pla-Martin et al., 2013). This change in the contact between mitochondria and ER seems to influence calcium homeostasis and results in a reduced calcium influx through SOCE (Pla-Martin et al., 2013). Additionally, the re-localization of mitochondria towards plasma membrane induced by depletion of the ER-calcium store is disturbed (Pla-Martin et al., 2013). In addition to influencing mitochondrial morphology, GDAP1 protein co-localizes with some peroxisomes besides its major localization at mitochondria and influences the morphology of peroxisomes by inducing peroxisomal fission, which is dependent on its HD (Huber et al., 2013). The analysis of cultured sensory neurons of *Gdap1* knockout mice in dorsal root ganglia explants revealed an additional effect in mitochondrial transport (Niemann et al., 2014). Mitochondria

show increased pausing when travelling in anterograde direction along the axons and the pausing of retrograde moving mitochondria last longer, however, the transport is not impaired in general (Niemann et al., 2014).

In the past, we identified *Gdap1* as a transcript up-regulated in the glutamate-resistant HT22R cells and because of this studied its role in oxidative stress (Noack et al., 2012). We could show that over-expression of GDAP1 protein, but not GDAP1 protein with recessively inherited disease-causing mutations like the R310Q point mutation, increases the total cellular GSH content in HT22S cells (Noack et al., 2012). This increase in total GSH level protects GDAP1 over-expressing cells against oxidative stress induced by GSH depletion (Noack et al., 2012). At the same time, GDAP1 affects mitochondria in several other parameters (Noack et al., 2012). GDAP1 increases the mitochondrial membrane potential, decreases mitochondrial superoxide production, reduces mitochondrial calcium content and results in a reduced mitochondrial activity of isolated mitochondria, however, stable over-expression of *Gdap1* R310Q does not alter these parameters (Noack et al., 2012). In addition, the analysis of two fibroblast cell lines from patients with autosomal-recessive CMT4A showed a reduction in total glutathione as well as reduced mitochondrial membrane potential, while the mitochondrial morphology remained unaffected (Noack et al., 2012). The effect of GDAP1 on glutathione content and protection against oxidative stress accompanied by the observed changes in the glutathione content of patient fibroblasts suggest a role of oxidative stress in CMT disease and disease progression. The analysis of GSH levels in drosophila after knockdown and over-expression of *Gdap1* confirmed our observation that *Gdap1* over-expression increases GSH levels (Lopez Del Amo et al., 2014). But in drosophila this effect is only detectable in old flies (Lopez Del Amo et al., 2014). The knockdown of *Gdap1* as well increases the GSH content, however, to a lower extent (Lopez Del Amo et al., 2014). In line with the recognized effect of *Gdap1* over-expression on mitochondrial activity, Cassereau and colleagues realized a reduced mitochondrial complex I activity in fibroblasts from patient with autosomal dominant CMT2K (Cassereau et al., 2009). In agreement, over-expression and knockdown of *Gdap1* in drosophila changes the mitochondrial function and enhances the ATP production in young drosophila flies (Lopez Del Amo et al., 2014). In contrast, old flies with over-expressed *Gdap1* display increased ATP levels, whereas flies with silenced *Gdap1* show decreased ATP production (Lopez Del Amo et al., 2014). These observations might suggest an influence of GDAP1 on mitochondrial respiration and activity, which was analysed in this study besides studying it influence on mitochondrial dynamics.

1.4 The Anti-Apoptotic Protein Bcl-x_L

Bcl-2-related protein, long isoform (Bcl-x_L, also named B-cell lymphoma-extra large) is another mitochondrial protein (Gonzalez-Garcia et al., 1994; Kaufmann et al., 2003) that protects against cell death including apoptosis (Boise et al., 1993; Gonzalez-Garcia et al., 1994). Apoptosis is a form of programmed cell death (PCD) that can induce the controlled elimination of a single cell as well as small clusters of cells in an energy-dependent process (Elmore, 2007). Bcl-x_L belongs together with Bcl-2 to the anti-apoptotic and first class of proteins containing conserved Bcl-2 homology (BH) domains 1 to 4 in the Bcl-2 family of proteins, a family of proteins which consists of three classes of proteins depending on their anti- or pro-apoptotic function as well as sequence similarities in their BH domains (Chipuk et al., 2010; Pradelli et al., 2010; Youle and Strasser, 2008). The role of Bcl-2 family members in preventing and supporting mitochondrial outer membrane permeabilization (MOMP) is a well-known and central event during the intrinsic pathway of apoptosis (Brunelle and Letai, 2009; Pradelli et al., 2010; Vander Heiden and Thompson, 1999; Youle and Strasser, 2008). Bcl-2 was the first identified enzyme of this family (Tsujimoto et al., 1984) and was recognized as an apoptosis inhibitor by inhibiting IL-3 (Interleukin-3)-deprivation-induced death in a lymphoid cell line (Vaux et al., 1988) few years after its recognition as an oncogene in human follicular lymphoma (Bakhshi et al., 1985; Cleary and Sklar, 1985; Tsujimoto et al., 1985). The *bcl-x* gene was identified as a *bcl-2*-related gene that encodes two protein products through alternative splicing by the use of two different 5'-splice sites within the first exon (Boise et al., 1993). The larger mRNA encodes Bcl-x_L, a protein of 233 amino acids which is similar in size and structure to Bcl-2, while the shorter mRNA encodes Bcl-x_S with only 170 amino acids (Boise et al., 1993). The anti-apoptotic action of human and murine Bcl-x_L was recognized upon growth factor withdrawal in IL-3-dependent mouse FL5.12 cells (Boise et al., 1993; Gonzalez-Garcia et al., 1994). During embryonic and postnatal development *bcl-x_L* is the dominant mRNA expression product of the *bcl-x* gene in murine tissues (Gonzalez-Garcia et al., 1994). Especially *bcl-x_L* had been recognized in the adult brain (Boise et al., 1993). The predominant expression of *bcl-x_L* during embryonic development has already suggested an important role of Bcl-x_L protein during this stage (Gonzalez-Garcia et al., 1994). In mice *bcl-x* knockout even results in substantial apoptotic cell death of postmitotic immature neurons in the developing brain, spinal cord, and dorsal root ganglia which causes the dead of *bcl-x*-deficient mice at embryonic stage (Motoyama et al., 1995).

The Bcl-x_L protein is located at the outer mitochondrial membrane (Gonzalez-Garcia et al., 1994; Kaufmann et al., 2003), but can additionally be found in a subcellular cytosolic location as well as in a membrane-bound state (Hsu et al., 1997), which is its favoured state (Kaufmann et al., 2003). The localization change of Bcl-x_L from cytosol to a membrane-

bound state can be induced by induction of apoptosis in murine thymocytes (Hsu et al., 1997). Bcl-x_L is in comparison to Bcl-2, which is localized on several intracellular membranes, specifically targeted to the outer mitochondrial membrane by a particular signalling sequence in its C-terminal region (Kaufmann et al., 2003). Additionally, others have even described its location on the ER because interaction with reticulon-x_s results in an increased localization from their predominant position at mitochondria to the ER (Tagami et al., 2000). Interestingly, Eno and colleagues examined the role of mitochondria- and ER-localized Bcl-x_L in preventing apoptosis (Eno et al., 2012). They established a mouse embryonic fibroblast (MEF) cell line with *bcl-x* gene knockout (Bcl-x_L-KO) which no longer shows Bcl-x_L protein expression and re-expressed Bcl-x_L targeted to the ER, mitochondria or in the cytoplasm (Eno et al., 2012). Knockout of *bcl-x* increases the susceptibility to apoptotic cell death and enhances H_2O_2-induced oxidative stress, while WT MEFs expressing endogenous Bcl-x_L are protected (Eno et al., 2012). In comparison, re-expression of mitochondrially targeted Bcl-x_L in the KO background restores its anti-apoptotic action, whereas ER-localized Bcl-x_L fails to do this (Eno et al., 2012). At the ER, Bcl-x_L interacts with all three isoforms of the inositol 1,4,5-trisphosphate ($InsP_3$) receptor ($InsP_3R$) Ca^{2+} release channel (White et al., 2005), whereas the interaction between Bcl-x_L and the different types of $InsP_3R$ seems to trigger the same or different cellular responses in the case of calcium homeostasis and apoptosis (Li et al., 2007). First results showed that Bcl-x_L's interaction with the carboxyl terminal of the $InsP_3R$ increases the sensitivity of $InsP_3R$ to low levels of $InsP_3$ resulting in an enhanced regulation of single channel activity by $InsP_3$ and Ca^{2+}, a reduced ER calcium content under Bcl-x_L over-expressing conditions, an enhancement in spontaneous cytosolic calcium oscillations and increases cellular apoptotic resistance (White et al., 2005). Bcl-x_L over-expression can even enhance mitochondrial activity and leads to an elevated NAD(P)H auto-fluorescence (White et al., 2005). A subsequent study realised that the interplay of Bcl-x_L with all three $InsP_3R$ is responsible for the increase in sensitivity to low levels of $InsP_3$ as well as its sensitivity to apoptotic stimuli, while the ER calcium concentration is only reduced in cells expressing Bcl-x_L and type 3 $InsP_3R$ (Li et al., 2007). Especially Bcl-x_L-KO MEFs display an impaired ER Ca^{2+} homeostasis which cannot be restored by re-expression of mitochondria-targeted Bcl-x_L, whereas ER-localized Bcl-x_L is able do this (Eno et al., 2012). This shows that ER-localized and mitochondria-localized Bcl-x_L have different function (Eno et al., 2012).

In addition, Bcl-x_L interacts with the voltage-dependent anion channel (VDAC) in the outer mitochondrial membrane (Arbel et al., 2012; Huang et al., 2013; Shimizu et al., 1999; Shimizu et al., 2000; Vander Heiden et al., 2001). While several studies report that Bcl-x_L induces closing of the VDAC1 channel (Arbel et al., 2012; Shimizu et al., 1999; Shimizu et al., 2000), two additional studies, including a most recent one, favour the open configuration

of VDAC induced by Bcl-x_L (Huang et al., 2013; Vander Heiden et al., 2001). Addition of recombinant Bcl-x_L protein to isolated mitochondria allows metabolite exchange like ADP across the outer mitochondrial membrane by inhibiting VDAC1 closure under conditions promoting its closed configuration, whereas cytochrome c is not released from the intermembrane space (Vander Heiden et al., 2001). The interaction of Bcl-x_L is restricted to VDAC1 and -3 isoforms (Huang et al., 2013). VDAC is responsible for the regulated crossing of metabolites, like ATP and ADP as the most important ones, as well as ions, such as Ca^{2+} through the outer mitochondrial membrane (Colombini, 2012). Huang and co-workers realized when they analysed the already mentioned MEF WT and Bcl-x_L-KO cell lines that ATP, which induces $InsP_3$-induced cytosolic Ca^{2+} transients, results in a larger mitochondrial Ca^{2+} uptake in WT compared to Bcl-x_L-KO cells (Huang et al., 2013). Re-expression of mitochondria-targeted Bcl-x_L in the KO background restores the capacity of mitochondrial Ca^{2+} and responsible for the mitochondrial calcium uptake is the interaction of Bcl-x_L with VDAC (Huang et al., 2013). By influencing mitochondrial Ca^{2+} homeostasis, Bcl-x_L might even directly influence mitochondrial function because mitochondrial Ca^{2+} uptake can directly elevate mitochondrial activity including OXPHOS by increasing the activity of four dehydrogenases including the pyruvate-, isocitrate- and alpha-ketoglutarate dehydrogenase of the TCA cycle as well as the activity of the ATP synthase itself (Das and Harris, 1990; Hansford and Zorov, 1998). Thus, an impaired mitochondrial calcium uptake in Bcl-x_L-KO MEFs (Huang et al., 2013) suggests a reduced mitochondrial activity. Even though WT and Bcl-x_L-KO MEFs show no differences in mitochondrial biomass, mitochondrial membrane potential and ER-mitochondrial contact sites (Huang et al., 2013), impacts of Bcl-x_L on mitochondria have already been described. In response to diverse death stimuli, Bcl-x_L is able to regulate the mitochondrial membrane potential and mitochondrial volume homeostasis and thereby prevents the loss of outer mitochondrial membrane integrity through the prevention of inner mitochondrial membrane hyperpolarization as well as matrix swelling (Vander Heiden et al., 1997). In hippocampal neurons Bcl-x_L over-expression caused an enhanced and more efficient energy metabolism, based on an increase in ATP production and decreased mitochondrial oxygen uptake reflecting a efficient coupling between ATP production and oxygen uptake (Alavian et al., 2011). In this study, an additional localization of Bcl-x_L in the inner mitochondrial membrane in GFP-Bcl-x_L-expressing neurons and native brain mitochondria, and a direct interaction with the β-subunit of the F_1F_0 ATP synthase was proposed, which seems to be responsible for increasing F_1F_0 ATPase activity caused by recombinant Bcl-x_L on prepared submitochondrial vesicles of the inner mitochondrial membrane containing enriched F_1F_0 ATP synthase complexes (Alavian et al., 2011). Neurons deficient for *bcl-x* display an increase in mitochondrial membrane potential, reduction in ROS production and subsequent increase in NAD(P)H (Chen et al.,

2011). Bcl-x_L reduces useless ion fluxes across the inner mitochondrial membrane and contributes by stabilizing the inner mitochondrial membrane potential to an efficient mitochondrial energetic (Chen et al., 2011).

In addition, Bcl-x_L influences directly mitochondrial dynamics. Bcl-x_L interacts with the mitochondrial fusion proteins Mfn1 and Mfn2 (Cleland et al., 2011) as well as the mitochondrial fission factor Drp-1 leading to increased activity (Li et al., 2008). However, in one other study, the interaction to mitofusins has been restricted to Mfn2 only, while no interaction with Mfn1 was recognized (Delivani et al., 2006). According to this, Bcl-x_L promotes both mitochondrial fusion and fission, which seems to be dependent on the protein expression level in over-expressing cells (Delivani et al., 2006; Sheridan et al., 2008). In cultured neurons, Bcl-x_L changes the mitochondrial dynamics by increasing both the rate of mitochondrial fission and fusion, but the rate of fission is still higher than the rate of fusion (Berman et al., 2009). Nevertheless, mitochondria of rat cortical neurons over-expressing Bcl-x_L are elongated compared to mitochondria in control cells (Berman et al., 2009). In comparison, a conditional knockout of *bcl-x* in mouse induces a shortened mitochondrial morphology in cortical neurons, so that the mitochondrial morphology appears more fragmented (Berman et al., 2009). Thus, the function of Bcl-x_L is not limited to its function as an anti-apoptotic protein that can influence and regulate calcium homeostasis. It has as well a role in influencing mitochondrial morphology and function which was further analysed in this study.

1.5 The Aim of this Project

Mitochondria are implicated in far more processes than being only essential for ATP production because they contribute to the production of metabolites, play a central role during apoptosis, are important for calcium homeostasis and are a major source for ROS (Dringen, 2000; Finkel and Holbrook, 2000; MacAskill and Kittler, 2010; Wallace, 1999; Westermann, 2010). In particular, mitochondrial defects like impaired mitochondrial dynamics and glutathione metabolism are associated with neurodegenerative diseases (Dringen, 2000; Dringen and Hirrlinger, 2003; Itoh et al., 2013). The aim of this project was to identify the effects including similarities on the mitochondrial form and function caused by acute stressors and by mechanisms against stress including adaptations through chronic oxidative stress and the two cytoprotective, mitochondrial proteins, GDAP1 and Bcl-x_L.

For this reason, I studied the effects of glutamate-induced oxidative stress in the model system of HT22S cells (Davis and Maher, 1994) and of oxidative stress induced by the two GSH depleting reagents EA and MQ (Chiou and Tzeng, 2000; Kim et al., 2014; Seyfried et al., 1999; Wullner et al., 1999) in human SH-SY5Y cells on mitochondria. We have generated a glutamate-resistant HT22R cell line (Lewerenz et al., 2006), which is a great

model to study the consequences of chronic oxidative stress and associated prolonged adaptations including mitochondrial form and function in this project. Increased mitochondrial membrane potential in HT22R cells (Noack et al., 2012) together with recent investigations demonstrating the influence of oxidative glutamate toxicity on mitochondrial form and function in HT22S cells (Grohm et al., 2010; Kumari et al., 2012) have already suggested an impact on mitochondria under acute oxidative stress and in glutamate resistance. Additionally, I analysed the effect of the mitochondrial, cytoprotective protein GDAP1 on mitochondrial form and function because GDAP1 protects against oxidative stress (Noack et al., 2012), is a mitochondrial fission factor (Niemann et al., 2005), seems to directly impact mitochondrial function and increases mitochondrial membrane potential (Noack et al., 2012), but when mutated induces predominantly CMT4A diseases (Baxter et al., 2002). Thus, I included wild type, disease-associated GDAP1 R310Q, GDAP1 S34A with a point mutation of the predicted GST active residue (S34; Shield et al., 2006) and a *GDAP1* knockdown condition in my study. We hypothesized due to its fission activity (Niemann et al., 2005), recently demonstrated GST activity (Wagner, 2009) and ability to increase GSH (Noack et al., 2012) that it acts even as a redox sensor causing mitochondrial adaptation in form and function. For this reason, I studied the effect of these various types of GDAP1 under oxidative stress on mitochondria. The second studied mitochondrial, cytoprotective protein Bcl-x_L, which protects against apoptosis (Boise et al., 1993; Gonzalez-Garcia et al., 1994), is important for calcium homeostasis (Eno et al., 2012; Li et al., 2007; White et al., 2005) as well as it directly influences mitochondria by interacting with the outer mitochondrial membrane protein VDAC regulating crossing of metabolites like ADP and Ca^{2+} (Huang et al., 2013; Vander Heiden et al., 2001) and influencing mitochondrial dynamics (Berman et al., 2009; Delivani et al., 2006; Sheridan et al., 2008). Because of this, I studied the influence of Bcl-x_L deficiency and mitochondria-localized Bcl-x_L on mitochondrial form and function.

2 MATERIALS AND METHODS

2.1 Materials

2.1.1 Materials for Molecular Biological Methods

2.1.1.1 Chemicals

Chemical	Supplier
2-Propanol	Merck KGaA, Darmstadt, Germany
Agarose, Agarose basic	Sigma-Aldrich, Steinheim, Germany AppliChem GmbH, Darmstadt, Germany
Calcium chloride ($CaCl_2$)	Sigma-Aldrich, Steinheim, Germany
Dimethyl sulfoxide (DMSO)	Sigma-Aldrich, Steinheim, Germany Carl Roth, Karlsruhe, Germany
Ethanol absolute AnalaR NORMAPUR®	VWR BDH Prolabo, Darmstadt, Germany
Ethanol Rotipuran 99,8 %	Carl Roth, Karlsruhe, Germany
Ethidium bromide	Sigma-Aldrich, Steinheim, Germany
Glycerol	Sigma-Aldrich, Steinheim, Germany
Magnesium chloride hexahydrate ($MgCl_2 \cdot 6H_2O$)	Sigma-Aldrich, Steinheim, Germany

2.1.1.2 Media

Media	Supplier
LB Agar, powder (Lennox L agar)	Invitrogen, Darmstadt, Germany
LB Broth Base (Lennox L Broth Base)	Invitrogen, Darmstadt, Germany
S.O.C. Medium	Invitrogen, Darmstadt, Germany

2.1.1.3 Antibiotics

Antibiotics	Supplier
Ampicillin sodium salt	Sigma-Aldrich, Steinheim, Germany
Kanamycin sulfate	Sigma-Aldrich, Steinheim, Germany

2.1.1.4 Kits

Kit	Supplier
Gateway™ System	Invitrogen, Darmstadt, Germany
pGEM T Easy Vector System	Promega, Madison, WI, USA
NucleoBond® Xtra Midi/Maxi Kit	Machery and Nagel, Düren, Germany
ZR RNA MiniPrep Kit	Zymo Research Cooperation, Irvine, USA
Zymoclean™ Gel DNA Recovery Kit	Zymo Research Cooperation, Irvine, USA
Zyppy™ Plasmid Miniprep Kit	Zymo Research Cooperation, Irvine, USA

2.1.1.5 Bacterial Strains

Bacterial Strain	Genotype	Supplier
DH5α	F– Φ80*lac*ZΔM15 Δ(*lac*ZYA-*arg*F) U169 *rec*A1 *end*A1 *hsd*R17 (rK–, mK+) *pho*A *sup*E44 λ– *thi*-1 *gyr*A96 *rel*A1	Invitrogen, Darmstadt, Germany
*ccd*B Survival™ 2 T1R	F^- *mcr*A Δ(*mrr-hsd*RMS-*mcr*BC) Φ80*lac*ZΔM15 Δ*lac*X74 *rec*A1 *ara*Δ139 Δ(*ara-leu*)7697*gal*U *gal*K *rps*L (Str^R) *end*A1 *nup*G *fhu*A::*IS2*	Invitrogen, Darmstadt, Germany

2.1.1.6 Restriction enzymes

Restriction enzymes were purchased from New England Biolabs (New England Biolabs, Frankfurt, Germany) and used in combination with the appropriate reaction buffer and if necessary under addition of bovine serum albumin (BSA) provided by the supplier.

2.1.1.7 Other Enzymes and Enzyme Mixes

Enzyme and Enzyme Mixes	Supplier
Gateway® LR Clonase® II Enzyme Mix	Invitrogen, Darmstadt, Germany
Platinum PCR SuperMix	Invitrogen, Darmstadt, Germany
High Capacity cDNA Reverse Transcription Kit	Applied Biosystems, Darmstadt, Germany
T4 DNA Ligase	New England Biolabs, Frankfurt, Germany
RNase-free DNase I	Zymo Research Cooperation, Irvine, USA

2.1.1.8 Buffers and Loading Buffers

Buffer and Loading Buffer		Supplier
10x BlueJuice Gel Loading Buffer		Invitrogen, Darmstadt, Germany
TAE, 1x	40 mM Tris base, 20 mM acetic acid, 1 mM EDTA, pH 8.4	Merck KGaA, Darmstadt, Germany Sigma-Aldrich, Steinheim, Germany
UltraPure™ 10x TBE Buffer		Invitrogen, Darmstadt, Germany

2.1.1.9 Other Materials

Material	Supplier
1 kb plus DNA ladder	Invitrogen, Darmstadt, Germany
Nuclease-Free Water (not DEPC-treated)	Ambion, Darmstadt, Germany
peqGreen	Peqlab Biotechnologie GmbH, Erlangen; Germany

2.1.1.10 Plasmid DNA

Table 1 shows a list of all used plasmid DNAs in this work. A description of the backbone and insert is included.

Table 1: Plasmid DNA.
Listed are all used plasmids including a description about the backbone and the insert.

Plasmid	Description	Supplier/Reference
pENTR3C:GDAP1	Full-length mouse *Gdap1* cDNA in entry vector pENTR3C	generated in the lab
pENTR3C:R310Q	mouse *Gdap1* cDNA with point mutation R310Q in entry vector pENTR3C	generated in the lab
pcDNA:S34A	mouse *Gdap1* cDNA with point mutation S34A in pcDNA3.1	Kind gift of Axel Niemann, Zürich, Switzerland
pENTR3C:S34A	mouse *Gdap1* cDNA with point mutation S34A in pENTR3C	this work
pPB-CAG-HA-IRES-Venus dest	*piggy*Bac transposon destination vector/empty vector	generated in the lab
pPB-CAG-HA-GDAP1-IRES-Venus	mouse *Gdap1* cDNA in *piggy*Bac transposon destination vector	this work
pPB-CAG-HA-R310Q-IRES-Venus	mouse *Gdap1* cDNA with point mutation R310Q in *piggy*Bac transposon destination vector	this work
pPB-CAG-HA-S34A-IRES-Venus	mouse *Gdap1* cDNA with point mutation S34A in *piggy*Bac transposon destination vector	this work
pCMV-HA hyPBase	hyperactive *piggy*Bac transposase expression vector	(Yusa et al., 2011)
pDsRed-mito	Mitochondrially targeted DsRed2	Kind gift of Axel Niemann, University of Zürich, Switzerland
peGFP-C1	empty vector	Clontech Laboratories, Mountain View, CA, USA
peGFP-G6PD	full-length rat *G6pd* cDNA in peGFP	kind gift of Juan P. Bolanos, University of Salamanca, Spain; (Garcia-Nogales et al., 2003)
pGW1:xCT-GFP	cDNA of mouse *Slc7a11*(xCT)-GFP in pGW1-CMV	kind gift of Andy Shih, University of British Columbia,

		Vancouver, Canada; (Shih and Murphy, 2001)

2.1.1.11 PCR Primers

Table 2 lists the primer pairs used for verification of the stable cell lines SH-SY5Y GDAP1, SH-SY5Y R310Q and SH-SY5Y S34A including their sequence, length and melting temperature.

Table 2: Primer pairs for verification of the cell lines SH-SY5Y S34A and SH-SY5Y R310Q.
Listed are the primer pairs used for verification of the SH-SY5Y cell lines S34A and R310Q compared to SH-SY5Y GDAP1 by PCR and subsequent sequencing of the PCR product. The sequence, length and melting temperature of the forward (fwd) and reverse (rev) primer is specified.

Primer	Sequence (5' → 3')	Length (bp)	Melting Tempera-ture (°C)	Purpose
PiggyCAG_2346_fwd	CAGCCATTGCCTTTTATGGT	20	59.96	Primer pair for verification of the cell line SH-SY5Y S34A
GDAP1_209_rev	CGCATAAACCAAGGCTCATT	20	60.1	
GDAP1_809_fwd	TGGAAAGAGACCGAACTTGG	20	60.22	Primer pair for verification of the cell line SH-SY5Y R310Q
PiggyCAG_4585_rev	CGCCTTTGCAGGTGTATCTT	20	60.27	

2.1.2 Material for Cell Culture, Cell-Based Assays and Biochemical Methods

2.1.2.1 Cell Lines

Table 3 shows a list of eukaryotic cell lines which were used in this work. The list includes a detailed description of the cell line's characteristics.

Table 3: Eukaryotic cell lines.
Listed are all used cell lines including their characteristics.

Cell Line	Characteristics	Supplier and Reference
HT22S	mouse hippocampal cell line, a sub-line derived from the parental cell line HT4	(Davis and Maher, 1994)
HT22R	glutamate-resistant HT22 cells, sub-population of HT22S cells, generated through the repetitive exposure to glutamate	(Lewerenz et al., 2006)
MEF WT	wild type (WT) mouse embryonic fibroblasts (MEF)	kind gift of Carl White, North Chicago, IL, USA; (Eno et al., 2012)
MEF Bcl-x_L-KO	Bcl-x_L-knockout MEF	kind gift of Carl White, North Chicago, IL, USA;

		(Eno et al., 2012)
MEF ActA	Bcl-x_L-knockout MEF stably over-expressing mitochondria-localized Bcl-x_L	kind gift of Carl White, North Chicago, IL, USA; (Eno et al., 2012)
SH-SY5Y	human neuroblastoma cell line, sub-clone parental cell line SK-N-SH	kind gift of Carsten Korth, Düsseldorf, Germany; (Biedler et al., 1978)
SH-SY5Y EV	SH-SY5Y stably transfected with pPB-CAG-HA-IRES-Venus dest (empty vector, EV)	this work
SH-SY5Y GDAP1	SH-SY5Y stably transfected with pPB-CAG-HA-GDAP1-IRES-Venus, over-expressing mouse GDAP1	this work
SH-SY5Y R310Q	SH-SY5Y stably transfected with pPB-CAG-HA-R310Q-IRES-Venus, over-expressing mouse GDAP1 mutant R310Q	this work
SH-SY5Y S34A	SH-SY5Y stably transfected with pPB-CAG-HA-S34A-IRES-Venus, over-expressing mouse GDAP1 mutant S34A	this work
SH-SY5Y pLKO-NT	SH-SY5Y stably transfected with pLKO.1 containing a non-targeted shRNA (pLKO-NT)	kind gift of Francesc Palau, Valencia, Spain; (Pla-Martin et al., 2013)
SH-SY5Y *GDAP1* KD	SH-SY5Y stably transfected with pLKO.1 containing a shRNA directed against *GDAP1* (G4)	kind gift of Francesc Palau, Valencia, Spain; (Pla-Martin et al., 2013)

2.1.2.2 Cell Culture Media, Supplements and Solutions

Media, Supplements and Solutions	Supplier
Dulbecco's modified eagle medium (DMEM) high glucose with L-glutamine and sodium pyruvate	PAA, Pasching, Austria Sigma-Aldrich, Steinheim, Germany Gibco, Paisley, United Kingdom
DMEM high glucose without phenol red	PAA, Pasching, Austria
DMEM/F12 (1:1 mixture of DMEM and Ham's F12) without L-glutamine	Gibco, Paisley, United Kingdom
DMEM without glucose	Gibco, Paisley, United Kingdom
Dulbecco's PBS (D-PBS) without calcium and magnesium	PAA, Pasching, Austria Sigma-Aldrich, Steinheim, Germany
HyClone fetal bovine serum, research grade	Thermo Scientific, Rockford, IL, USA
L-glutamine (200 mM)	Gibco, Paisley, United Kingdom
MEM non-essential amino acids solution (100x)	Gibco, Paisley, United Kingdom
Opti-MEM® I Reduced Serum Medium	Gibco, Paisley, United Kingdom
Sodium pyruvate (100 mM)	Gibco, Paisley, United Kingdom

Trypsin-EDTA (0.05 %)	Gibco, Paisley, United Kingdom

2.1.2.3 Antibiotics for Cell Culture

Antibiotics	Supplier
Blasticidin (10 mg/ml)	InvivoGen, Toulouse, France
Penicillin-Streptomycin (10,000 U/ml penicillin and 10 mg/ml streptomycin in 0.9 % NaCl)	Gibco, Paisley, United Kingdom Sigma-Aldrich, Steinheim, Germany
Puromycin (10 mg/ml)	InvivoGen, Toulouse, France

2.1.2.4 Solutions for Cell Viability Assays

Solution	Formulation and Concentration	Supplier for Chemicals
D-(+)-Galactose	500 mM in H_2O	Sigma-Aldrich, Steinheim, Germany
Ethacrynic acid (EA)	30 mg/ml in ethanol absolute	Santa Cruz Biotechnology, Heidelberg, Germany
L-Glutamic acid	250 mM in 1x PBS pH 7.4 adjusted with NaOH	Sigma-Aldrich, Steinheim, Germany
Menadione (MQ)	10 mM in ethanol absolute	Sigma-Aldrich, Steinheim, Germany

2.1.2.5 Transfection Reagents

Transfection Reagent	Supplier
Attractene	Qiagen, Hilden, Germany
TransFast™ Transfection Reagent	Promega, Madison, WI, USA

2.1.2.6 Chemicals

Chemical	Supplier
2-Mercaptoethanol	Sigma-Aldrich, Steinheim, Germany
5,5'-Dithiobis-(2-nitrobenzoic-acid) (DTNB)	Sigma-Aldrich, Steinheim, Germany
5-Sulfosalicylic acid dihydrate	Sigma-Aldrich, Steinheim, Germany
β-Nicotinamide adenine dinucleotide 2′-phosphate reduced tetrasodium salt hydrate (NADPH)	Sigma-Aldrich, Steinheim, Germany
Dimethyl sulfoxide	Sigma-Aldrich, Steinheim, Germany
Ethanol absolute AnalaR NORMAPUR®	VWR BDH Prolabo, Darmstadt, Germany
Ethanol Rotipuran 99,8 %	Carl Roth, Karlsruhe, Germany
L-Glutathione reduced	Sigma-Aldrich, Steinheim, Germany
Milk powder	Sigma-Aldrich, Steinheim, Germany
n-Octyl-β-D-glucopyranoside	Carl Roth, Karlsruhe, Germany
Powdered milk, blocking grade	Carl Roth, Karlsruhe, Germany

Triethanolamine	Sigma-Aldrich, Steinheim, Germany
Sodium hydroxide (NaOH)	Carl Roth, Karlsruhe, Germany Sigma-Aldrich, Steinheim, Germany
Triton X-100	Sigma-Aldrich, Steinheim, Germany
Tween 20	Sigma-Aldrich, Steinheim, Germany

2.1.2.7 Assay Kits, Enzymes for Cell-Based Assays and Biochemical Methods

Kit	Supplier
BC Assay Protein Quantification Kit	Interchim, Montlucon, France
CellTiter-Blue® Cell Viability Assay	Promega, Madison, WI, USA
NAD/NADH-Glo™ Assay	Promega, Madison, WI, USA
NADP/NADPH-Glo™ Assay	Promega, Madison, WI, USA
Glutathione reductase from baker's yeast (*S. cerevisiae*)	Sigma-Aldrich, Steinheim, Germany

2.1.2.8 Standard Solutions and Buffers for Cell Biological and Biochemical Methods

Solution	Supplier
4 % Roti®-Histofix (acid free (pH 7), phosphate-buffered formaldehyde solution 4 %)	Carl Roth, Karlsruhe, Germany
4x Laemmli Sample Buffer	Bio-Rad Laboratories GmbH, München, Germany
4x LDS Sample Buffer	Invitrogen, Darmstadt, Germany
10x Tris/glycine/SDS Running Buffer	Bio-Rad Laboratories GmbH, München, Germany
10x NuPAGE Sample Reducing Agent	Invitrogen, Darmstadt, Germany
10x PBS	Gibco, Paisley, United Kingdom
MOPS Running Buffer (20x)	Invitrogen, Darmstadt, Germany
Ponceau S Solution	Sigma-Aldrich, Steinheim, Germany
RIPA Buffer	Thermo Scientific, Rockford, IL, USA
Roti®-ImmunoBlock (10x)	Carl Roth, Karlsruhe, Germany
Trypan Blue stain, 0.4%	Invitrogen, Darmstadt, Germany Logos Biosystems, Anyang, Korea

2.1.2.9 Assay Buffers and Buffers for Cell Biological and Biochemical Methods

Buffer and Solution	Formulation and Concentration	Supplier for Chemicals
GSH assay buffer	100 mM Na_2PO_4 1 mM EDTA pH 7.5	Sigma-Aldrich, Steinheim, Germany
Immunoblotting (IB) blocking buffer	3 % (w/v) milk powder in PBS-T	Carl Roth, Karlsruhe, Germany Gibco, Paisley, United Kingdom

		Sigma-Aldrich, Steinheim, Germany
IB washing buffer (PBS-T)	1x PBS 0.05 % (v/v) Tween 20	Gibco, Paisley, United Kingdom Sigma-Aldrich, Steinheim, Germany
Immunocytochemistry (ICC) blocking buffer	1x ROTI-Immunoblock in PBS	Carl Roth, Karlsruhe, Germany

2.1.2.10 Antibodies and Dies for Cell Biological and Biochemical Methods

Table 4 lists the primary and secondary antibodies used for immunoblotting, immunocytochemistry analysis as well as the dies applied in cell viability experiments with the BD Pathway and for analysis of the mitochondrial morphology of the HT22 cell lines. The applied concentration of a dye and the dilution of an antibody are mentioned.

Table 4: Antibodies and dies used for immunoblotting, immunocytochemistry analysis, cell viability assays and analysis of mitochondrial morphology.
The table includes a list of primary and secondary antibodies including the dilution used for immunoblotting (IB) and immunocytochemistry (ICC) analysis. The concentration of dyes applied in experiment is specified.

Antibody or Dye	Antigen	Dilution/ Concentration	Supplier
Primary Antibody			
anti-Actin, clone 4, monoclonal, mouse	purified chicken actin, epitope recognizes a N-terminal part near amino acids 50 to 70	IB: 1:4,000	Merck Millipore, Darmstadt, Germany
anti- Bcl-$x_{S/L}$ (S-18), polyclonal, rabbit	peptide corresponding to N-terminus of human Bcl-$x_{S/L}$	IB: 1:100 to 1:200	Santa Cruz Biotechnology, Heidelberg, Germany
anti-Bcl-x_L (54H6), monoclonal, rabbit	synthetic peptide surrounding Asp61 of human Bcl-x_L	ICC: 1:200	Cell Signaling, Frankfurt, Germany
anti-G6PD (D5D2), monoclonal, rabbit	synthetic peptide corresponding to C-terminus of human G6PD	IB: 1:1,000	Cell Signaling, Frankfurt, Germany
anti-GDAP1	GDAP1 recombinant epitope signature tag (PrEST)	IB: 1:500 ICC: 1:100	Sigma-Aldrich, Steinheim, Germany
Secondary Antibody			
anti-mouse IgG (H+L) (DyLight 680 conjugate), goat	-	IB: 1:15,000	Cell Signaling, Frankfurt, Germany

anti-rabbit IgG (H+L) (DyLight 800 conjugate), goat	-	IB: 1:15,000	Cell Signaling, Frankfurt, Germany
IRDye 800 goat anti-mouse IgG (H+L)	-	IB: 1:30,000	Licor, Königstein, Germany
IRDye 680 goat anti-rabbit IgG (H+L)	-	IB: 1:30,000	Licor, Königstein, Germany
anti-rabbit IgG (H+L) FITC conjugate, goat	-	ICC: 1:500	Merck Millipore, Darmstadt, Germany
Dye			
4',6-diamidino-2-phenylindole, dilactate (DAPI)	-	300 nM	Molecular Probes, Eugene, OR, USA
Hoechst 33342	-	0.5 µg/ml	Sigma-Aldrich, Steinheim, Germany
MitoTracker Red CMXRos	-	200 nM	Molecular Probes, Eugene, OR, USA
SYTOX Orange nucleic acid stain (5 mM solution)	-	0.5 µM	Molecular Probes, Eugene, OR, USA

2.1.2.11 Other Materials for Cell Biological and Biochemical Methods

Material	Supplier
8 – 16 % Precise protein gels, 10 wells	Thermo Scientific, Rockford, IL, USA
4 – 15 % Mini-PROTEAN® TGX Stain-Free™ gels, 10 wells	Bio-Rad Laboratories GmbH, München, Germany
Dako Fluorescence Mounting Medium	Dako, Glostrup, Denmark
iBlot Transfer Stack, Regular (Nitrocellulose)	Invitrogen, Darmstadt, Germany
Immu-Mount	Thermo Scientific, Rockford, IL, USA
MagicMark™ XP Western Protein Standard	Invitrogen, Darmstadt, Germany
one cOmplete, Mini Protease Inhibitor Cocktail tablets	Roche Diagnostics, Mannheim, Germany
Trans-Blot® Turbo™ Mini/Midi PVDF Transfer Packs	Bio-Rad Laboratories GmbH, München, Germany

2.1.3 Solutions and Medium for High-Resolution Respirometry

Medium and Solution	Formulation and Concentration	Supplier for Chemicals
Mitochondrial respiration medium		
MiR05	0.5 mM EGTA 3 mM $MgCl_2$ * 6 H_2O 60 mM Lactobionic acid 20 mM Taurine 10 mM KH_2PO_4 20 mM HEPES 110 mM D-Sucrose 1 g/l BSA, essentially fatty acid free pH 7.1	Sigma-Aldrich, Steinheim, Germany PAA, Pasching, Austria
Substrates		
Malate	0.8 M L-Malic acid in H_2O pH 7.0	Sigma-Aldrich, Steinheim, Germany
Glutamate	2 M L-Glutamic acid, monosodium salt hydrate in H_2O, pH 7.0	Sigma-Aldrich, Steinheim, Germany
Succinate	1 M Succinate disodium salt, hexahydrate in H_2O, pH 7.0	Sigma-Aldrich, Steinheim, Germany
Cytochrome c	4 mM Cytochrome c (from equine heart) in H_2O	Sigma-Aldrich, Steinheim, Germany
ADP+Mg^{2+}	0.5 M Adenosine 5'diphosphate potassium salt, 0.3 mM $MgCl_2$ in H_2O, pH 7.0	Sigma-Aldrich, Steinheim, Germany
Uncoupler		
FCCP	1 mM Carbonyl cyanide 4-(trifluoromethoxy)phenylhydrazone in ethanol absolute	Sigma-Aldrich, Steinheim, Germany
Inhibitors		
Rotenone	1 mM Rotenone in ethanol absolute	Sigma-Aldrich, Steinheim, Germany
Antimycin A	5 mM Antimycin A (from *Streptomyces sp.*) in ethanol absolute	Sigma-Aldrich, Steinheim, Germany
Oligomycin	4 mg/ml Oligomycin (from *Streptomyces diastatochromogenes*; mixture of oligomycins A, B, and C) in ethanol absolute	Sigma-Aldrich, Steinheim, Germany
Cell Permeabilization		
Digitonin	10 mg/ml Digitonin in DMSO	Sigma-Aldrich, Steinheim, Germany

2.1.4 Equipment

Instrument	Supplier
Analytical balance 770	Kern & Sohn GmbH, Balingen-Frommern, Germany
Analytical balance	Sartorius, Göttingen, Germany
BD Pathway 855	Becton Dickinson, Heidelberg, Germany
Biofuge Stratos	Heraeus Instruments, Osterode, Germany
CaptairBio PCR workstation	Erlab, Cologne, Germany
Cellometer™ Auto T4	Nexcelom Bioscience, Lawrence, MA, USA
Centrifuge 5415R/ 5415C	Eppendorf, Hamburg, Germany
Centrifuge 5804R/ 5810R	Eppendorf, Hamburg, Germany
GDS-Gel Imaging System	Intas, Gottingen, Germany
GENios Pro microplate reader	Tecan, Männedorf, Switzerland
GloMax® Multi+ Detection System	Promega, Madison, WI, USA
BX51 Fluorescence Microscope	Olympus, Hamburg, Germany
Eating Table	Medax, Neumünster, Germany
HERAcell 240i incubator	Thermo Scientific, Rockford, IL, USA
Heraeus™ Fresco™ 17 Microcentrifuge	Thermo Scientific, Rockford, IL, USA
HERAsafe Class II Biological Safety Cabinet	Thermo Scientific, Rockford, IL, USA
iBlot® Dry Blotting System	Invitrogen, Darmstadt, Germany
Incubator 1000	Heidolph, Schwabach, Germany
Incubator Forma® 310	Thermo Scientific, Rockford, IL, USA
Incubator Innova 4230	New Brunswick Scientific/ Eppendorf, Hamburg, Germany
Infinite M200 Pro microplate reader	Tecan, Männedorf, Switzerland
JuLI™ BR Live Cell Analyzer	NanoEnTek Inc., Seoul, Korea
Laboratory balance	Faust, Schaffhausen, Switzerland
Luna™ Automated Cell Counter	Logos Biosystems, Anyang, Korea
Microscope Wilovert/ Wilovert S	Helmut Hund GmbH, Wetzlar, Germany
Micro Star 17R Microcentrifuge	VWR Thermo Electron LED GmbH, Osterode am Harz, Germany
Mini-PROTEAN® Tetra Cell electrophoresis system	Bio-Rad Laboratories GmbH, München, Germany
MoFlo™ XDP	Beckman-Coulter, Krefeld, Germany
NanoDrop 2000 Spectrophotometer	Thermo Scientific, Rockford, IL, USA
Neubauer-improved Counting Chamber	Marienfeld, Lauda-Königshofen, Germany
Odyssey Infrared Imaging System	Licor, Königstein, Germany
Odyssey Sa Infrared Imaging System	Licor, Königstein, Germany
Orbital Shaker	Heidolph,
Oxygraph-2k	Oroboros Instruments, Innsbruck, Austria
PowerPac™ Basic Power Supply PowerPac 300 Power Supply	Bio-Rad Laboratories GmbH, München, Germany
P25 Power Pack	Biometra, Göttingen, Germany
Platform Shaker	Heidolph, Schwabach, Germany
Radiometer ABL800 basic	Radiometer GmbH, Willich, Germany
Sub-Cell GT System	Bio-Rad Laboratories GmbH, München,

	Germany
T1 Thermocycler	Biometra, Gottingen, Germany
TC10™ Automated Cell Counter	Bio-Rad Laboratories GmbH, München, Germany
TCS SP5 confocal microscope	Leica Microsystems, Wetzlar, Germany
TGradient Thermocycler	Biometra, Gottingen, Germany
Thermomixer Compact	Eppendorf, Hamburg, Germany
Trans-Blot® Turbo™ Transfer System	Bio-Rad Laboratories GmbH, München, Germany
Water bath	Memmert, Schwallbach, Germany
Water bath 006T with heating thermostats E100	Lauda-Brinkmann, Delran, NJ, USA
XCell SureLock™ Mini-Cell Electrophoresis System	Invitrogen, Darmstadt, Germany

2.1.5 Software

Data generated with the BD Pathway 855 system were analysed with the Attovision software provided by BD and processed with Microsoft Excel. Western blots were processed with the software Image Studio Lite Ver 3.1 (Licor) and analysed with ImageJ (http://imagej.nih.gov/ij/). Sequence data were viewed with FinchTV Version 1.4 (Geospiza) and a multiple sequence alignment was performed online using MultAlign (http://multalin.toulouse.inra.fr/multalin/; Corpet, 1988). Nucleotide sequences were translated in a protein sequence using the Expasy translation tool (http://www.web.expasy.org/translate/). For the pairwise alignment of nucleotide and protein sequences the EMBOSS Needle tool (http://www.ebi.ac.uk/Tools/psa/emboss_needle/) was used which is based on the Needleman-Wunsch alignment algorithm to find an optimum alignment. For data acquisition and analysis of high-resolution respirometry experiments the DatLab software Version 5.1.0.20 (Oroboros Instruments) was used. Confocal pictures were taken with the Leica Application Suite (LAS) Advanced Fluorescence (AF) 2.4.1 software and processed using Adobe Photoshop. All collected data were illustrated and analysed with GraphPad Prism5.

2.2 Methods

2.2.1 Molecular Biological Methods

2.2.1.1 Plasmid DNA Purification

Plasmid DNA was purified from bacterial cultures grown in LB (Luria-Bertani) medium containing the appropriate selective antibiotic (100 µg/ml ampicillin or 50 µg/ml kanamycin) and incubated at 37 °C and 260 rpm overnight. Bacterial cultures were inoculated with a single cell colony picked from an agar plate or material from a glycerol stock.

For isolation of small scale endotoxin-free plasmid DNA, the Zyppy™ Plasmid Miniprep Kit from Zymo Research was used according to the manufacture's instruction. In brief, plasmid DNA was isolated from 1.2 ml bacterial overnight culture. Cells were lysed by an alkaline lysis, the lysate was neutralized and cell debris was removed by centrifugation before the supernatant was loaded onto a spin column. Plasmid DNA bound to the spin column were washed twice and eluted with 20 µl of nuclease-free water.

For large scale plasmid DNA purification, the NucleoBond® Xtra Midi/Maxi Kit from Machery and Nagel was used. Plasmid DNA was isolated from a 150 ml bacterial overnight culture according to the manufacture's protocol. A bacterial culture was harvested by centrifugation, resuspended and lysed by alkaline lysis based on the method of Birnboim and Doly (Birnboim and Doly, 1979). The lysate was cleared through an equilibrated column filter and simultaneously loaded onto an equilibrated silica-based anion-exchanger resin column by gravity flow. After two following washing steps, the plasmid DNA was eluted with an elution buffer under high-salt conditions. Plasmid DNA was precipitated with isopropanol, centrifuged and washed with 70 % (v/v) ethanol. After an additional centrifugation, the DNA pellet was dried at room temperature before it was reconstituted with an appropriated volume of nuclease-free water.

The DNA concentration was measured using the NanoDrop 2000 Spectrophotometer (Thermo Scientific). The accepted ratio of absorbance at 260 to 280 nm was around 1.80 for pure plasmid DNA.

2.2.1.2 Restriction Enzyme Digest

Restriction enzyme digests were performed to analyse plasmid DNA or to prepare DNA for cloning. Plasmid DNA was restricted with restriction endonucleases according to the manufacture's instruction. In general, a restriction digest was performed in a double digest in a total volume of 25 µl or 50 µl. 3 to 5 µl plasmid DNA purified in a small scale were digested in a 25 µl reaction containing 5 units of each enzyme, 2.5 µl of the appropriate 10x enzyme buffer and if necessary BSA. 1 to 2 µg of plasmid DNA from large scale isolations were

digested in a 50 µl reaction containing 10 units of each enzyme, 5 µl of the appropriate 10x enzyme buffer and if required BSA. Restriction enzyme digests were incubated at 37 °C for 1-2 h.

2.2.1.3 Agarose Gel Electrophoresis

Plasmid DNA after restriction enzyme digest and polymerase chain reaction (PCR) products were analysed in an agarose gel electrophoresis. DNA mixed with 1x BlueJuice™ Gel Loading Buffer (10x) was separated alongside the 1 kb plus DNA ladder in an 1 % (w/v) agarose gel with 0.6 µg/ml ethidium bromide or peqGreen at 120 constant voltages in 1x TBE or 1x TAE buffer in a horizontal chamber.

2.2.1.4 Gel Extraction of DNA Fragments

After separation of DNA in an agarose gel electrophoresis, fragments of the correct size were excised from the gel using a scalpel and the DNA was purified from the gel with the Zymoclean™ Gel DNA Recovery Kit from Zymo Research according to the manufacture's protocol. DNA was eluted with 10 µl nuclease-free water and used in ligation reactions or send for sequencing.

2.2.1.5 Ligation of DNA Fragments

For cloning of restriction fragments, DNA fragments were ligated using T4 DNA Ligase. In general, the reaction mix contained plasmid and insert in an appropriate ratio, for example in a ration of 1:5, 1 µl T4 DNA Ligase, 1/10 volume of 10x T4 DNA Ligase Reaction Buffer in a total volume of 10 µl. The reaction mix was either incubated at room temperature for 1 h or at 4 °C overnight.

2.2.1.6 Preparation of Chemically Competent Bacteria

Chemically competent *Escherichia coli* of the bacterial strains DH5α and *ccd*B Survival™ 2 T1R were prepared for cloning after the adapted protocol of Cohen and colleagues (Cohen et al., 1972). A 2 ml starter culture of the respective bacterial strain was grown in antibiotic-free S.O.C. medium at 37 °C and 260 rpm overnight. The following day, 150 ml antibiotic-free LB-medium was inoculated 1:1,000 with the starter culture. The culture was grown up to an OD_{600} of 0.5. The cells were pelleted by centrifugation at 5,000 g and 4 °C for 10 min. The cell pellet was resuspended in 10 ml of ice-cold 100 mM $MgCl_2$ and incubated on ice for 15 min. After a second centrifugation, the cell pellet was resuspended in ice-cold 100 mM

$CaCl_2$ containing 15 % (v/v) glycerol. 100 µl aliquots were prepared, shock frozen in liquid nitrogen and stored at -80 °C.

2.2.1.7 Transformation of Chemically Competent *Escherichia coli*

To transform chemically competent bacteria with plasmid DNA, bacterial cells were thawed on ice. Plasmid DNA (0.5 to 1 µl) or 5 to 10 µl ligation mix were added to the cells. After a 30 min-incubation on ice, bacterial cells were heat-shocked for 60 sec at 42 °C and placed on ice for 2 min. 250 µl S.O.C. medium was added and the cells were incubated at 37 °C and 260 rpm for 1 h. For selection, bacteria were finally spread on a LB-agar plate containing 100 µg/ml ampicillin or 50 µg/ml kanamycin and incubated at 37 °C overnight.

2.2.1.8 Cloning of *Gdap1* cDNAs into the pENTR3C Vector

The full-length mouse complementary DNA (cDNA) of wild type *Gdap1* and *Gdap1* cDNA with the point mutation R310Q had been subcloned from pcDNA:GDAP1 or pcDNA:R310Q (kind gift of Axel Niemann, Niemann et al., 2005) into the pBluescript II SK(+) cloning vector using the restriction endonucleases BamHI and XbaI. With help of BamHI and NotI, the cDNAs were further cloned into the pENTR3C vector. This subcloning had been carried out by the former lab member Rebecca Noack.
The pENTR3C:S34A vector was prepared by the isolation of a small sequence encoding the GDAP1 point mutation S34A from pcDNA:S34A (kind gift of Axel Niemann) with the restriction enzymes BamHI and AgeI following ligation of this fragment into the BamHI/AgeI-linearized pENTR3C:GDAP1 vector. The cloning was verified by restriction enzyme digest and sequencing.

2.2.1.9 Gateway Cloning

For the cloning of various plasmid DNAs, the Gateway technology was used which is based on the properties of the bacteriophage lambda site-specific recombination (Landy, 1989). The gateway technique allows the transfer of a DNA sequence into a vector without the use of DNA restriction endonucleases and ligase, while the orientation and reading frame is maintained (Hartley et al., 2000). The DNA transfer occurs by recombination between specific attachments (*att*) sites of an entry clone and the destination vector mediated by enzymes in the clonase enzyme mix. For the generation of the entry clone, the gene of interest had been cloned in a conventional way into the pENTR vector pENTR3C, where it is flanked by the necessary *att*L sites for recombination. The destination vector contains all necessary features for protein expression and a cassette flanked by *att*R sites containing the *ccd*B gene for negative selection. During a recombination, the *ccd*B gene is replaced by the

gene of interest in the destination vector. Because of the lethal effect of the CcdB protein, transformed CcdB-sensitive bacteria, which took up an unchanged destination vector still containing the *ccd*B cassette, fail to grow and die.

To perform a recombination between the entry clone and the destination vector pPB-CAG-HA-IRES-Venus dest, a LR Clonase recombination reaction contained 50 to 150 ng of the entry clone, 1 µl of the destination vector at 150 µg/ml and TE Buffer (pH 8.0) up to a total volume of 8 µl and 1 µl LR Clonase™ II enzyme mix. The reaction mix was mixed by vortexing. After one hour incubation at 25 °C, 1 µl of the 2 µg/ml Proteinase K solution was added and incubated at 37 °C for 10 min to terminate the reaction. 5 µl reaction mixed were subsequently transformed in the CcdB-sensitive and chemically competent DH5α *E. coli*. Expression clones were selected over the ampicillin resistance and analysed by restriction enzyme digest following an agarose gel electrophoresis.

2.2.1.10 Cryopreservation of Bacterial Strains

For long-time storage of plasmid DNA and respective bacterial strains, bacterial glycerol stocks were prepared. 800 µl of a bacterial overnight culture was mixed with 200 µl of a sterile 80 % (v/v) glycerol solution and stored in a cryovial at -80 °C.

2.2.1.11 Isolation of RNA from Eukaryotic Cell Lines

For total RNA purification from eukaryotic cells, the ZR RNA MiniPrep Kit from Zymo Research was used. In brief, cell samples were pelleted by gentle centrifugation and the cell pellet was resuspended in 400 µl RNA Lysis Buffer before the RNA was isolated according to the manufacture's instruction. A DNAse treatment was performed to remove any DNA contamination of the RNA sample. For this reason, RNA loaded onto a column was treated in an in-column DNAse digestion with DNAse I for 15 min at room temperature. RNA was finally eluted with 30 µl of nuclease-free water and stored at -80 °C or directly converted to single-stranded cDNA for downstream applications.

2.2.1.12 Reverse Transcription

For the conversion of RNA to single-stranded cDNA a reverse transcription was performed using the High Capacity cDNA Reverse Transcription Kit from Applied Biosystems. According to the manufacture's instruction, the reaction mix contained 2 µl 10X RT Buffer, 1.6 µl 25X dNTP Mix (100 mM), 4 µl 10X RT Random Primers, 2 µl MultiScribe™ Reverse Transcriptase, 8.4 µl nuclease-free water and 20 µl RNA sample. The reaction mix with a total volume of 40 µl was incubated in a thermal cycler. The reverse transcription run

included a step at 25 °C for 10 min, a step at 37 °C for 120 min and one step at 85 °C for 5 min.

2.2.1.13 Polymerase Chain Reaction

A polymerase chain reaction (PCR) was performed for the amplification of a specific region of DNA strand using the ready-to-use Platinum PCR SuperMix from Invitrogen, which contains a necessary mixture of recombinant *Taq* Polymerase, dNTPs and $MgCl_2$ for amplification. In general, a reaction mix consisted of 2 µl template DNA, 1 µl of the respective forward as well as reverse primer (10 pmol/µl; final concentration of 200 nM per primer), 45 µl Platinum PCR SuperMix and nuclease-free water up to a final volume of 50 µl. For a 25 µl reaction mix, half the amount of template DNA, forward and reverse primer and Platinum PCR SuperMix was used. The reaction mix was placed in a thermal cycler and the DNA was amplified in a five step program:

1. Initial denaturation and activation	94 °C for 2 min,
2. Denaturation	94 °C for 30 sec,
3. Primer annealing	50 to 60 °C for 30 sec,
4. Elongation	72 °C for 1 min per kb,
5. A final elongation	72 °C for 10 min.

Steps 2 to 4 were repeated 34 times. The PCR products were analysed in a following agarose gel electrophoresis.

2.2.1.14 Sequencing of PCR Products and Plasmid DNA

For sequencing of PCR products and plasmid DNA was send to GATC. The DNA was prepared according to the company's guidelines.

2.2.2 Methods in Cell Biology

2.2.2.1 Culturing of Eukaryotic Cell Lines

All eukaryotic cell lines were cultured in their appropriate growth medium in 10 cm tissue culture plates or T-75 tissue culture flasks in a humidified incubator at 5 % CO_2 and 95 % air at 37 °C. When cells were 80 to 95 % confluent, cells were passaged into new tissue culture vessels under aseptic conditions in a laminar-flow hood every 3 to 4 days. For sub-culturing, the medium was removed, cells were washed with D-PBS and detached with 1 to 1.5 ml of 0.05 % Trypsin-EDTA. After a 3 to 5 min-incubation at 37 °C, the reaction was stopped by

adding fresh growth medium. Cells were resuspended and sub-cultured in an appropriate dilution into new cell culture vessels. If necessary, trypsin was removed by centrifugation (1,200 rpm, 3 min). Cells in 10 cm plates were grown in a total of 10 ml medium, while 15 ml medium were used for the growth in T-75 flasks.

For cell counting an improved Neubauer Counting Chamber, the Cellometer™ Auto T4 (Nexcelom Bioscience), the TC10™ (Bio-Rad) or the Luna™ Automated Cell Counter (Logos Biosystems) was used. In order to count only viable cells, a Trypan blue staining solution was applied.

2.2.2.2 Culturing of HT22 cell lines

Mouse hippocampal HT22 cell lines were cultured in DMEM high glucose supplemented with 5 % (v/v) FBS, 100 U/ml penicillin and 100 µg/ml streptomycin. The parental HT22 cell line is a well accepted model for studying glutamate-induced oxidative stress (Albrecht et al., 2010). Through a repetitive exposure of this cell line to glutamate, a glutamate-resistant cell line had been generated (Lewerenz et al., 2006). This glutamate-resistant cell line was continuously expanded under a 10 mM glutamate. In the following, the glutamate-sensitive cells is designated HT22S, while the glutamate-resistant cells are named HT22R. The HT22 cell lines were passaged in a 1:5 or 1:10 ratio.

2.2.2.3 Culturing of Mouse Embryonic Fibroblasts (MEFs)

The mouse embryonic fibroblast (MEF) cell lines wild type (WT), Bcl-x_L-knockout (Bcl-x_L-KO) and ActA were grown in DMEM high glucose supplemented with 10 % (v/v) FBS, 100 U/ml penicillin and 100 µg/ml streptomycin. The Bcl-x_L-KO cell line showing no Bcl-x_L expression is derived from an embryo of an 11 day pregnant mouse heterozygous for the *bcl-x* gene (bcl-$x^{+/-}$) and had been immortalized by SV40 T antigen expression (Eno et al., 2012). The ActA MEFs stably express mitochondrially targeted Bcl-x_L (Eno et al., 2012) and were grown in medium additionally supplemented with 1.5 µg/ml blasticidin. This cell line had been generated by the stable transfection of the Bcl-x_L-KO cell line with the pEF6 plasmid encoding a mitochondrially targeted Bcl-x_L by replacement of the C-terminal transmembrane region of *bcl-x_L* gene with the membrane-targeting sequence of the listerial actin assembly-inducing protein ActA (Eno et al., 2012). The MEF cells were sub-cultured in a 1:20 to 1:40 ratio.

2.2.2.4 Culturing of SH-SY5Y Cell Lines

The human neuroblastoma cell line SH-SY5Y was cultured in DMEM-F12 supplemented with 10 % (v/v) FBS, 100 U/ml penicillin, 100 µg/ml streptomycin, 2 mM L-Glutamine and 1x MEM non-essential amino acids. SH-SY5Y cells are a clonal subline of the neuroblastoma cell line SK-N-SH that derived from a metastatic bone tumour of a 4-year-old girl. The parental cell line SK-N-SH was sub-cloned three times to receive the subclone SH-SY5Y (Biedler et al., 1978).

The stably over-expressing SH-SY5Y cell lines EV, GDAP1, R310Q and S34A were cultured in the general growth medium of SH-SY5Y cells. These cell lines were stably transfected with the empty vector pPB-CAG-HA-IRES-Venus or this vector encoding mouse wild type GDAP1, GDAP1 with the mutation R310Q and S34A, respectively.

The control SH-SY5Y cell line pLKO-NT and *GDAP1*-silenced *GDAP1* KD (G4) were cultured in the general growth medium supplemented with 2 µg/ml puromycin. These cell lines had been stably transfected with pLKO.1 containing a shRNA of GDAP1 (G4) or a non-targeted shRNA (pLKO-NT; Pla-Martin et al., 2013). The SH-SY5Y cell lines were sub-cultured in a 1:3 to 1:6 ratio.

2.2.2.5 Transfection of Eukaryotic Cells

For transfection of HT22 cells and MEFs the Attractene Transfection Reagent from Qiagen was used according to the manufacture's instruction. In brief, 200,000 cells per well were seeded into 6-well plates and left to adhere overnight. Next day, the transfection mix was prepared containing 4 µg plasmid DNA and 4.5 µl Attractene Transfection Reagent in 100 µl OptiMEM medium. The transfection mix was mixed and incubated for 10 to 15 min at room temperature for complex formation. Meanwhile, the culture medium was removed and fresh growth medium was added to the cells. The transfection mix was added drop wise to the plate and distributed by rocking the plate. The cells were incubated under normal growth conditions.

Neuroblastoma SH-SY5Y cells were transfected using the TransFast™ Transfection Reagent from Promega. The transfection was performed according to the manufacture's recommendations. In total, 250,000 to 300,000 cells per well were seeded into 6-well plates one day before transfection. Optimal transfection efficiency was achieved using a 1:1 charge ratio of TransFast™ Transfection Reagent to DNA. Therefore, 2.5 µg plasmid DNA and 7.5 µl TransFast Transfection reagent were added to 1 ml DMEM-F12 without supplements and mixed by vortexing. After 10 to 15 min incubation at room temperature, the growth medium of the cells was removed and 1 ml transfection mix was added. The cells were incubated under normal growth conditions for 1 h before 2 ml of complete growth medium was added.

24 h to 48 h after transfection the cells were used and analysed in following experiments.

2.2.2.6 Generation of Stably Transfected SH-SY5Y Cell Lines

Stably transfected SH-SY5Y cell lines were generated with help of the *piggy*Bac transposon vector system (System Biosciences) and following fluorescence-activated cell sorting. Cells were co-transfected with the bicistronic *piggy*Bac (PB) transposon vector (pPB-CAG-HA-IRES-Venus dest, pPB-CAG-HA-GDAP1-IRES-Venus, pPB-CAG-HA-R310Q-IRES-Venus or pPB-CAG-HA-S34A-IRES-Venus) and the helper vector pCMV-HA hyPBase encoding the hyperactive *piggy*Bac Transposase (PBase; Yusa et al., 2011) necessary for transposition. For co-transfection the TransFast Transfection Reagent was used and cells were transfected as described in the previous paragraph. A 1:2.5 ratio of transposase to transposon vector was applied. According to this, cells in 6-well plates were transfected with 1 µg of pCMV-HA hyPBase and 2.5 µg of transposon vector. The PB transposon vector includes transposon-specific inverted terminal repeat sequences (ITRs) located on both ends of a mammalian expression cassette. These ITRs get recognized by the PBase, which catalyses the transfer of the PB transposon from the vector into the host genome at TTAA sites (Bauser et al., 1999; Fraser et al., 1996). Here, the mammalian expression cassette included a mammalian promoter, the gene of interest followed by an internal ribosomal entry site (IRES) and a sequence of the fluorescence protein Venus. 48 h after transfection, transfected cells were identified by an IRES-mediated co-expression of the fluorescence marker Venus along the expression of the gene of interested and hence, sorted and collected by fluorescence-activated cell sorting with a MoFlo^{TM} XDP (Beckman Coulter) equipped with a 488 nm laser. For cell sorting, cells were detached using trypsin and the cell suspension was filtered through a 40 µM cell strainer (BD Falcon). Shortly before sorting, cells were pelleted by centrifugation (1,000 rpm, 3min) and resuspended in an appropriate volume of sorting buffer containing 1 % (v/v) FBS in PBS. Venus-positive cells were collected in complete growth medium. The cells were centrifuged, resuspended in an appropriate volume of growth medium and transferred into a suitable culture vessel for cultivation. The sorting step was repeated until about 82 up to 98 % of the cells were Venus-positive.

2.2.2.7 Cryopreservation of Eukaryotic Cell Lines

For cryopreservation of eukaryotic cell lines, cells were grown to 80 -90 % confluence, detached with trypsin and collected by centrifugation (1,000 rpm, 3 – 5 min). The cell pellet was resuspended in an appropriate volume of freezing medium containing 90 % (v/v) FBS and 10 % (v/v) of the cryoprotectant dimethyl sulfoxide (DMSO) and divided into 1 ml aliquots in cryovials. The cryovials were placed into the Nalgene Mr. Frosty Freezing container and

frozen at a cooling rate of 1 °C per min at -80 °C. The next day, the cryovials were moved to the vapour face of liquid nitrogen.
For thawing frozen cells, the cryovial was placed into a 37 °C water bath. The thawed cell suspension was quickly transferred to a 15 ml tube with 9 ml pre-warmed growth medium. After centrifugation, the cell pellet was resuspended in complete growth medium, transferred into tissue culture vessel and placed into the incubator.

2.2.2.8 Cell Viability Assay

For analysis of the cell viability after incubation with cell death inducing agent, HT22 cells were seeded at a density of 5,000 cells per well in 100 µl growth medium into 96-well plates. Next day, glutamate was added at indicated concentrations, whereas HT22R cells were additionally maintained under their regular 10 mM glutamate exposure. Cell viability was quantified 22 to 24 h later using the CellTiter-Blue® (CTB) reagent from Promega. According to the manufacture's guidelines, 20 µl CTB reagent was added to each well and incubated for 3 h under normal growth conditions. During this incubation time, metabolic active cells convert resazurin in the CTB reagent to the fluorescence-detectable resorufin. The resorufin fluorescent signal was recorded at 562 nm excitation with an emission at 590 nm using the GENios Pro or the Infinite M200 Pro microplate reader (Tecan).
For cell viability assays with MEFs, 4,000 cells per well in 100 µl of DMEM high glucose without phenol red supplemented with 10 % (v/v) FBS, 100 U/ml penicillin, and 100 µg/ml streptomycin were seeded into 96-well plate. The following day, the cell death inducing agent glutamate was added at indicated concentrations. 24 h later, cells were stained with 0.5 µg/ml Hoechst 33342 and 0.5 µM SYTOX Orange nucleic acid stains in 30 min at 37 °C and analysed using the BD Pathway 855. While Hoechst stains the nuclei of all cells, SYTOX orange stains only dead cells because it cannot cross the plasma membrane of viable cells, but enters and stains dead cells with damaged membranes. With help of the Attovision and BD Image Explorer Software the percentage of dead cells per well was determined. Thus, Hoechst staining was used to designate region of interests (ROIs) and the percentage of dead cells was calculated as percentage of double-positive cells.
Alternatively, to access the susceptibility of MEFs to oligomycin and antimycin A, MEF cells were seeded at the same density of 4,000 cells per well into 96-well plates. The next day, the cell death inducing agents were added at indicated concentrations. In order to enhance the sensitivity against the ATP synthase-inhibitor oligomycin (Lardy et al., 1958) and complex III-inhibitor antimycin A (Herrero and Barja, 1997), the medium was changed to DMEM without glucose supplemented with 25 mM galactose, 10 % FBS, 100 U/ml penicillin, 100 µg/ml streptomycin and 1 mM sodium pyruvate as well as the reagents were added in this medium. Cell viability was determined using the CTB reagent as described above 24 h later.

2.2.2.9 Cell Proliferation Assay

The cell proliferation of MEFs was examined with help of the CTB reagent. At the beginning, the CTB reagent necessary for the entire experiment was diluted 1:20 with complete growth medium. In total 6,250 cells per well were plated into a 24-well plate and the cells were left to adhere within 3 to 4 h before the experiment was started. Then the general growth medium was replaced by medium supplemented with CTB reagent. The plate was incubated for 3 h before 100 µl samples (three of each well) were transferred to a 96-well plate and the fluorescent signal was recorded using the Infinite M200 Pro microplate reader (Tecan). The rest of the CTB-medium mix was removed, fresh growth medium was added and the cells were left to proliferate under standard growth conditions. The cell proliferation was determined on day 0, 2 and 3.

In order to calculate the cell number on each day, a standard curve of each cell line was prepared. Hence, different cell numbers (100,000 cells, 50,000 cells, 25,000 cells, 12,500 cells and 6,250 cells) in duplicates were plated into a 24-well plate and left to adhere within 3 to 4 h before the corresponding fluorescent signal was determined using the CTB reagent as described before.

2.2.2.10 Enzymatic Measurement of Total Cellular Glutathione Content

The total cellular glutathione (GSH and GSSG) content was analysed in an enzymatic recycling assay. In total, 200,000 cells per well were seeded into 6-well plates and were treated with a GSH decreasing agent in the indicated concentration and for the mentioned time period the next day. After washing cells twice with ice-cold PBS, cells were resuspended in 200 µl PBS. The cell suspension was transferred into 100 µl of 10 % (w/v) sulfosalicylic acid to remove proteins from the sample. The sample was vortexed and incubated on ice for 10 min. After a centrifugation (10 min, 16,000 g at 4 °C), the supernatant was transferred into 24 µl of 50 % (v/v) triethanolamine in H_2O for neutralization. For detection of total cellular glutathione, samples were diluted in GSH Assay Buffer supplemented with 0.8 mM NADPH, 0.6 mM 5,5'-dithiobis-(2-nitrobenzoic-acid) (DTNB) and 1 U/ml glutathione reductase. During the assay, DTNB and GSH react which lead to oxidation of GSH and generation of the yellow and photometric-detectable 5′-thio-2-nitrobenzoic acid (TNB) and a mixed disulfide GS-TNB (Giustarini et al., 2013; Rahman et al., 2006). GS-TNB can be reduced to GSH under the release of one molecule TNB as well as glutathione disulfide (GSSG) can be recycled to GSH by glutathione reductase under NADPH consumption (Giustarini et al., 2013; Rahman et al., 2006). The formation of TNB was measured kinetically at 390 nm using the GENios Pro microplate reader (Tecan). To quantify the total glutathione content in a sample, a standard curve with known glutathione

concentration (20 µM, 10 µM, 5 µM, 2.5 µM, 1.25 µM, 0.625 µM, 0 µM) was generated and carried along.

Total cellular glutathione content was normalized to cellular protein amounts. For this reason, after the centrifugation step, pellets were solubilised in 100 µl of 0.2 N NaOH at 37°C overnight and the protein concentration was quantified using a BC Assay Protein Quantification Kit (Interchim).

2.2.2.11 Analysis of total NAD/NADH and NADP/NADPH

In order to analyse total cellular NAD^+ and NADH (NAD) as well as total cellular $NADP^+$ and NADPH (NADP), the NAD/NADH-Glo™ Assay and NADP/NADPH-Glo™ Assay from Promega were used. Both assays were performed according to the manufacture's instruction. In brief, for the NAD/NADH-Glo™ Assay cells were detached using trypsin, centrifuged and washed with D-PBS before 25,000 cells resuspended in 50 µl D-PBS were transferred to a white flat-bottom polystyrene 96-well plate (Greiner Bio-one) and an equal volume of freshly prepared NAD/NADH-Glo™ Detection Reagent containing reconstituted Luciferin Detection Reagent, Reductase, Reductase Substrate, NAD Cycling Enzyme and NAD Cycling Substrate was added. After moderate shaking of the plate to mix and lyse cells, the plate was incubated for 30 min at room temperature before the luminescence was recorded using the GloMax® Multi+ Detection System (Promega). The NAD/NADH-Glo™ Assay allows the detection of total cellular NAD based on the activity of a NAD Cycling Enzyme which converts NAD^+ to NADH, while a NAD Cycling Substrate is converted into a NAD Cycling product in the meantime. In a following reaction, a reductase under NADH-consumption enzymatically turns a proluciferin reductase substrate to luciferin, which can be then measured by light produced through the activity of an Ultra-Glo™ rLuciferase under ATP-consumption. The light signal can be detected by a luminescence reader and is proportional to the total amount of cellular NAD^+ and NADH of the biological sample.

According to this, the NADP/NADPH-Glo™ Assay was performed in the same way, but here a NADP Cycling Enzyme and a corresponding NADP Cycling Substrate was used that turned into a NADP Cycling product. Hence, the use of the NAD corresponding NADP Cycling Enzyme and the NAD corresponding NADP Cycling Substrate as well as the cycling between the cycling enzyme and reductase ensures the specificity of the assays to detect either total cellular NAD or NADP.

2.2.2.12 Measurement of Extracellular Glucose and Lactate

HT22 cells were seeded at a density of 300,000 cells, whereas MEF cells were seeded at a density of 200,000 cells per well into 6-well plates. The medium was replaced by fresh

growth medium 24 h later. After a 24 h incubation, the medium was collected, cells were removed by centrifugation (1,200 rpm, 5 min) and the glucose and lactate concentration were quantified in the central diagnostic laboratory of the University Medical Centre Mainz of the Johannes Gutenberg University or with help of the Radiometer ABL800 basic (Radiometer).

2.2.3 High-Resolution Respirometry

The high-resolution respirometer Oxygraph-2k (Oroboros Instruments) was used to measure the mitochondrial oxygen consumption of cells. Using the DatLab Software 5.1, the oxygen concentration in nmol/ml and the oxygen consumption expressed as oxygen flow per million cells in pmol/(s*10^6 cells) were recorded in 2 s intervals at a gain of 2. All experiments were carried out under instrumental background correction and after daily calibration of the polarographic oxygen sensors with the respective experimental medium. The oxygen consumption of cells was monitored under continuous stirring at 750 rpm and 37 °C in the two 2 ml-glass chambers. Substrates and inhibitors were titrated manually using Hamilton gastight syringes.

2.2.3.1 Phosphorylation-Control Protocol (PCP)

The oxygen consumption of intact cells was examined in a phosphorylation-control protocol. Cells resuspended in their growth medium at a density of 1 – 2 x 10^6 cells/ml (Table 5) were filled into the 2 ml glass chambers. The exact cell number after dilution to the appropriate cell number was quantified each time before the start of the experiment. After approximately 10 min, the chambers were closed to record routine respiration (R). The ATP synthase was inhibited by adding 2 µg/ml of oligomycin to determine leak respiration (L). For evaluation of the electron transfer system (ETS) capacity (E), the protonophore carbonyl cyanide 4-(trifluoromethoxy) phenylhydrazone (FCCP) was titrated in 0.5 µM steps until a maximum flow per million cells was reached. Respiration was inhibited by the addition of 0.5 µM rotenone (inhibitor of complex I) and 2.5 µM antimycin A (inhibitor of complex III) and the non-mitochondrial residual oxygen consumption (ROX) was measured.

2.2.3.2 Substrate-Uncoupler-Inhibitor Titration (SUIT) Protocol

For the study of respiratory control and oxidative phosphorylation (OXPHOS), a mitochondrial substrate-uncoupler-inhibitor titration (SUIT) protocol was carried out with digitonin-permeabilized cells, which allows an *in situ* analysis of mitochondria. When a SUIT protocol was performed the mitochondrial respiration medium MiR05 (Gnaiger et al., 2000) was used. Cells were detached using trypsin, centrifuged (1,000 rpm, 3 min), and washed

with D-PBS before they were resuspended in MiR05. Measurements were carried out at a density of 1 – 2 x 10^6 cells/ml (Table 5). After dilution to the appropriate cell number for the experiment, the exact cell number was quantified before the start of the experiment.

To determine the optimum concentration of digitonin (dig) sufficient to completely permeabilize plasma membranes, but not the mitochondrial membranes of each cell line, the procedure described by Pesta and Gnaiger (Pesta and Gnaiger, 2012) was followed. In brief, after air calibration of the polarographic oxygen sensor with MiR05, cells resuspended in MiR05 were filled into the glass chamber. After 10 min, the chambers were closed and endogenous routine respiration was recorded, followed by the addition of 0.5 µM rotenone, 1 mM ADP and 10 mM succinate. While the addition of ADP and succinate did not induce respiration, the following stepwise titration of digitonin in 2-3 µg/cm^3 steps resulted in gradual permeabilization of plasma membranes accompanied by a stepwise increase in respiration until a maximum induction of respiration was reached at optimum digitonin concentration. The further addition of digitonin resulted in inhibition of respiration and allowed the determination of the optimum concentration of digitonin for plasma membrane permeabilization.

In the SUIT protocol, cells resuspended in MiR05 were filled into the glass chamber and the chamber was closed to measure routine endogenous respiration. 2 mM malate (M) and 10 mM glutamate (G) were added, which allow complex I-linked respiration by feeding electrons via NADH into the respiratory system. The appropriate amount of digitonin (Table 6) was added for complete plasma membrane permeabilization and the leak state GM_N (no adenylates added, N) was recorded. To study the OXPHOS capacity state (P) GM_P, respiration was induced by adding 1 and 2 mM ADP, respectively. 10 mM of the complex II-linked substrate succinate (S) was added which induced respiration with convergent electron input of complex I and II into the Q-junction and allowed the determination of the respiratory state GMS_P. Additional 2 mM ADP was added to exclude a limitation by ADP supply. By adding 10 µM cytochrome c (c) the intactness of the outer mitochondrial membrane was tested ($GMSc_P$). Only experiments with an increase of less than 15 % were used for analysis. The ATP synthase was inhibited adding 2 µg/ml oligomycin and the leak state GMS_L was recorded. Respiration was stimulated by the titration of FCCP in 0.5 µM steps and the ETS state GMS_E was evaluated, followed by the inhibition of complex I adding 0.5 µM rotenone and the respiratory capacity on succinate alone in the ETS state $S(Rot)_E$ was determined. ROX was measured after the addition of 2.5 µM antimycin A.

Table 5: Cell density used in high-resolution respirometry.
Listed is the cell density which was used to measure the oxygen consumption of the various cell types in phosphorylation-control protocols (PCP) and substrate-uncoupler-inhibitor titration (SUIT) protocols.

Cell type	PCP	SUIT Protocol
HT22	1 x 10^6 cells/ml	1 x 10^6 cells/ml
SH-SY5Y	1.5 - 2.0 x 10^6 cells/ml	1.5 – 2.0 x 10^6 cells/ml
MEF	1.2 x 10^6 cells/ml	1.0 - 1.2 x 10^6 cells/ml

Table 6: Digitonin concentrations used in SUIT protocols.
Listed is the appropriate digitonin concentration to permeabilize the plasma membrane of various cell types in SUIT protocols.

Cell type	Digitonin concentration (µg/10^6 cells)
HT22	10 µg/10^6 cells
SH-SY5Y	6 µg/10^6 cells
MEF	13 µg/10^6 cells

2.2.4 Analysis of Mitochondrial Morphology

Two different approaches were used for the analysis of the mitochondrial morphology in cells. HT22 cells were seeded onto cover slips. The next day, HT22 cells were treated with 200 nM MitoTracker Red CMXRos in serum-free medium which specifically stains mitochondria of live cells depending on their membrane potential. After a 15 min-incubation under growth conditions the staining solution was removed, cells were washed with D-PBS and incubated for further 15 min with complete growth medium at 37 °C. Alternatively, SH-SY5Y cells and MEFs were transfected with a plasmid encoding mitochondrially targeted DsRed2 (pDsRed2-mito), seeded onto cover slips the following day and left to adhere over night.

Without any previous treatment or after the indicated treatment with glutamate, menadione or ethacrynic acid, cells were fixed with 4 % Roti®-Histofix in 15 min at room temperature. After three subsequent washing steps with PBS, cells were permeabilized with 0.2 % (v/v) Triton X-100 in PBS for 10 min following three additional washing steps with PBS. Cell nuclei were stained with 300 nM DAPI (5 min, room temperature). Cells were washed twice with PBS and once with dH_2O before cover slips were mounted onto microscope slides using Immu-Mount or Dako Fluorescence Mounting Medium. On an Olympus BX51 fluorescence microscope using a 60x oil immersion objective, the mitochondrial morphology was categorized by blinded observers. In total, 100 or 200 cells per condition were analysed and categorized in a aggregated, tubular, mixed, vesicular and fragmented mitochondrial morphology as described by Niemann and colleagues (Niemann et al., 2005). Representative pictures were taken with either the Olympus BX51 fluorescence microscope equipped with a 60x oil

immersion objective or the confocal microscope TCS SP5 from Leica Microsystems GmbH using a 63x oil immersion objective. Representative fluorescence pictures of MEFs were taken with the same settings. Confocal images from the same experiment were obtained from one optical section with the same settings concerning zoom factor, resolution (8 bit), pinhole (1 a.u.), frame/line average and format width and height. Confocal images of HT22 cells were taken with a zoom of 2.6, a resolution of 8 bits, a pinhole of 1 a.u., a format width and height of 1024 pixels and a frame-average of 3, while confocal images of SH-SY5Y cells were taken with the same resolution, pinhole, format width and height, but with a zoom of 3.0, a line-average of 8 and a frame-accumulation of 2. For better visualization of printed confocal images and fluorescence images, images of the same experiment were adjusted concerning the gradation curve, brightness and contrast of each channel in the same way afterwards.

2.2.5 Live-Cell Imaging

For the live-cell imaging of HT22S and HT22R cells, the live cell imaging system JuLI^{TM} BR Live Cell Analyzer from NanoEnTek Inc. was used. In total 160,000 cells were plated into one well of a 6-well plate and left to adhere overnight. The next day the medium was changed to complete growth medium supplemented with 10 mM glutamate, whereas HT22R cells in comparison to HT22S cells were maintained under their additional 10 mM glutamate exposure. Hence, the glutamate concentration in the experiment with HT22R constituted 20 mM glutamate in total. The cell lines were examined under normal growth condition for 24 h. The JuLI^{TM} BR Live Cell Analyzer, equipped with a 4x microscope objective, took a picture every 5 min.

2.2.6 Biochemical Methods

2.2.6.1 Preparation of Total Protein Cell Lysates

To prepare total protein cell lysates, cells were detached using trypsin, resuspended in growth medium and pelleted by centrifugation (1,000 rpm, 3 min). The supernatant was discarded and the pellet was washed with D-PBS. Cells were pelleted in a subsequent centrifugation step before they were lysed in an appropriate volume of RIPA Buffer containing Protease Inhibitors (one cOmplete, Mini Protease Inhibitor Cocktail tablet per 15 ml RIPA Buffer). Cell debris was removed by centrifugation at 16,000 g in 30 min at 4 °C. The supernatant was transferred to a pre-cooled 1.5 ml-tube on ice and the protein concentration was quantified using the BC Assay Protein Quantification Kit (Interchim)

according to the manufacture's instruction. Cell lysates were subsequently analysed by western blotting.

2.2.6.2 SDS-Polyacrylamid Gel Electrophoresis (PAGE) and Western Blotting (adapted from Laemmli, 1970; Towbin et al., 1979)

For western blot analysis, protein samples were diluted with water to obtain equal protein concentrations and mixed either with 4x LDS Sample Buffer and 10x Sample Reducing Agent, or 4x Laemmli sample buffer containing β-mercaptoethanol to a final 1 x concentration. Protein samples were denatured at 95 °C for 5 min and equal amounts of proteins were separated in a sodium dodecyl sulfate (SDS)-polyacrylamid gel electrophoresis on 8 – 16 % Precise protein or 4 – 15 % Mini-PROTEAN® TGX Stain-Free™ gels alongside the MagicMark™ XP Western Protein Standard at 120-150 V. Afterwards, the proteins were transferred onto a nitrocellulose membrane using the iBlot® Dry Blotting System (Invitrogen) or onto a PVDF membrane using the Trans-Blot® Turbo™ Transfer System (Bio-Rad). The protein transfer was verified with Ponceau S solution before the membrane was blocked with Immunoblotting (IB) blocking buffer for 1 h at room temperature. Proteins were detected by immunolabelling using the appropriate primary and secondary antibodies diluted in IB blocking buffer (Table 4). The membrane was incubated with the primary antibodies overnight at 4 °C, followed by the incubation with the secondary antibodies for 1 h at room temperature. Between each incubation step, the membrane was washed three times with IB washing buffer for 10 min per wash. The infrared fluorescence conjugated-secondary antibodies were detected with the Odyssey Infrared or Odyssey Sa Infrared Imaging System.

2.2.6.3 Immunocytochemistry (ICC)

In order to address the localization of proteins inside cells, an immunocytochemistry (ICC) was performed. For ICC analysis of SH-SY5Y cell lines an appropriate number of cells were platted onto cover slips and left to adhere over night. The next day, the medium was removed, cells were washed with D-PBS and fixed with 4 % Roti®-Histofix in 15 min at room temperature. After two additional washing steps, cells were permeabilized with 0.25 % (v/v) Triton X-100 in PBS for 10 min following three further washing steps for 5 min. To block unspecific binding of antibodies, the cells were incubated with ICC blocking buffer for 30 min. The primary antibodies were diluted in ICC blocking buffer containing 0.1 % (v/v) Tween and cells were incubated with the primary antibodies overnight at 4 °C. The fluorophore-conjugated secondary antibodies were diluted in the ICC blocking buffer containing 0.1 % (v/v) Tween. The cells were incubated with the secondary antibody for 1 h at room temperature in the dark. After removing the secondary antibody, cell nuclei were stained with

300 nM DAPI (5 min, room temperature) and cover slips were mounted with Dako Fluorescent Mounting Medium onto microscope slides. Between each incubation step, the cells were washed thoroughly three times with PBS for 5 min per wash.

Alternatively, for ICC analysis of the intracellular localization of Bcl-x_L in MEFs, an appropriate number of cells transfected with pDsRed2-mito were plated onto glass cover slips and left to adhere overnight. The next day, the cells were fixed the same way as described before, but after this step, cells were permeabilized and blocked with ICC blocking buffer supplemented with 0.5 % (w/v) n-octyl-β-D-glucopyranoside within 60 min at room temperature. In the following steps, like during the incubation with the primary and secondary antibody, the same ICC blocking buffer containing 0.5 % (w/v) n-octyl-β-D-glucopyranoside was used, but the procedure was carried out as described before.

Fluorescence pictures were taken with the confocal microscope TCS SP5 from Leica Microsystems GmbH using a 63x oil immersion objective. Confocal images from the same experiment were taken from one optical section with the same settings. A zoom of 3.0, a resolution of 8 bits, a pinhole of 1 a.u., a format width and height of 1024 pixels and a frame-average of 8 were used at a scan speed of 600 Hz. Afterwards the gradation curve, brightness and contrast of each channel of confocal images of the same experiment were adjusted for better visualization of printed images.

2.2.7 Statistical Analysis

The GraphPad Prism 5 software was used to carry out statistical analysis. Data are displayed as mean ± standard deviation (S.D.). Statistical significance between results was evaluated by the two-tailed t-test, one-way Analysis of Variance (ANOVA) followed by the Tukey's multiple comparison test or the two-way ANOVA followed by the Bonferroni's *post hoc* test. A *p*-value less than 0.05 was considered as statistically significant.

3 RESULTS

3.1 Effects of Acute Oxidative Stress on Mitochondrial Form and Function

3.1.1 Oxidative Glutamate Toxicity Does Not Influence Mitochondrial Morphology in Mouse Hippocampal HT22S Cells

The mouse hippocampal cell line HT22S is an exceptional model system for studying oxidative stress caused by glutamate, named oxidative glutamate toxicity (Albrecht et al., 2010; Tan et al., 2001). Oxidative glutamate toxicity seems to directly affect mitochondria by inducing a breakdown of the mitochondrial membrane potential (Landshamer et al., 2008; Noack et al., 2012; Pallast et al., 2009) and subsequent activated 12/15-LOX target and directly damage mitochondria (Pallast et al., 2009). Mitochondria are highly dynamic organelles because of constant fusion and fission events (Chan, 2012; Westermann, 2010). Oxidative glutamate toxicity even seems to influence directly mitochondrial dynamics because a treatment of HT22S cells with glutamate provoked perinuclear accumulation and mitochondrial fragmentation (Grohm et al., 2010; Kumari et al., 2012). An exposure to hydrogen peroxide (H_2O_2) even induced an elongation of mitochondria in human Chang liver cells (Yoon et al., 2006) and the treatment of isolated mitochondria with either H_2O_2 or oxidized glutathione (GSSG) resulted in mitochondrial fusion in HeLa cells (Shutt et al., 2012). For this reason, I investigated the mitochondrial morphology of HT22S cells after an exposure to 10 mM glutamate for 6 h by staining mitochondria with the mitochondrial-specific dye MitoTracker Red. The mitochondrial morphology was classified as described by Niemann and colleagues (Niemann et al., 2005) into the five categories: aggregated, tubular, mixed, vesicular and fragmented. Cells with aggregated mitochondria show an aggregation of mitochondria, while cells with mainly elongated mitochondria were categorized as tubular and cells with completely fragmented mitochondria as fragmented. The category mixed describes the appearance of both tubular and vesicular mitochondria in a cell, whereas cells with the category vesicular displayed mainly fragmented mitochondria besides some tubular ones. Representative single-section confocal images of each category, apart from category aggregated as this was not observed, are shown in Figure 10A. The analysis of three independent experiments by two blinded observers categorizing 100 cells per condition in each experiment showed no significant changes in the mitochondrial morphology of HT22S cells exposed to glutamate compared to the untreated control (Figure 10B). Consequently, a treatment of HT22S cells with glutamate did not change their mitochondrial morphology.

3.1.2 Oxidative Glutamate Toxicity Increases Mitochondrial Respiration in HT22S Cells

The direct effect of a glutamate-exposure on the mitochondrial membrane potential (Landshamer et al., 2008; Noack et al., 2012; Pallast et al., 2009) together with the recent observation demonstrating an increase in the mitochondrial respiration of glutamate-treated HT22S cells (Kumari et al., 2012) already showed the influence of endogenous oxidative stress on mitochondria in the HT22S cell line. For this reason, I examined the mitochondrial respiration of glutamate-treated HT22S cells by high-resolution respirometry and as in the previous experiment treated HT22S cells with 10 mM glutamate for 6 h before measuring their mitochondrial respiration. Figure 10C shows representative traces of the mitochondrial oxygen consumption of untreated and glutamate-treated HT22S cells. At the beginning, the basal routine respiration (R) of intact HT22S cells was recorded in their regular growth medium. Then the ATP synthase was inhibited by addition of oligomycin, which allowed the recording of the resting or non-phosphorylating leak respiration, state L. The leak respiration is the leak oxygen flux after inhibition of ATP production and compensates mainly proton leak at maximum mitochondrial membrane potential as well as proton slip and electron slip, which redirects electrons toward ROS production, besides cation cycling (K^+, Ca^{+2}; Gnaiger, 2008; Pesta and Gnaiger, 2012). In the following, the titration of the protonophore and uncoupler FCCP stimulated the oxygen consumption and the electron transfer system (ETS) capacity (E) state was measured at the maximum oxygen flux with optimum FCCP concentration. This is a state of experimentally induced maximum non-coupled respiration (Pesta and Gnaiger, 2012). By addition of the complex I-inhibitor rotenone and complex III-inhibitor antimycin A the mitochondrial respiration was inhibited and the non-mitochondrial residual oxygen consumption (ROX) was determined. ROX was used for the correction of routine, leak and ETS capacity. This allows the comparison of only mitochondrial oxygen consumption between cell lines and experimental conditions. ROX can be explained mostly by non-mitochondrial oxygen consumption of cellular auto-oxidation reaction and by the activity of oxygen consuming enzymes, like for example peroxidase and oxidase, which in part contribute to ROS production (Gnaiger, 2008; Pesta and Gnaiger, 2012). In agreement with the observations by Kumari and colleagues (Kumari et al., 2012), a treatment of HT22S cells with glutamate induced a significant increase of the oxygen flow per cells at basal routine respiration, leak respiration and ETS capacity compared to untreated cells (Figure 10D). But the untreated and treated HT22S cells displayed both an excess in the capacity of their ETS because the oxygen flow per cells at maximum ETS capacity was higher than the part being used in basal routine respiration.

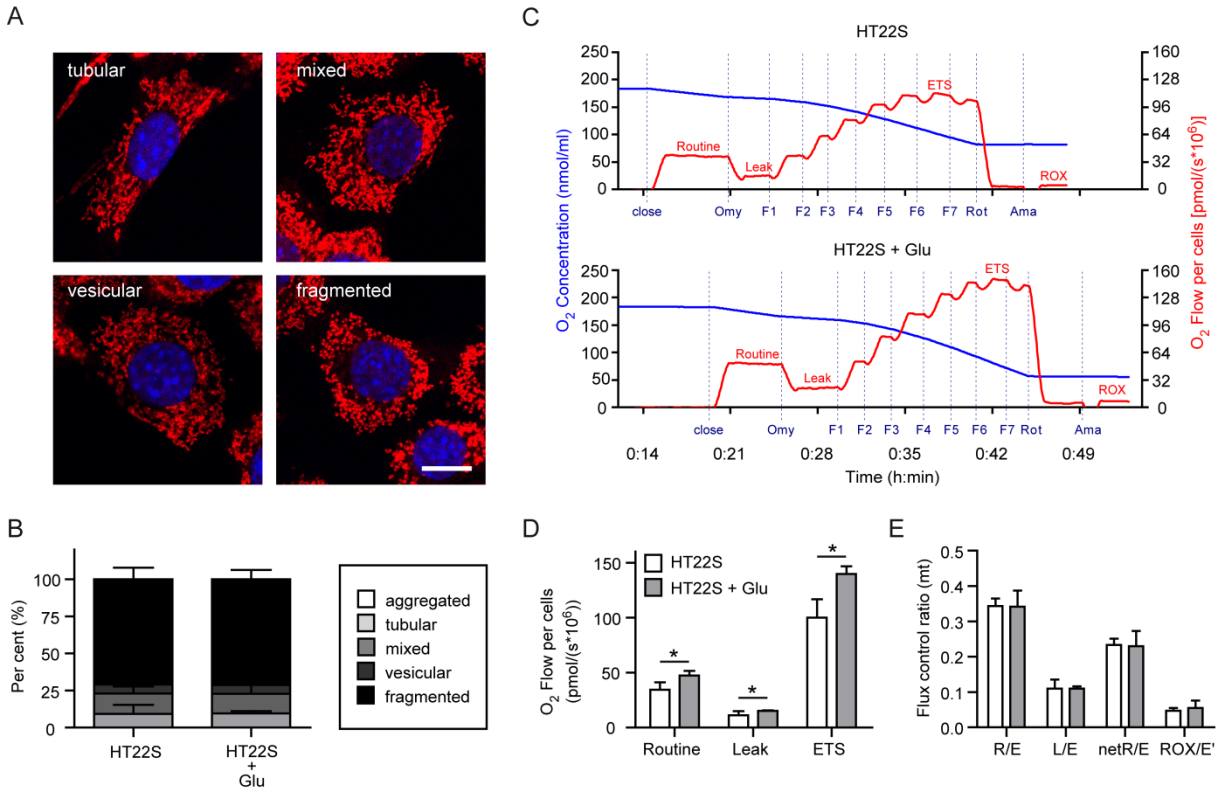

Figure 10: Mitochondrial respiration is decreased in glutamate-treated HT22S cells, but their mitochondrial morphology is not affected.
HT22S cells were treated for 6 h with glutamate (Glu) before their mitochondrial morphology and their mitochondrial oxygen consumption was analysed by high-resolution respirometry in comparison to untreated HT22S cells as a control. **(A/B)** Mitochondria of living cells were stained with MitoTracker Red and their nuclei were visualized with DAPI (blue). The mitochondrial morphology was analysed by fluorescence microscopy. The mitochondrial morphology was categorized in an aggregated, tubular, mixed, vesicular and fragmented category. Cells possessing a mixed category showed a mixture of tubular as well as fragmented mitochondria, while cells with a vesicular phenotype showed mainly fragmented mitochondria besides few tubular mitochondria. **(A)** Representative confocal images of the category tubular, mixed, vesicular, fragmented are shown. The aggregated category is not shown since no cell exhibited this category. Scale bar represents 20 µm. **(B)** The exposure of HT22S cells to glutamate caused no overall change in the mitochondrial morphology. Cells were categorized by two blinded investigators. Shown data were obtained in three independent experiments and are represented as mean ± S.D.. **(C)** Shown are representative traces of each experimental condition showing the oxygen concentration (blue line) and the oxygen flow per cells (red line) measured by high-resolution respirometry. The addition of oligomycin (Omy), FCCP (F), rotenone (Rot) and antimycin A (Ama) are indicated with dashed lines. Sections reflecting routine respiration, leak respiration induced by the ATP synthase-inhibitor oligomycin, electron transfer system (ETS) capacity at maximum FCCP concentration and residual oxygen consumption (ROX), after inhibition of complex I with rotenone and complex III with antimycin A, are labelled. **(D)** Quantitative analysis of the ROX-corrected mitochondrial (mt) oxygen flow per cells at the corresponding respiratory state indicated that the 6 hour-exposure of HT22S cells to glutamate induced an increase in routine, leak and ETS capacity. **(E)** Calculated mitochondrial flux control ratios by normalizing routine respiration (R), leak respiration (L) and the fraction used for ATP production (netR as R-L) to the maximum ETS capacity state E. In addition, ROX was normalized to the total uncoupled respiratory flux, the uncorrected ETS capacity state E'. The exposure to glutamate induced no changes in the flux control ratios of HT22S cells. Data displayed in (D) and (E) were obtained from three independent experiments done in duplets and show the mean ± S.D.. Statistical significance was calculated using Student's two-tailed t-test and is indicated by an asterisks (p<0.05).

In order to compare the fraction of the ETS capacity used for routine (R), leak (L) and phosphorylating respiration (netR=R-L), the respiratory states were expressed in relation to the maximum ETS capacity state E (calculation of the flux control ratios). The fraction of the ETS capacity utilized for routine respiration (R/E) as well as the fraction of the ETS capacity, which is directly used for ATP production and hence, for phosphorylation of ADP to ATP (netR/E), were comparable in untreated and treated HT22S cells (Figure 10E). Untreated

and glutamate-treated HT22S cells utilized 0.34 ± 0.02 and 0.34 ± 0.05 (mean ± S.D., n=3) of their ETS capacity for basal routine respiration (R/E). Consequently, the cells used approximately 34 % of their ETS capacity for basal routine respiration in their regular growth medium with and without a prior exposure to glutamate, which underlines the excess in their capacity of the ETS. The fraction of the ETS capacity used for non-phosphorylating leak respiration compensating mainly proton leak (Gnaiger, 2008; Pesta and Gnaiger, 2012) is also unaffected by oxidative glutamate toxicity. In addition, the flux control ratio of oxidative side-reactions, which is ROX relative to the total and uncorrected uncoupled respiratory flux E' (ROX/E') is comparable in glutamate-treated and untreated HT22S cells. In summary, although an acute exposure to glutamate does not influence mitochondrial form, it increases the respiratory activity in HT22S cells as described before (Kumari et al., 2012).

3.1.3 Ethacrynic Acid and Menadione Alter the Mitochondrial Morphology in Human Neuroblastoma SH-SY5Y Cells

In the next experiment, I investigated the effect of acute oxidative stress on the mitochondrial morphology of a human neuronal cell line and selected the human neuroblastoma cell line SH-SY5Y as a model system. In comparison to the experiment with HT22S cells, I used ethacrynic acid (EA) and menadione (MQ) to induce oxidative stress by GSH depletion in SH-SY5Y cells because these cells do not die in response to excessive extracellular glutamate. EA induces oxidative stress by a complete loss of total glutathione in both cytosol and mitochondria (Seyfried et al., 1999; Wullner et al., 1999), while MQ triggers oxidative stress by inducing ROS production through redox cycling and GSH depletion (Chiou and Tzeng, 2000; Criddle et al., 2006; Kim et al., 2014; Loor et al., 2010). Both reagents have been claimed to affect mitochondrial dynamics. A treatment of human fibroblasts and BSC-1 cells with EA induced mitochondrial fusion and the formation of mitochondrial reticulum within a short time (Bowes and Gupta, 2005; Soltys and Gupta, 1994), while a treatment of cardiomyocytes with MQ resulted in mitochondrial fragmentation (Loor et al., 2010). In order to study the mitochondrial morphology in SH-SY5Y cells, cells were transfected with a mitochondrially targeted DsRed2 (pDsRed-mito) and oxidative stress was induced by treating cells with 30 µg/ml EA or 20 µM MQ for 1 h. The mitochondrial morphology was categorized as described above by a blinded investigator using fluorescence microscopy. Representative confocal images of SH-SY5Y cells with an aggregated, tubular, mixed, vesicular and fragmented mitochondrial morphology are shown in Figure 11A. The treatment of SH-SY5Y cells with EA resulted in a dramatic increase of cells with tubular mitochondria compared to vehicle-treated cells as a control (Figure 11B). Hence, EA induced mitochondrial fusion in agreement with previous observations (Bowes and Gupta, 2005; Soltys and Gupta, 1994) in SH-SY5Y cells. In comparison to this, MQ provoked mitochondrial fission because the

number of cells with a vesicular and fragmented mitochondrial shape increased in contrast to the control (Figure 11B), which is in line with observations by Loor and colleagues (Loor et al., 2010). Since EA and MQ were solved in absolute ethanol and the treatment of cells with this vehicle resulted in a similar distribution of cells in the five categorize, the results of all six experiments were combined in the column with vehicle-treated SH-SY5Y cells (Figure 11B). Thus, within one hour EA and MQ triggered a change in the mitochondrial morphology of SH-SY5Y cells by inducing oxidative stress linked to most likely GSH depletion and induced mitochondrial fusion and fission, respectively.

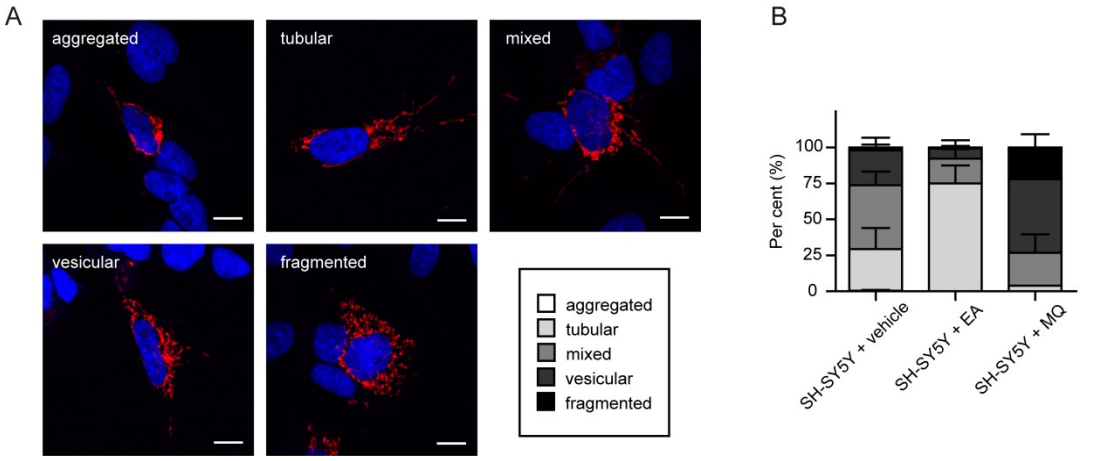

Figure 11: Oxidative stress induced by ethacrynic acid and menadione alters the mitochondrial morphology in human neuroblastoma SH-SY5Y cells.
SH-SY5Y cells transfected with mitochondrially targeted DsRed2 (pDsRed2-mito) were treated with 30 µg/ml ethacrynic acid (EA) or 20 µM menadione (MQ) for 1 h. After fixation nuclei were stained with DAPI (blue) and their mitochondrial morphology was analysed by fluorescence microscopy. The mitochondrial morphology was categorized in an aggregated, tubular, mixed, vesicular and fragmented category as described before by a blinded investigator, who classified 100 cells per condition. **(A)** Representative confocal images of the category aggregated, tubular, mixed, vesicular and fragmented are shown. Scale bars represent 10 µm. **(B)** The quantification of three independent experiments revealed an increase in the cell number with tubular mitochondria after EA-treatment, while MQ induced an increase of cells with a vesicular and fragmented mitochondrial shape. Vehicle-treated cell from experiments with EA and MQ are combined in the column SH-SY5Y + vehicle. Data are represented as mean ± S.D..

3.1.4 Ethacrynic Acid Reduces Mitochondrial Respiration in SH-SY5Y Cells

Because glutamate-induced oxidative stress changed the mitochondrial respiration in HT22S cells (Figure 10; Kumari et al., 2012), I analysed the effect of EA on mitochondrial oxygen consumption in SH-SY5Y cells. The rapid and drastic change of the mitochondrial morphology in SH-SY5Y cells and the results of previous investigations showing impaired mitochondrial enzyme activity induced by EA in other cell types (Seyfried et al., 1999; Wullner et al., 1999) suggest that the mitochondrial respiration is probably as well influenced by EA in SH-SY5Y cells. In comparison to Seyfried and colleagues, who recognized a decrease of mitochondrial respiratory complexes' activities in isolated mitochondria of EA-treated cells (Seyfried et al., 1999), I investigated its effect on intact cells by high-resolution respirometry. Like in the previous experiment, SH-SY5Y cells were treated with 30 µg/ml EA

for 1 h before the mitochondrial respiration was analysed. Figure 12 shows representative traces of the mitochondrial respiration of intact SH-SY5Y cells in their regular growth medium after treatment with EA or the vehicle as a control. EA reduced significantly the mitochondrial basal routine respiration as well as the ETS capacity in SH-SY5Y (Figure 12B), but the leak respiration was not influenced by EA. The routine respiration and ETS capacity of EA-treated cells was reduced to about 69.9 % and 66.6 % (n=4). The part of the ETS capacity used for routine (R), leak (L) and phosphorylating respiration (netR) as well as the flux control ratio of oxidative side-reactions (ROX/E') was comparable under both experimental conditions (Figure 12C). As a result, EA certainly induced rapidly a reduction of the routine respiration and ETS capacity, but consequently the part of ETS capacity used for routine respiration and the fraction utilized for ATP production remained unchanged in SH-SY5Y cells because of a reduced ETS capacity. Hence, EA provokes a change in the mitochondrial morphology as well as mitochondrial respiration in SH-SY5Y cells within a short period of time.

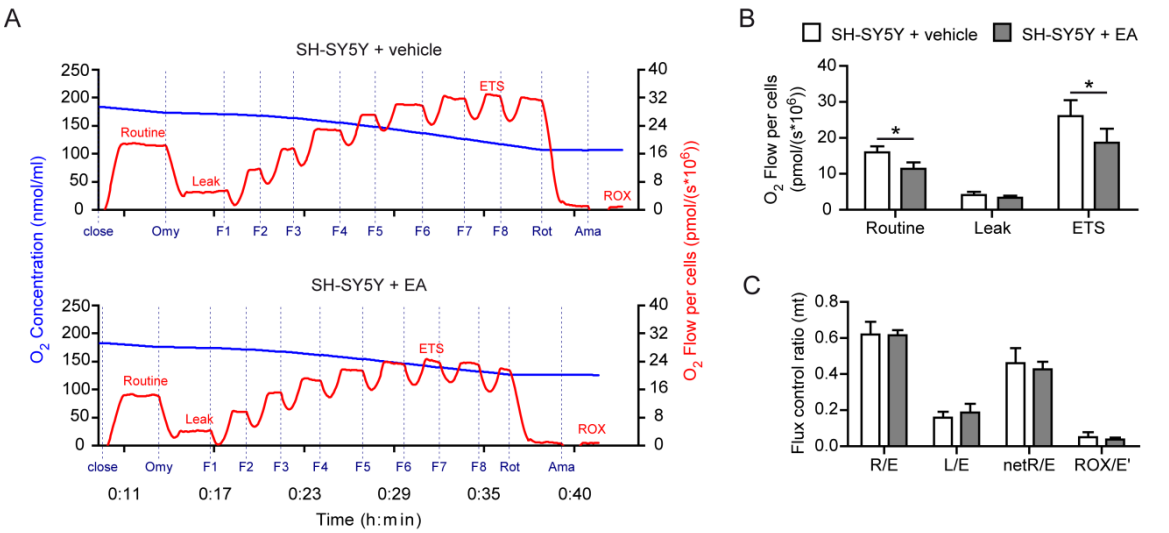

Figure 12: Ethacrynic acid induces a reduction in mitochondrial respiration in SH-SY5Y cells.
The mitochondrial respiration was analysed in SH-SY5Y cells after a 1 h-treatment with 30 µg/ml ethacrynic acid (EA) or the vehicle as a control by high-resolution respirometry. **(A)** Representative traces of vehicle-treated and EA-treated SH-SY5Y cells are represented showing the oxygen concentration (blue line) and the oxygen flow per cells (red line). Dashed lines mark the addition of oligomycin (Omy), titration of FCCP (F including step number) as well as application of rotenone (Rot) and antimycin A (Ama). Respiratory states reflecting routine respiration, leak respiration, ETS capacity and ROX are indicated. **(B)** The quantitative analysis of the ROX-corrected oxygen flow per cells of the control (1.6 ± 0.4*10^6 cells/ml; mean ± S.D.) and EA-treated (2.2 ± 0.1*10^6 cells/ml) SH-SY5Y cells showed a reduction of routine respiration and ETS capacity induced by EA. The leak respiration was comparable in both conditions. **(C)** Normalization of the ROX-corrected, mitochondrial (mt) routine respiration (state R), leak respiration (state L) and the fraction used for ATP production (netR=R-L) to the ETS capacity (state E) revealed no changes in EA-treated cells in contrast to the control. In addition, the flux control ratio of oxidative side reaction ROX normalized to the ROX-uncorrected total ETS capacity (E') was similar in vehicle- and EA-treated SH-SY5Y cells. Data shown in (B) and (C) were collected in four independent experiment performed in duplets and are presented as mean O_2 flow per cells or mean flux control ratio ± S.D.. Statistical significance is indicated with an asterisk (p<0.05) and was verified using Student's two-tailed t-test.

3.1.5 Menadione Decreases the Mitochondrial Respiration in SH-SY5Y Cells

Menadione altered the mitochondrial morphology of SH-SY5Y cells to a more fragmented appearance (Figure 11). It is most likely that MQ as well as an exposure of HT22S cells to glutamate (Figure 10; Kumari et al., 2012) and a treatment of SH-SY5Y cells (Figure 12) and other cell types with EA (Seyfried et al., 1999; Wullner et al., 1999) changes the mitochondrial oxygen consumption of this cell line. Hence, I investigated the mitochondrial respiration of intact cells in their general growth medium after an exposure to MQ. In comparison to the previous experiment, I treated cells with 10 and 20 µM MQ for 1 h before the mitochondrial oxygen consumption was analysed. Representative measurements of SH-SY5Y cells under each experimental condition are shown in Figure 13A. The analysis of the ROX-corrected oxygen flow per cells at routine respiration, leak respiration and ETS capacity in three separate experiments showed an impact of MQ on the mitochondrial respiration in a concentration-dependent manner. 10 µM of MQ decreased slightly the basal routine respiration, whereas the ETS capacity was significantly reduced compared to control cells (Figure 13B). A treatment with 20 µM MQ did not only reduce significantly the ETS capacity, but also the basal routine respiration. The ETS capacity was even significantly decreased in cells treated with 20 µM MQ compared to cells exposed to half of the dose with 10 µM MQ. In contrast to this, the leak respiration remained comparable under all three conditions. The routine respiration was reduced to 85.4 % in cells treated with 10 µM MQ, and 64.9 % in cells treated with 20 µM MQ, whereas the ETS capacity was decreased to 87.5 % in 10 µM and 58.8 % (n=3) in 20 µM MQ-treated SH-SY5Y cells in relation to the control. Thus, the impact of MQ on the ETS capacity was stronger than on the basal routine respiration.

Calculation of the flux at the respiratory states routine and leak in relation to the ETS capacity showed that only the routine control ratio was significantly enhanced after a treatment with 20 µM MQ compared to a treatment with 10 µM (Figure 13C). Nevertheless, the routine and leak control ratio was increased slightly, but not significantly by 20 µM MQ. The portion of the ETS capacity utilized for phosphorylating respiration (netR/E) remained unchanged. However, the flux control ratio of oxidative side-reactions (ROX/E') was enhanced significantly in cells treated with 20 µM MQ in comparison to untreated and cells treated with half of the dose, which suggested an increase in ROX. Analysis of the residual oxygen consumption showed that ROX was increased from an oxygen flow per cells of 1.29 ± 0.4 pmol/(s*10^6) (mean ± S.D., n=3) in untreated cells to 1.49 ± 0.4 pmol/(s*10^6) in cells treated with 10 µM and than further to 2.41 ± 0.8 pmol/(s*10^6) in cells treated with 20 µM MQ. The changes in ROX between untreated and cells treated with 20 µM MQ were significantly different as well as the increase in ROX between treated cells (not shown).

In conclusion, oxidative stress induced by MQ did not only impact the mitochondrial morphology, but altered additionally the mitochondrial function by impairing mitochondrial

oxygen consumption in a concentration-dependent manner in SH-SY5Y cells. The effects of MQ on mitochondria emerged already after a short period of one hour. In comparison to EA, MQ had as well an effect on non-mitochondrial oxygen consumption and increased ROX.

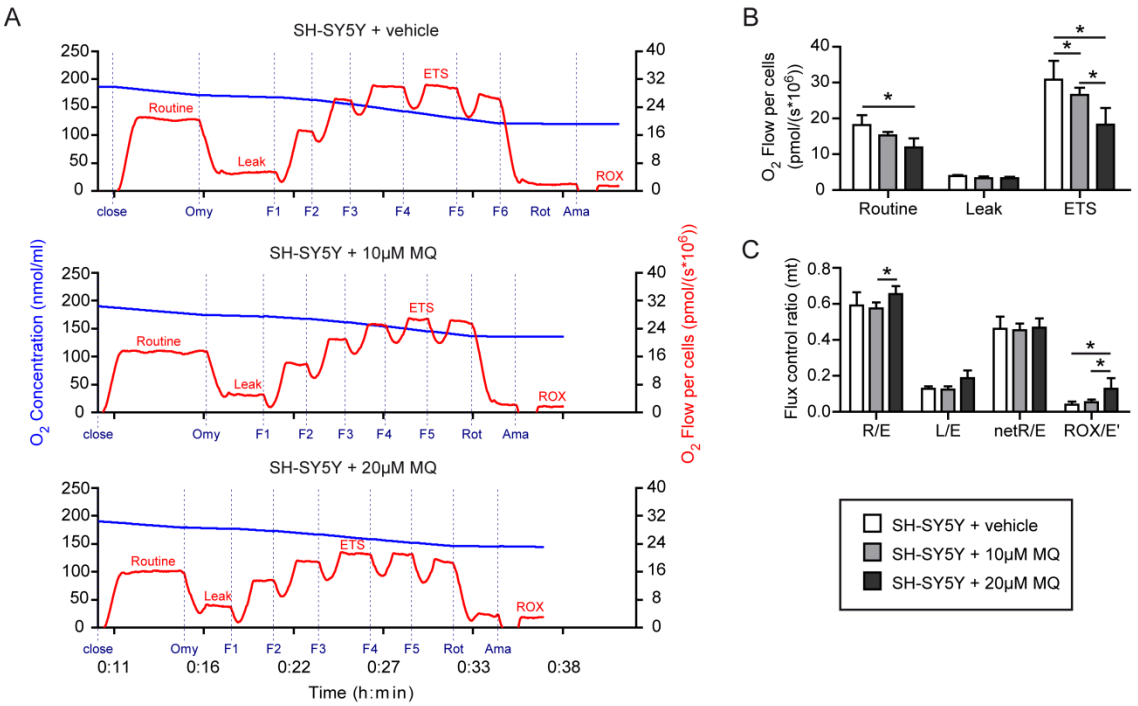

Figure 13: A treatment with menadione reduces the mitochondrial respiration of SH-SY5Y cells. After a treatment with 10 µM and 20 µM menadione (MQ) for 1 h, the mitochondrial oxygen consumption was analysed by high-resolution respirometry in SH-SY5Y cells compared to vehicle-treated cells as a control. **(A)** A representative trace of each condition is displayed showing the oxygen concentration with a blue line and the oxygen flow per cells with a red line. The addition of oligomycin (Omy), FCCP-titration (F including step number) as well as the addition of rotenone (Rot) and antimycin A (Ama) are labelled with dashed lines, while the respiratory states reflecting routine respiration, leak respiration, ETS capacity and ROX are indicated. **(B)** The oxygen flow per cells was corrected for ROX to compare only mitochondrial respiration. The mitochondrial oxygen flow per cells of SH-SY5Y cells treated with 10 µM MQ or 20 µM MQ ($2.0 \pm 0.2*10^6$ cells/ml; mean ± S.D.) was reduced at routine respiration and at non-coupled respiration reflecting ETS capacity compared to vehicle-treated ($2.0 \pm 0.3*10^6$ cells/ml) cells. At leak respiration comparable oxygen consumptions were measured. **(C)** Calculated fraction of the ETS capacity (state E) used for routine respiration (state R), leak respiration (state L) and for ATP production (netR=R-L). A treatment with 20 µM menadione increased the routine control ratio (R/E), while all other flux control ratios were comparable under all three experimental conditions. The flux control ratio of oxidative side-reactions (ROX) normalized to the ROX-uncorrected total non-coupled respiratory flux, ETS capacity (E'), was increased in both MQ-treated SH-SY5Y cells compared to the control. Data represented in (B) and (C) were obtained from three independent experiments performed in duplets and are represented as mean ± S.D.. Statistical significance was verified using two-way ANOVA Bonferroni posttest. An asterisk indicates a $p<0.05$.

3.2 Effect of Adaptations including Mitochondrial Form and Function against Oxidative Stress in Glutamate-Resistant HT22R cells

3.2.1 The Glutamate-Resistant Cell Line HT22R

Glutamate-resistant HT22R cells are a great model to analyse the effect of chronic oxidative stress and associated adaptations against oxidative stress (Lewerenz et al., 2006) including mitochondrial form and function as a mechanism against stress. We have created the glutamate-resistant cell line HT22R (Lewerenz et al., 2006) by the repetitive exposure of the parental glutamate-sensitive HT22S cell line (Maher and Davis, 1996) to glutamate. The live cell-imaging of parental HT22S cells treated with 10 mM showed that these cells displayed the first sign of cell death in form of rounded cells already approximately 8 h after the beginning of the experiment (Figure 14A). At this time point, HT22S cells began to lose their adherence. 16 h after the start of the experiment, all HT22S cells were dead compared to HT22R cells, which were still viable at this time point. HT22R cells had even continued to proliferate. In comparison to HT22S cells, HT22R cells were additionally maintained under their regular exposure to 10 mM glutamate in this experiment, so that the total glutamate-concentration during the experiment was 20 mM of glutamate.

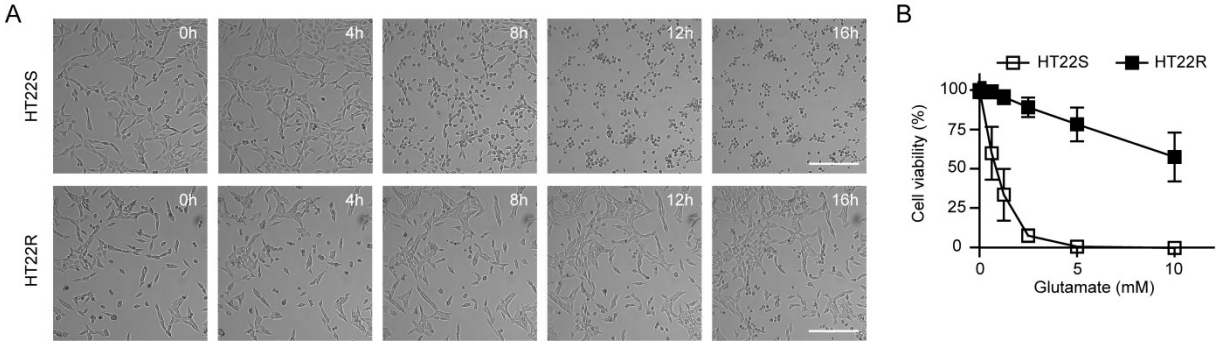

Figure 14: The hippocampal mouse cell line HT22R is resistant to oxidative stress induced by glutamate. **(A)** Glutamate-sensitive HT22S and glutamate-resistant HT22R seeded in a 6-well plate were treated with 10 mM glutamate to induce oxidative stress and monitored in a live-cell imaging experiment for 24 h. HT22R cells were additionally maintained under their regular 10 mM glutamate exposure, so that the final glutamate concentration added up to 20 mM glutamate. Shown are representative pictures after 0, 4, 8, 12 and 16 h. While HT22R cells are resistant to glutamate and continued to proliferate, HT22S cells showed clear signs of cell death after 8 h. Scale bar represents 250 µm. **(B)** Cells were subjected to the indicated concentration of glutamate. HT22R cells were additionally maintained under their usual 10 mM glutamate exposure besides the indicated concentration of glutamate. 22 h later, the cell viability was quantified using the CellTiter-Blue reagent. The cell viability in per cent, represented as mean ± S.D. of five replicates obtained from three independent experiments were plotted against the used glutamate concentrations.

In a cell viability assay the sensitivity of parental HT22S cells and the resistance of HT22R cells to a glutamate exposure was additionally proved. Cells were exposed to different concentrations of glutamate and their viability was measured using the CellTiter-Blue (CTB) reagent. Within 22 h, HT22S cells were killed in a concentration-dependent manner by glutamate (Figure 14B), whereas 57.5 ±15.6 % (mean ± S.D., n=3) of HT22R cells were still

viable when exposed to the highest concentration of 10 mM glutamate (already published in Pfeiffer et al., 2014). Like in the previous experiment, HT22R cells were additionally maintained under their regular 10 mM glutamate exposure in this experiment. All HT22S cells were killed at a concentration of 5 and 10 mM of glutamate, while only 7.4 ± 3.9 % were surviving an exposure to 2.5 mM glutamate.
Thus, the HT22R cells are significantly protected against oxidative glutamate toxicity as described before (Lewerenz et al., 2006). HT22R cells are even capable to proliferate when exposed to 20 mM glutamate, which is 200 % of the amount of glutamate they are exposed to under general growth conditions.

3.2.2 Altered Mitochondrial Morphology in Glutamate-Resistant HT22R Cells

Mitochondrial dynamics plays an important role in the maintenance of functional mitochondria and is consequently not only critical for mitochondrial bioenergetics, but also important for cell survival (Westermann, 2010; Youle and van der Bliek, 2012). The recent examination of the mitochondrial membrane potential in HT22S and R cells showed a significant increase in the mitochondrial membrane potential for the glutamate-resistant HT22R cell line (Noack et al., 2012), which suggested an involvement of mitochondria in the glutamate resistant phenotype. For this reason, I investigated the mitochondrial morphology of HT22R and HT22S cells and stained mitochondria of living cells with the mitochondrial-specific dye MitoTracker Red. In three independent experiments, 100 cells from each cell line were categorized by two blinded observers. The result of HT22S cells in Figure 15A has already been shown in Figure 10. In contrast to HT22S cells, glutamate-resistant HT22R cells showed a decrease in the fragmented category at the expense of an increase in cells with tubular mitochondria (Figure 15A; already published in Pfeiffer et al., 2014). Therefore, the prolonged exposure of glutamate changed the mitochondrial morphology in HT22R cells towards a more elongated character suggesting changes in mitochondrial respiration in the glutamate-resistant HT22R cell line.

3.2.3 Reduced Mitochondrial Oxygen Consumption Induced by the Continuous Exposure to Glutamate in HT22R Cells

Since the mitochondrial membrane potential is altered in the glutamate-resistant HT22R cells (Noack et al., 2012) as well as I could observe a change in the mitochondrial morphology of these cells, I examined their mitochondrial respiration by high-resolution respirometry to

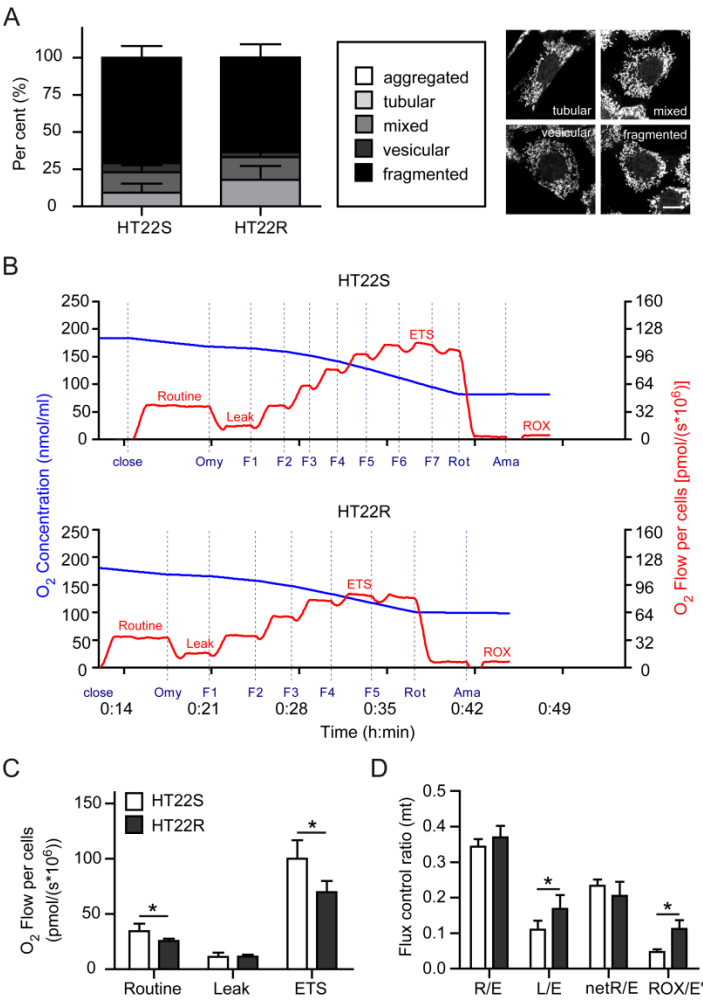

Figure 15: Glutamate-resistant HT22R cells show increasingly elongated mitochondria with decreasing respiratory activity.
(A) HT22R and HT22S cells were analysed after a staining with MitoTracker Red and DAPI (blue) by two blinded observers using fluorescence microscopy. The mitochondrial morphology was categorized as described before in a tubular, mixed, vesicular and fragmented category. The analysis of three independent experiments is represented as mean ± S.D.. The quantification indicated a reduction of HT22R cells with fragmented mitochondria at the expense of an increase with cells showing a tubular mitochondrial morphology. Previously shown exemplary confocal images of the category tubular, mixed, vesicular, fragmented are displayed in smaller magnification. Scale bar represents 20 µm. **(B)** The mitochondrial respiration of HT22S cells and HT22R cells was analysed by high-resolution respirometry. Displayed are representative traces showing the oxygen concentration (blue line) and the oxygen flow per cells (red line) of HT22S and R cells. Dashed lines indicate the addition of oligomycin (Omy), FCCP (F), rotenone (Rot) and antimycin A (Ama) and the respiratory states routine, leak, ETS capacity and ROX are labelled. **(C)** The quantitative analysis of the ROX-corrected oxygen flow per cells at the corresponding respiratory state indicated that the continuous exposure to glutamate resulted in a decreased routine respiration and ETS capacity in the glutamate-resistant HT22R cell line. **(D)** The calculated mitochondrial flux control ratios were calculated by normalizing routine respiration (R), leak respiration (L) and the fraction used for ATP production (netR) to the maximum ETS capacity which showed that in HT22R cells the leak control ratio (L/E) as well as the flux control ratio of oxidative non-mitochondrial side-reactions normalized to the total uncoupled respiratory state (ROX/E') is enhanced. Data shown in (C) and (D) were obtained from three independent experiments done in duplets and show the mean ± S.D.. Results from HT22S cells have already been shown in Figure 10. Statistical significance was calculated using Student's two-tailed t-test and is indicated by an asterisks (p<0.05).

find out whether this cell line differs in their mitochondrial respiratory activity to parental HT22S cells. A representative measurement of H22R is shown in Figure 15B in comparison to a representative trace of HT22S cells, which has already been displayed in Figure 10 together with the quantitative analysis. The prolonged exposure of HT22R cells to glutamate reduced the routine respiration and induced a significant decrease in the ETS capacity compared to parental HT22S cells (Figure 15C; already published in Pfeiffer et al., 2014). Both cell lines consumed similar oxygen levels at leak respiration as well as both cell lines revealed an excess in their capacity of the ETS. Calculation of the flux control ratios showed that the fraction of the ETS capacity utilized for routine respiration (R/E) as well as the fraction of ETS capacity which is directly used for phosphorylating respiration (netR/E) were comparable in the glutamate-sensitive HT22S and glutamate-resistant HT22R cells (Figure 15D, already published in Pfeiffer et al., 2014). HT22R cells used about 37 % of their ETS capacity for basal routine respiration compared to 34 % (n=3) in glutamate-sensitive

HT22S cells. This underlines the excess in the capacity of the ETS. But the fraction of the ETS capacity used for non-phosphorylating leak respiration was significantly enhanced and closer to the upper limit of the ETS capacity in HT22R cells compared to the glutamate-sensitive HT22S cells (already published in Pfeiffer et al., 2014). In addition, the flux control ratio of oxidative side-reactions (ROX/E') is significantly increased in HT22R cell line in contrast to HT22S cells. This increase in the fraction of the total ETS capacity used for non-mitochondrial residual oxygen consumption suggests an elevation in for example oxygen consuming enzymes and cellular auto-oxidation reactions (Gnaiger, 2008; Pesta and Gnaiger, 2012). The analysis of ROX in both cell lines proved a significant increase in ROX from an oxygen flow per cells of 4.82 ± 0.4 pmol/(s*10^6) (mean ± S.D., n=3) in HT22S cells up to 8.55 ± 0.5 pmol/(s*10^6) in HT22R cells. These finding indicate that the glutamate resistance induced an increase in ROX combined with a reduction in the respiratory activity. Thus, HT22R cells seem to be less reliable on ATP production during OXPHOS than parental HT22S cells.

3.2.4 Increased Oxidative Phosphorylation Capacity in Glutamate-Resistant HT22R Cells

In order to further analyse the respiratory states and in particular the OXPHOS capacity of the glutamate-sensitive and the glutamate-resistant HT22 cell lines, the oxygen consumption was investigated in digitonin-permeabilized cells in a substrate-uncoupler-inhibitor titration (SUIT) protocol by high-resolution respirometry. In a SUIT protocol, the oxygen consumption of digitonin-permeabilized cells in mitochondrial respiration medium MiR05 gets activated upon addition of mitochondrial substrates and ADP. Figure 16A shows a representative result of a SUIT protocol with HT22S and HT22R cells. At the beginning, the routine endogenous respiration depending on intracellular substrates was measured. In comparison to HT22S cells, HT22R cells showed a reduced routine endogenous respiration (Figure 16B; already published in Pfeiffer et al., 2014). This observation is in agreement to the routine respiration in intact cells (Figure 15C). Glutamate and malate were added and the plasma membrane was permeabilized with digitonin. In both cell lines comparable leak states GM_N with no adenylates added (N) were measured. Respiration was then stimulated adding 2 mM ADP and the OXPHOS state GM_P which is dependent on electron input through complex I into the respiratory system was quantified (illustrated in Figure 16E, left). The OXPHOS state GM_P was significantly enhanced in HT22R cells compared to HT22S cells. Adding succinate further increased the oxygen consumption and the OXPHOS state GMS_P was determined. Here, a convergent electron input over complex I and II into the Q-junction of the respiratory system occurs (illustrated in Figure 16E, centred). The respiratory activity at this respiratory state was additionally significantly increased in HT22R cells (already published in Pfeiffer et

al., 2014). The following second addition of 2 mM was without any major increase in the respiratory activity and thus, a limitation of ADP supply at the OXPHOS state GMS_P could be excluded. By adding cytochrome c the intactness of the outer mitochondrial membrane was confirmed when an increase of less than 15 % was recognized and these experiments were used for analysis. With the ATP synthase inhibitor oligomycin the mitochondrial respiration was inhibited and the respiratory leak state GMS_L was measured, which was similar in both cell lines. The titration of the uncoupler FCCP up to a maximum concentration to induce respiration and to measure the ETS capacity state GMS_E resulted as well in a comparable oxygen flow per cells (illustrated in Figure 16E, right), but the ETS capacity state $S(Rot)_E$, which is dependent on electron input over complex II alone, is significantly increased in HT22R cells in contrast to parental HT22S cells (already published in Pfeiffer et al., 2014). In both cell lines the higher respiratory activity in the ETS capacity states GMS_E compared to the OXPHOS capacity state GMS_P indicated a high excess in their ETS capacity. Thus, the capacity of electron transfer by the respiratory system is not fully used during OXPHOS. Consequently the phosphorylation system limits the OXPHOS capacity in both cell lines. In the last step of the SUIT protocol the complex III-inhibitor antimycin A was added to inhibit mitochondrial respiration and measure ROX which was used for correction of the former measured respiratory states to compare only mitochondrial-dependent oxygen consumption.
In order to compare the fraction of the ETS capacity used for leak respiration GMS_L and OXPHOS capacity state GMS_P, both states were normalized to the maximum flux at state GMS_E (Figure 16C). In comparison to the leak control ratio in intact cells, the L/E (GMS_L/GMS_E) coupling control ratio was comparable in permeabilized HT22S and HT22R cells. The phosphorylation system control ratio or OXPHOS/ETS (P/E) expresses the restriction of the OXPHOS capacity by the phosphorylation system (Gnaiger, 2009). The phosphorylation system control ratio P/E was significantly increased to 0.78 ± 0.04 (mean ± S.D.) in HT22R cells in contrast to 0.62 ± 0.1 in HT22S cells. According to this, HT22S cells utilized only 62 % of their ETS capacity during OXPHOS, while HT22R cells used 78 %. A P/E control ratio smaller 1 ($P/E<1$) in HT22S and R cells reflects that the phosphorylation system executed control over OXPHOS capacity and underlined an excess in the ETS capacity in both cell lines. The decrease of P/E in HT22S compared to HT22R cells reflects a higher limitation of the phosphorylation system in the HT22S cell line and demonstrates a higher capacity of the phosphorylation system in HT22R cells. In addition, the quantified L/P coupling control ratio, which links the result of coupling and restriction by the phosphorylation system ($L/P=(L/E)/(P/E)$; Gnaiger, 2009), was slightly, but not significantly, reduced in the HT22R cells compared to HT22S cells (Figure 16D).

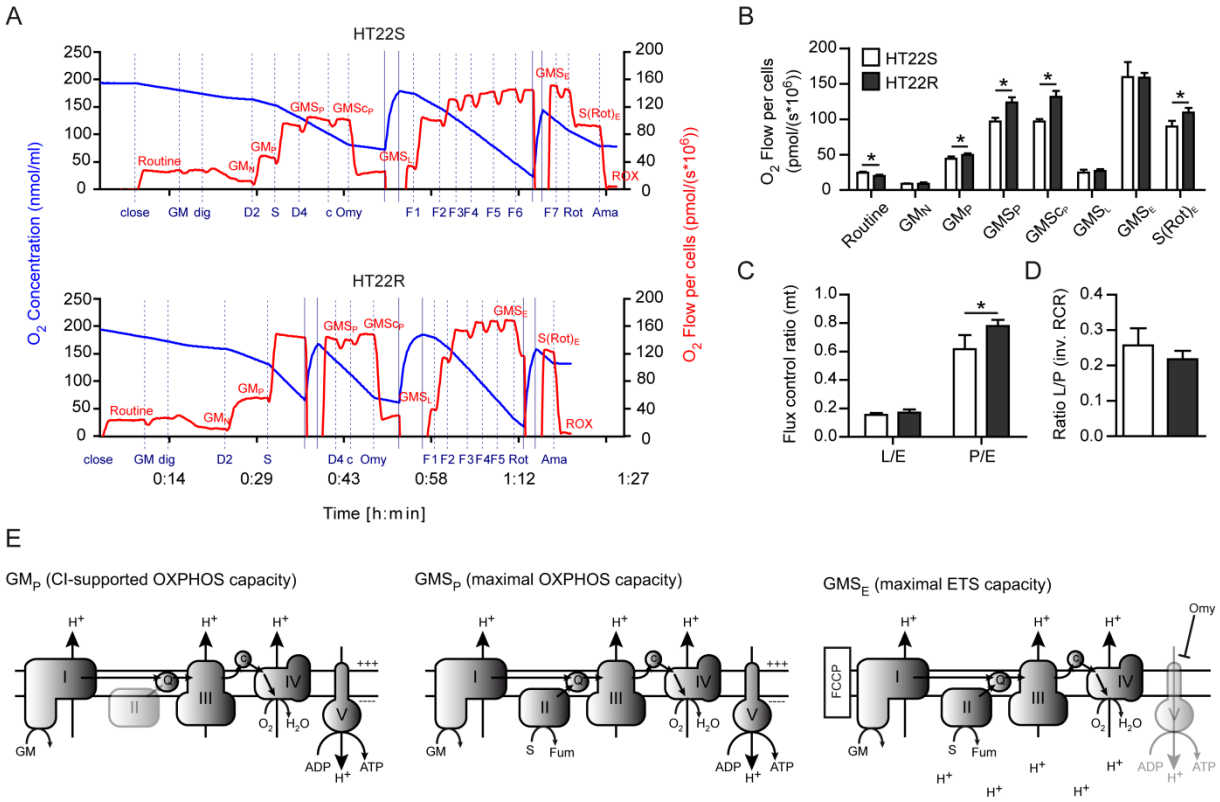

Figure 16: Increased oxidative phosphorylation capacity in glutamate-resistant HT22R cells.
(A) Analysis of the mitochondrial respiration and oxidative phosphorylation capacity was done by high-resolution respirometry with digitonin-permeabilized HT22S and R cells. Shown are representative traces of each cell line representing the oxygen concentration (blue line) and the oxygen flow per cells (red line), whereas the addition of glutamate and malate (GM), digitonin (dig), ADP-Mg^{2+} (D), succinate (S), cytochrome c (c), oligomycin (Omy), FCCP (F), rotenone (Rot) and antimycin A (Ama) are labelled with dashed lines. The re-oxygenation, including opening and closing of the chamber, is marked with solid lines. Sections representing specific respiratory states are labelled in red. The routine endogenous respiration was measured after closing of the chamber. After adding glutamate + malate and permeabilizing the cells with digitonin, the leak state GM_N with no adenylates added (N) was measured. Respiration was stimulated by the addition of 2 mM ADP-Mg^{2+} (D2) and the respiratory state GM_P was recorded followed by adding succinate and ADP-Mg^{2+} to a final concentration of 4 mM (D4) to measure the OXPHOS capacity state GMS_P in which a convergent input of electrons via complex I and II occurs. Addition of cytochrome c proved the intactness of the outer mitochondrial membrane ($GMSc_P$) following application of oligomycin to measure the leak state GMS_L. The titration of FCCP allowed the recording of the ETS capacity at maximum O_2 flow per cells and consequently the determination of the ETS state GMS_E. By inhibition of complex I with rotenone, the ETS state $S(Rot)_E$, which is depending on electron input over complex II alone, was measured and ROX was determined after adding antimycin A in the end. **(B)** Analysis of the ROX-corrected oxygen flow per cells at the indicated mitochondrial respiratory state showed a reduction in endogenous routine respiration beside an increase in the OXPHOS capacity GM_P and GMS_P as well as an increase in the ETS-capacity $S(Rot)_E$ in the glutamate-resistant HT22R cells compared to the glutamate-sensitive cell line HT22S. **(C)** The calculation of the fraction used for leak respiration at state GMS_L (L) and the fraction used for complex I and II-dependent OXPHOS capacity state GMS_P (P) relative to the ETS state GMS_E showed a enhanced P/E ratio in HT22R cells. **(D)** The calculation of the inverse respiratory control ratio (RCR) as L/P revealed no significant differences between both cell lines. Data shown in (B), (C) and (D) come from four independent experiments done in duplets. Bar graphs show the mean ± S.D.. Statistical significance was calculated using Student's two-tailed t-test and is indicated by an asterisks representing a $p<0.05$. **(E)** Illustration of the respiratory states GM_P reflecting complex I-supported respiration (left), GMS_P illustrating maximal OXPHOS capacity with convergent electron input via complex I and II into the Q-junction (Q) (centre; Fum, fumarate) and the respiratory state GMS_E demonstrating the maximal ETS capacity after titration of the protonophore FCCP causing an collapse of the mitochondrial membrane potential by depolarization under inhibition of the ATP synthase through oligomycin (right).

Thus, the analysis of mitochondrial function in glutamate-resistant cells showed a reduced respiration of intact cells in their general growth medium as well as of unpermeabilized cells depending on intracellular substrates in mitochondrial respiratory medium in this experiment. But the OXPHOS capacity depending on complex I alone and with convergent electron input

into the Q-junction through complex I and II were unexpectedly increased in the glutamate-resistant HT22R cells as well as the OXPHOS capacity was less limited by the phosphorylation system in HT22R. Because of this, the functioning of the mitochondrial system seems to be not impaired. Rather the reduced respiratory activity and capacity in intact HT22R cells suggest a deficiency of substrates or even alternative use of substrates in other pathways for energy production to maintain their metabolic activity.

3.2.5 Decreased Lactate Production in Glutamate-Resistant HT22R Cells

The decreased mitochondrial oxygen consumption of intact HT22R cells suggest an alternative use of substrates in other energy producing metabolic pathways with an increase in glucose metabolism in either glycolysis or the parallel pentose phosphate pathway. While NADH is produced in glycolysis, but primarily by β-oxidation of fatty acid and in the tricarboxylic acid (TCA) cycle in mitochondria (Hirst, 2013), NADPH is generated in the pentose phosphate pathway (Stincone et al., 2014). NADPH is used by the GSH reductase for catalyzing the reduction of GSSG to GSH, and hence, for the recovery of the important antioxidant GSH (Dringen, 2000). Enhanced glucose consumption through both the glycolysis and the pentose phosphate pathway and coupled enhanced production of NADH as well as NADPH resulted in a neuroprotective effect against oxidative stress (Soucek et al., 2003). For this reason, we analysed conditioned medium of both cell lines for its glucose and lactate content. The analysis of 24 h-conditioned medium of HT22S and R cells revealed a significant reduction in lactate production by HT22R cells (Figure 17B; already published in Pfeiffer et al., 2014), while the same amount of glucose was consumed by both cell lines (Figure 17A). We assume by this observation that the HT22R cells most likely consume glucose in the pentose phosphate pathway which will be helpful in the production of NADPH that can be used for GSH recovery and can help in the defence against a prolonged glutamate exposure.

3.2.6 G6PD Over-Expression Enhances Total Cellular Glutathione in Glutamate-Sensitive HT22S Cells

The production of NADPH is catalyzed in part by glucose-6-phosphate dehydrogenase (G6PD), the first enzyme of the pentose phosphate pathway, which is often referred to as the rate-limiting enzyme of this pathway (Stincone et al., 2014). Previous studied showed that the over-expression of G6PD induced a protection against oxidative stress caused by increasing GSH production (Salvemini et al., 1999). In order to examine the effect of G6PD in the protection against oxidative glutamate toxicity, I transiently over-expressed G6PD in HT22S cells and analysed enzymatically their total glutathione (GSSG and GSH) content. In

agreement with the observations by Salvemini and colleagues (Salvemini et al., 1999), I saw a significant basal (untreated) increase in total cellular glutathione levels in HT22S cells over-expressing G6PD protein compared to empty vector (EV, peGFP-C1) expressing cells (Figure 17C). The level of total glutathione was comparable enhanced to the level of xCT-expressing cells which were carried along as a control. As described before, xCT is a subunit of the cystine/glutamate antiporter system x_c^- (Sato et al., 1999) which, on the one hand, is up-regulated in HT22R cells (Lewerenz et al., 2006) and, on the other hand, can protect xCT over-expressing HT22S cells against glutamate (Lewerenz et al., 2006; Noack, 2011; Noack et al., 2012). In a time course of 6 h, the treatment with 10 mM glutamate reduced the total glutathione levels in EV, G6PD and xCT over-expressing cells (Figure 17C), but the over-expression of xCT retained a significant increase of total glutathione compared to control cells after 2 and 4 h, while the over-expression of G6PD tended to result in enhanced glutathione levels at all time points. The exposure of G6PD and xCT over-expressing cells to different concentrations of glutamate in a cell viability assay underlined the already described protective effect of xCT against oxidative glutamate toxicity (Figure 17D; Lewerenz et al., 2006; Noack, 2011; Noack et al., 2012). Nevertheless EV and G6PD-expressing cells were similarly susceptible to the induction of oxidative stress by glutamate and died, while approximately 50 % of xCT-expressing cells were still viable at a concentration of 10 mM glutamate after 18 h.

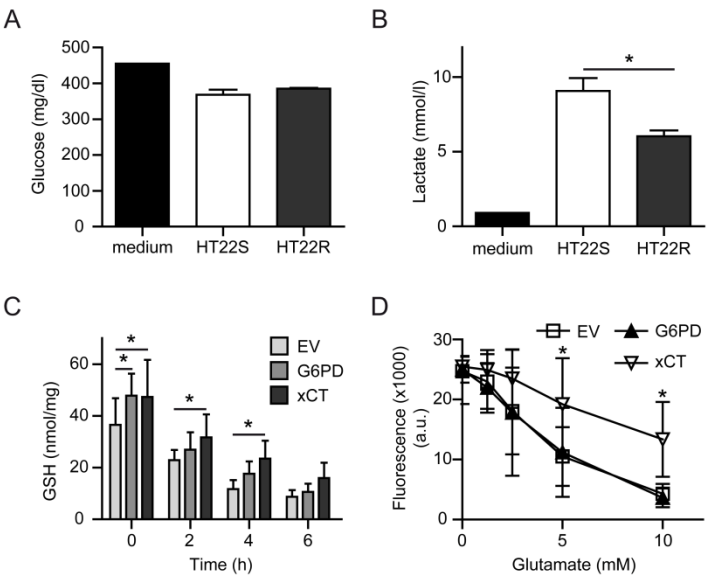

Figure 17: Decreased lactate production in HT22R cells and enhanced total cellular glutathione content in G6PD over-expressing HT22S cells.
(A, B) Analysis of the glucose (A) and lactate (B) content of 24 h-conditioned medium. Medium conditioned by HT22R cells showed a reduced lactate, but similar glucose concentration as medium of HT22S cells. Fresh medium had a glucose concentration of 455 mg/dl and a lactate concentration of 0.9 mmol/l. Data shown in bar graphs display the mean ± S.D. of two independent experiments done in duplets. Statistical significance was proved using Student's two-tailed t-test. **(C)** HT22S cells transiently over-expressing G6PD, xCT or empty vector (EV) were treated with 10 mM glutamate for the indicated time. Their total cellular glutathione content (GSH; GSH and GSSG) was measured enzymatically. Data were collected in three independent experiments done in duplets and are represented as mean ± S.D.. **(D)** To analyse the susceptibility of G6PD, xCT and EV over-expressing HT22S cells to the indicated concentration of glutamate, cells seeded into 96-well plates were treated with glutamate for 18 h. The cell viability was quantified with the CTB reagent. The fluorescence values, represented as mean ± S.D., were plotted against the used glutamate concentrations and were obtained in three independent experiments done in five replicates. Statistical significance in (C) and (D) were calculated using two-way ANOVA posthoc Bonferroni test. Asterisks indicate a $p<0.05$.

As a result, a transient over-expression of G6PD in HT22S cells increased the total glutathione level comparable to xCT-expressing cells, but could only faintly prevent a

glutamate-induced decline down to levels in control cells. In agreement with this observation, control cells as well as G6PD-expressing cells died in a concentration-dependent manner by glutamate, so that G6PD could not prevent cell death induced by glutamate in HT22S cells.

3.3 Effect of Mitochondrial, Cytoprotective GDAP1 on Mitochondrial Form and Function

3.3.1 The Wild Type and Mutated *Gdap1* Over-Expressing and *GDAP1* Knockdown Human Neuroblastoma SH-SY5Y Cell Lines

Previous work in our laboratory identified the outer mitochondrial membrane (Niemann et al., 2005) and novel GST-like protein (Marco et al., 2004) GDAP1 up-regulated in glutamate-resistant HT22R cells (Noack et al., 2012). Even the over-expression of GDAP1 in parental HT22S cells protects this cell line against cell death induced by oxidative glutamate toxicity, and by 12/15-Lox as well as truncated, active BH3-interacting domain death agonist (tBID) over-expression, which induce a subsequent breakdown of the mitochondrial membrane potential and mitochondrial membrane integrity, because GDAP1 increases cellular glutathione (Noack et al., 2012). Therefore, GDAP1 is a mitochondria-localized cytoprotective protein. For this reason, we wanted to study its effect on mitochondrial form and function as an example for another mechanism against stress. Because mutations in *GDAP1* cause in humans the most frequently recessively inherited subtype CMT4A (Baxter et al., 2002; Cuesta et al., 2002) and GDAP1 is expressed in the peripheral and central nervous system, particularly in neurons (Noack et al., 2012; Pedrola et al., 2005), I studied its effect on mitochondria in the human neuroblastoma cell line SH-SY5Y which even expresses endogenously GDAP1 (Pedrola et al., 2005). I generated SH-SY5Y cell lines stably over-expressing full-length wild type *Gdap1*, the disease-causing mutation R310Q (Azzedine et al., 2003) and a control cell line transfected with the empty vector (EV) in addition to cells over-expressing the point mutation S34A. The serine (S) residue at position 34 in the GST-N domain of the amino acid sequence of GDAP1 was predicted to be the responsible amino acid for its potential GST activity (Shield et al., 2006). The stable cell lines were generated with help of the *piggy*Bac transposon technology and subsequent repetitive fluorescence-activated cell sorting (FACS) for the reason that the *piggy*Bac vector is a bicistronic vector encoding the N-terminal hemagglutinin (HA)-tagged protein of interest followed by an internal ribosome entry site (IRES) element and the sequence of the fluorescence marker protein Venus downstream of a strong CAG-promoter. This allows the integration of the transgene into the genome as well as selection and enrichment of Venus-positive clones by repetitive cell sorting without the use of antibiotic selection causing alterations. Figure 18A shows

exemplary the last sort of the SH-SY5Y cell line stably over-expressing wild type GDAP1. The generated cell lines are further referred to as EV, GDAP1, R310Q and S34A.

In order to verify the successful stable transfection of the four cell lines, reverse transcriptase-polymerase chain reaction (RT-PCR) proved the mRNA expression of *Gdap1*, *Gdap1* R310Q and *Gdap1* S34A in the respective cell line in contrast to EV cells showing no PCR product (Figure 18B). EV cells showed no PCR product because one of the primers of each used primer pair was binding outside of the *Gdap1* sequence in the transposon sequence, while the other was binding inside it. These results evidenced the integration of the *piggy*Bac transposon encoding wild type or mutated *Gdap1* into the genome and subsequent mRNA expression. By sequencing of the RT-PCR product, the mutation R310Q and S34A were verified (Supplementary data S1 and S2). In addition, a western blot analysis of total protein extracts of the four cell lines proved the endogenous expression of GDAP1 protein with a predicted size of 40 to 41 kDa in all cell lines (Figure 18C; Pedrola et al., 2005) besides the over-expression of the respective HA-tagged GDAP1 protein in the cell lines GDAP1, R310Q and S34A in contrast to no expression in EV cells. Equal protein loading was proved by detection of β-Actin. The analysis of the cell lines by fluorescence immunocytochemistry using an antibody directed against GDAP1 verified additionally the over-expression of GDAP1 protein in the GDAP1, R310Q and S34A cell line (Figure 18E). In the EV cell line only low GDAP1 protein expression was detectable, which can be explained by endogenous GDAP1 expression (Pedrola et al., 2005). GDAP1 even co-localized with a transiently expressed mitochondrially targeted DsRed2 (mtDsRed) in these cell lines. On the one hand, this confirmed the over-expression of *Gdap1* and on the other hand, the already described localization of GDAP1 to mitochondria (Niemann et al., 2005) in the new generated stable SH-SY5Y cell lines.

In addition, I included the recently described stable SH-SY5Y *GDAP1* knockdown cell line, named *GDAP1* KD, and the control cell line, named pLKO-NT (kind gift of Pla-Martin; Pla-Martin et al., 2013) in my study to corroborate the findings under over-expressing conditions with those under GDAP1 deficiency. Immunoblotting of total cell extracts of *GDAP1* KD and pLKO-NT cells confirmed the silencing of *GDAP1* on protein levels in the *GDAP1* KD cell line, whereas equal protein loading was verified by the detection of β-Actin (Figure 18C).

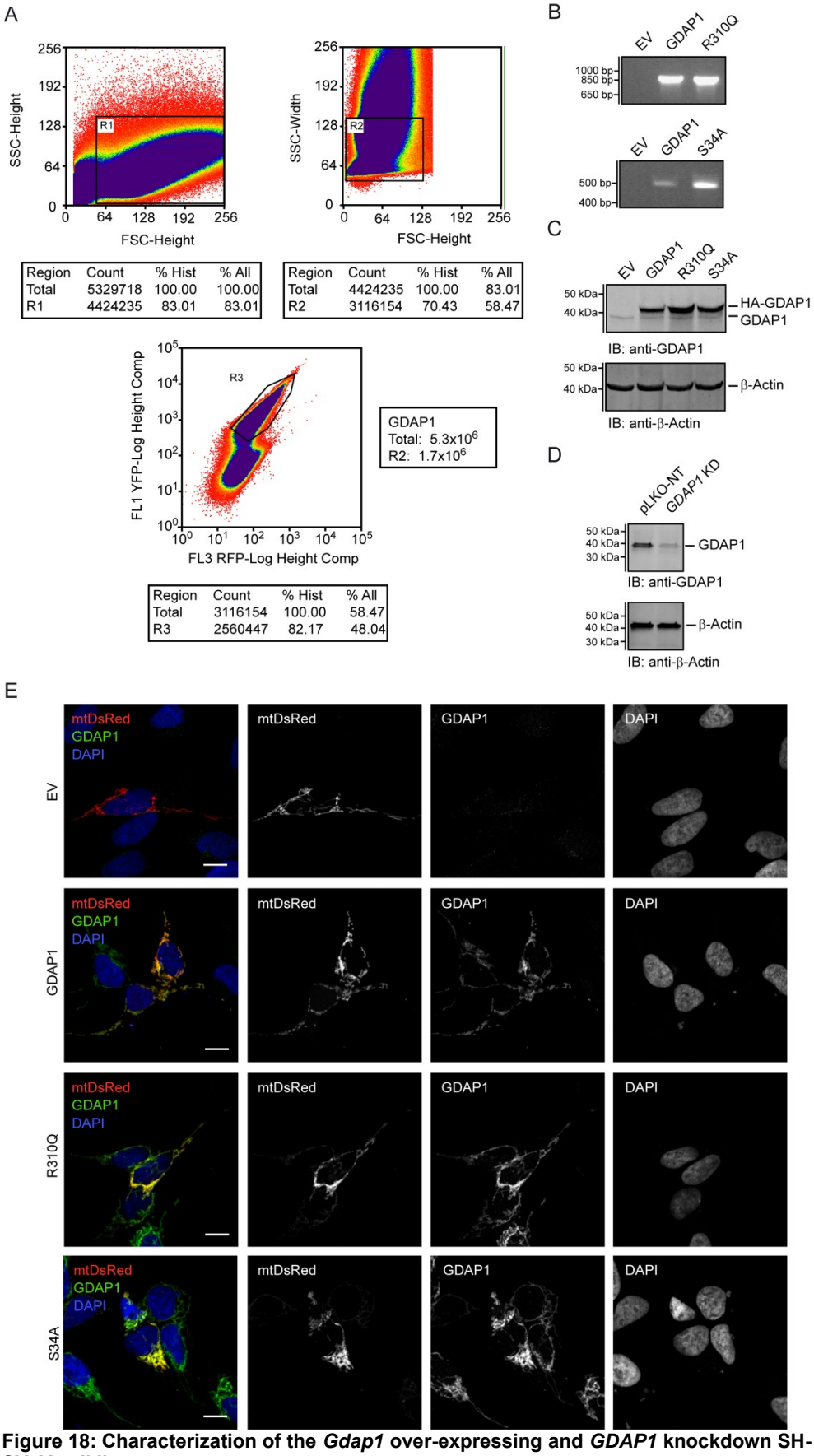

Figure 18: Characterization of the *Gdap1* over-expressing and *GDAP1* knockdown SH-SY5Y cell lines.

(A) The stable SH-SY5Y cell lines EV (empty vector), GDAP1, R310Q and S34A were prepared with help of the *piggy*Bac transposon system and repetitive fluorescence-activated cell sorting to collect and enrich transfected and Venus-positive (yellow fluorescent marker protein) cells. Cells had been transfected with a bicistronic *piggy*Bac vector encoding the

gene of interest (*Gdap1, Gdap1* R310Q and *Gdap1* S34A) followed by the reporter gene (Venus fluorescence protein) downstream of an internal ribosome entry site (IRES) element. Representative, the sixth and final sort of the cell line GDAP1 is displayed. 82.17 % of the gated cells (R3) were Venus-positive and collected. **(B)** The stable over-expression of wild type or mutated *Gdap1* was verified by reverse transcription-polymerase chain reaction (RT-PCR) in SH-SY5Y EV, GDAP1, R310Q and S34A cells. The PCR products for GDAP1 and R310Q in the upper panel and for GDAP1 and S34A in the lower panel evidenced the successful integration of the *piggy*Bac transposon into the genome and the expression of the *Gdap1* mRNA. EV cells showed no PCR product because one primer of the used primer pair binds inside the GDAP1 sequence, while the other anneals in the transposon sequence. **(C)** Western blot analysis of total protein lysates of SH-SY5Y EV, GDAP1, R310Q and S34A cells with an antibody directed against GDAP1 detected a band for the endogenous GDAP1 with a predicted molecular weight of 40 to 41 kDa in all cell lines and an upper band of over-expressed and hemagglutinin (HA)-tagged GDAP1 protein with a predicted size of approximately 42 kDa in GDAP1, R310Q and S34A cells. Equal protein loading was proved with an antibody directed against β-Actin. **(D)** Immunoblot analysis of total protein extracts from SH-SY5Y pLKO-NT and *GDAP1* knockdown (*GDAP1* KD) cells with an GDAP1 antibody detected a band for endogenous GDAP1. Equal protein loading was proved with β-Actin, which verified that the expression of GDAP1 protein is reduced in *GDAP1* KD cells. **(E)** A fluorescence immunocytochemistry analysis of SH-SY5Y EV, GDAP1, R310Q and S34A cells transiently transfected with a mitochondrially targeted DsRed2 (mtDsRed; pDsRed2-mito) proved the mitochondrial localization of GDAP1 detected with an anti-GDAP1 antibody (green), while cell nuclei were stained with DAPI (blue). Exemplary confocal images from one single section show co-localization of GDAP1 expression and mitochondrially targeted DsRed2 (yellowish staining in merge image) in SH-SY5Y GDAP1, R310Q and S34A in mitochondria. SH-SY5Y EV cells display only low levels of endogenous GDAP1 expression. Scale bar represents 10 µm.

3.3.2 Wild Type GDAP1 is a Mitochondrial Fission Factor and GDAP1 S34A Induces Mitochondrial Fusion

Because mitochondrial GDAP1 regulates mitochondrial dynamics and induces mitochondrial fission in COS-7 (Niemann et al., 2005) and HT22S cells (Noack et al., 2012), whereas the disease-associated recessively inherited mutation R310Q lost the ability to induce mitochondrial fragmentation (Niemann et al., 2005; Noack et al., 2012), I investigated the mitochondrial morphology in the new stable SH-SY5Y cell lines EV, GDAP1, R310Q and S34A cells in addition to analyse the mitochondrial appearance in *GDAP1* KD and control (pLKO-NT) cells. Previous investigation claimed that *GDAP1* knockdown induces mitochondrial elongation in NE1-115 cells (Niemann et al., 2005) as well as a similar mitochondrial elongation index, reflecting most likely a similar mitochondrial morphology, had been described for *GDAP1* KD and control cells (Pla-Martin et al., 2013). Therefore, cells transfected with a mitochondrially targeted DsRed2 (mtDsRed) were analysed as described above by a blinded investigator. *GDAP1* KD and pLKO-NT cells possessed surprisingly a difference in their mitochondrial morphology (Figure 19A). *GDAP1* KD cells exposed an increase in cells with fragmented mitochondria at the expense of a decrease in cells with tubular mitochondria, which could explain the previously described reduced mitochondrial interconnectivity in *GDAP1* KD cells (Pla-Martin et al., 2013). Thus, silencing of *GDAP1* changed the mitochondrial shape in SH-SY5Y cells. In comparison to this, wild type GDAP1 acted as described before as a mitochondrial fission factor (Niemann et al., 2005; Noack et al., 2012) and induced mitochondrial fission in SH-SY5Y GDAP1 cells, while disease-

associated mutated GDAP1 R310Q failed to induce mitochondrial fragmentation (Figure 19B). The stable over-expression of S34A induced drastically mitochondrial fusion because in total about 74 % of S34A cells showed a tubular mitochondrial morphology. Previous experiments have already demonstrated that GDAP1 S34A almost completely lost the ability to induce mitochondrial fragmentation in COS-7 cells (Wagner, 2009). As a result, GDAP1 acts as a non-classical mitochondrial fission factor in various cell types including SH-SY5Y cells. Changes in the mitochondrial morphology caused by knockdown or over-expression of wild type GDAP1 protein in addition to the loss-of-function of the disease causing point mutation R310Q suggests an effect of GDAP1 on mitochondrial activity by influencing mitochondrial dynamics. Additionally, the result of the point mutation S34A, the predicted active side residue (Shield et al., 2006), shows that this amino acid and its possible GST activity seems to be important for or connected with GDAP1's fission activity as claimed before (Wagner, 2009). The mutation S34A prevents completely GDAP1's activity as a fission factor, so that it acts dominant negative and induces mitochondrial elongation.

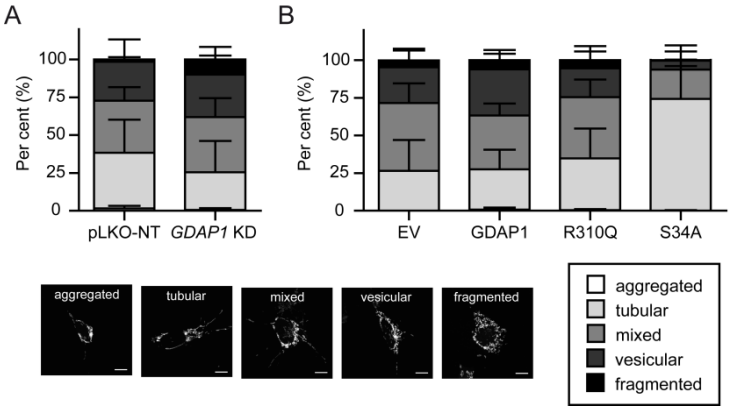

Figure 19: *GDAP1* knockdown and GDAP1 protein over-expression changes the mitochondrial morphology in SH-SY5Y cells.
SH-SY5Y cells were transiently transfected with mitochondrially targeted DsRed2 (pDsRed2-mito) and their mitochondrial morphology was analysed by a blinded investigator. It was distinguished between an aggregated, tubular, mixed, vesicular and fragmented mitochondrial morphology. **(A)** *GDAP1* knockdown resulted in an increase in fragmented mitochondria at the expense of a decrease in cells with tubular mitochondria. **(B)** Over-expression of GDAP1 protein induced mitochondrial fragmentation whereas GDAP1 with the mutation R310Q failed to induce mitochondrial fission. The over-expression of S34A GDAP1 protein caused a drastic increase in mitochondrial fusion. Data in (A) and (B) are represented in mean ± S.D. and were obtained in nine separate experiments. A total of 900 cells were categorized of each cell line. A representative confocal image of each category is shown in the lower section. These images have been already presented in Figure 6. They are shown here in smaller magnification and are displaying only mtDsRed2 expression. Scale bars represent 10 µm.

3.3.3 Silencing of *GDAP1* Enhances Mitochondrial Respiration in Intact SH-SY5Y Cells

The change in the mitochondrial morphology induced by a knockdown of *GDAP1* in SH-SY5Y cells (Figure 19) suggests an impact of GDAP1 on mitochondrial activity. Indeed, investigating the mitochondrial respiration in intact cells in their normal growth medium by high-resolution respirometry revealed a significant increase in mitochondrial respiratory activity under GDAP1 depletion, which is even directly recognizable in the exemplary measurement of the knockdown and control SH-SY5Y cell line in Figure 20A. Knockdown of *GDAP1* increased the basal routine respiration and leak respiration compared to the control (Figure 20B). The ETS capacity was only slightly, but not significantly, enhanced after depletion of GDAP1. Normalization of the routine respiration and ETS capacity in *GDAP1* KD cells to the corresponding respiratory state in pLKO-NT cells showed that the routine respiration was increased by about 1.4-fold and the ETS capacity about 1.1-fold by a knockdown of *GDAP1* (Figure 20D). In addition, the calculation of the flux control ratios indicated that the routine (R/E), leak (L/E) and net routine control ratio (netR/E) used for phosphorylating respiration were significantly enhanced as well as the flux control ratio of oxidative side-reactions normalized to the ROX-uncorrected ETS capacity E' in *GDAP1* KD cells (Figure 20C). Hence, not only the mitochondrial respiration is enhanced by silencing of *GDAP1*, but also the fraction of the total ETS capacity used for non-mitochondrial residual oxygen consumption suggesting an increase in, for example, oxygen consuming enzymes and cellular auto-oxidation reactions (Gnaiger, 2008; Pesta and Gnaiger, 2012). The analysis of ROX in both cell lines showed that ROX was significantly increased from an oxygen flow per cells of 1.14 ± 0.5 pmol/(s*10^6) (mean ± S.D.; n=11) in control cells to 1.91 ± 1.1 pmol/(s*10^6) in *GDAP1* KD cells.

As a consequence, knockdown of *GDAP1* in SH-SY5Y cells increased the basal routine respiration and leak respiration as well as these cells utilized a larger fraction of their maximum ETS capacity for routine respiration, non-phosphorylating leak respiration and phosphorylating respiration. These findings suggest an overall higher mitochondrial respiratory activity caused by silencing of *GDAP1* and support the hypothesis of GDAP1 regulating mitochondrial activity.

3.3.4 Wild Type and Mutated GDAP1 Attenuates the Part of the ETS Capacity Used for Routine and Phosphorylating Respiration

Because *Gdap1* (wild type and mutated) over-expression changes mitochondrial morphology in SH-SY5Y cells, this suggests as well an effect of GDAP1 on mitochondrial activity. According to this, we could previously observe that stable over-expression of *Gdap1*

increases mitochondrial membrane potential and decreased mitochondrial superoxide production and mitochondrial Ca^{2+} content, while the disease-associated GDAP1 point mutation R310Q failed to induce these changes in HT22S cells (Noack et al., 2012). Isolated intact mitochondria of these cells showed even a reduced mitochondrial activity for wild type *Gdap1* over-expressing cells (Noack et al., 2012). For this reason, I studied the effect of wild type and mutated GDAP1 protein over-expression on mitochondrial oxygen consumption in the stable SH-SY5Y cells. Representative respiratory measurements are shown in Figure 20E. The analysis of the ROX-corrected oxygen flow per cells revealed no changes in the routine and non-phosphorylating leak respiration as well as in the ETS capacity between the various *Gdap1* over-expressing cell lines (GDAP1, R310Q and S34A) and in addition in comparison to the EV control cell line (Figure 20F). Only the calculation of the flux control ratios showed differences in the routine control ratio and the net routine control ratio (Figure 20G). The over-expression of wild type GDAP1 significantly decreased the routine control ratio in contrast to the control. The routine control ratio for the cell line over-expressing the disease-causing point mutation R310Q was further significantly reduced in contrast to GDAP1 cells, whereas over-expression of the point mutation S34A significantly enhanced the R/E ratio compared to R310Q cells up to a similar level as in GDAP1 cells. The routine control ratio of S34A cells was not significantly different to control cells. The fraction of the maximum ETS capacity directly utilized for ATP production, as expressed in the net routine ratio, was significantly decreased in all over-expressing cells independent of the expression of either wild type or mutated GDAP1 in contrast to the control. But the S34A cell line showed a similar netR/E ratio as the wild type GDAP1 over-expressing cell line.

Thus, the stable over-expression of either wild type *Gdap1* or mutated *Gdap1* with the point mutation R310Q and S34A did not change the overall mitochondrial oxygen consumption of intact cells. But the observed changes in the flux control ratio indicated that over-expression of *Gdap1* and *Gdap1* R310Q reduced the fraction of the ETS capacity used for routine respiration. More remarkable was the effect on the net routine ratio, which was significantly reduced in all over-expressing cells. According to this, the cells use a smaller fraction of their ETS capacity for phosphorylating respiration in their basal routine respiration that let us assume an impaired OXPHOS capacity in over-expressing cells.

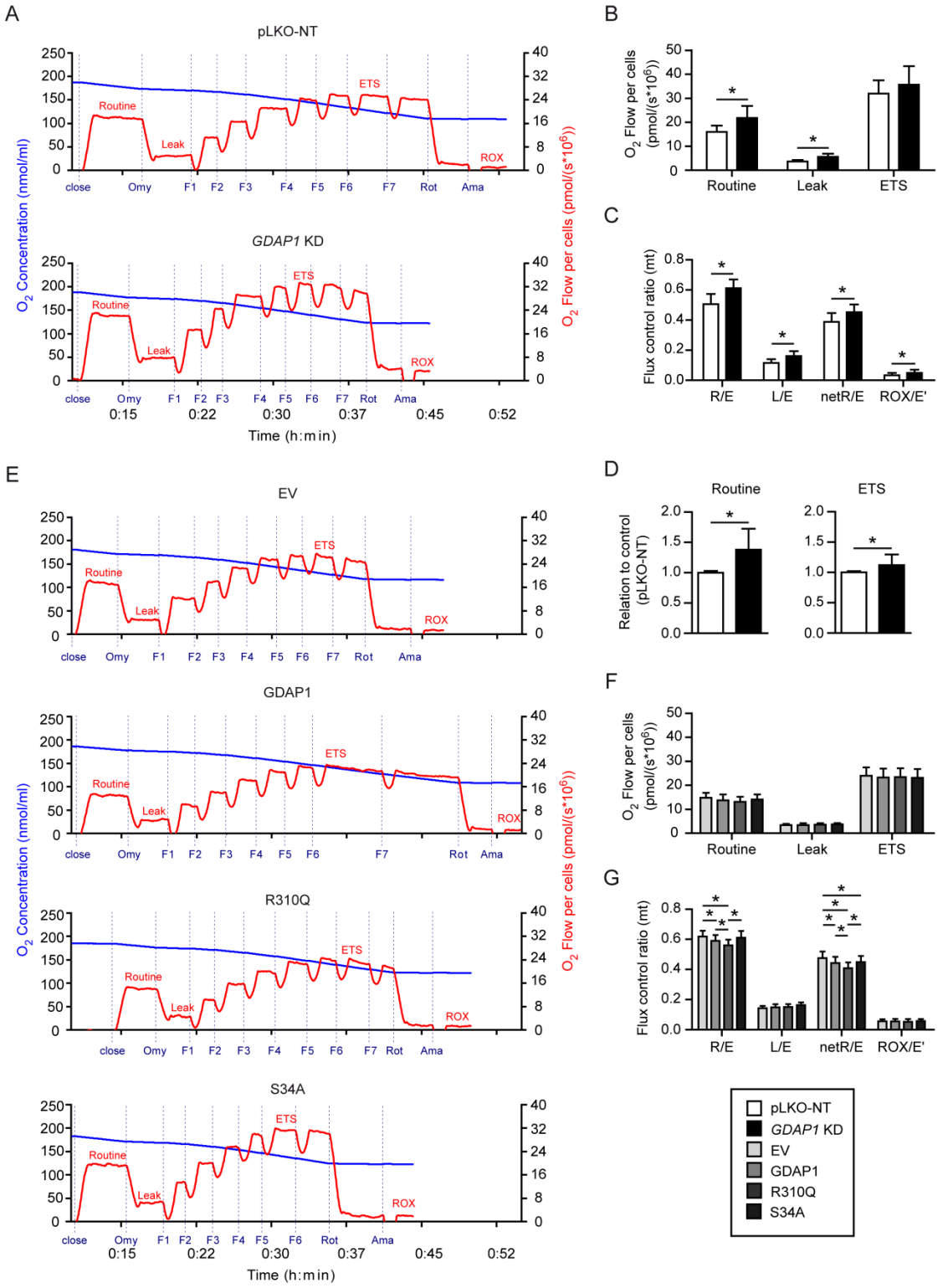

Figure 20: *GDAP1* knockdown induces an increase in mitochondrial respiration, whereas wild type and mutated *Gdap1* over-expression decreases the fraction of the ETS capacity used for routine and phosphorylating respiration in SH-SY5Y cells.

The mitochondrial oxygen consumption of the SH-SY5Y cell lines pLKO-NT, *GDAP1* KD, EV, GDAP1, R310Q and S34A was analysed by high-resolution respirometry. Displayed are measured typical traces of the SH-SY5Y cell lines pLKO-NT and *GDAP1* KD **(A)** and of SH-SY5Y EV, GDAP1, R310Q as well as S34A cells **(E)** showing the oxygen concentration (blue line) and the oxygen flow per cells (red line). The addition of the inhibitors oligomycin (Omy), rotenone (rot) and antimycin A (Ama) and titration of the uncoupler FCCP (F including step number) are marked with dashed lines, whereas the determined corresponding respiratory states are labelled. **(B)** *GDAP1* KD ($1.5 \pm 0.4*10^6$ cells/ml; mean ± S.D) induced an increased ROX-corrected oxygen flow per cells at routine respiration and leak respiration, while the ETS capacity remained unchanged compared to pLKO-NT cells (control; $1.7 \pm 0.5*10^6$ cells/ml). **(C)** Normalization of the ROX-corrected, mitochondrial (mt) routine respiration (state R), leak respiration (state L) and the fraction of phosphorylating respiration (netR=R-L) to the ETS capacity (state E) as well as

the normalization of oxidative side reaction ROX to the ROX-uncorrected total ETS capacity (E') showed an increase upon *GDAP1* KD of all flux control ratios compared to the control. **(D)** The routine respiration and ETS capacity of the *GDAP1* KD cells was expressed in relation to the corresponding respiratory state in the control. The routine respiration was 1.4-fold and the ETS capacity 1.1-fold higher in *GDAP1* KD cells in contrast to control cells. **(F)** The quantitative analysis of the ROX-corrected oxygen flow per cells of EV ($1.9 \pm 0.3*10^6$ cells/ml; mean ± S.D.), GDAP1 ($1.9 \pm 0.4*10^6$ cells/ml), R310Q ($2.0 \pm 0.2*10^6$ cells/ml) and S34A ($2.1 \pm 0.4*10^6$ cells/ml) SH-SY5Y cells revealed no changes in the overall mitochondrial oxygen consumption. **(G)** Calculation of the flux control ratio R/E, L/E, netR/E and ROX/E' showed a reduction of the routine control ratio (R/E) in GDAP1 and R310Q cells and in the fraction of the ETS capacity used for ATP production (netR/E) in the SH-SY5Y cell lines GDAP1, R310Q and S34A compared to EV cells. The leak control ratio (R/E) and the flux control ratio of oxidative side reactions (ROX/E') remained comparable in all cell lines. Data presented in bar graphs in (B, C and D) as well as (F and G) show mean ± S.D. which were collected in eleven separate experiments done in duplets. Statistical significance is indicated with an asterisk ($p<0.05$) and was verified using Student's two-tailed t-test (B, C and D) and two-way ANOVA followed by Bonferroni posttests (F and G).

3.3.5 Silencing of *GDAP1* Elevates Mitochondrial Respiratory Activity Including OXPHOS Capacity

The respiratory measurement of the intact SH-SY5Y cell lines pLKO-NT and *GDAP1* KD demonstrated that silencing of *GDAP1* induced an overall increase in the mitochondrial respiratory activity. To further analyse the mitochondrial oxygen consumption and to investigate especially the OXPHOS capacity, I examined the mitochondrial respiration in digitonin-permeabilized cells in mitochondrial respiration medium in a SUIT protocol. One typical measurement of each cell line is shown in Figure 21A. The routine respiration was significantly increased in *GDAP1* KD cells compared to the control (Figure 21B). Thus, the result from the previous experiment with intact cells (Figure 20B) could be reproduced in this experiment, however, intact cells have access to substrates from the growth medium, whereas permeabilized cells are depending on endogenous substrates. In addition to the routine respiration, the leak respiration GM_N, but more impressively the OXPHOS capacity GM_P depending on electron input over complex I as well as the OXPHOS capacity GMS_P with convergent complex I and II electron input into the Q-junction were significantly enhanced in *GDAP1* KD cells. Additionally, knockdown of *GDAP1* increased the leak state GMS_L, ETS state GMS_E with convergent complex I and II electron input and the ETS state $S(Rot)_E$ depending on electron input over complex II into the respiratory system. Thus, the respiratory activity of *GDAP1* KD cells was not only increased in intact cells, but also the OXPHOS analysis in digitonin-permeabilized cells showed an increase in the OXPHOS capacity and ETS capacity induced by a knockdown of *GDAP1*. As a result, these cells show a drastic increase in the respiratory capacity which suggests that *GDAP1* KD cells provide their energy supply mainly through OXPHOS. Consequently, a knockdown of *GDAP1* appears to induce a shift towards mitochondrial energy production and GDAP1 seems to be important to regulate mitochondrial function.

3.3.6 Over-Expression of Wild Type or Mutated *Gdap1* Causes Decreasing OXPHOS and ETS Capacity in SH-SY5Y Cells

Previous experiments analysing the ATP production in isolated mitochondria of stable HT22S cells demonstrated a significant reduced mitochondrial respiratory activity for GDAP1 cells, while the respiratory activity of R310Q cells was only slightly decreased (Noack et al., 2012). In order to analyse OXPHOS in the stably over-expressing wild type or mutated GDAP1 SH-SY5Y cell lines, I next investigated the respiratory activity of digitonin-permeabilized cells as described before by high-resolution respirometry. In agreement with the respiratory activity of intact cells (Figure 20F), the routine endogenous respiration as well as the two measured leak states GM_N and GMS_L were comparable in all cell lines (Figure 21D). The OXPHOS capacity state GM_P induced by glutamate/malate and subsequent ADP addition after digitonin permeabilization were similar in all cell lines. Over-expression of wild type and S34A GDAP1 protein slightly, but comparably decreased the OXPHOS state GM_P. The disease-associated R310Q mutation further decreased OXPHOS state GM_P, although this reduction was still not remarkably different to the control. In addition, stable over-expression of *Gdap1* or *Gdap1* with the point mutation S34A induced a similar slight decrease of the OXPHOS state GMS_P, while GMS_P was significantly reduced in R310Q cells compared to control EV cells. However, the ETS state GMS_E depending on convergent complex I and II electron input proved to be significantly different between the cell lines. Over-expression of wild type *Gdap1* and disease-causing mutated *Gdap1* R310Q significantly decreased the ETS state GMS_E, whereas the reduction was stronger in the stable cell line with the disease-associated point mutation. The S34A cell line showed only a slight reduction in GMS_E compared to the control. The final quantification of the ETS state $S(Rot)_E$ with an electron input over complex II alone after inhibiting complex I with rotenone revealed only minor changes between the cell lines.

In conclusion, over-expression of wild type and mutated *Gdap1* changed to various degrees the mitochondrial respiration and respiratory capacity of SH-SY5Y cells. The most severe changes were detectable for the disease-causing mutation R310Q. The stable over-expression of this point mutation decreased the OXPHOS state GMS_P and the ETS state GMS_E, while GDAP1 slightly influenced the mitochondrial respiration. This indicates that GDAP1, but even stronger the disease-associated GDAP1 R310Q, influences certain aspects of mitochondrial respiration and diminishes the mitochondrial respiratory activity, which suggests a role of GDAP1 in regulating mitochondrial respiratory activity. Surprisingly, R310Q seems not to lose its decreasing effect on mitochondrial respiratory activity although it fails to induce mitochondrial fission.

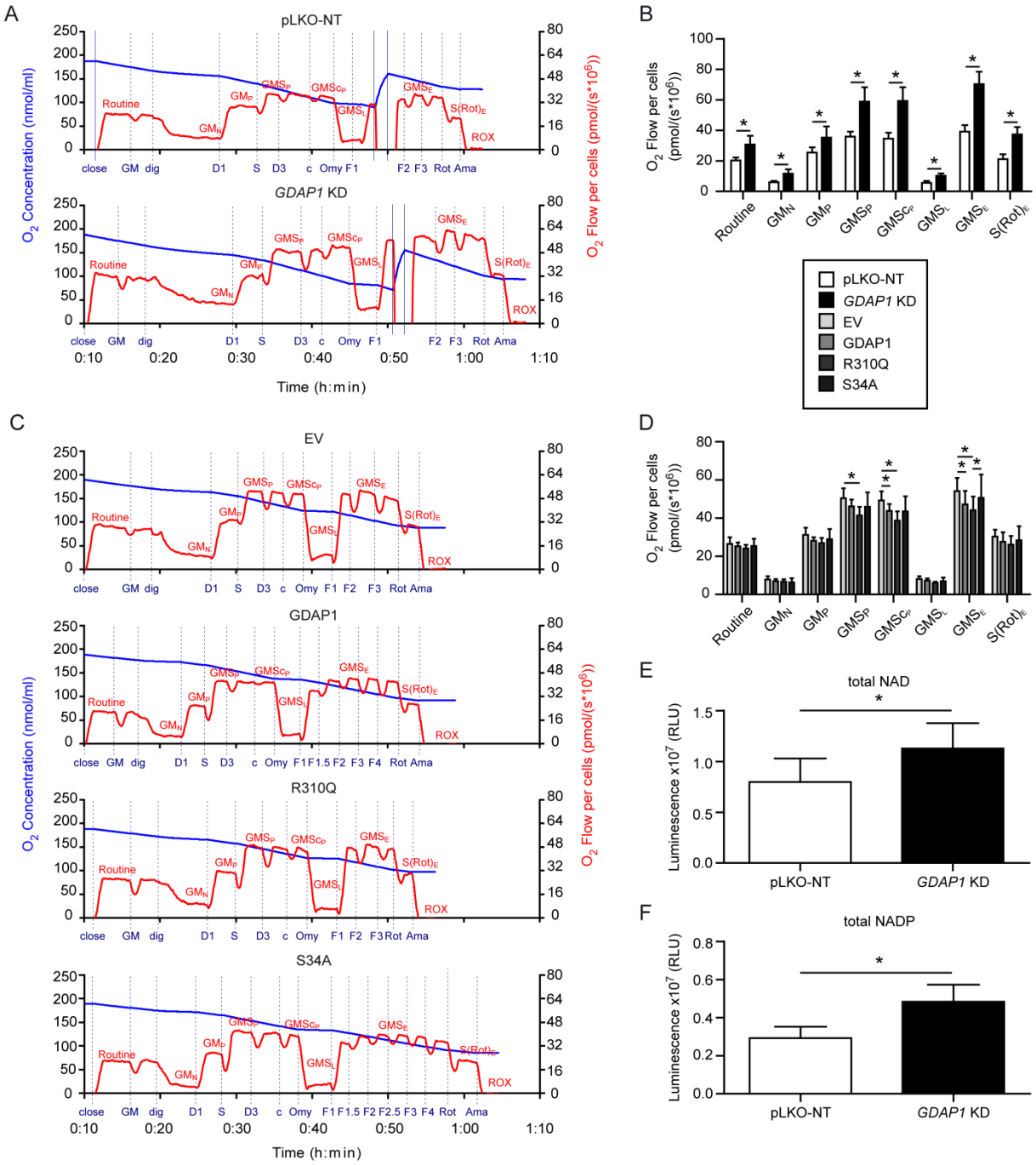

Figure 21: *GDAP1* knockdown increases mitochondrial respiration and *Gdap1* over-expression decreases in varying extent the OXPHOS and ETS capacity in permeabilized SH-SY5Y cells.
The mitochondrial respiration and oxidative phosphorylation capacity was analysed in the *GDAP1* knockdown and *Gdap1* over-expressing cell lines in digitonin-permeabilized cells with the Oxygraph-2k. One typical measurement of mitochondrial respiration in the *GDAP1* KD and pLKO-NT control cell line are displayed in **(A)** and representative traces of the over-expressing cell lines EV, GDAP1, R310Q and S34A are presented in **(C)**. The oxygen concentration is indicated with a blue line, the oxygen flow per cells with a red line and the application of glutamate and malate (GM), digitonin (dig), ADP-Mg^{2+} (D; D-1mM (D1) and D-3mM (D3)), succinate (S), cytochrome c (c), oligomycin (Omy), FCCP (F), rotenone (Rot) and antimycin A (Ama) are labelled with vertical dashed lines. Re-oxygenation of the chamber (opening and closing) is marked with solid lines. The sections presenting defined respiratory states are labelled in red. **(B)** *GDAP1* knockdown (*GDAP1* KD) showed a clear increase in the ROX-corrected oxygen flow per cells at all respiratory states compared to the control cell line pLKO-NT. In the analysed experiments in average $1.9 \pm 0.1*10^6$ cells/ml (mean ± S.D.) pLKO-NT cells and $1.4 \pm 0.2*10^6$ cells/ml *GDAP1* KD cells were used. **(D)** Over-expressing wild type or mutated *Gdap1* did not influence the respiratory states routine, GM_N, GM_P, GMS_L and $S(rot)_E$, but the OXPHOS state GMS_P and the ETS capacity state GMS_E, both depending on convergent electron input through complex I and II in the respiratory system, were attenuated in variable degree. For analysis $1.2 \pm 0.1*10^6$ cells/ml EV, $1.2 \pm 0.2*10^6$ cells/ml GDAP1, $1.5 \pm 0.3*10^6$ cells/ml R310Q, and $1.3 \pm 0.2*10^6$ cells/ml S34A cells were used in each experiment. **(E)** Detection of total oxidized and reduced nicotinamide adenine dinucleotides (NAD^+ and NADH; total NAD) in SH-SY5Y

pLKO-NT and *GDAP1* KD cells using the bioluminescent assay NAD/NADH-Glo Assay. Total NAD was increased in *GDAP1* KD cells compared to the control, which is visible in an increase in the luminescence measured in relative light units (RLU). **(F)** Using the bioluminescent assay NADP/NADPH-Glo Assay total oxidized and reduced nicotinamide adenine dinucleotides phosphates ($NADP^+$ and NADPH; total NADP) were detected which showed that total NADP was increased in *GDAP1* KD cells compared to the control. Data in (E) and (F) were collected in three independent experiments conducted in quadruplicates, while data shown in (B) and (D) were obtained in five and six independent experiments, respectively. Bar graphs represent the mean ± S.D. and an asterisk reflects a $p<0.05$. Statistical significance in (B), (E) and (F) was calculated using Student's two-tailed t-test, while two-way ANOVA followed by Bonferroni posttest was conducted in (D).

3.3.7 Increased total NAD and NADP in *GDAP1* Knockdown Cells

GDAP1 KD SH-SY5Y cells displayed increased mitochondrial respiratory activity and capacity. These observations suggest that these cells seem to sustain their energy demand mainly by mitochondrial activity through OXPHOS. NADH is the substrate for complex I which is the largest and one of the key enzymes of the mitochondrial respiratory system in eukaryotic cells (reviewed in Hirst, 2013). NADH gets produced mainly by β-oxidation of fatty acid and in the TCA cycle in mitochondria and to a lesser extent in glycolysis (Hirst, 2013). Because of the increased mitochondrial respiration in SH-SY5Y cells under *GDAP1* knockdown, I analysed the total oxidized and reduced nicotinamide adenine dinucleotides (NAD^+ and NADH) content of this cell line compared to its control cell line pLKO-NT using a bioluminescent assay. This analysis indicated a significant increase in total NAD in the *GDAP1* KD cells (Figure 21E). Thus, this increase is matching with an enhanced mitochondrial activity. The increased total NAD seems to demonstrate a sufficient supply of probably NADH for complex I-supported respiration in mitochondria. Combined with the increased mitochondrial respiration, this let us assume an enhanced mitochondrial production of NADH in the TCA cycle, through β-oxidation of fatty acid and glycolysis. For the reason that increased glucose consumption in glycolysis and pentose phosphate pathway protect against oxidative stress by elevating the production of NADH and NADPH (Soucek et al., 2003), I analysed additionally total oxidized and reduced nicotinamide adenine dinucleotides phosphates ($NADP^+$ and NADPH) in both cell lines using a respective bioluminescent assay. The analysis proved that in addition to total NAD, even total NADP is increased by a knockdown of *GDAP1* in SH-SY5Y cells (Figure 21F). These results suggest that *GDAP1* knockdown increases glucose consumption in glycolysis and pentose phosphate pathway besides increasing strongly mitochondrial respiratory activity.

3.4 The Effect of Cytoprotective GDAP1 in Preventing Alterations of Mitochondrial Form and Function Induced by Acute Oxidative Stress

3.4.1 *Gdap1* Over-Expression Protects SH-SY5Y Cells from Ethacrynic Acid-Induced Mitochondrial Fusion

Because of GDAP1's function as a cytoprotective protein protecting against oxidative stress by increasing cellular glutathione (Noack et al., 2012), its demonstrated GST activity (Wagner, 2009) in combination with its role as a non-classical fission factor (Niemann et al., 2005) and in this study observed influence on mitochondrial function (Figure 20/21), we hypothesize that GDAP1 can recognize the cellular or local redox state with its GST domains inducing an adjustment of the mitochondrial morphology and function. It may even change the energy production of the cell, although its function as a GST protein (Wagner, 2009) and its cytoprotective effect by increasing cellular glutathione (Noack et al., 2012) is contradictory to the classical function of GSTs catalyzing the nucleophilic addition of reduced GSH to electrophilic substrates, non-polar compounds containing an electrophilic nitrogen, carbon or sulphur atom, which reduces GSH levels (Hayes et al., 2005). In order to prove this hypothesis, I analysed whether over-expression of *Gdap1* in SH-SY5Y cells can prevent the mitochondrial changes induced by EA and MQ as observed in the parental SH-SY5Y cells (Figure 11). We expected that the GSH depleting activity of EA (Seyfried et al., 1999; Wullner et al., 1999) and MQ (Chiou and Tzeng, 2000; Kim et al., 2014) induces a change in the redox state which forces GDAP1 to react. In addition, I investigated if GDAP1 with the disease-associated point mutation R310Q and the point mutation S34A with mutation of the possible active amino acid residue (S34) in the GST-N domain (Shield et al., 2006) influences the hypothesized function as a redox sensor. In order to examine the mitochondrial morphology in the stable SH-SY5Y cell lines under the same experimental conditions as before, oxidative stress was induced in cells transiently transfected with mitochondrially targeted DsRed2 by a treatment with 30 µg/ml EA or 20 µM MQ for 1 h. Because both EA and MQ were solved in absolute ethanol and the treatment of the different cell lines with this vehicle resulted in a similar distribution of cells in the five categories in every cell line, the results of vehicle-treated cells of each cell line were combined in one column (Figure 22). Treating the stable SH-SY5Y cell lines with EA induced mitochondrial fusion as expected (Figure 11; (Bowes and Gupta, 2005; Soltys and Gupta, 1994) in EV, R310Q and S34A cells (Figure 22A). In S34A cells, which show mainly a tubular mitochondrial morphology in vehicle-treated cells, EA further increased mitochondrial fusion (Figure 22A). Nevertheless, GDAP1 prevented the induction of mitochondrial fusion induced by EA. EA- and vehicle-treated GDAP1 cells displayed a quite similar distribution in the five mitochondrial categories. However, a treatment with MQ, which induces mitochondrial

fragmentation (Figure 11; Loor et al., 2010), induced an increase in the mitochondrial categories vesicular and fragmented in EV, R310Q, S34A as well as in GDAP1 cells. In GDAP1 cells which showed increased mitochondrial fission in vehicle-treated cells, mitochondrial fragmentation was further increased after a treatment with MQ (Figure 22A), which is probably due to the fact that GDAP1 is a mitochondrial fission factor (Niemann et al., 2005). Thus, GDAP1 prevented mitochondrial fusion induced by EA, while EA provoked mitochondrial elongation in S34A and R310Q cells. In comparison to the effect of EA on GDAP1 cells, these results suggest that the point mutations have resulted in a lost activity of GDAP1 to prevent mitochondrial fusion. The importance and already claimed possible connection (Wagner, 2009) of the predicted GST active side residue S34 (Shield et al., 2006) for its fission activity gets supported by this observation.

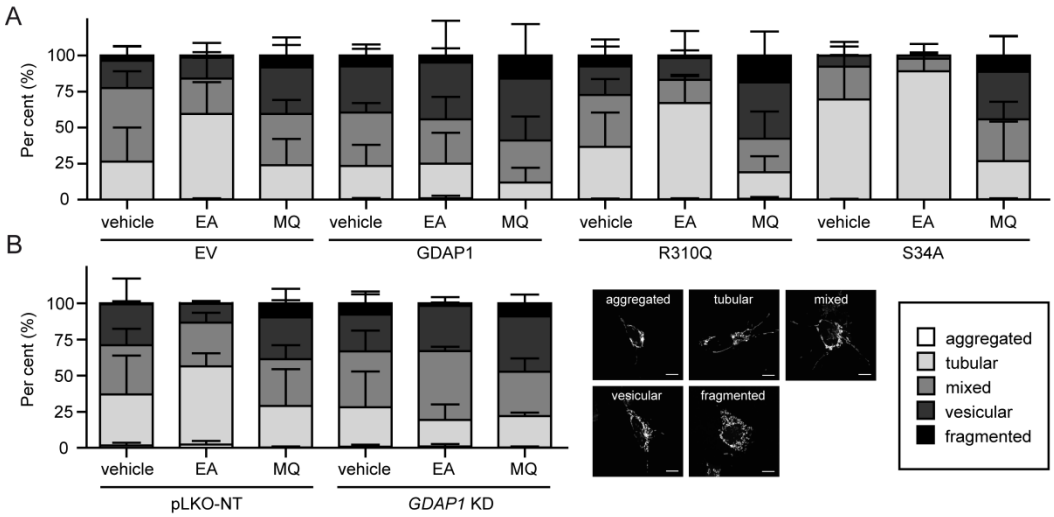

Figure 22: Induction of oxidative stress by ethacrynic acid or menadione influences the mitochondrial morphology of *Gdap1* over-expressing and *GDAP1* knockdown SH-SY5Y cells.

The stable SH-SY5Y cell lines EV, GDAP1, R310Q and S34A as well as SH-SY5Y pLKO-NT and *GDAP1* KD were transfected transiently with mitochondrially targeted DsRed2 (pDsRed2-mito). After a 1 h-treatment with 30 µg/ml ethacrynic acid (EA) or 20 µM menadione (MQ), the mitochondrial morphology was analysed by fluorescence microscopy and categorized by a blinded investigator. It was distinguished between an aggregated, tubular, mixed, vesicular and fragmented category as described before. As a control, each cell line was treated with the vehicle ethanol. The results from vehicle-treated cells for each cell line were combined in the respective vehicle treated column. Confocal images of each category displayed in the right lower section had been represented before and are shown here in smaller magnification. These images are displaying only mitochondrially targeted DsRed2 expression. Scale bars represent 10 µm. **(A)** Treating SH-SY5Y cells EV, R310Q and S34A with EA induced elongation of mitochondria, whereas wild type GDAP1 prevented this change in mitochondrial morphology. The treatment with MQ triggered mitochondrial fission in all four cell lines and further increased basal mitochondrial fragmentation in GDAP1 cells. **(B)** Treating SH-SY5Y cell lines pLKO-NT and *GDAP1* KD with EA induced mitochondrial elongation in control cells, whereas *GDAP1* KD cells showed an increased mixed mitochondrial shape. MQ-treatment changed the mitochondrial morphology of both cell lines to a more fragmented phenotype. The results shown in (A) and (B) are presented in mean ± S.D. and were conducted in three independent experiments in which per cell line and condition 100 cells were categorized.

3.4.2 Ethacrynic Acid-Induced Mitochondrial Fusion Activity Is Impaired in *GDAP1* KD Cells

Since GDAP1 prevents mitochondrial fusion induced by EA, but cannot avoid an increase in MQ-induced mitochondrial fission, I investigated the changes in mitochondrial morphology of *GDAP1* KD cells after initiation of oxidative stress. As previously, cells transfected with mitochondrially targeted DsRed2 were either treated with 30 µg/ml EA or 20 µM MQ for 1 h before analysing their mitochondrial morphology. MQ triggered mitochondrial fission in *GDAP1* KD cells as well as in the control pLKO-NT cell line (Figure 22B). However, EA induced mitochondrial fusion only in the control cell line. The *GDAP1* KD cells showed astonishingly an increase in the category vesicular and mixed at the expense of a decrease of cells with elongated mitochondria. To remember, the mixed category describes the appearance of fragmented as well as tubular mitochondria in the same cell. According to these observations, MQ induced mitochondrial fission in *GDAP1* KD and control pLKO-NT cells as well as in the wild type and mutated *Gdap1* over-expressing SH-SY5Y cell lines. But EA did not trigger remarkably mitochondrial fusion in *GDAP1* KD cells. In comparison, EA was able to induce considerably mitochondrial fusion in control pLKO-NT cells. Thus, *GDAP1* KD cells as well as wild type *Gdap1* over-expressing cells are surprisingly both excluded from the induction of mitochondrial fusion induced by EA.

3.4.3 Mitochondrial Respiration is Less Severely Reduced by Ethacrynic Acid in *Gdap1* Over-Expressing SH-SY5Y Cells

Because of the function of GDAP1 to protect HT22S cells against oxidative glutamate toxicity through an increase of total cellular glutathione (Noack et al., 2012), I analysed if GDAP1 can reduce or even prevent the induced reduction of mitochondrial respiration observed in EA-treated SH-SY5Y cells (Figure 12) or described impaired mitochondrial enzyme activity like in other cell types (Seyfried et al., 1999; Wullner et al., 1999) and tested whether the point mutation R310Q or S34A can change the outcome of this experiment. For the reason that GDAP1 cells are protected against mitochondrial fusion (Figure 22), it is more likely that they also have an advantage to prevent changes in the mitochondrial respiration induced by EA. As described before, cells were treated with 30 µg/ml EA for 1 h before the mitochondrial respiration was investigated. The analysis of the ROX-corrected oxygen flow per cells showed that the basal routine respiration and ETS capacity was not only significantly reduced in EV and GDAP1 cells, but also in R310Q and S34A cells (Figure 23A). But the EA-induced reduction in routine respiration and ETS capacity of R310Q and S34A cells were even significantly stronger than the reduction in GDAP1 cells as well as the ETS capacity was further decreased in comparison to EV cells. The leak respiration remained comparable

in all vehicle- and EA-treated cell lines. Calculation of the flux control ratio revealed only minor differences between the cell lines because the fraction of the maximal ETS capacity used for routine respiration (R/E) and the fraction of the uncorrected-ETS capacity used for compensating ROX (ROX/E') were similar in all cell lines (Figure 23B). However, the leak control ratio (L/E) of EA-treated S34A cells was significantly enhanced compared to treated EV and R310Q cells and in contrast to the vehicle-treated S34A cells. The net routine control ratio, representing the part of routine respiration used for phosphorylating respiration normalized with state E, was significantly decreased in EA-treated GDAP1 and S34A cells, whereas the reduced netR/E ratio of EA-treated S34A cells was even further significantly reduced in contrast to EV and GDAP1 cells. In order to recognize changes in the reduction of the routine respiration and ETS capacity between vehicle-treated and treated cells of each cell line, I normalized the ROX-corrected oxygen flow per cells of EA-treated to that of vehicle-treated cells of the same cell line. Besides a significant relative reduction in the routine and ETS capacity of vehicle-treated versus EA-treated cells of each cell line (not indicated), I realised that the reduction of the routine respiration and the ETS capacity was less severe in treated GDAP1 cells in contrast to that of treated EV cells (Figure 23C). The routine respiration of GDAP1 cells was reduced to approximately 71.3 % (n=4) and in EV cells to roughly 61.7 % after an exposure to EA in relation to the untreated counterpart of vehicle-treated GDAP1 and EV cells, respectively. In EA-treated GDAP1 cells the ETS capacity was only reduced to about 73.2 %, while in EV cells it was further decreased to approximately 65.3 % in relation to vehicle-treated cells. Furthermore, in S34A cells the reduction of the routine respiration and the ETS capacity was in relation significantly stronger than in GDAP1 cells (Figure 23C) as well as the reduction of the ETS capacity was significantly stronger in R310Q compared to GDAP1 cells. Thus, EA had the strongest impact on S34A cells. In conclusion, these findings showed that in addition to preventing mitochondrial fusion induced by EA, wild type GDAP1 is able to avoid a less severe reduction of the routine respiration and ETS capacity. Additionally, the relative reduction in the routine respiration and ETS capacity of S34A cells was comparable to control EV cells, so that in contrast to wild type GDAP1, GDAP1 S34A is not able to prevent this decrease suggesting that the amino acid S34, the predicted active side residue for GST activity (Shield et al., 2006), is necessary for inhibiting this reduction. In addition, its function as a mitochondrial fission factor is very important to avoid a severe relative reduction in mitochondrial respiration because both GDAP1 R310Q and S34A with lost fission activity could not prevent it.

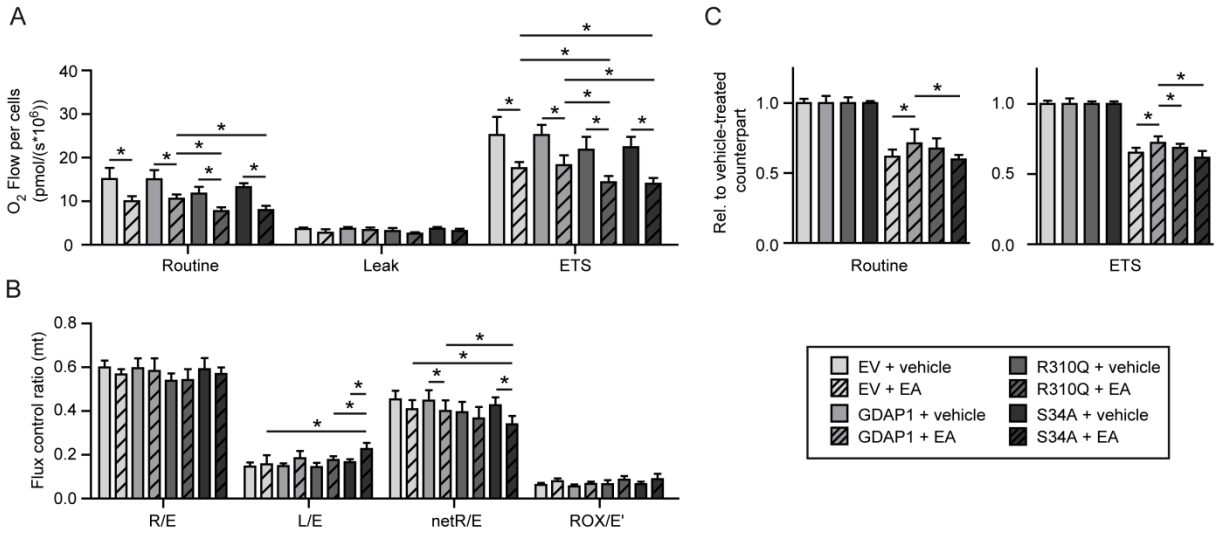

Figure 23: A less severe EA-induced reduction of mitochondrial respiration in GDAP1 cells.
The SH-SY5Y cell lines were examined for their mitochondrial oxygen consumption in their general growth medium after a treatment with 30 µg/ml EA for 1 h using the Oxygraph-O2k. Vehicle-treated cells were carried along for comparison. **(A)** Quantitative analysis of the ROX-corrected respiratory states routine, leak and the ETS capacity showed significant reductions of routine respiration and ETS capacity after an exposure to EA. In comparison to EA-treated GDAP1 cells, the cell lines with over-expressing mutated GDAP1 R310Q and S34A protein showed further reductions of routine respiration and ETS-capacity after a treatment with EA. **(B)** Calculated flux control ratios indicated similar results in the routine control ratio (R/E) and the flux of oxidative side-reaction normalized to the uncorrected total state E' (ROX/E') in all vehicle-treated compared to EA-treated cell lines. The leak control ratio (L/E) was increased in EA-treated compared to vehicle-treated S34A cells as well as it was significantly enhanced compared to EV and R310Q-treated cells. The net routine control ratio (netR/E) was decreased after EA-treatment in GDAP1 and S34A cells, whereas the decrease in treated S34A cells was significantly different to treated control EV and GDAP1 cells. **(C)** Calculation of the routine respiration and ETS capacity of EA-treated cells in relation (rel.) to the vehicle-treated counterpart underlined the reductions in the routine respiration and ETS capacity. In addition, changes in the reductions between the cell lines became visible. Besides the indicated significant (*) changes, the relative reductions in routine respiration and ETS capacity were significantly different between vehicle-treated and EA-treated cells of each cell line (not indicated). Wild type GDAP1 prevented a less severe reduction of the routine respiration and ETS capacity. Data were collected in four independent experiments performed in duplets and are presented as mean ± S.D.. In average $2.0 \pm 0.2*10^6$ cells/ml were used in each measurement. Statistical significance is indicated with an asterisk ($p<0.05$) and was verified using two-way ANOVA followed Bonferroni posttests in (A) and (B) and one-way ANOVA followed by Tukey's multiple comparison test in (C).

3.4.4 Reduced and Impaired Mitochondrial Respiration in Ethacrynic Acid-Treated *GDAP1* KD SH-SY5Y Cells

In order to analyse whether silencing of *GDAP1* changes the result of an EA treatment on mitochondrial activity in the human neuroblastoma SH-SY5Y cells, I analysed the mitochondrial oxygen consumption of *GDAP1* KD cells comparative to pLKO-NT control cells. A 1 h-treatment with 30 µg/ml EA decreased the mitochondrial routine respiration and ETS capacity in both cell lines in contrast to cells treated with the vehicle (Figure 24A). The reduction of the basal routine respiration and the ETS capacity was in both cell lines significantly different to the respiratory state in vehicle-treated cells of the same cell line, whereas the leak respiration was unaffected (Figure 24A). Calculation of the decrease in the routine respiration and the ETS capacity of the treated cell line in relation to the vehicle-treated counterpart revealed that both respiratory states were reduced to similar levels in

GDAP1 KD and control cells (Figure 24C). Thus, the EA-treatment seems to have a similar effect on both cell lines and reduced the mitochondrial oxygen consumption to a comparable degree. Nevertheless, the calculation of the flux control ratios relativised this observation because significant changes were recognizable in the routine, leak and net routine control ratio, while the ROX/E' control ratio was similar (Figure 24B). The R/E, L/E and netR/E ratio was significantly increased in EA-treated *GDAP1* KD cells in contrast to treated pLKO-NT cells. This showed that *GDAP1* KD cells had to utilize a larger fraction of their ETS capacity for basal routine, leak and phosphorylating respiration. In addition, the leak control ratio was even significantly increased in treated *GDAP1* KD cells compared to vehicle-treated *GDAP1* KD cells. The part of the ETS capacity used for phosphorylating respiration was reduced in the EA-treated pLKO-NT cell line compared to vehicle-treated cells. Thus, a treatment with EA induced more changes in *GDAP1* KD cells than in the pLKO-NT cell line, which was especially noticeable in the alterations of the flux control ratios, although the reduction in routine respiration and ETS capacity is comparable in GDAP1 depleted cells and control cells.

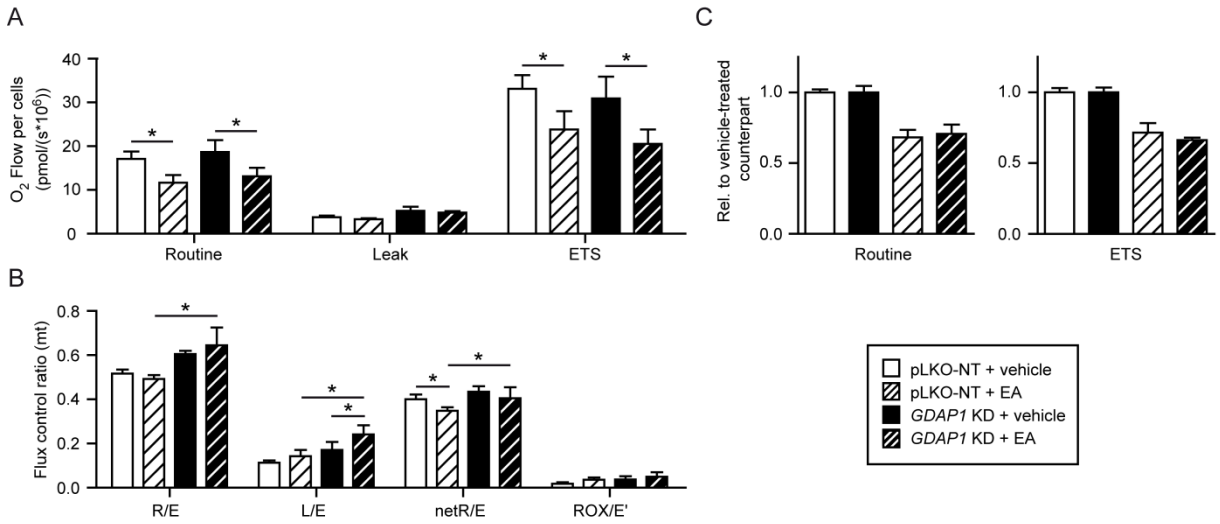

Figure 24: Ethacrynic acid induces a reduction in mitochondrial oxygen consumption in *GDAP1* KD and control SH-SY5Y cells.
Mitochondrial oxygen consumption was analysed in stable SH-SY5Y pLKO-NT and *GDAP1* KD cells were analysed after induction of oxidative stress by EA using high-resolution respirometry. Oxidative stress was induced by a treatment with 30 µg/ml EA for 1 h, while vehicle-treated cells were carried along for comparison. **(A)** The ROX-corrected respiratory states routine and ETS capacity were reduced in both cell lines, pLKO-NT and *GDAP1* KD, after exposure to EA, while the leak respiration remained unaffected. **(B)** Treatment of *GDAP1* KD with EA induced an increase in the routine (R/E), leak (L/E) and net routine (netR/E) control ratio compared to the EA-treated control cells pLKO-NT, while the flux control ratio of oxidative side reaction normalized to the total ETS capacity (ROX/E') was uninfluenced. **(C)** Calculation of the routine respiration and ETS capacity of EA-treated cells in relation (rel.) to the vehicle-treated counterpart underlined the reduction in both respiratory states and showed that the reduction was similarly severe in both cell lines, while the relative reduction between vehicle- and EA-treated cells of each cell line was significant (not indicated). Data are presented as mean ± S.D. and were obtained in four independent experiments performed in duplets. In average 2.1 ± 0.2*10^6 cells/ml were used in each measurement. Statistical significance was calculated with two-way ANOVA followed Bonferroni posttests in (A) and (B) and one-way ANOVA followed by Tukey's multiple comparison test in (C). An asterisk indicates statistical significance and represents a $p<0.05$.

3.4.5 Menadione Reduces the ETS Capacity in Wild Type and Mutated *Gdap1* Over-Expressing Cells

A treatment with MQ impaired the mitochondrial respiration in parental human neuroblastoma SH-SY5Y cells (Figure 13), which was much more drastic than the effect caused by EA (Figure 12). MQ induced mitochondrial fission in the wild type and disease-associated mutated *Gdap1* over-expressing SH-SY5Y cells (Figure 22) and thus, it is possible that it as well changes the mitochondrial respiration of this cell lines. In order to test whether induction of oxidative stress by MQ has an effect on the mitochondrial activity of these cell lines, I treated the cells with 20 µM MQ prior to measuring mitochondrial oxygen consumption. Within 1 h MQ induced a significant decrease of the ETS capacity in all cell lines (Figure 25A). It reduced significantly the basal routine respiration of mutated GDAP1 R310Q and S34A cells, but the leak respiration compensating mainly proton leak (Gnaiger, 2008; Pesta and Gnaiger, 2012) was comparable in all cell lines. GDAP1 and EV cells displayed by tendency a reduced respiration, however, these changes were not significant. The impact of MQ on mitochondrial respiration was in this experiment stronger on the ETS capacity. Calculating the relative reduction of the routine and ETS capacity of MQ-treated cells compared to vehicle-treated cells of the same cell line, underlined this effect. While the routine respiration of each cell line was reduced by MQ to comparable levels in all cell lines and this reduction was not significantly different to the vehicle-treated counterpart (Figure 25C, left panel), the ETS capacity was significantly decreased (not indicated). This decrease was even more severe for R310 cells compared to EV and S34A cells (Figure 25C, right panel). Calculation of the flux control ratios showed that not only the fraction of the ETS capacity used for compensating leak respiration (L/E) in all cell lines and for ATP production (netR/E) in GDAP1 and R310Q was increased, but also the fraction used for routine respiration (R/E; Figure 25B). This is due to the drastically reduced ETS capacity, while the routine respiration was only partly impaired. The R/E and L/E ratio of MQ-treated R310Q was even more enhanced in contrast to treated EV cells. The part of the ETS capacity which was used for phosphorylating respiration (netR/E) was decreased in S34A after a treatment with MQ compared to treated GDAP1 and EV cells. In addition, the ROX/E' ratio, which is the part of the ROX-uncorrected ETS capacity used for oxidative side reaction, was significantly increased in all cell line. This suggests that MQ induced an increase in non-mitochondrial oxygen consumption. In fact, ROX was enhanced in MQ-treated cells in contrast to the vehicle-treated counterpart of the same cell line (not shown). This effect was already recognized in MQ-treated parental SH-SY5Y cells (paragraph 3.1.5).

Thus, MQ altered the mitochondrial oxygen consumption of wild type and mutated *Gdap1* over-expressing SH-SY5Y cells and this effect was especially detectable in a reduced ETS capacity. In conclusion, GDAP1 could not prevent the MQ-induced changes in mitochondrial

respiration although the impact on mitochondrial activity was stronger in mutated *Gdap1* over-expressing cells.

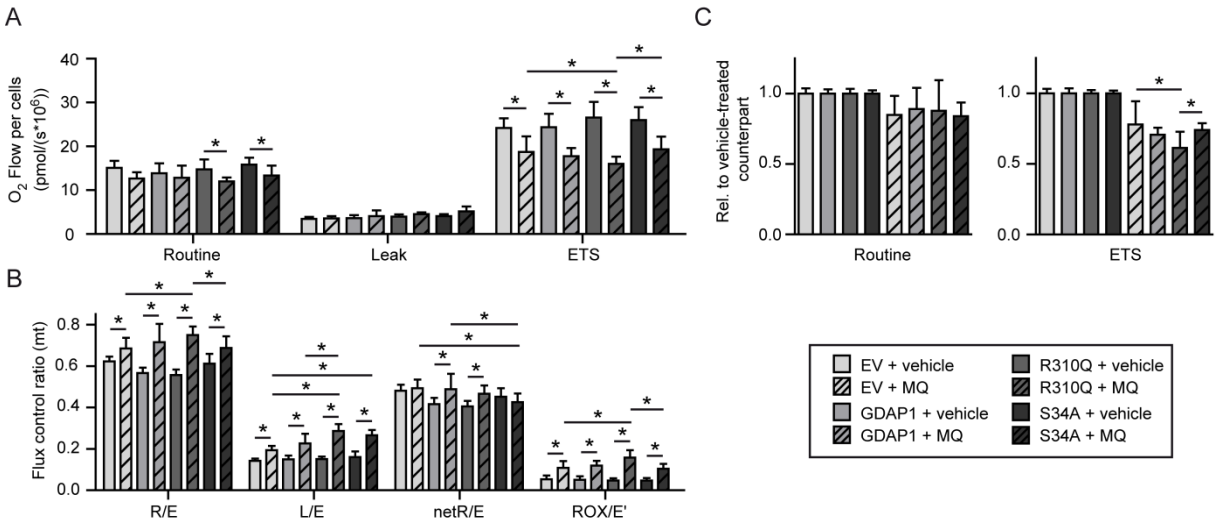

Figure 25: Menadione induces a reduction in the ETS capacity of EV, GDAP1, R310Q and S34A cells. The mitochondrial respiration after induction of oxidative stress by MQ was measured in the four SH-SY5Y cell lines in their general growth medium using the Oxygraph-O2k. Cells were treated with 20 µM MQ or the vehicle as a control for 1 h before analysis. **(A)** The oxygen flow per cells at the respiratory states routine, leak and ETS capacity was corrected for ROX. The comparison of the mitochondrial oxygen consumption showed a MQ-induced significant reduction of the ETS capacity in all cell lines. The routine respiration was only decreased in MQ-treated R310Q and S34A cells, while the leak respiration of vehicle-treated and MQ-treated cells was similar in all cell lines. **(B)** Calculation of the flux control ratio by normalizing routine respiration (R), leak respiration (L), phosphorylating respiration (netR) to the ETS capacity (E) as well as ROX was set into relation to the total and uncorrected ETS capacity (E'). MQ induced an increase of the routine control ratio (R/E), leak control ratio (L/E) and the ROX/E' flux control ratio in all cell lines. The net routine control ratio representing the part of ETS capacity used in phosphorylating respiration was only enhanced in cells over-expressing wild type GDAP1 and GDAP1 R310Q protein after a MQ-treatment. **(C)** The routine respiration and ETS capacity of MQ-treated cells were normalized to the corresponding state of the vehicle-treated counterpart. This showed that the ETS capacity was decreased drastically and significantly in the MQ-treated cell line compared to the corresponding vehicle-treated cells (not indicated). Additionally, the relative decrease in ETS capacity was even more severe for R310 cells compared to EV and S34A cells. Data presented as mean ± S.D were obtained from four independent experiments performed in duplets. In average $1.8 \pm 0.3*10^6$ cells/ml were used in each measurement. Statistical significance was verified using two-way ANOVA followed Bonferroni posttests in (A) and (B) or one-way ANOVA followed by Tukey's multiple comparison test in (C). An asterisk represents a $p<0.05$.

3.4.6 Reduced Mitochondrial Respiration after Induction of Oxidative Stress by Menadione in *GDAP1* KD Cells

Since MQ induced a reduction of the mitochondrial respiration in a concentration-dependent manner in SH-SY5Y cells (Figure 13) and affected mitochondrial respiration in *Gdap1* over-expressing cells (Figure 25), I analysed whether *GDAP1* knockdown makes the cells more susceptible to oxidative stress induced by MQ and influences their mitochondrial respiration. Because MQ induces a more pronounced change in the mitochondrial morphology than EA (Figure 22A), it is possible that the mitochondrial respiration is stronger impaired in MQ-treated than in EA-treated *GDAP1* KD cells. In fact, a treatment with 20 µM MQ induced a reduction of both the basal routine respiration and the ETS capacity in *GDAP1* KD cells and pLKO-NT cells within 1 h (Figure 26A). The leak respiration was not influenced by MQ,

however, was still increased in *GDAP1* KD cells. Like in the previous experiment with EA (Figure 24C), the relative decrease of the routine respiration and ETS capacity of treated cells normalized to vehicle-treated cells of the same cell line showed that MQ induced a similar reduction of both respiratory states in *GDAP1* KD compared to pLKO-NT cells (Figure 26C). Nevertheless, the calculated flux control ratios revealed more severe changes in the control pLKO-NT cell line than in the *GDAP1* KD cell line (Figure 26B). While only the mitochondrial L/E ratio was increased in *GDAP1* KD cells, the R/E, L/E and netR/E ratio was significantly enhanced in pLKO-NT cells. Thus, the *GDAP1* KD cells can better coupe with the effect of oxidative stress induced by MQ. One further effect of MQ on both cell lines was the previously described effect on SH-SY5Y cells (Figure 13C) and *Gdap1* over-expressing SH-SY5Y cells (Figure 25B). A treatment with MQ increased the ROX/E' ratio (Figure 26B) and ROX was actually enhanced in MQ-treated cells compared to the vehicle-treated counterpart in both cell lines (not shown). As a result, MQ reduced the mitochondrial respiratory activity in *GDAP1* KD and control cells within one hour. But the effects are stronger for the pLKO-NT cells since this cell line displayed changes in the routine control ratio and net routine control ratio, which were not detectable in *GDAP1* KD cells.

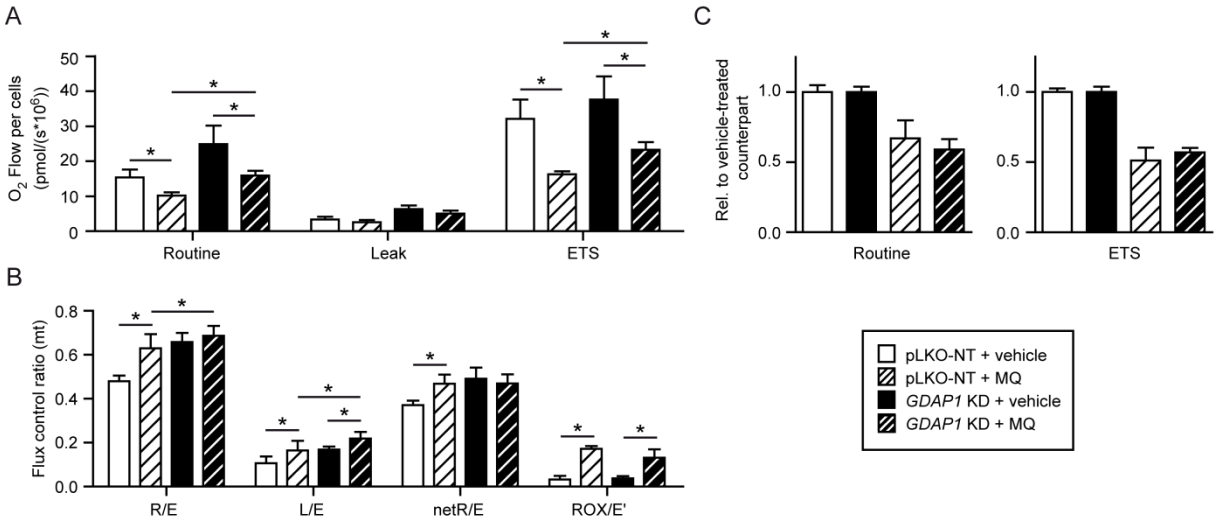

Figure 26: Oxidative stress induced by menadione decreases the mitochondrial oxygen consumption in the *GDAP1* KD and control cell line.
The mitochondrial respiration of the stable SH-SY5Y cell lines pLKO-NT and *GDAP1* KD were examined by high-resolution respirometry using the Oxygrapg-2k after induction of oxidative stress with 20 µM MQ for 1 h. Cells treated with the vehicle were carried along for comparison. **(A)** Analysis of the ROX-corrected respiratory states revealed a reduction of both routine respiration and ETS capacity in the *GDAP1* KD and the control cell line pLKO-NT induced by a treatment with MQ. The leak respiration remained comparable in both vehicle- and MQ-treated cells of both cell lines. **(B)** The flux control ratios routine control ratio (R/E), leak control ratio (L/E), net routine control ratio (netR/E) and the flux control ratio of oxidative side reaction normalized to the total ETS capacity (ROX/E') were calculated. A treatment of pLKO-NT cells with MQ in contrast to a vehicle treatment resulted in an enhancement of all flux control ratios, whereas a treatment of the *GDAP1* KD cell line induced only an increase in the leak control ratio and the flux control ratio of oxidative side-reactions. **(C)** Calculation of the routine respiration and ETS capacity of MQ-treated cells in relation (rel.) to the vehicle-treated counterpart revealed that the reduction was similarly and significantly severe in both cell lines. Data collected in four separate experiments done in duplets are shown as mean ± S.D.. In each measurement an average of $1.5 \pm 0.4*10^6$ cells/ml were used. The two-way ANOVA followed Bonferroni posttest was applied in (A) and (B) and one-way ANOVA followed by Tukey's multiple comparison test in (C) to analyse statistical significance, which is indicated with an asterisk representing a $p<0.05$.

3.5 Effect of the Cytoprotective Protein Bcl-x_L on Mitochondrial Form and Function

3.5.1 Characterization of the Mouse Embryonic Cell Lines Deficient in Bcl-x_L Protein Expression and Re-Expressing Mitochondrially Targeted Bcl-x_L

Another mitochondrial and cytoprotective protein is the anti-apoptotic B-cell lymphoma 2 (Bcl-2) protein family member B-cell lymphoma-extra large (Bcl-x_L; Boise et al., 1993; Gonzalez-Garcia et al., 1994) which is localized in the cytosol as well as at both the ER and mitochondria (Gonzalez-Garcia et al., 1994; Hsu et al., 1997; Tagami et al., 2000). Thus, Bcl-x_L is one further mitochondrial, cytoprotective protein suitable to identify mechanisms against stress on mitochondria. In order to study the role of mitochondrial Bcl-x_L on mitochondrial form and function, we received as a kind gift from Carl White the well-characterized Bcl-x_L-KO mouse embryonic fibroblasts (MEFs) cell line, this cell line re-expressing mitochondria-targeted Bcl-x_L (ActA) and a wild type (WT) MEF cell line (Eno et al., 2012). These cell lines have already been analysed to study the cytoprotective role of ER- and mitochondria-localized Bcl-x_L, the function of Bcl-x_L in regulating Ca^{2+} homeostasis (Eno et al., 2012) besides studying the interaction of Bcl-x_L with the outer mitochondrial membrane voltage-dependent anion channel (VDAC) influencing mitochondrial calcium signalling (Huang et al., 2013). In an immunoblot analysis using an antibody directed against Bcl-$x_{S/L}$, I verified the deficiency of Bcl-x_L protein expression in Bcl-x_L-KO MEFs. These cells showed no Bcl-x_L protein expression compared to WT and ActA cells (Figure 27A). However, ActA cells expressed higher levels of Bcl-x_L than WT cells with endogenous Bcl-x_L protein expression, which was proved by equal protein loading detecting β-Actin as a loading control. The protein expression of the alternative splicing variant Bcl-x_s of the *bcl-x* gene (Boise et al., 1993) was undetectable in all three cell lines. Thus, Bcl-x_L is the predominant splicing variant expressed in these MEF cell lines as previously observed (Eno et al., 2012).

In order to verify the intracellular localization of Bcl-x_L protein in the MEF cell lines, I performed a fluorescence immunocytochemistry analysis. Cells transfected transiently with mitochondrially targeted DsRed2 (mtDsRed; pDsRed2-mito) were stained with an antibody directed against Bcl-x_L. In ActA cells the localization of Bcl-x_L at mitochondria was nicely detectable by the co-localization of Bcl-x_L protein with the mitochondrially targeted DsRed2, whereas Bcl-x_L protein was unverifiable in Bcl-x_L-KO cells (Figure 27B). A very low expression of Bcl-x_L protein was visualized in WT cells, but Bcl-x_L seemed to be as well localized mainly at mitochondria. In conclusion, the Bcl-x_L-KO cells are deficient in Bcl-x_L protein as verified by immunoblotting and immunocytochemistry analysis. The successful re-expression of mitochondria-localized Bcl-x_L protein in ActA cells in the KO background was detected by western blotting and co-localization of Bcl-x_L protein with mitochondrially targeted DsRed2.

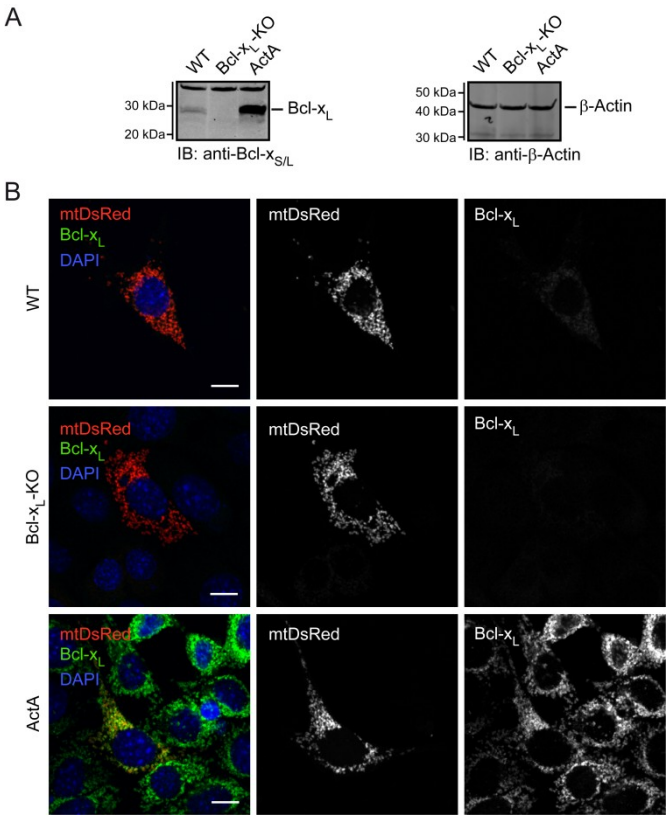

Figure 27: *Bcl-x* knockout and over-expression of mitochondria-localized Bcl-x_L in MEF cells.
(A) Western blot analysis of total protein lysates with an antibody directed against Bcl-$x_{S/L}$ proved the silencing of Bcl-x_L protein expression in Bcl-x_L-KO cells and the over-expression of mitochondria-targeted Bcl-x_L protein (predicted size: 30 kDa) in ActA cells in contrast to wild type (WT) MEF cells. Equal protein loading was verified by detection of β-Actin. **(B)** Analysis of Bcl-x_L protein localization by fluorescence immunocytochemistry using an antibody directed against Bcl-x_L showed the mitochondrial co-localization of Bcl-x_L with transiently transfected mitochondrially targeted DsRed2 (mtDsRed) in ActA cells. Bcl-x_L-KO cells displayed no Bcl-x_L protein expression, whereas only faint endogenous Bcl-x_L protein expression was detectable in WT cells at mitochondria. Scale bar represents 10 µm.

3.5.2 Deficiency in Bcl-x_L Protein Changes the Mitochondrial Morphology

Previous studies recognized the interaction between Bcl-x_L and proteins of the mitochondrial dynamics machinery. Bcl-x_L supports fission and fusion because it interacts with the mitochondrial fusion mediating protein Mfn1 and/or Mfn2 (Cleland et al., 2011; Delivani et al., 2006) as well as it interacts and increases the activity of the mitochondrial fission factor Drp-1 (Li et al., 2008). It even affects the dynamic of mitochondrial fission and fusion in cultured neurons by increasing the rate of both fission and fusion although it induces a longer mitochondrial morphology, while the conditional knockout of *bcl-x* changes the mitochondrial morphology towards a more fragmented phenotype (Berman et al., 2009). In line with the observations by Berman and colleagues (Berman et al., 2009), I expected a more tubular morphology of mitochondria in WT and ActA cells and a reduction in this category along with an increase in mitochondrial fragmentation in Bcl-x_L-KO cells. The mitochondrial morphology was examined after the transient expression of mitochondrially targeted DsRed2. I distinguished between the four observed mitochondrial categories tubular, mixed, vesicular and fragmented as shown in Figure 28A. The analysis of the mitochondrial morphology indicated that WT cells expressing endogenous Bcl-x_L protein showed mainly tubular mitochondria (Figure 28B). Deficiency of Bcl-x_L changed the mitochondrial shape. Bcl-x_L-KO cells displayed a reduction of cells with tubular mitochondria besides an increase in cells with

vesicular and fragmented mitochondria in contrast to WT cells. In the ActA cell line, the re-expression of Bcl-x_L at mitochondria changed the mitochondrial morphology towards WT cells. Comparison of Bcl-x_L-KO and ActA cells indicated a raise in the tubular category under re-expression of mitochondrially localized Bcl-x_L, while the percentage of cells with vesicular and fragmented mitochondria was similar to WT cells, although the category of cells with a mixed morphology was larger in ActA cells. Thus, as expected Bcl-x_L influences mitochondrial dynamics. The deficiency of Bcl-x_L caused a more fragmented mitochondrial shape, while re-expression of Bcl-x_L at mitochondria changes the mitochondrial morphology towards a more elongated form like in WT cells. As a conclusion, mitochondria-localized Bcl-x_L a is important for preventing changes in mitochondrial morphology.

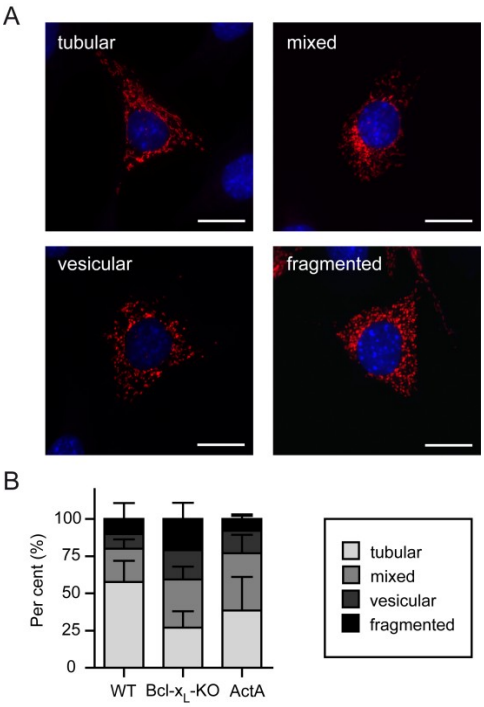

Figure 28: Bcl-x_L deficiency and mitochondria-localized Bcl-x_L alter the mitochondrial morphology.
MEF cells were transiently transfected with a mitochondrially targeted DsRed2 and analysed by fluorescence microscopy by a blinded observer for their mitochondrial morphology. The mitochondrial morphology was categorized as described before in a tubular, mixed, vesicular and fragmented appearance. Cells with aggregated mitochondria were not observed. **(A)** Exemplary fluorescence microscopy images of the category tubular, mixed, vesicular and fragmented. Scale bar represents 20 µm. **(B)** The data of three independent experiments, in which 200 cells per cell line were categorized in each experiment, showed a decrease in a tubular mitochondrial morphology at the expense of an increase in the three categories mixed, vesicular and fragmented in Bcl-x_L-KO cells in contrast to WT MEF cells. Cells over-expressing mitochondria-targeted Bcl-x_L (ActA) displayed an increase in the tubular and mixed category and a decrease in both vesicular and fragmented category compared to knockout cells. The data are presented as mean ± S.D..

3.5.3 Comparable Mitochondrial Oxygen Consumption in WT, Bcl-x_L-KO and ActA Cells

Besides influencing mitochondrial dynamics in supporting fission and fusion (Delivani et al., 2006; Sheridan et al., 2008) by enhancing the rate of these two processes (Berman et al., 2009), Bcl-x_L seems to influence mitochondrial activity by stabilizing the mitochondrial membrane potential (Chen et al., 2011). In addition, it can interact with outer mitochondrial membrane localized VDAC (Arbel et al., 2012; Huang et al., 2013; Shimizu et al., 2000; Vander Heiden et al., 2001) and in this way controls crossing of metabolites including ATP and ADP as well as it regulates mitochondrial calcium uptake by supporting the open configuration of this channel (Huang et al., 2013; Vander Heiden et al., 2001). Because mitochondrial calcium uptake is impaired in Bcl-x_L-KO cells (Huang et al., 2013) and mitochondrial Ca^{2+} uptake can elevate mitochondrial activity including OXPHOS by

increasing the activity of dehydrogenases of the TCA cycle and ATP synthase (Das and Harris, 1990; Hansford and Zorov, 1998), we expected a reduced mitochondrial respiration

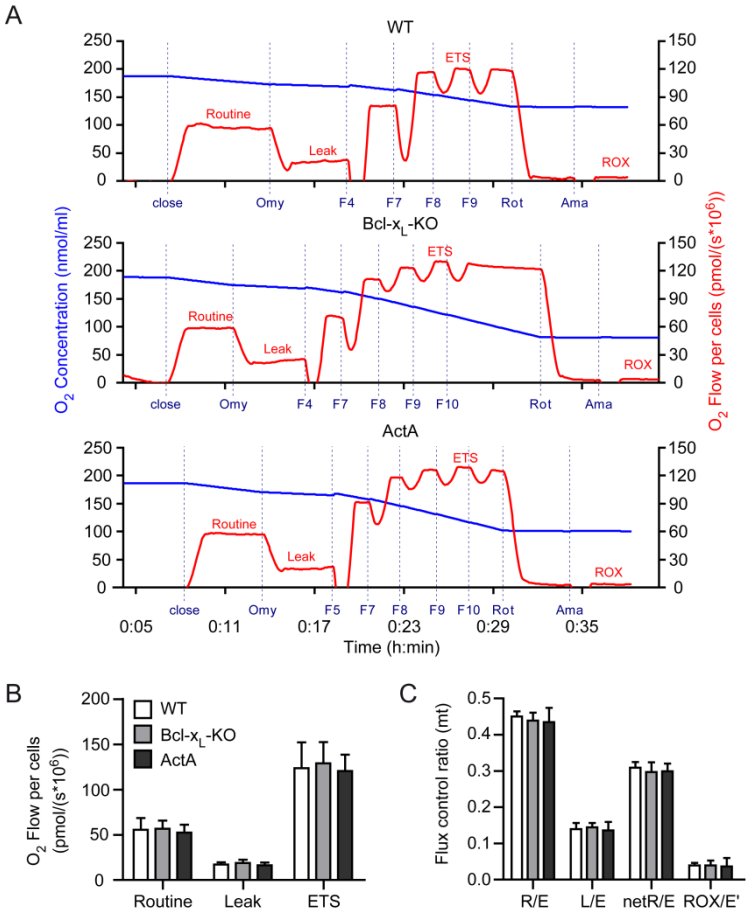

Figure 29: Unchanged mitochondrial respiration in intact Bcl-x_L-KO and mitochondria-localized over-expressing Bcl-x_L ActA MEF cells.

WT, Bcl-x_L-KO and ActA cells were analysed by high-resolution respirometry. **(A)** Representative respiratory measurements show the oxygen concentration with a blue trace and the oxygen flow per cells with a red trace plotted against the time. With dashed vertical lines the addition of oligomycin (Omy), FCCP (F including step number), rotenone (Rot) and antimycin A are marked, while the quantified respiratory states routine, leak, ETS capacity and ROX are labelled in red. **(B)** Analysis of the ROX-corrected and hence, mitochondrial oxygen flow per cells revealed no differences in basal routine and leak respiration as well as in the ETS capacity between the cell lines. **(C)** By normalization of the routine (R), leak (L) and net routine (netR=R-L, representing phosphorylating respiration) respiration to the ETS capacity (E), the flux control ratios R/E, L/E and netR/E were calculated, which did not differ between the cell lines. In addition, the flux control ratio of oxidative side reactions in relation to the ROX-uncorrected ETS capacity E' remained unaffected. Data represented as mean ± S.D. result from seven separate experiments performed in duplets. Statistical significance was proved by two-way ANOVA followed Bonferroni posttests.

under Bcl-x_L deficiency. The described changes in the mitochondrial morphology of Bcl-x_L-KO cells even suggest a change in mitochondrial activity. For this reason, we analysed the mitochondrial respiration of intact cells in their general growth medium. This experiment was

performed by the former student Julia Schneider under my supervision in the context of her bachelor thesis (Schneider, 2014). Neither the MEF cell line Bcl-x_L-KO nor the ActA cell line with mitochondria-localized Bcl-x_L showed any differences in the ROX-corrected routine respiration, leak respiration and ETS capacity compared with each other or with WT cells (Figure 29B). However, all cell lines displayed an excess in their ETS capacity, which was detectable in a higher oxygen flow per cells at ETS capacity than the part being used in basal routine respiration (Figure 29A/B). In addition, when the routine respiration (R), leak respiration (L) and phosphorylating respiration (netR=R-L) was set into relation to the ETS capacity no differences were detectable between the cell lines as well as the flux control ratio of non-mitochondrial oxidative side-reactions (ROX) in relation to the uncorrected ETS capacity (E') was not significantly influenced (Figure 29C). Thus, in contrast to our expectation, alterations in the mitochondrial morphology (Figure 28) and mitochondrial calcium homeostasis (Huang et al., 2013) are not combined with a reduction in mitochondrial respiration of Bcl-x_L-KO cells. Huang and colleagues have already shown that the basal mitochondrial membrane potential of WT and Bcl-x_L-KO are comparable (Huang et al., 2013), which could in part explain a similar mitochondrial oxygen consumption in both cell lines.

3.5.4 Silencing of Bcl-x_L Protein Expression Reduces the OXPHOS and ETS Capacity with Convergent Complex I and II Electron Input

In order to exclude that *bcl-x* knockout does not influence mitochondrial activity as suggested by the analysis of mitochondrial oxygen consumption in intact cells, the mitochondrial respiration and especially OXPHOS was analysed in permeabilized MEF cells. This experiment was carried out in part by the bachelor student Julia Schneider (Schneider, 2014) under my supervision and partly by myself. According to basal routine respiration in the previous experiment with intact cells (Figure 29B), the routine endogenous respiration was comparable in WT, Bcl-x_L-KO and ActA cells (Figure 30B). In addition, the first measured leak respiratory state GM_N (no adenylates added) after addition of glutamate + malate and permeabilization of cells with digitonin as well as the later in the experiment determined leak respiratory state GMS_L after inhibition of the ATP synthase with oligomycin were similar in all three cell lines. But quantification of the OXPHOS state GM_P with glutamate/malate-supported respiration through complex I showed a reduction by trend in Bcl-x_L-KO compared to WT and ActA cells. In particular, the OXPHOS state GMS_P with convergent complex I and

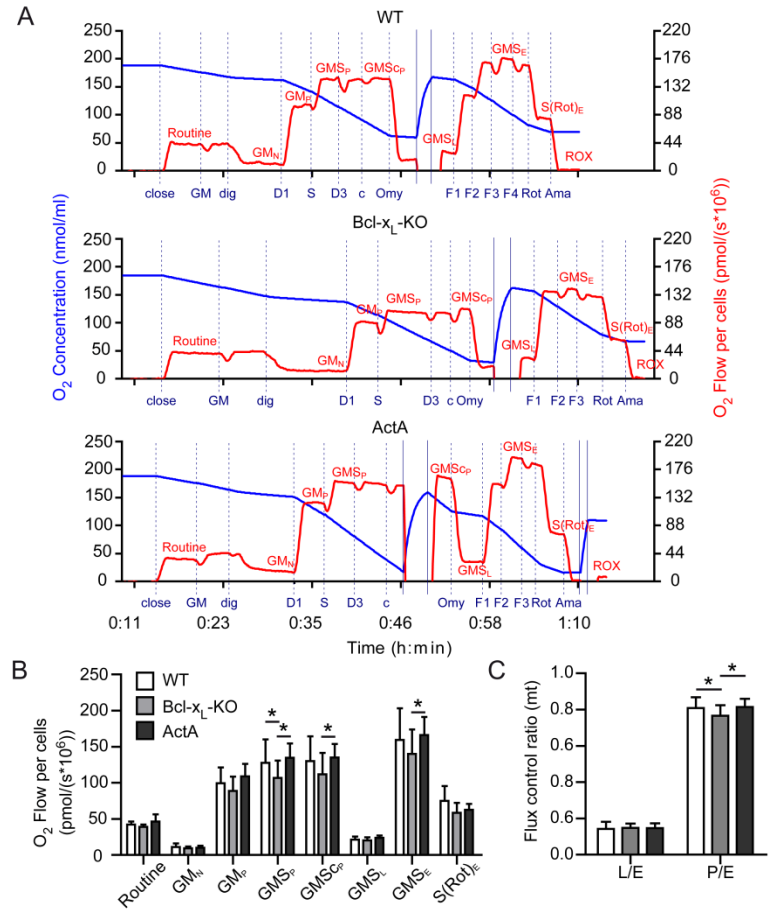

Figure 30: *Bcl-x* gene knockout decreases the OXPHOS and ETS capacity of the mitochondrial respiratory system.
The OXPHOS capacity of mitochondrial respiration was analysed in digitonin-permeabilized cells of WT, Bcl-x_L-KO and ActA cells by using the high-resolution respirometer Oxygraph-2k. **(A)** Shown are exemplary and representative measurements of WT, Bcl-x_L-KO and ActA cells. The blue trace represents the oxygen concentration and the red trace the oxygen flow per cells, which are plotted against the time. Vertical dashed lines mark the addition of glutamate + malate (GM), digitonin (dig), ADP-Mg^{2+} (D including final concentrations: 1, 1 mM; 3, 3 mM), succinate (S), cytochrome c (c), oligomycin (Omy), FCCP (F including step number), rotenone (Rot) and finally antimycin A (Ama). In addition, re-oxygenation of the chambers, including opening and closing, is indicated with vertical solid lines. The measured respiratory states used for analysis are labelled in red. **(B)** The ROX-correction and analysis of the measured respiratory states revealed that MEF cells deficient in Bcl-x_L protein expression (Bcl-x_L-KO) have a reduced OXPHOS capacity with convergent complex I and II electron input in the respiratory system (GMS_P) as well as a reduced ETS capacity with convergent electron input (GMS_E) compared to WT and ActA cells. The over-expression of mitochondria-localized Bcl-x_L rescued the effect of Bcl-x_L deficiency and increased GMS_P and GMS_E in ActA cells up to comparable levels in WT cells. **(C)** Calculation of the mitochondrial leak control ratio ($L/E=GMS_L/GMS_E$) and the OXPHOS control ratio ($P/E=GMS_P/GMS_E$) indicated a significant reduction in the OXPHOS control ratio of Bcl-x_L-KO in contrast to WT and ActA cells. Data presented in mean ± S.D. were collected in eight separate experiments, which were performed in duplets. An asterisk represents statistical significance ($p<0.05$), which was proved by two-way ANOVA following Bonferroni posttests.

II electron input was significantly decreased in Bcl-x_L-KO cells in contrast to WT and ActA cells after addition of succinate. Consistent with this result, the ETS capacity GMS_E with convergent complex I and II electron input was significantly reduced in Bcl-x_L-KO compared to ActA cells. In contrast to WT cells, the KO of *bcl-x* in the Bcl-x_L-KO cell line tends to result in a slightly reduced ETS capacity state GMS_E. Hence, re-expression of mitochondria-localized Bcl-x_L (ActA cells) rescued the observed changes of Bcl-x_L deficiency and increased both respiratory states up to comparable levels in WT cells. The inhibition of complex I allowed the quantification of the ETS capacity $S(Rot)_E$ depending on succinate alone. In all three cell lines no significant differences in this respiratory state were detected, however, the ETS capacity on succinate alone was low, which indicated a low capacity of succinate-supported respiration. In all cell lines the respiration seems to be limited by the phosphorylation system because the oxygen flow per cells at the OXPHOS capacity state GMS_P is lower than the maximum ETS capacity state GMS_E. Thus, all cell lines revealed a clear excess in their ETS capacity. The limitation by the phosphorylation system also limited the stimulation of respiration after addition of succinate, which suggests that the phosphorylation system retains control over respiratory flux. Calculation of the OXPHOS control ratio P/E (GMS_P/GMS_E) revealed that WT and ActA cells with a P/E ratio of about 0.809 and 0.814 (n=8) approached in a similar degree the upper limit of their ETS capacity, while the OXPHOS control ratio was significantly reduced to approximately 0.767 in Bcl-x_L-KO cells (Figure 30C). The reduced P/E ratio in Bcl-x_L-KO cells suggests that the control of the phosphorylation system is bigger in this cell line than in the WT and ActA cell line. Nevertheless, the leak control ratio L/E (GMS_L/GMS_E) was comparable in all three cell lines. In conclusion these results suggest that knockout of *bcl-x* reduces considerably the OXPHOS and ETS capacity state with convergent complex I and II electron input in Bcl-x_L-KO MEF cells, whereas over-expression of mitochondria-localized Bcl-x_L protein can rescue these effects. This even demonstrates that Bcl-x_L at mitochondria is important to prevent a reduction in mitochondrial capacity.

3.5.5 Knockout of *bcl-x* Does Not Influence the Glycolytic Activity

Since Bcl-x_L-KO MEFs display an impaired OXPHOS and ETS capacity, we investigated whether an increase in the glycolytic activity might compensate the deteriorated mitochondrial capacity in Bcl-x_L-KO cells. NADH is produced predominantly in mitochondria in the TCA cycle and through β-oxidation of fatty acids as well as to a lower extent in glycolysis (Hirst, 2013). Therefore, I studied the influence of Bcl-x_L on the total NAD (NAD^+ and NADH) pool. The NAD pool of Bcl-x_L-KO cells was slightly, but not significantly increased compared to WT and ActA cells (Figure 31A). Re-expression of mitochondria-localized Bcl-x_L

protein in ActA cells reduced the slight increase recognized in Bcl-x_L-KO cells and decreased total NAD to a comparable level in WT cells. This result suggests comparable and sufficient levels of NAD for subsequent mitochondrial respiration in all three MEF cell lines, which could in part explain why the mitochondrial respiration of cells in their regular growth medium was comparable.

Instead of using pyruvate as a substrate for the TCA cycle, excess pyruvate can be converted by the lactate dehydrogenase to lactate under NADH consumption at the end of glycolysis (Wallace, 1999). In order to further exclude a change in the glycolytic activity as a consequence of an impaired mitochondrial function in Bcl-x_L-KO MEFs, I analysed conditioned media of all three cell lines for its glucose and lactate content after 24 h. Bcl-x_L-KO cells utilized comparable amounts of glucose than WT and ActA cells (Figure 31B). In addition, the metabolized glucose levels in Bcl-x_L-KO was not converted in a higher extent to lactate (Figure 31C), which suggested a similar glycolytic activity in all three cell lines.

These observations suppose that Bcl-x_L-KO MEFs do not compensate a reduction in their mitochondrial capacity by increasing glycolytic activity, which let us assume that Bcl-x_L-KO cells most likely compensate an impaired mitochondrial capacity through enhanced glucose metabolism in the pentose phosphate pathway.

3.5.6 Increasing Susceptibility to Inhibition of Mitochondrial Energy Production in Bcl-x_L-KO MEFs

In a subsequent experiment, I analysed the cell viability of cells treated with the mitochondrial toxins antimycin A to inhibit complex III (Herrero and Barja, 1997) and oligomycin to inhibit ATP synthase (Lardy et al., 1958) which will force cells achieving their energy demand rather through glycolysis and/or the pentose phosphate pathway than through OXPHOS in mitochondria. In their regular growth medium containing 25 mM glucose, neither antimycin A nor oligomycin reduced the cell viability up to more than approximately 55 to 60 % and 36 to 45 %, respectively (Figure 31D and G). Under this condition the MEF cell lines had still excess to glucose which allowed to provide their energy demand through glycolysis and/or the pentose phosphate pathway. Therefore, I replaced glucose by galactose in the medium. This forces cells to sustain their energy demand by mitochondrial OXPHOS and most probably cells use glutamine as a source to produce ATP in mitochondria (Reitzer et al., 1979) and hence, this approach has been used before to enhance the effect of mitochondrial toxins on cell lines (Gohil et al., 2010; Marroquin et al., 2007). In fact, changing glucose to galactose increased the susceptibility to induce cell death in the MEF cell lines by antimycin A (Figure 31E) and oligomycin (Figure 31H) when used in the same concentrations

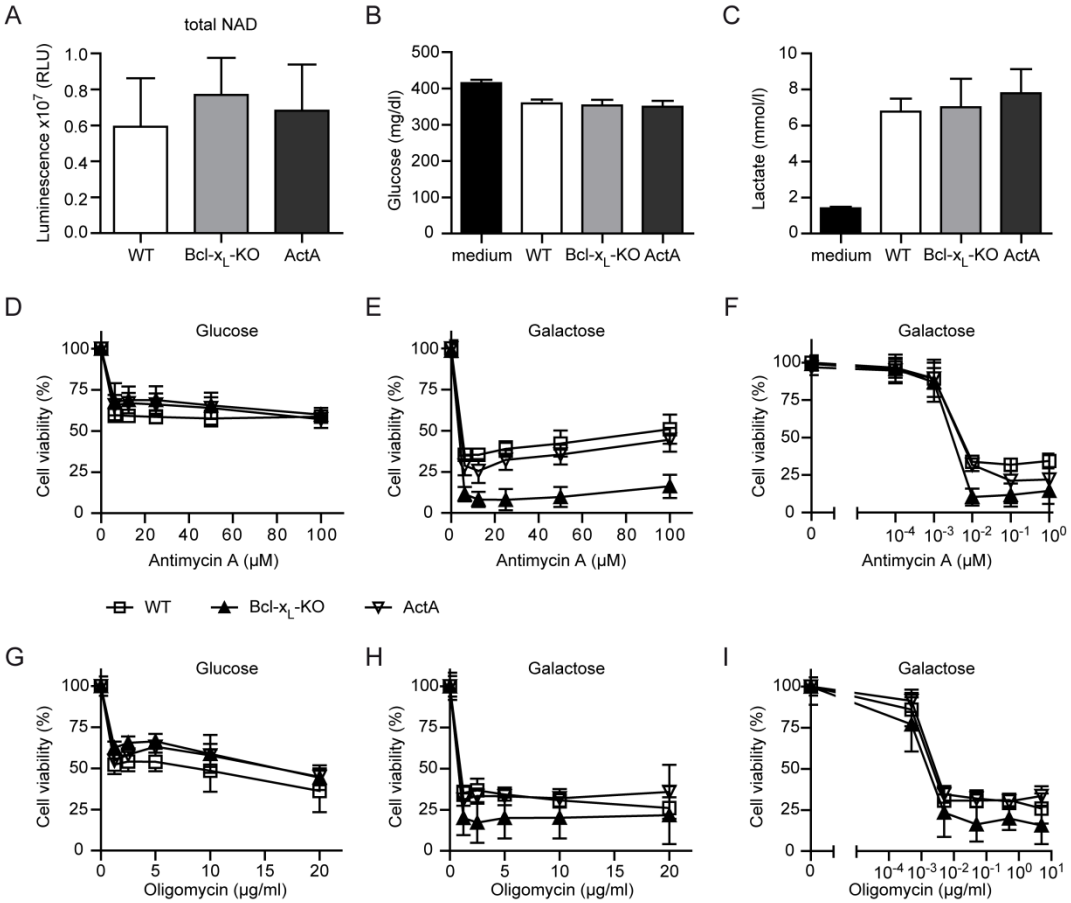

Figure 31: Bcl-x_L-KO MEFs do not display an increased glycolytic activity, but are more susceptible to the inhibition of mitochondrial respiration by mitochondrial toxins.
(A) The total oxidized and reduced nicotinamide adenine dinucleotides (NAD^+ and NADH; total NAD) were quantified in WT, Bcl-x_L-KO and ActA cells using the bioluminescence assays NAD/NADH-Glo assay and measuring of the produced luminescent in relative light units (RLU). Total NAD was slightly increased in Bcl-x_L-KO cells compared to WT and ActA cells. Data are derived from four independent experiments done in quintuplicate. **(B/C)** Analysis of 24-h conditioned medium of MEF cells. The glucose (B) and lactate (C) concentration in the conditioned medium was quantified using the Radiometer abi800 basic. Data shown in bar graphs display the mean ± S.D. of four independent experiments done in duplets. Statistical significance was proved using one-way ANOVA following Tukey's multiple comparison test. **(D-I)** Cells were treated with the indicated concentration of the complex III-inhibitor antimycin A (D-F) or ATP synthase-inhibitor oligomycin (G-I) in medium containing either 25 mM glucose (D/G) or 25 mM galactose (E/F/H/I). After 24 h, cell viability was determined using CTB reagent and normalized. **(D)** Cells treated with different concentrations of antimycin A in glucose medium showed a slightly reduced cell viability at all concentrations, but the susceptibility did not differ between the cell lines. **(E/F)** Changing glucose medium to galactose containing medium increased the sensitivity to antimycin A in a concentration-dependent manner. Bcl-x_L-KO cells displayed a higher mortality rate than WT and ActA cells. **(G)** Treatment of oligomycin in glucose medium reduced the cell viability up to approximately 50 % in all MEF cell lines. **(H/I)** The change of glucose to galactose containing medium increased the susceptibility of all cell lines to the mitochondrial toxin and ATP synthase-inhibitor oligomycin. The mortality of Bcl-x_L-KO cells was increased compared to both other cell lines. Each experiment was performed three (D-F, H,I) or four (G) times in triplicates. The cell viability in per cent as mean ± S.D. was plotted against the used antimycin A and oligomycin concentration, respectively.

as before. However, Bcl-x_L-KO cells were more influenced by a complex III-inhibition with antimycin A and by inhibition of the ATP synthase with oligomycin than WT and ActA cells. For this reason, the cell viability was significantly decreased by a concentration of 6.25 to 100 µM antimycin A in contrast to WT and ActA cells as well as the reduction in cell viability

significantly differed in Bcl-x_L-KO cells at a concentration of 1.25 to 5 µg/ml of oligomycin compared to WT and at concentrations of 2.5 to 20 µg/ml of oligomycin in contrast to ActA cells. Nearly all Bcl-x_L-KO cells died by a treatment with antimycin A, while oligomycin reduced the cell viability of this cell line down to about 21 %. WT and ActA cells were similarly influenced by both toxins. In these experiments with antimycin A and oligomycin the cell survival had already been impaired relatively strong in medium with galactose. Because of this, I decided to treat the cell lines with lower concentrations of both toxins. Reducing the concentrations of both antimycin A (Figure 31F) and oligomycin (Figure 31I) resulted in cell death induced in a concentration-dependent manner in all cell lines. But still at these lower concentrations Bcl-x_L-KO MEFs were more severely influenced than WT cells and ActA cells. At a lower concentration of 0.01 to 1 µM antimycin A the decrease in cell viability was significantly different compared to WT cells as well as Bcl-x_L-KO cells were significantly more susceptible to 0.05 and 0.5 µg/ml oligomycin and 0.0005 to 0.05 as well as 5 µg/ml oligomycin in contrast to WT and ActA cells, respectively.

Thus, Bcl-x_L-KO cells are more dependent on glucose consumption through glycolysis or the pentose phosphate pathway under inhibiting situations of mitochondrial respiration. According to these results together with the observation of an impaired mitochondrial OXPHOS and ETS capacity and comparable glycolytic activity under Bcl-x_L deficiency, we assume that *bcl-x* gene knockout leads to an increase in the pentose phosphate pathway, whereas re-expression of Bcl-x_L at mitochondria can prevent this change in energy metabolism.

3.5.7 Bcl-x_L Deficiency Increases G6PD Protein Expression, the Total NADP Pool and Cell Proliferation

In order to analyse whether deficiency of Bcl-x_L induces an increase in the pentose phosphate pathway in Bcl-x_L-KO cells, I examined the expression of the G6PD protein. The analysis of total protein lysates of WT, Bcl-x_L-KO and ActA cells by immunoblotting and normalization of G6PD abundance to β-Actin protein expression as a loading control verified a significant increase in G6PD protein expression in Bcl-x_L-KO cells in contrast to WT cells (Figure 32A). Re-expression of mitochondrially targeted Bcl-x_L slightly lowered the expression of G6PD in ActA cells compared to Bcl-x_L-KO cells, but G6PD abundance was still significantly enhanced in contrast to WT cells.

Because NADPH is a product of the pentose phosphate pathway which gets produced at two steps in the oxidative branch by the activity of the first enzyme G6PD and by 6-phosphogluconate dehydrogenase (6PGDH; Stincone et al., 2014), the NADP pool was analysed with help of a specific bioluminescence assay. Bcl-x_L-KO cells displayed an increase in the total NADP pool, which was significantly enhanced in contrast to WT cells

(Figure 32B). Once more, stable re-expression of mitochondrially targeted Bcl-x_L in the KO background reduced the increase in total NADP in the ActA cell line, however, the total NADP pool was still significantly elevated in contrast to WT cells. This result reflects and matches in trend the result observed of G6PD abundance.

After a period of time culturing the MEF cells, I even realized a difference in the proliferation rate between WT, Bcl-x_L-KO and ActA cells. Analysing the proliferation with help of the CTB reagent over three days indicated an enhanced proliferation rate under Bcl-x_L knockout. Already after one day, the cell number of Bcl-x_L-KO MEFs was significantly higher compared to WT cells and after two further days in culture the cell number of Bcl-x_L-KO cells was not only significantly higher in contrast to WT cells, but also to ActA cells (Figure 34C). Thus, re-expression of mitochondria-localized Bcl-x_L decreased cell proliferation, although a comparison of WT and ActA cells showed that the proliferation of ActA cells was significantly faster.

In conclusion, the increase in G6PD expression in addition to an enhanced total NADP pool suggest an increase in pentose phosphate pathway activity under *bcl-x* gene knockout which we assume is an adaptation to impaired mitochondrial capacity in Bcl-x_L-KO cells and to *bcl-x* gene knockout in general. In this cell line, an increase in the pentose phosphate pathway can even explain a increasing proliferation rate because the pentose phosphate pathway is a source for the production of precursors for nucleotide- and amino acid synthesis besides being important for NADPH production (Stincone et al., 2014).

3.5.8 Bcl-x_L Deficiency Increases the total Cellular Glutathione Pool

Due to the fact that the total NADP pool was notably increased in Bcl-x_L-KO cells and NADPH is necessary for the recovery of the antioxidant GSH (Dringen, 2000), we hypothesis an increase in the total glutathione content of Bcl-x_L-KO cells. For this reason, I examined enzymatically the total glutathione content of WT, Bcl-x_L-KO and ActA cells and induced a reduction of GSH by a treatment with 10 mM glutamate. As expected, comparing the total GSH content of untreated WT, Bcl-x_L-KO and ActA cells, the Bcl-x_L-KO cells showed a significantly increased GSH content (Figure 32D). But by a treatment with glutamate the GSH content decreased and already within 4 h the GSH content was comparable in Bcl-x_L-KO as well as WT and ActA cells.

An increased GSH content can protect against oxidative stress as observed, for example, in HT22R cells and GDAP1 protein over-expressing HT22S cells (Noack et al., 2012). In order to examine a protective effect of enhanced glutathione content in Bcl-x_L-KO cells, I induced oxidative stress through treating cells with various concentrations of glutamate. The exposure to glutamate induced cell death in a concentration-dependent manner in all three

cell lines within 19 h (Figure 32E). A major difference in the susceptibility to oxidative stress was not detectable. Neither silencing of *bcl-x* nor re-expression of mitochondrially targeted Bcl-x_L changed the cell viability compared to WT cells.

We concluded from these observations that even though Bcl-x_L-KO cells show an increase in the basal total glutathione content, this increased total cellular glutathione content cannot protect these cells against oxidative stress induced by glutamate. But the enhanced total NADP content in Bcl-x_L-KO cells seems to be beneficial for the production and especially recovery of the antioxidant GSH.

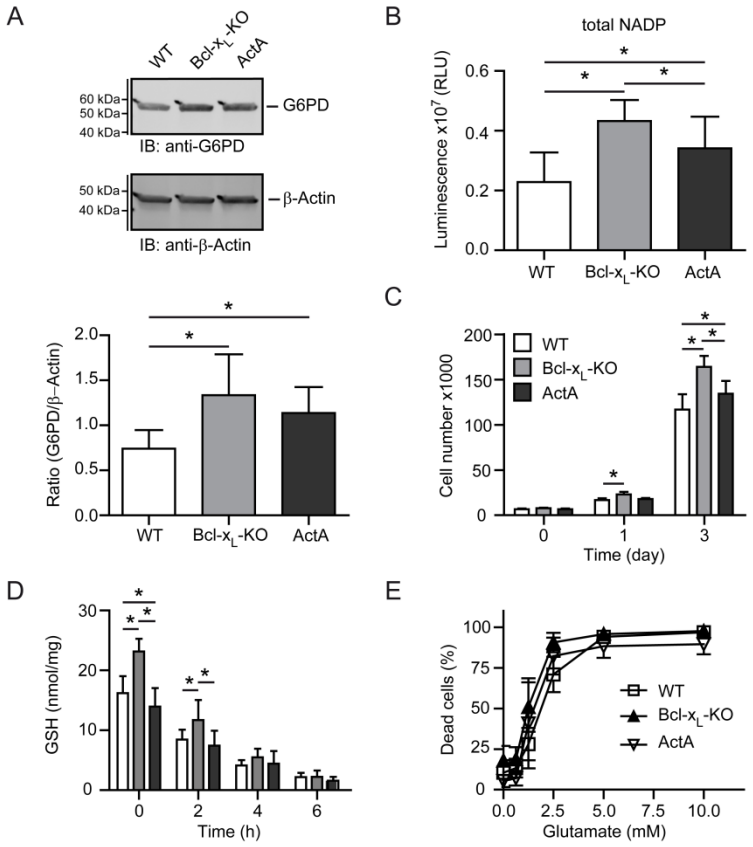

Figure 32: Bcl-x_L deficiency increased total NADP and cellular glutathione. **(A)** The expression of Glucose-6-phosphate dehydrogenase (G6PD) was analysed by western blotting using an antibody detecting G6PD with a predicted molecular weight of 58 kDa. An antibody directed against β-Actin was used for normalization and to proof equal protein loading. The relative expression of G6PD was determined by quantifying the relative intensity of the band for G6PD and β-Actin using ImageJ and subsequent normalization. The analysis of nine independent immunoblots showed a significant increase in the relative expression of G6PD in Bcl-x_L-KO cells. **(B)** The total oxidized and reduced nicotinamide adenine dinucleotide phosphates ($NADP^+$ and NADPH, total NADP) was quantified in WT, Bcl-x_L-KO and ActA cells using the bioluminescence assay NADP/NADPH-Glo assay and measuring of the produced luminescent in relative light units (RLU). Total NADP in Bcl-x_L-KO was significantly enhanced compared to WT and ActA cells. Data derived from four independent experiments done in quintuplicate. **(C)** Cell proliferation of MEF cells analysed using CTB reagent. 6,250 cells were seeded into 24-well plates. The cell proliferation was analysed on day 0, 1 and 3 and the cell number was calculated with help of a standard curve. Bcl-x_L-KO cells displayed an enhanced proliferation rate compared to both WT and ActA cells. Data were obtained from three independent experiments performed in triplets. **(D)** The total cellular glutathione (GSH; GSH and GSSG) content was measured enzymatically in cells treated for the indicated time with 10 mM glutamate. The quantified total glutathione content was normalized to the total protein content. Data were collected in three independent experiments done in duplets. **(E)** MEF cells seeded into 96-well imaging plates were subjected to the indicated concentration of glutamate. About 19 h later, the cell viability was determined with a staining of dead cells with SYTOX Orange and all cells with Hoechst. The percentage of dead cells per well was quantified using the pathway and subsequent analysis. All cells were similarly susceptible to glutamate induced oxidative glutamate toxicity. Data were obtained in four independent experiments done in triplicates. All data are presented as mean ± S.D.. Statistical significance was proved performing one-way ANOVA following Tukey's multiple comparison test (A/B) or two-way ANOVA followed by Bonferroni posttest (C-D). Asterisks indicate a $p<0.05$.

4 DISCUSSION

4.1 Influence of Acute Oxidative Stress on Mitochondrial Form and Function in HT22S and SH-SY5Y Cells

As described in the beginning, oxidative stress results from an imbalance between the antioxidant defence mechanisms and the production of ROS in which the equilibrium is shifted towards an increase in ROS production and accumulation (reviewed in Dringen, 2000; Finkel and Holbrook, 2000). In this study, we demonstrated although mitochondria are a major source for ROS production (Finkel and Holbrook, 2000), they are directly affected by oxidative stress in the model of system of hippocampal HT22S and neuroblastoma SH-SY5Y cells. Even though previous studies demonstrated a perinuclear accumulation and mitochondrial fission induced by glutamate-induced oxidative stress in HT22S cells (Grohm et al., 2010; Kumari et al., 2012), I did not observe a changed mitochondrial morphology after an exposure to glutamate (Figure 10B). In comparison to examine the mitochondrial morphology after a 6 h-exposure to 10 mM glutamate, the previous studies examined the mitochondrial morphology after a 24 h- and 18 h-exposure with 4 mM and 5 mM of glutamate, respectively (Grohm et al., 2010; Kumari et al., 2012). In this study, HT22S cells died from a treatment with 5 and 10 mM glutamate within 22 h (Figure 14B), whereby an analysis of the mitochondrial morphology would be impossible after 18 to 24 hours. But although the mitochondrial morphology was still unaffected, a treatment with glutamate affected directly the mitochondrial respiration and induced an increased routine respiration and ETS capacity (Figure 10D), as described before (Kumari et al., 2012). Most likely the increase in ROS production and especially depletion in GSH during oxidative glutamate toxicity (Tan et al., 1998a) has not yet induced activation of 12/15-LOX (Li et al., 1997b; Pallast et al., 2009) to such a point that mitochondria are damaged by a decreasing mitochondrial membrane potential and increasing mitochondrial permeability (Pallast et al., 2009) which would directly impair mitochondrial respiration. Additionally, it has not come to a complete breakdown of the mitochondrial membrane potential, yet (Landshamer et al., 2008; Noack et al., 2012; Pallast et al., 2009). Considering the chronological sequence of oxidative glutamate toxicity (Figure 6), after a 6 h-exposure to glutamate an enhancement in intracellular cGMP causes an elevation of intracellular calcium by the influx of calcium (Li et al., 1997a) through the plasma membrane-localized calcium channel ORAI1 (Henke et al., 2013). Because mitochondrial Ca^{2+} uptake can directly enhance mitochondrial activity including OXPHOS by increasing the activity of dehydrogenases of the TCA cycle as well as the activity of the ATP synthase itself (Das and Harris, 1990; Hansford and Zorov, 1998), an increasing mitochondrial calcium influx can possibly cause an increase in mitochondrial

respiration in HT22S cells after a 6 h exposure to glutamate, but this needs to be further analysed.

In contrast to the effect of glutamate on mitochondria in HT22S cells, mitochondria of SH-SY5Y cells were influenced in their form and function by oxidative stress induced by ethacrynic acid (EA) and menadione (MQ). I demonstrated that a treatment with EA triggered extensive fusion of mitochondria, whereas MQ provoked mitochondrial fragmentation (Figure 11B) as expected (Bowes and Gupta, 2005; Loor et al., 2010; Soltys and Gupta, 1994). The effect was so drastic that about 75 % of the cells showed the described morphology after only one hour. Loor and colleagues have already concluded that the effect of MQ on mitochondrial shape is an early and critical event for inducing cell death, however, they examined the mitochondrial form after a 4 h exposure to MQ (Loor et al., 2010) and according to our results, the effect is much faster. In comparison, the rapid mitochondrial re-organization by EA inducing the development of a mitochondrial reticulum has already been observed by an exposure for only 15 min (Soltys and Gupta, 1994). EA is well-known for its glutathione depleting activity and induces loss of both cytosolic and mitochondrial glutathione (Seyfried et al., 1999; Wullner et al., 1999), but its glutathione depleting activity is not responsible for the induction of mitochondrial fusion (Bowes and Gupta, 2005). Its alkylating activity on cysteine residues seems to be responsible for changing mitochondrial morphology because the cysteine-alkylator N-ethylmaleide had a similar effect on mitochondria than EA (Bowes and Gupta, 2005) which suggests that cysteine-alkylation by EA caused mitochondrial morphology changes in SH-SY5Y cells as well. Since mitochondrial fusion was induced so rapidly, it might be that EA-induced cysteine-alkylation of critical cysteine residue(s) of proteins involved in the fusion process (Bowes and Gupta, 2005) were inducing mitochondrial fusion. In a subsequent study, Bowes and Gupta claimed that EA-induced mitochondrial elongation is even caused by restraining the recruitment or activity of fission proteins like Drp1 whereby mitochondrial fission is blocked (Bowes and Gupta, 2008). In comparison, menadione triggers oxidative stress through ROS production by redox cycling and GSH depletion (Chiou and Tzeng, 2000; Criddle et al., 2006; Kim et al., 2014; Loor et al., 2010), but it has not been investigated which function of menadione is inducing mitochondrial morphology changes, so that I cannot rule out that GSH depletion is in charge of influencing mitochondrial morphology in SH-SY5Y cells. Especially, since it induces mitochondrial fission instead of leading to mitochondrial fusion like EA.

Although EA and MQ affect mitochondria in different ways and induced mitochondrial fusion or fission, the effect on mitochondrial respiration was similar in SH-SY5Y cells. In both cases the basal mitochondrial respiration as well as the ETS capacity was reduced by a treatment with EA (Figure 12) and MQ (Figure 13). Especially the fact that both fragmented and tubular mitochondria showed a decreased mitochondrial respiration is surprising because

fragmented mitochondria are associated with resting cells and mitochondrial fusion are beneficial under situations of high energy demand (reviewed in Westermann, 2012). A recent publication even showed that cellular stress induced by apoptotic stimuli like UV irradiation and cycloheximide resulted in a drastically increased mitochondrial network displaying stress-induced mitochondrial hyperfusion which was accompanied by enhanced ATP production (Tondera et al., 2009). According to this, the effect of MQ on mitochondrial respiration comes up to our expectation that mitochondrial fission impairs mitochondrial respiration. Most probably a decrease in the mitochondrial membrane potential is responsible for the observed reduction in respiration given that a treatment of cardiomyocytes with MQ significantly decreased the mitochondrial potential within 1 h (Loor et al., 2010) as well as MQ induced a reduction in the mitochondrial membrane potential of isolated pancreatic acinar cells (Gerasimenko et al., 2002), in human epithelial ovarian carcinoma OVCAR-3 cells (Kim et al., 2014) and in Jurkat T cells in which MQ also reduces the inner membrane mass (Laux and Nel, 2001). A breakdown of the mitochondrial membrane potential even induces a reversible mitochondrial fragmentation (Legros et al., 2002) suggesting that MQ triggers a reduction in the mitochondrial membrane potential which provokes mitochondrial fission. The MQ-induced reduction in the mitochondrial membrane potential in Jurkat T cells and OVCAR-3 cells can be abolished or attenuated by N-acetylcysteine (Kim et al., 2014; Laux and Nel, 2001) which can increase intracellular GSH levels (Issels et al., 1985; Issels et al., 1988; Thor et al., 1979). This suggests that the MQ-induced changes in mitochondrial morphology and function are linked with the loss of the mitochondrial membrane potential and its GSH-depleting activity.

Because EA-treated cerebellar granule neurons revealed a decrease in mitochondrial membrane potential (Wullner et al., 1999), a possible reduction in the mitochondrial membrane potential of EA-treated SH-SY5Y cells can be responsible for the observed impaired mitochondrial respiration, however, others did not observe a change in the membrane potential in EA-treated human fibroblasts (Soltys and Gupta, 1994). In addition, EA-treatment reduces the activity of mitochondrial complex II/III and complex IV in cerebellar granule neurons (Wullner et al., 1999) as well as PC12 cells, whereas complex II/III activity was completely abolished after a treatment with EA for 4 h (Seyfried et al., 1999). EA is decreasing mitochondrial and cytosolic glutathione levels and increasing the mitochondrial production of ROS (Seyfried et al., 1999), which can also directly affect mitochondrial function. Seyfried and colleagues supposed that complex III inhibition is caused by EA-induced direct alkylation of thiol groups which are important for enzyme function or through changes in the stability and permeability of the mitochondrial inner membrane (Seyfried et al., 1999). There is no evidence that MQ is directly affecting mitochondrial respiratory complexes, but a decrease in mitochondrial membrane potential is induced by activation of

mitochondrial permeability transition pores (Gerasimenko et al., 2002) as well as the effect on mitochondrial membrane potential can be prevented by GSH-increasing N-acetylcysteine (Kim et al., 2014; Laux and Nel, 2001).

Thus, glutamate as well as EA and MQ affect mitochondrial function even though the effect of oxidative glutamate toxicity in HT22S cells is different than the effect of acute oxidative stress induced by EA and MQ in SH-SY5Y cells in which both impaired mitochondrial respiration within one hour, although not up to a level where the damage completely blocks mitochondrial activity. Additionally in contrast to glutamate, EA and MQ changed mitochondrial dynamics very rapidly and effectively, so that the effects of EA and MQ on mitochondrial shape and function seem to be early events. Together these results indicate that the effect on mitochondrial form and function is dependent on the cellular changes induced by the oxidative stress-inducing reagent.

4.2 Chronic Oxidative Stress Induces a Shift in Energy Metabolism towards the Pentose Phosphate Pathway in Glutamate-Resistant HT22R Cells

The glutamate-resistant HT22R cells proved to be a great model system to identify adaptations in mitochondrial form and function as mechanisms against chronic oxidative stress. As previously been shown in several studies, glutamate-resistant HT22R cells are resistant to oxidative glutamate toxicity (Henke et al., 2013; Lewerenz et al., 2006; Lewerenz et al., 2012; Noack et al., 2012) in contrast to their parental HT22S cell line which die in a concentration-dependent manner by a glutamate exposure (Figure 14B; Davis and Maher, 1994; Dittmer et al., 2008; Henke et al., 2013; Landshamer et al., 2008; Noack et al., 2012). The HT22R cells are even remarkably resistant to a higher amounts of glutamate (20 mM) than the cells are usually exposed to (10 mM) under regular growth conditions (Figure 14). The live cell-imaging of both cell lines revealed that glutamate-resistant HT22R cells are slightly affected at the beginning, but continue to proliferate in the end, whereas the cell viability of HT22S cells has already been impaired after approximately 8 h when the cells showed a rounded and less adhered phenotype (Figure 14A). This is usually the time-point when the level of the very important antioxidant GSH drops below 20 % and the ROS production begins to increase exponentially (Tan et al., 1998a). We have previously demonstrated that the linear increase in ROS during the first 6 h (Tan et al., 1998a) is accompanied with a decrease in the mitochondrial membrane potential (Noack et al., 2012). An increase in the cellular GSH content, a reduced glutamate-induced GSH depletion caused by an increased GSH synthesis rate through the up-regulation of the subunit xCT of the cystine/glutamate antiporter system x_c^- (Lewerenz et al., 2006) is valuable for the

resistant phenotype of HT22R cells. Even the over-expression of the xCT subunit in glutamate-sensitive HT22S cells is supporting a decreased cell susceptibility to oxidative stress and enhanced glutathione synthesis (Figure 17C/D; Lewerenz et al., 2006; Noack et al., 2012), whereas the glutamate-resistant phenotype of HT22R cells can be impaired by silencing xCT or inhibiting xCT pharmacological (Lewerenz et al., 2012). For the reason that mitochondria seem to be a major source of ROS production (Finkel and Holbrook, 2000) and HT22R cells showed increased mitochondrial membrane potential and decreased ROS production (Noack et al., 2012), I further studied the role of mitochondria in the resistant phenotype of HT22R cells. Chronic oxidative stress influenced in HT22R cells the mitochondrial network and reduced mitochondrial fragmentation (Figure 15A) in addition to decreasing the mitochondrial respiration in intact cells (Figure 15C), which suggests that HT22R cells are less dependent on OXPHOS and hence, ATP production in mitochondria. This assumption is supported by the observation that a treatment of HT22R cells with the ATP synthase-inhibitor oligomycin induced less cell death of HT22R cells than the cell viability of HT22S cells was affected (Pfeiffer et al., 2014). Thus, we expected a shift from OXPHOS towards non-mitochondrial pathways of energy production like glycolysis and/or the pentose phosphate pathway in HT22R cells.

Cancer cells often display a decrease in their energy production in mitochondria towards glycolysis, although they have sufficient supply to oxygen and produce up to 50 % of their ATP through glucose metabolism in this pathway (Pedersen, 2007). In the end, glucose is converted to lactate which is transported out of the cell (Pedersen, 2007). This phenotype is known as the Warburg effect (Pedersen, 2007). Cancers displaying the Warburg effect show up-regulation of the first enzyme in glycolysis, the hexokinase isoform 2, which binds to VDAC in the outer mitochondrial membrane (Pedersen, 2007). The binding to VDAC prevents its inhibition through its product glucose-6-phosphate as well as hexokinase 2 gets direct access to mitochondrially produced ATP increasing its activity (Pedersen, 2007). The analysis of hexokinase 1 and hexokinase 2 in cytosolic and mitochondrial-enriched fractions of HT22S and R cells excluded the Warburg effect in the resistant phenotype of HT22R cells because even though they showed an up-regulation of hexokinase 1 and 2, both hexokinases are primarily localized in the cytosol (Pfeiffer et al., 2014). In addition, HT22R cells displayed a reduced lactate production, while they utilized the same amount of glucose than HT22S cells (Figure 17A/B) which suggests an increase in the pentose phosphate pathway for energy production, whereas mitochondrial respiration is reduced. In fact, the activity of the first and rate-limiting enzyme of the pentose phosphate pathway, the G6PD (Stincone et al., 2014), is increased in HT22R cells (Pfeiffer et al., 2014). It is well-known that the pentose phosphate pathway is important for the synthesis of ribonucleotides and is a very important source for NADPH (Patra and Hay, 2014). It splits from the glycolytic pathway

after the first step when glucose is converted to glucose-6-phosphate by hexokinases (Patra and Hay, 2014). NADPH is necessary for the recovery of GSH from its oxidized form GSSG by the glutathione reductase (Dringen, 2000; Dringen and Hirrlinger, 2003). Previous studies even demonstrated a relationship between the pentose phosphate pathway and the antioxidant defence system and showed that a treatment of various cell types with glutathione-reducing drugs, H_2O_2 or peroxynitrite induced a stimulation of the pentose phosphate pathway, an increase in G6PD expression and/or G6PD activation (Ben-Yoseph et al., 1996; Garcia-Nogales et al., 2003; Salvemini et al., 1999; Ursini et al., 1997). We hypothesize that in HT22R cells an increase in glucose metabolism in the pentose phosphate pathway leading to increased NADPH production as well as the already recognized increased expression of xCT (Lewerenz et al., 2006) is especially beneficial for increased glutathione production and recovery. These adaptations help HT22R cells to survive a prolonged exposure to glutamate and are part of their glutamate-resistant phenotype. Interestingly, the transient over-expression of G6PD in HT22S cells also induced an increase in total cellular glutathione content comparable to cells over-expressing xCT (Figure 17C). Salvemini and colleagues have already shown that a stable over-expression of human G6PD in HeLa cells induces an increase in G6PD protein expression and activity as well as it enhances GSH level, which is accompanied by reduced ROS production under basal levels, but cannot prevent an increase in ROS production under BSO-induced glutathione depletion (Salvemini et al., 1999). Nevertheless, the activities of the GSH reductase and GSH peroxidase, which are enzymes of the glutathione metabolism as well as the H_2O_2-removing enzyme catalase and 6-phosphogluconate dehydrogenase of the pentose phosphate pathway are unaffected in these cells (Salvemini et al., 1999). A glutamate treatment of G6PD-transfected HT22S cells induced as well glutathione depletion in our hands, but this glutathione depletion was slower as in control cells, but faster than in xCT over-expressing HT22S cells (Figure 17C). Extracellular glutamate induces an inhibition of the cystine/glutamate antiporter x_c^-, which results in GSH depletion and increased ROS production (Murphy et al., 1989). This induced GSH depletion has most probably happened in G6PD-expressing cells as well, whereas the over-expression of xCT has possibly induced an increased cystine uptake as recognized in HT22R cells with increased xCT expression, which is inhibited by higher concentrations of glutamate than in HT22S cells (Lewerenz et al., 2006). We assume that in xCT over-expressing cells a higher concentration of glutamate probably induces the same effect as in control cells as well as the same effect is induced after a longer time. Nevertheless, the increased total cellular glutathione content is not preventing glutamate-induced cell death in G6PD over-expressing HT22S compared to xCT over-expressing cells (Figure 17D; Lewerenz et al., 2006; Noack et al., 2012). This could

also be due to a more rapid inhibition of the cystine/glutamate antiporter x_c^-, reduced GSH production and decrease in GSH in the end.

The supposed increase in glucose metabolism in the pentose phosphate pathway and reduced mitochondrial respiration of intact HT22R cells in growth medium (Figure 15), whereas the OXPHOS states are enhanced in permeabilized HT22R cells (Figure 16), let to the hypothesis that basal mitochondrial respiration is limited by a use of substrates in the pentose phosphate pathway resulting in a limited availability of substrates for glycolysis and mitochondrial function. In both experimental settings, the basal mitochondrial respiration was consistently reduced in HT22R cells because prior to permeabilization cells are dependent on endogenous substrates in mitochondrial respiration medium, which reflects a limited availability of substrates. The observed increase in mitochondrial membrane potential in HT22R cells (Noack et al., 2012) would expect an increase in mitochondrial respiration and OXPHOS, however, HT22S cells and HT22R used a comparable fraction of their ETS capacity for phosphorylating respiration (netR/E ration) in addition to an impaired mitochondrial respiration in HT22R cells. Even though the leak respiration is similar in HT22R and HT22S cells, the calculation of the fraction of their ETS capacity used for compensating proton slip, electron slip, electron leak and cation cycling (Pesta and Gnaiger, 2012) is remarkably elevated (Figure 16), which might be the source for increased mitochondrial superoxide production in HT22R cells (Pfeiffer et al., 2014). In addition, the flux control ratio of oxidative side-reactions, which is ROX relative to the total and uncorrected uncoupled respiratory flux E' (ROX/E'), as well as ROX were remarkably increased in HT22R cells. It can be assumed that this is caused by an increase in auto-oxidation reactions and the activity of oxygen consuming enzymes like peroxidases and oxidases, which in part contribute to ROS production (Pesta and Gnaiger, 2012). Further experiments are necessary to explain the origin of an increased flux control ratio of oxidative side-reactions and ROX.

Thus, we came to the conclusion that a change in energy metabolism by a shift from energy production through OXPHOS in mitochondria towards the pentose phosphate pathway for increasing NADPH production, glutathione production and recovery allows HT22R cells to survive a prolonged exposure to glutamate and are part of their glutamate-resistant phenotype. The observed changes in mitochondrial form and function including adaptations in energy metabolism can be counted as resistance mechanisms against oxidative stress.

4.3 Possible Reasons for Changes in Glucose Metabolism in Glutamate-Resistant HT22R Cells

The recognition of increased pentose phosphate pathway activity as an adaptation of HT22R cells to prolonged oxidative stress (Pfeiffer et al., 2014) raised the question, how a transition

in glucose metabolism is induced. It has already been recognized that as a consequence of oxidative stress a change in glucose metabolism can be induced through the cooperation of rapid metabolic and subsequent slower gene regulatory mechanisms resulting in transitions in the glycolysis/pentose phosphate pathway, whereby the pentose phosphate pathway activity gains rapidly in importance (reviewed in Stincone et al., 2014). Within seconds oxidative stress can inhibit glycolytic enzymes including glyceraldehyde-3-phosphate dehydrogenase (GAPDH; Ralser et al., 2007; Ralser et al., 2009) and the pyruvate kinase (Anastasiou et al., 2011), while a reduced activity of the pyruvate kinase can even lead to accumulation of its substrate phosphoenolpyruvate which inhibits the glycolytic enzyme triosephosphate isomerase (Gruning et al., 2011). Under these conditions, the activity of the pentose phosphate pathway is not influenced, while glycolysis is inhibited (Ralser et al., 2007; Ralser et al., 2009; Shenton and Grant, 2003). These adaptations are only short-lived before post-translational and transcriptional changes occur which sustain increased pentose phosphate pathway activity (Stincone et al., 2014). Changes in post-translational modifications, like for example SIRT2-mediated deacetylation of G6PD induced by oxidative stress through menadione, subsequently enhances G6PD activity in mouse erythrocytes and MEF cells resulting in increased pentose phosphate pathway activity (Wang et al., 2014). In addition, analysis of oxidative stress induced by for example H_2O_2 results in rapid, but transient increased G6PD mRNA expression levels in human HepG2, Hep3B and Jurkat T-cells which show increased G6PD activity (Ursini et al., 1997) as well as a treatment of Hep3B cells with the GSH-decreasing drug diamide enhances G6PD protein expression and transiently increases its activity (Salvemini et al., 1999). But the recognized increase in G6PD protein activity (Pfeiffer et al., 2014) and resulting pentose phosphate pathway activity in HT22R cells is an effect of long-term transcriptional changes rather than an effect of post-translational or transient transcriptional changes. Certain transcription factors and signalling complexes are associated with an up-regulation of the pentose phosphate pathway activity (Patra and Hay, 2014) which may even mediate the alterations in HT22R cells. Activation of the mammalian target of rapamycin complex 1 (mTOR1) can stimulate glycolysis and the pentose phosphate pathway by inducing gene expression including enzymes of the oxidative branch of the pentose phosphate pathway like G6PD, 6PGDH and ribulose-5-phosphate isomerase and epimerase (Duvel et al., 2010). Nevertheless, studying two targets of mTOR signalling, the ribosomal protein S6 and S6 kinase, excluded mTOR signalling being responsible for the transition in energy metabolism in HT22R cells (Pfeiffer et al., 2014).

The transcription factor nuclear factor erythroid 2-related factor 2 (Nrf2) is activated by electrophiles, ROS and xenobiotics and induces the expression of detoxifying enzymes and antioxidants protein genes by binding to antioxidant response elements (ARE), a cis-regulatory element important for gene induction (Uruno and Motohashi, 2011). We could

show that a treatment of HT22S cells with the neuroprotective antibiotic ceftriaxone (Lewerenz et al., 2009) as well as with dimethyl fumarate (Albrecht et al., 2012) increased Nrf2 expression inducing increased protection against oxidative stress by enhancing GSH levels (Albrecht et al., 2012; Lewerenz et al., 2009). Nrf2 is a known inducer of the cystine/glutamate antiporter x_c^- and is responsible for an increased expression of the subunit xCT and enhanced x_c^- activity in ceftriaxone-treated HT22S cells (Lewerenz et al., 2009) and a raise in nuclear Nrf2 caused by a DMF-treatment in HT22S increased xCT expression (Albrecht et al., 2012). In a study with *Nrf2*-knockout mice, it has been recognized that Nrf2 is also important for gene expression of several proteins of the pentose phosphate pathway (Wu et al., 2011). This was further confirmed in a study with cancer cell lines in which *NRF2* knockdown decreased the mRNA and protein expression of various enzymes of the pentose phosphate pathway including G6PD and 6PGDH, transketolase and transaldolase 1 (Mitsuishi et al., 2012). Thus, Nrf2 activates enzymes of the oxidative and non-oxidative branch of the pentose phosphate pathway and is beneficial for NADPH and nucleotide production (Mitsuishi et al., 2012). Since HT22R cells show increased xCT expression (Lewerenz et al., 2006) and increased G6PD protein activity (Pfeiffer et al., 2014), these changes could be induced by Nrf2. But HT22R cells display a comparable Nrf2 accumulation than HT22S cells, so that Nrf2 plays a minor role in their glutamate-resistant phenotype (Lewerenz et al., 2012). Responsible for increased xCT expression in HT22R cells is an up-regulation of the nuclear factor activating transcriptional factor-4 (ATF4) due to a 13 bp deletion in the upstream open reading frame overlapping the ATF4 open reading frame and the formed fusion protein is effectively translated under usual suppressing conditions (Lewerenz et al., 2012). In HT22S cells enhanced resistance against oxidative glutamate toxicity can be achieved by over-expression of ATF4 and a subsequently induced increase in system x_c^- activity and GSH content (Lewerenz and Maher, 2009). ATF4 has already been recognized as a transcription factor regulating glutathione metabolism because ATF4 over-expression increases intracellular GSH, whereas knockdown of ATF4 decreases genes involved in glutathione metabolism (Igarashi et al., 2007) as well as *Atf4*$^{-/-}$ mouse fibroblasts show reduced expression in genes for glutathione biosynthesis and amino acid import (Harding et al., 2003). A direct relationship of ATF4 and cellular metabolism has not been reasoned, but up-regulation and activation of ATF4 in the heart of transgenic mice carrying a single nucleotide polymorphism in the gene of aldehyde dehydrogenase 2 stimulates expression of enzymes for amino acid biosynthesis and transport which give rise to precursors for GSH synthesis resulting in elevated GSH levels as well as the myocardial NADPH/$NADP^+$ ratio enhances and the levels of intermediate metabolites like 6-phosphogluconate and ribose-5-phosphate in the pentose phosphate pathway increase (Endo et al., 2009). Therefore, ATF4 and to a smaller part Nrf2 seem to be important for the

glutamate-resistant phenotype of HT22R cells. We assume that these two transcription factors may mediate the change in glucose metabolism observed in this study. Interestingly, a direct interaction of ATF4 and Nrf2 has been recognized and a dimer of both proteins seems to bind to ARE (He et al., 2001).

In conclusion, the alterations in energy metabolism are of an adaptive nature in the glutamate-resistant HT22R cell line and are part of their resistant phenotype rather than being a pronounced change in mitochondrial form and/or function as induced by acute stressors in HT22S and SH-SY5Y cells.

4.4 GDAP1 Triggers Mitochondrial Fission in SH-SY5Y Cells

Because GDAP1 is up-regulated in HT22R cells and its over-expression protects against oxidative stress (Noack et al., 2012), it was tremendously interesting to even study the direct effect of this protein on mitochondrial form and function. Previous studies identified the outer mitochondrial membrane (Niemann et al., 2005) and cytoprotective protein (Noack et al., 2012) GDAP1 as a factor influencing mitochondrial dynamics and inducing mitochondrial fission (Niemann et al., 2005). Even though the mitochondrial morphology can vary between different cell types (Collins et al., 2002), over-expression of GDAP1 protein in monkey COS-7 cells, mouse HT22S and human HeLa cells induces mitochondrial fission (Niemann et al., 2005; Noack et al., 2012; Pla-Martin et al., 2013) as well as I could show here that over-expression of GDAP1 protein caused mitochondrial fragmentation in SH-SY5Y cells (Figure 19B). Thus, the function of GDAP1 as a non-classical mitochondrial fission factor is cell type independent. It is not only limited to mammalian cells, because a similar effect of GDAP1 on mitochondrial dynamics has been recognized recently in drosophila (Lopez Del Amo et al., 2014). Although mitochondrial fission is an early and critical step in apoptosis (Suen et al., 2008; Youle and Karbowski, 2005), GDAP1 causes mitochondrial fission without enhancing the risk of apoptosis and without interfering with mitochondrial fusion (Niemann et al., 2005). Induction of mitochondrial fragmentation by GDAP1 is dependent on the fission factors Drp1 and Fis1 (Niemann et al., 2009), however, it is still not fully understood how GDAP1 initiates mitochondrial fission. But the Charcot-Marie-Tooth disease-associated and recessively inherited point mutation R310Q (Azzedine et al., 2003) fails to induce mitochondrial fission in COS-7 cells (Niemann et al., 2005), HT22S cells (Noack et al., 2012) and as well in SH-SY5Y cells as we could show here. This is not caused by a relocation of GDAP1, because GDAP1 R310Q is still localized at mitochondria (Figure 18E; Niemann et al., 2005; Wagner et al., 2009). The mutation R310Q is located within a non-specific region, C-terminally to the hydrophobic domain (Wagner et al., 2009). This amino acid is especially important for mitochondrial fission and hence, for proper function concerning changes in

mitochondrial dynamics (Wagner et al., 2009). SH-SY5Y S34A cells containing a mutation of the predicted active amino acid serine for catalytic activity in the GST-N domain (Shield et al., 2006) lost almost completely their mitochondrial fission activity (Figure 20B), which is in line with observations in COS-7 cells (Wagner, 2009). This suggests that this amino acid is important for mitochondrial fission. However, the mutation S34A, although this protein is still mitochondrially localized (Figure 18E), drastically induced mitochondrial elongation in SH-SY5Y cells suggesting that it rather affects GDAP1's mitochondrial fission activity in a negative and dominant way. GDAP1's mitochondrial fission activity seems to be connected with its putative GST-activity because point mutations of various highly conserved key amino acids of the GST-N domain including S34A resulted in the loss of its fission activity although it was still localized at mitochondria (Wagner, 2009). It should be noted that mutations causing CMT are especially located within the GST domains of the protein (Cassereau et al., 2011a). Thus, regarding mitochondrial fission activity, the mutation R310Q and S34A are both lost-of-function mutation, while GDAP1 S34A especially dominant negatively affects GDAP1's fission activity.

4.5 *Gdap1* Silencing Affects Mitochondrial Dynamics in SH-SY5Y Cells

Previous analysis of the mitochondrial morphology in different *Gdap1* silenced cell lines resulted in contradictory findings (Niemann et al., 2005; Niemann et al., 2009; Pla-Martin et al., 2013). *Gdap1* silencing in N1E-115 cells supports mitochondrial elongation (Niemann et al., 2005) compared to SH-SY5Y *GDAP1* KD cells displaying a comparable mitochondrial elongation index to controls cells, but with a reduced mitochondrial interconnectivity (Pla-Martin et al., 2013). By analysing the mitochondrial morphology of *GDAP1* KD cells in the same way as the over-expressing cells, we observed that the mitochondrial morphology actually differs between *GDAP1* KD and control cells. Silencing of *GDAP1* changed the mitochondrial morphology towards a more fragmented phenotype in SH-SY5Y cells (Figure 19A). This result might reflect the recognized reduced mitochondrial interconnectivity in *GDAP1* KD cells (Pla-Martin et al., 2013). In addition, knockdown of *Drosophila Gdap1* increased mitochondrial fusion and induced larger mitochondria in the retina as well as very large and elongated mitochondria in thorax muscle fibres (Lopez Del Amo et al., 2014). In the muscle progressive aggregation of mitochondria was induced by *Gdap1* knockdown (Lopez Del Amo et al., 2014). In contrast to this observation, cultured primary motor neurons of *Gdap1* knockout (*Gdap1*$^{-/-}$) mice with early-onset neuropathy displayed scattered mitochondria with a round or spheroid morphology, while more severely affected neurons showed large tubular mitochondria that cristae were swollen (Barneo-Munoz et al., 2015).

The mitochondrial network interconnectivity was additionally reduced in cultured *Gdap1*$^{-/-}$ motor neurons (Barneo-Munoz et al., 2015). Thus, *GDAP1/Gdap1* silencing affects mitochondrial dynamics and alters the balance between mitochondrial fusion and fission in various extents. Interestingly, the paralogue of GDAP1, GDAP1L1, which is mainly cytosolic and expressed in the central nervous system, but not in the peripheral nervous system, translocates upon increasing concentrations of GSSG (oxidized glutathione) to mitochondria and inserts into the outer mitochondrial membrane (Niemann et al., 2014). In *Gdap1* silenced N1E-115 cells, re-expression of *Gdap1* can abrogate the elongated mitochondrial morphology and induced mitochondrial fission (Niemann et al., 2009) as well as expression of *Gdap1l1* provoked mitochondrial fragmentation (Niemann et al., 2014). Thus, GDAP1L1 can compensate the loss of GDAP1. In agreement with this observations, increasing levels of GDAP1L1 were associated with mitochondria in the spinal cord of aged *Gdap1*$^{-/-}$ mice, where it can compensate the deficiency of GDAP1 (Niemann et al., 2014) and this effect might affect silencing of *Gdap1*/*GDAP1* even in other cell types.

4.6 Influence of GDAP1 on Mitochondrial Respiratory Activity

Because dysfunction in mitochondrial dynamics has been implicated in neurodegenerative diseases like Parkinson's disease, Huntington disease and even in subtypes of Charcot-Marie-Tooth disease (Itoh et al., 2013; Westermann, 2010; Youle and van der Bliek, 2012) together with the observation that GDAP1 influences mitochondrial morphology (Niemann et al., 2005; Noack et al., 2012) even in SH-SY5Y cells, I further analysed the effect of cytoprotective GDAP1 on mitochondrial respiratory activity. Initial analysis studying the influence of GDAP1 on mitochondrial function showed a reduced mitochondrial respiratory activity of isolated intact mitochondria from stable HT22S GDAP1 cells which displayed an increased mitochondrial membrane potential (Noack et al., 2012). Here, I could show that GDAP1 (wild type and mutated) affected mitochondrial respiration in intact SH-SY5Y cells (Figure 20F) by reducing the part of their maximal ETS capacity used for routine and/or phosphorylating respiration (Figure 20G). Thus, the mitochondrial respiration is affected by over-expression of wild type and mutated GDAP1. By tendency the measured OXPHOS capacity states in permeabilized GDAP1 cells are reduced (Figure 21D) in agreement with observations in HT22S GDAP1 cells (Noack et al., 2012). However, stable over-expression of R310Q further reduced the OXPHOS capacity. The OXPHOS state with convergent electron input was significantly decreased in R310Q cells (Figure 21D) in contrast to previous results in which stable HT22S R310Q cells exhibited no significant changes in the mitochondrial respiratory activity (Noack et al., 2012). In both GDAP1 and R310Q cells the ETS capacity was impaired in contrast to control cells, which may influence ATP production

through OXPHOS. Interestingly, in S34A cells with elongated mitochondria we expected that here a more tubular network also induces increased ATP production as observed for a stress-induced highly interconnected mitochondrial network (Tondera et al., 2009) as well as mitochondrial fusion are linked to high energy demand (reviewed in Westermann, 2012). In fact, I only recognized a comparable respiratory activity to GDAP1 cells. We did not find out the cause of the reduction in mitochondrial respiratory activity in GDAP1 (wild type and mutant) over-expressing cells. In our previous study we postulated that the reduced mitochondrial activity together with an increased mitochondrial respiration might indicate an inhibitory effect of GDAP1 on later stages of oxidative phosphorylation like the ATP synthase (Noack et al., 2012). Since all cell lines displayed a reduced ETS capacity and hence reduced maximal respiration, it would be interesting to study the mitochondrial activity depending on electron input through complex I, complex II or complex IV separately to find out whether one of the complexes is influenced. However, we can conclude by our observations that both mutated GDAP1 forms did not lose their ability to reduce mitochondrial respiration and induced a comparable reduction of mitochondrial activity like wild type GDAP1 although GDAP1 R310Q even can further reduce mitochondrial respiration. Thus, disease-causing GDAP1 R310Q presents a pathological gain-of-function regarding its ability to reduce mitochondrial respiration in contrast to its loss-of-function in inducing mitochondrial fission.

The analysis of the *GDAP1* silenced cells suggested that GDAP1 regulates mitochondrial respiration, because *GDAP1* KD cells have an increased mitochondrial respiratory activity (Figure 20/21) even though the mitochondrial morphology was increasingly fragmented. In particular, *GDAP1* KD cells seem to have sufficient supply to NADH due to an increase in the total NAD (NAD^+ and NADH) pool (Figure 21E) and a possible increase in NADH can especially support complex I-supported respiration. Interestingly, young *Gdap1* over-expressing and *Gdap1* RNAi flies revealed a decrease in ATP levels compared to control flies, but the ATP levels in *Gdap1* knockdown cells was increased in contrast to over-expressing cells (Lopez Del Amo et al., 2014), which in some way reflects our observations in tendency. In our analysis, *GDAP1* KD cells possessed evidently an excess in their ETS capacity state (GMS_E) indicating a limiting phosphorylating respiration, whereas in all other cell lines the mitochondrial respiration seemed to be restricted by the ETS capacity for the reason that stimulation with FCCP did not cause a much higher oxygen consumption than in the OXPHOS state with convergent electron input (Figure 21). This was especially detectable in SH-SY5Y cells GDAP1, R310Q and S34A and less severe in both control cell lines. *GDAP1* silenced cells seem to meet their energy demand to a higher extent through ATP production during OXPHOS, while the existence of GDAP1 gives the impression to prevent this change in energy supply. The increase in total NADP levels under *GDAP1* knockdown

even suggests an elevated pentose phosphate pathway activity with increased NADPH production which together with a possible increase in NADH production in *GDAP1* KD cells may indicate a way to avoid an increasing susceptibility to oxidative stress when cytoprotective GDAP1 is down-regulated. Soucek and colleagues demonstrated that increased glucose consumption in glycolysis and pentose phosphate pathway resulting in elevated production of NADH and NADPH protect against oxidative stress (Soucek et al., 2003). But an increasing activity in the pentose phosphate pathway needs to be proved in *GDAP1* KD cells. Interestingly, silencing of *GDAP1* also enhanced the flux control ratio of oxidative side-reactions which is ROX relative to the total and uncorrected uncoupled respiratory flux E' (ROX/E'). This is caused by an increase in ROX through auto-oxidation reactions and the activity of oxygen consuming enzymes like peroxidases and oxidases which in part contribute to ROS production (Pesta and Gnaiger, 2012). The existence of GDAP1 protein seems to prevent this effect, because the control cell lines as well as the over-expressing cells lines did not exhibit this effect. It has already been shown that over-expression of GDAP1 decreases mitochondrial superoxide production (Noack et al., 2012) as well as overall ROS production (Lopez Del Amo et al., 2014; Noack et al., 2012), whereas knock down of *Gdap1* is associated with increased ROS production in aged flies (Lopez Del Amo et al., 2014). Since mitochondria especially contribute to ROS production (Finkel and Holbrook, 2000), the increased mitochondrial respiration in *GDAP1* KD cells and a possibly increased activity of oxygen consuming enzymes might cause a general increase in ROS production and in particular mitochondrial superoxide production. Under these circumstances, an increasing production of NADH and NADPH to protect against oxidative stress might prevent damages by increasing ROS production in *GDAP1* KD cells and maybe are adaptations against stress in *GDAP1* KD cells, but this needs to be proved additionally to proving increasing ROS production.

The recognized changes in energy supply under alteration of GDAP1 protein expression levels propose metabolic adjustments, however, further analysis are necessary to allow a conclusion whether a change in mitochondrial respiration contributes to the progression in CMT disease associated with mutations in *GDAP1*. Studying the mitochondrial fusion proteins MFN1, MFN2 and OPA1 has already demonstrated a relationship between proper mitochondrial dynamics being important for key cellular function including mitochondrial ATP production during OXPHOS. A loss of mitochondrial fusion in MEF cells lacking both mitofusin 1 and 2, or in *OPA1* RNA interference cells was accompanied by reduced and heterogeneous mitochondrial membrane potential and diminished mitochondrial respiration caused by defects in multiple respiratory complexes (Chen et al., 2005). Knockdown of Mfn2 protein in muscle cells reduced mitochondrial glucose and fatty acid oxidation, mitochondrial membrane potential and induced down-regulation of the protein expression of nuclear-

encoded subunits of respiratory complexes I, II and III as well as the ATP synthase which results in decreased complex I+III and complex III activity (Pich et al., 2005). Fibroblast cell lines of patients with CMT2A caused by mutations in *MFN2* manifested a reduced mitochondrial membrane potential and a defect in mitochondrial coupling although the mitochondrial morphology was unaffected (Loiseau et al., 2007) and the analysis of further CMT2A patients' fibroblast cell lines displayed a similar mitochondrial coupling defect (Guillet et al., 2010). In both cases the coupling defect reduced the OXPHOS efficiency although the ATP production was unaltered because of increasing oxygen consumption (Guillet et al., 2010; Loiseau et al., 2007). A first evidence supporting a change in mitochondrial respiration contributing to the progression in CMT disease associated with mutations in *GDAP1* come from a study by Cassereau and colleagues in which fibroblasts cell lines from patients with autosomal dominant CMT2K caused by the point mutation C240Y in *GDAP1* (c.719G>A) showed a mitochondrial complex I deficiency (Cassereau et al., 2009). Thus, mutations in the mitochondrial fission factor GDAP1 causing Charcot-Marie-Tooth disease can affect mitochondrial dynamics which might result in mitochondrial dysfunction. In addition, GDAP1 seems to be important for proper mitochondrial transport because *GDAP1/Gdap1* knockdown and knockout impairs mitochondrial transport and alters mitochondrial distribution (Lopez Del Amo et al., 2014; Niemann et al., 2014; Pla-Martin et al., 2013). All the changes seem to contribute to the progression of CMT disease caused by mutations in the gene of *GDAP1*.

In conclusion, GDAP1 belongs to cytoprotective proteins that directly affect mitochondrial form and function. It seems to be even necessary to prevent a dependency on energy production through especially OXPHOS as demonstrated under GDAP1 deficiency. Similarity to adaptations under chronic oxidative stress in glutamate-resistant HT22R cells which even show increasing levels of GDAP1 expression (Noack et al., 2012), is a by trend reduced mitochondrial respiratory activity under GDAP1 over-expression, however, not as strong as in HT22R cells.

4.7 The Cytoprotective Glutathione Transferase GDAP1 Prevents EA-Induced Mitochondrial Fusion

The analysis to prove our hypothesis that GDAP1 acts as a redox sensor sensing the redox state in the cytosol and transmitting information to mitochondria which may induce adaptations in mitochondrial form and function resulted in some presumable clues. As a reminder, our hypothesis came up because recent findings demonstrated a GST enzyme activity with an insect cell-expressed recombinant GDAP1 protein (Wagner, 2009), while we identified GDAP1 as a cytoprotective protein increasing levels of GSH to protect against

oxidative stress (Noack et al., 2012) as well as GDAP1 over-expressing old flies show enhanced GSH levels and an increased GSH/GSSG ratio resulting in reduced ROS production (Lopez Del Amo et al., 2014). Usually GSTs catalyze the nucleophilic addition of reduced GSH to electrophilic substrates (Hayes et al., 2005) and thereby decrease the level of reduced glutathione by catalyzing its conjugation. In contrast to classical GSTs, GDAP1 increases the GSH content (Lopez Del Amo et al., 2014; Noack et al., 2012) as well as it acts as a non-classical mitochondrial fission factor, so that it is possible that GDAP1 rather acts as GSH sensor than being a classical GST. Interestingly, analysing the effect of oxidative stress by the known GSH depleting reagents EA and MQ (Chiou and Tzeng, 2000; Kim et al., 2014; Seyfried et al., 1999; Wullner et al., 1999) in GDAP1 over-expressing cells proved that GDAP1 inhibited mitochondrial fusion induced by EA and still functioned as a mitochondrial fission factor (Figure 22A) although mitochondrial fission induced by GDAP1 is dependent on Fis1 and Drp1 (Niemann et al., 2009) and EA is considered to inhibit mitochondrial fission (Bowes and Gupta, 2008). Thus, GDAP1 is a strong fission factor and a functional GST activity seems to be important for this effect because mitochondrial fusion was further increased in EA-treated S34A (Figure 22A), which show a general drastic increase in mitochondrial elongation (Figure 20B) and probably GDAP1 S34A is missing GST activity. In contrast, EA induced mitochondrial elongation in R310Q cells and control EV cells. We assume that this perhaps is an indication for GDAP1 being a redox sensor and adjusting the mitochondrial morphology. But it could also be that over-expression of GDAP1 increased total GSH levels (Lopez Del Amo et al., 2014; Noack et al., 2012), which might prevent mitochondrial fusion induced by cysteine-alkylation of EA (Bowes and Gupta, 2005) and instead EA forms spontaneously or mediated by GSTs a conjugate with GSH (Awasthi et al., 1993; Habig et al., 1974). In addition, EA is a substrate for GDAP1 that was used to prove its GST activity (Wagner, 2009). Surprisingly in contrast to our expectation, EA did not induce mitochondrial fusion in *GDAP1* KD cells compared to control pLKO-NT cells with enhanced mitochondrial fusion (Figure 22B). We do not know why silencing of *GDAP1* prevents mitochondrial elongation induced by EA, but perhaps there is a link between adjustments in cellular metabolism including increased mitochondrial activity, total NAD and total NADP which prevents the change in mitochondrial morphology. Even though the effect of EA-treatment on mitochondrial morphology varied between the different cell lines, the effect on mitochondrial respiration was comparable. In all cell lines EA induced a reduction in mitochondrial activity and impaired mitochondrial respiration (Figure 23 and 24). Nevertheless, GDAP1 cells exhibited a significantly lowered reduction in the relative decrease in routine respiration and ETS capacity (Figure 23D), which might be prevented because EA cannot influence the mitochondrial morphology in this cell line (Figure 22A).

However, the measured routine and maximum respiration was also reduced in a comparable manner as in the control and mutated *Gdap1* over-expressing cells.

Previous studies demonstrated that EA induces a reduction of the cytosolic and mitochondrial GSH pool as well as EA affects and impairs the activity of various mitochondrial complexes (Seyfried et al., 1999; Wullner et al., 1999). In these two studies and in a study by Muyderman and colleagues, it was recognized that the mitochondrial GSH pool is more rapidly affected than the cytosolic pool (Muyderman et al., 2004; Seyfried et al., 1999; Wullner et al., 1999). A similar concentration of EA as I used in this study induced a complete GSH depletion of the mitochondrial pool in astrocytes within 15 minutes (Muyderman et al., 2004). Therefore, it might be that we encountered a similar effect in SH-SY5Y cells which impaired mitochondrial respiration up to a level that no longer significant differences in the mitochondrial activity were detectable between the different cell lines. Maybe conditions in which a highly selective depletion of the mitochondrial GSH pool is induced, like they were determined for primary astrocytes (Muyderman et al., 2004), can help for the analysis of mitochondrial respiration under acute oxidative stress in SH-SY5Y cells.

The presumable clues of GDAP1 being a redox sensor were weakened studying the effect of GDAP1 in preventing changes in mitochondrial form and function caused by oxidative stress induced by GSH depletion through MQ (Chiou and Tzeng, 2000; Kim et al., 2014). MQ, which is known to induce mitochondrial fission (Loor et al., 2010) and also leads to mitochondrial fragmentation in SH-SY5Y cells (Figure 11), provokes mitochondrial fission independent of the existence of the mitochondrial fission factor GDAP1. We recognized that in all cell lines the mitochondrial categories fragmented and vesicular were increased (Figure 22) and even mitochondrial fragmentation was further pronounced in GDAP1 cells as well as in R310Q cells with lost mitochondrial fission activity. Astonishingly, the dominant negative effect of GDAP1 S34A was abolished and mitochondrial fission was induced. Thus, MQ has a strong effect on changing mitochondrial dynamics and inducing mitochondrial fragmentation. Most likely MQ induced a reduction in the mitochondrial membrane potential (Gerasimenko et al., 2002; Kim et al., 2014; Laux and Nel, 2001; Loor et al., 2010). For the reason that a protonophore-induced collapse of the mitochondrial membrane potential has been associated with induction of mitochondrial fragmentation caused by inhibiting mitochondrial fusion (Legros et al., 2002) and GDAP1 increases the mitochondrial membrane potential in HT22S cells (Noack et al., 2012), GDAP1 could not prevent further mitochondrial fragmentation induced by MQ in SH-SY5Y cells (Figure 22A). However, GDAP1 has been identified as a mitochondrial fission factor (Niemann et al., 2005) and hence, we would usually expect that it adjusts the mitochondrial morphology by inducing mitochondrial fragmentation when it really functions as a redox sensor and this coincidences with MQ-induced mitochondrial fragmentation (Loor et al., 2010). What argues against

GDAP1 being a redox sensor is that MQ induced a reduction in the maximal mitochondrial respiration (ETS capacity) in GDAP1 cells similar to all other cell lines (Figure 25). In addition, although GDAP1 increased total GSH levels in HT22S cells (Noack et al., 2012) and glutathione-increasing N-acetylcysteine can prevent MQ-induced mitochondrial membrane potential reduction (Kim et al., 2014; Laux and Nel, 2001), GDAP1 did not prevent further changes in the maximal mitochondrial respiration. Nevertheless, GDAP1 prevented a reduction in the routine respiration, which was recognized in SH-SY5Y cells R310Q and S34A, but which was also not detected in EV cells. Thus, SH-SY5Y cells with disease-associated GDAP1 R310Q missing mitochondrial fission activity and GDAP1 S34A with a mutation of the predicted active amino acid for GST activity (Shield et al., 2006) were most severely influenced by a treatment with MQ. MQ affected in a comparable manner mitochondrial respiration in *GDAP1* KD cells and control pLKO-NT cells and reduced routine respiration and ETS capacity and increased ROX (Figure 26).

In conclusion, our experiments could not completely confirm the hypothesis that GDAP1 functions as a redox sensor protein which senses the redox state in the cytosol and transmits information to mitochondria to adjust the mitochondrial morphology and function. Only a treatment with EA might indicate GDAP1 being a redox sensor. It is obvious that further experiments are necessary to prove our hypothesis because the treatment of cells with EA and MQ is very fatal and mitochondrial morphology and function is very strongly and rapidly affected. As a result, evidences are easily obscured and GDAP1's function as a redox sensor cannot be proved.

4.8 Absence of the Cytoprotective Protein Bcl-x_L Induces Mitochondrial Fission and Decreases Mitochondrial Function

The second studied mitochondrial and cytoprotective protein Bcl-x_L, which is well-known for its anti-apoptotic function (Boise et al., 1993; Gonzalez-Garcia et al., 1994), seems to even influence mitochondrial form and function as observed in this study. I demonstrated that in MEF cells with *bcl-x* gene knockout, deficiency of the cytoprotective Bcl-x_L protein induced a change in mitochondrial dynamics and increased mitochondrial fragmentation (Figure 28B) as observed before by conditional knockout of *bcl-x* in mouse cortical neurons (Berman et al., 2009). Re-expression of mitochondrially targeted Bcl-x_L restored mitochondrial dynamics because ActA cells showing re-expression of Bcl-x_L at mitochondria in the knockout background displayed a comparable mitochondrial morphology as WT MEF cells with a more elongated mitochondrial shape (Figure 28B). This proved that mitochondria-localized Bcl-x_L is important for regulating mitochondrial dynamics like it is as well important for its anti-apoptotic activity (Eno et al., 2012) and mitochondrial calcium uptake (Huang et al., 2013).

The phenomenon that Bcl-x_L over-expression leads to more elongated mitochondria has already been recognized in rat cortical neurons (Berman et al., 2009) and HeLa cells (Sheridan et al., 2008). Interestingly, I studied the mitochondrial morphology at a steady state, but real time analysis of mitochondrial dynamics showed that Bcl-x_L over-expression increases both the rate of mitochondrial fission and fusion (Berman et al., 2009). Bcl-x_L apparently influences mitochondrial dynamics by interacting with mitofusins responsible for mitochondrial fusion (Cleland et al., 2011; Delivani et al., 2006) and the mitochondrial fission factor Drp-1 (Li et al., 2008). Although, Berman and colleagues claimed that the elongated mitochondrial morphology observed in Bcl-x_L over-expressing cells cannot be explained by enhanced mitochondrial fusion and fission rates, but is rather a consequence of increasing mitochondrial biomass (Berman et al., 2009), MEF WT and Bcl-x_L-KO cells displayed no difference in their mitochondrial biomass (Huang et al., 2013) although they showed differences in mitochondrial morphology. Since Bcl-x_L-KO cells showed an increasing susceptibility to apoptotic cell death and oxidative stress (Eno et al., 2012) and extensive mitochondrial fragmentation occurs during apoptosis before caspases are activated (Youle and Karbowski, 2005), it might be that increased mitochondrial fragmentation is a hint for increased susceptibility to apoptosis or current apoptosis. Nevertheless, Bcl-x_L-KO cells did not show any difference in cell health under general growth conditions and cells had even an elevated proliferation rate compared to WT and ActA cells (Figure 32C), which makes this presumption unlikely.

Surprisingly, although Bcl-x_L deficient MEF cells have increasingly fragmented mitochondria and we expected a reduced mitochondrial respiration in Bcl-x_L-KO cells because of a reduced mitochondrial calcium uptake (Huang et al., 2013) and a most probably reduced crossing of metabolites including ADP in Bcl-x_L-KO for the reason that Bcl-x_L can regulate crossing of ADP (Vander Heiden et al., 2001), the analysis of mitochondrial oxygen consumption revealed a comparable mitochondrial activity in intact Bcl-x_L-KO, WT and ActA cells (Figure 29). But the comparable measured respiratory activity of WT and Bcl-x_L-KO cells reflects the comparable mitochondrial membrane potential in these cell lines (Huang et al., 2013). However, analysing mitochondrial respiration in permeabilized cells showed that, on the one hand, according to the routine respiration in intact cells, the basal respiration of the still unpermeabilized MEF cell lines was similar, but on the other hand, I recognized differences in the subsequent analysis of OXPHOS and ETS capacity (Figure 30). Bcl-x_L deficient MEF cells displayed a reduction in the OXPHOS and ETS capacity with especially convergent complex I and II electron input, whereas re-expression of mitochondria-localized Bcl-x_L in the Bcl-x_L-KO background restored mitochondrial activity in ActA cells comparable to WT cells. The reduced mitochondrial activity in permeabilized Bcl-x_L-KO cells suggests an impairment of the respiratory system under *bcl-x* gene knockout. But also another scenario

could reduce mitochondrial oxygen consumption in Bcl-x_L-KO cells. Bcl-x_L interacts with VDAC at the outer mitochondrial membrane (Arbel et al., 2012; Huang et al., 2013; Shimizu et al., 1999; Shimizu et al., 2000; Vander Heiden et al., 2001). VDAC can regulate the flux of ions across the outer mitochondrial membrane and is important for the movement of metabolic anions like succinate, pyruvate, phosphocreatine and phosphate between the cytosol and mitochondria as well as for the ATP/ADP exchange through the outer mitochondrial membrane (Hodge and Colombini, 1997; Vander Heiden et al., 2000). Efficient mitochondrial ATP/ADP exchange is required for coupled respiration and to avoid cell death because growth factor withdrawal from dependent cells results in disruption of metabolism by defective ADP and ATP exchange across the outer mitochondrial membrane, which can be prevented by Bcl-x_L (Vander Heiden et al., 2000; Vander Heiden et al., 1999). Bcl-x_L seems to favour the open configuration of VDAC (Huang et al., 2013; Vander Heiden et al., 2001) which is necessary for the movement of metabolic anions to cross the outer mitochondrial membrane (Hodge and Colombini, 1997). Adding recombinant Bcl-x_L protein to isolated mitochondria allows metabolite exchange such as ADP across the outer membrane by inhibiting VDAC1 closure under conditions promoting its closed configuration, while cytochrome c is not released from the intermembrane space (Vander Heiden et al., 2001). The interaction between Bcl-x_L and VDAC is also important for mitochondrial Ca^{2+} uptake (Huang et al., 2013). Hence, re-expression of mitochondria-localized Bcl-x_L in the knockout background re-stores the reduced mitochondrial calcium uptake of Bcl-x_L-KO cells (Huang et al., 2013) and mitochondrial Ca^{2+} uptake is even able to directly increase mitochondrial OXPHOS (Das and Harris, 1990; Hansford and Zorov, 1998). According to these results, even though there is a sufficient supply of substrates and ADP in the experimental setting, Bcl-x_L deficiency could limit metabolites crossing of the outer mitochondrial membrane because of a missing interaction between Bcl-x_L and VDAC which might reduce mitochondrial activity. This reduced mitochondrial activity is, however, re-stored by re-expression of mitochondrially targeted Bcl-x_L. Contradictory to this assumption is the comparable mitochondrial activity in intact cells. We assume that compensatory mechanisms exist which maintain exchange of metabolic anions across the outer mitochondrial membrane and help to avoid a reduction in mitochondrial activity. Especially a continuous exchange of metabolites is necessary to preserve the intactness of the outer membrane and to avoid the release of apoptosis-promoting proteins (Harris and Thompson, 2000). Decreasing movement of metabolites can result in enhanced ROS production, mitochondrial inner membrane hyperpolarisation and matrix swelling (Harris and Thompson, 2000). Loss of permeability can even lead to accumulation of stored metabolic energy in form of phosphocreatine within the intermembrane space (Vander Heiden et al., 2000). Bcl-x_L was shown to prevent both membrane hyperpolarisation and matrix swelling and thereby

preserves the integrity of the outer mitochondrial membrane under various death stimuli (Vander Heiden et al., 1997). In addition to Bcl-x_L, Bcl-2 can prevent the loss of mitochondrial outer membrane permeability in growth factor-deprived cells (Vander Heiden et al., 2000). According to this, Bcl-2 might compensate the Bcl-x_L deficiency in Bcl-x_L-KO cells and maintains mitochondrial respiration in intact cells, however, Bcl-x_L-KO cells display no compensatory up-regulation in the protein expression of other Bcl-2 proteins including Bcl-2 (Eno et al., 2012). Interestingly, over-expression of Bcl-x_L in hippocampal neurons increases the efficiency of energy metabolism by increasing ATP production and decreasing mitochondrial oxygen uptake, whereas Bcl-x_L deficiency reduces ATP synthesis (Alavian et al., 2011). Alavian and colleagues claimed that Bcl-x_L does not only localize in the outer mitochondrial membrane, but also in the inner mitochondrial membrane or the matrix (Alavian et al., 2011). They argue that a direct interaction with the β-subunit of the F_1F_0 ATP synthase can increase F_1F_0 ATPase activity (Alavian et al., 2011). However, Bcl-x_L with the membrane targeting sequence of listerial protein actin assembly-inducing protein (ActA) co-localized with the outer mitochondrial protein Tom20 (mitochondrial import receptor subunit Tom20 of the translocase of outer membrane; Eno et al., 2012) which suggests an localization at the outer mitochondrial membrane making an interaction with the β-subunit of the ATP synthase unlikely that looms into the matrix. Especially, Bcl-x_L interacts with VDAC1 and 3 in the outer mitochondrial membrane and re-expression of the mitochondria-localized Bcl-x_L (including the targeting sequence of ActA) can restore mitochondrial Ca^{2+} uptake in the Bcl-x_L knockout background (Huang et al., 2013), which makes an interaction with the ATP synthase in the mitochondrial matrix improbable. Thus, in ActA cells the re-stored OXPHOS and ETS capacity is not a result of such an interaction. However, our results cannot exclude that certain mitochondrial complexes are impaired. Consequently, the mitochondrial activity of single mitochondrial complexes needs to be examined as well as an analysis of the protein expression of the mitochondrial system can help to better understand the effect and consequences of a Bcl-x_L knockout on mitochondrial respiration.

Under the perspective of a decreased respiratory capacity, we expected an adaptation in the energy metabolism in Bcl-x_L-KO cells. One option would be an increasing glycolytic activity, but although Bcl-x_L-KO cells showed a slightly increased total NAD pool and NADH is in part produced during glycolysis (Stincone et al., 2014), Bcl-x_L-KO, WT and ActA cells consumed a comparable amount of glucose and displayed a similar lactate production (Figure 31A-C). These results suggest a comparable glycolytic activity in all three cell lines. A previous study showed that over-expression of Bcl-x_L in neurons increased the glycolytic activity and enhanced the lactate production (Alavian et al., 2011), but ActA cells over-expressing mitochondrially targeted Bcl-x_L did not show this effect. In addition, the inhibition of mitochondrial respiration by the complex III inhibitor antimycin A and the ATP synthase

inhibitor oligomycin demonstrated that especially Bcl-x_L-KO cells are more susceptible to the inhibition of mitochondrial respiration in galactose containing medium than WT and ActA cells (Figure 31E/F and H/I). The increasing susceptibility of Bcl-x_L-KO MEFs suggests that Bcl-x_L-KO cells depend more on glucose consumption for energy production through glycolysis and/or the pentose phosphate pathway to sustain their energy demand. Since an increase in the glycolytic activity was excluded, we consequently turned to study the pentose phosphate pathway and in fact, recognized an increased protein expression of the rate-limiting enzyme of the pentose phosphate pathway, G6PD (Stincone et al., 2014), and an enhanced total NADP pool (Figure 32A/B) in Bcl-x_L-KO cells which suggests an increased activity of the pentose phosphate pathway. Re-expression of mitochondria-targeted Bcl-x_L reduced the total NADP pool as well as the protein expression of the G6PD, but those two levels were still higher than in WT cells (Figure 32A/B). The significant increase in total NADP is in line with increased mitochondrial NAD(P)H in *bcl-x* knockout neurons (Chen et al., 2011) as well as Bcl-x_L over-expression decreased the mitochondrial to cytosolic NAD(P)H fluorescence in murine TAMH hepatocyte cells (Schwartz et al., 2007). Since NADPH is necessary for the recovery of GSH from its oxidized form GSSG (Dringen, 2000; Dringen and Hirrlinger, 2003), we expected and detected an increased total cellular glutathione content in Bcl-x_L-KO cells, which was reduced to comparable levels in WT cells under re-expression of mitochondria-localized Bcl-x_L (Figure 32D). Since the pentose phosphate pathway is a major source for NADPH production as well as it is necessary for the synthesis of ribonucleotides (Patra and Hay, 2014), the increased pentose phosphate pathway activity in Bcl-x_L deficient cells is, on the one hand, beneficial for an increased total NADP pool and subsequent increased GSH synthesis and recovery, but on the other hand, it can explain the increased proliferation rate of Bcl-x_L-KO cells (Figure 32E).

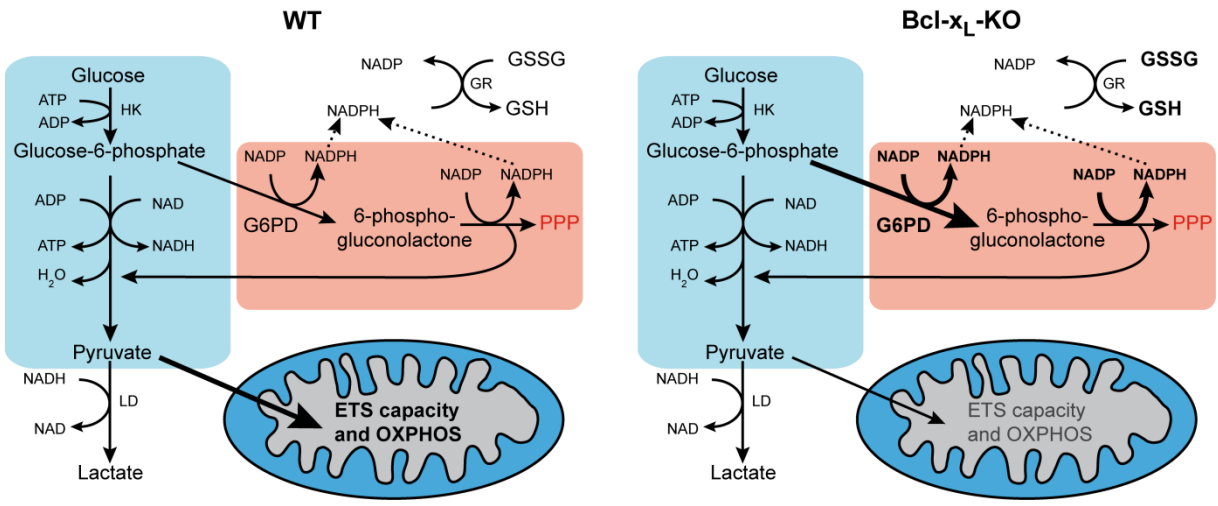

Figure 33: Changes in energy metabolism in Bcl-x_L-KO MEFs.
Illustrated is the energy metabolism in WT (left) and Bcl-x_L-KO cells. Silencing of Bcl-x_L increases G6PD protein expression, total NADP, total cellular glutathione and reduces OXPHOS as well as ETS capacity which suggest a change in energy metabolism with enhanced pentose phosphate pathway activity.
GR, glutathione reductase; HK, Hexokinase; LD, Lactate dehydrogenase; NAD, NAD^+; NADP, $NADP^+$

In conclusion, silencing of Bcl-x_L influences the mitochondrial morphology and affects energy metabolism. *Bcl-x* gene knockout and subsequent deficiency of Bcl-x_L protein expression impairs OXPHOS and ETS capacity, but increases the activity of the pentose phosphate pathway which increases NADPH production and subsequent cellular glutathione content and is beneficial for enhanced cell proliferation. The changes in energy metabolism are illustrated compared to WT cells in Figure 33. Re-expression of mitochondria-localized Bcl-x_L can restore the detected changes in energy metabolism. Thus, Bcl-x_L influences mitochondrial form and function and deficiency in Bcl-x_L even induces a change in energy metabolism to increasing activity in the pentose phosphate pathway.

4.9 Conclusion and Outlook

In this study, I could show that mitochondria are influenced under acute oxidative stress affecting their mitochondrial form and/or function, and that adaptation against chronic oxidative stress as well as the two mitochondrial and cytoprotective proteins Gdap1 and Bcl-x_L influence mitochondrial morphology and function.

I recognized that acute endogenous oxidative stress induced by glutamate did not alter the mitochondrial morphology, but increased mitochondrial respiration in hippocampal glutamate-sensitive HT22S. In contrast, analysing the consequences of oxidative stress induced by the well-known glutathione depleting reagents EA and MQ (Chiou and Tzeng, 2000; Kim et al., 2014; Seyfried et al., 1999; Wullner et al., 1999) showed that both reagents affected mitochondrial shape and function very rapidly in human neuroblastoma SH-SY5Y cells. But their effect was different than the influence of glutamate on mitochondria. EA induced extensive mitochondrial elongation and MQ triggered mitochondrial fragmentation, which both equally decreased mitochondrial respiration. Thus, it is not possible to come to a general conclusion in which way oxidative stress influences mitochondrial form and function. The effect on mitochondria is rather dependent on the cellular changes induced by the oxidative stress-inducing reagent.

The prolonged exposure of glutamate-resistant HT22R cells to glutamate induced consistent adaptations in their energy metabolism including changes in mitochondrial form and function. HT22R cells, which are remarkably protected against oxidative glutamate toxicity, adjusted their mitochondrial morphology towards a less fragmented phenotype and reduced their energy supply through oxidative phosphorylation in mitochondria. Reduced ATP production in mitochondria is compensated by an increasing activity in the pentose phosphate pathway, which is beneficial for increasing NADPH production and subsequent glutathione recovery. Thus, HT22R cells use most available glucose in the pentose phosphate pathway to increase glutathione recovery, which indicates that mitochondrial and metabolic adaptations are important in the resistance of cells to oxidative stress. It would be interestingly to further

study HT22R and find out what causes the persistent adaptations in energy metabolism and what is important for the glutamate-resistant phenotype on transcriptional level in which ATF4 and to a smaller part Nrf2 are good candidates.

In addition, analysing the function of the two mitochondrial, cytoprotective proteins GDAP1 and Bcl-x_L on mitochondria demonstrated that both proteins influence mitochondria. In agreement with previous observations (Niemann et al., 2005; Noack et al., 2012), I could confirm that the non-classical mitochondrial fission factor GDAP1 can effectively induce mitochondrial fission in SH-SY5Y cells and that GDAP1 with the Charcot-Marie-Tooth disease-causing mutation R310Q has lost this ability. As already claimed, its most likely GST activity seems to be connected with its mitochondrial fission activity (Wagner, 2009), because S34A cells with a mutation of the predicted active amino acid serine for catalytic activity in the GST-N domain (Shield et al., 2006) induced drastic mitochondrial elongation. Hence, the point mutation S34A had a dominant negative effect on GDAP1's fission activity. In addition, silencing of *GDAP1* influenced mitochondrial dynamics, but more serious was its effect on mitochondrial respiration. *GDAP1* knockdown significantly increased mitochondrial respiratory activity, whereas over-expression of wild type or mutated GDAP1 reduced mitochondrial activity and capacity. Especially, *GDAP1* knockdown was even accompanied by increasing NADP, proposing increased pentose phosphate pathway activity, which needs to be further investigated. Interestingly, in line with decreasing mitochondrial capacity under GDAP1 over-expression, HT22R cells with increasing GDAP1 expression (Noack et al., 2012) showed also reduced mitochondrial respiratory activity, however, reduced mitochondrial respiration in HT22R cells cannot be exclusively explained by increasing GDAP1 expression. It is more the result of several adaptations all together. But the results from *Gdap1* over-expressing and *GDAP1* KD SH-SY5Y cells suggest a physiological effect of GDAP1 on mitochondrial energy production besides influencing mitochondrial dynamics. Additionally, over-expression of GDAP1 prevented strongly mitochondrial elongation and induced a lower decline in the relative reduction of routine respiration and ETS capacity induced by EA in contrast to mutated *Gdap1*, control cells and even parental SH-SY5Y cells. We assume that these results indicate a possible function of GDAP1 as a redox sensor which recognizes the cellular or local redox state with its GST domains and especially adjusts mitochondrial morphology and slightly positively adapts mitochondrial respiration. But wild type GDAP1 could not prevent similarly to mutant GDAP1 changes in the mitochondrial morphology and respiratory activity induced by MQ. Thus, further experiments are necessary to prove its activity as a redox sensor. The consequences of EA and MQ on mitochondrial form and function in SH-SY5Y cells proved to be too fatal to clearly verify our hypothesis. Helpful for verification of our hypothesis can be the use of genetically-encode OxStress Donors targeted to mitochondria.

In addition, analysing of the effect of the mitochondrial and well-known anti-apoptotic protein (Boise et al., 1993; Gonzalez-Garcia et al., 1994) Bcl-x_L proved that silencing of Bcl-x_L induces a change in mitochondrial morphology and function which causes an adaptation in energy metabolism. Bcl-x_L-KO MEFs showed an increased fragmented mitochondrial morphology and an impaired mitochondrial respiratory OXPHOS and ETS capacity, although the cells can compensate this effect and displayed an unaffected mitochondrial respiratory activity in intact cells. At the same time, silencing of Bcl-x_L induced increased susceptibility to two mitochondrial toxins and an increase in the pentose phosphate pathway activity indicated by an increasing abundance of the key enzyme G6PD and an elevated total NADP pool. Enhanced levels of NADPH are especially helpful for GSH recovery (Dringen, 2000; Dringen and Hirrlinger, 2003), which can explain the elevated total cellular glutathione content under *bcl-x* gene knockout as well as an elevated pentose phosphate pathway activity favours the enhanced proliferation rate in Bcl-x_L-KO MEFs. Interestingly, over-expression of only mitochondria-localized Bcl-x_L can prevent the recognized changes in Bcl-x_L-KO cells. Thus, at mitochondria Bcl-x_L seems to be important for regulating mitochondrial morphology and function as well as it has previously been proved to be essential for apoptosis protection (Eno et al., 2012) and mitochondrial Ca^{2+} entry by interacting with VDAC (Huang et al., 2013). This interaction between Bcl-x_L and VDAC even proved to be essential allowing metabolite exchange such as ADP across the outer mitochondrial membrane under conditions preventing VDAC1 closure (Vander Heiden et al., 2001) and in consequence is important for mitochondrial energy production. The shift towards or additional increasing activity in the pentosephosphate pathway in HT22R cells and Bcl-x_L-KO MEFs seems to be a great mechanism against stress and/or to compensate impaired or decreasing respiratory function.

Fascinatingly, I recognized even some similarities between *Gdap1* over-expression and Bcl-x_L deficiency. Over-expression of GDAP1 protein and silencing of Bcl-x_L protein induce mitochondrial fission as well as both increase total cellular glutathione (shown here and Noack et al., 2012). In addition, both proteins impaired mitochondrial respiration because over-expressing GDAP1 and Bcl-x_L-KO cells displayed a reduction in the OXPHOS and ETS capacity. In consequence, there might be a direct interaction between GDAP1 and Bcl-x_L or a shared direct interaction partner. Since Bcl-x_L interacts with VDAC at the outer mitochondrial membrane and regulates the flux through this channel by adjusting its configuration (Arbel et al., 2012; Huang et al., 2013; Shimizu et al., 1999; Shimizu et al., 2000; Vander Heiden et al., 2001), we hypothesize VDAC as an interaction partner of both proteins. Thus, it needs to be investigated, if there is a direct interaction between GDAP1 and Bcl-x_L or if GDAP1 interacts directly with VDAC whereby the movement of metabolites through the outer mitochondrial membrane is regulated.

5 ATTACHMENT

```
GDAP1 wild type  801 CTGGGGACATGGAAAGAGACCGAACTTGGAAACCTATTATGAGCGTGTCT    850
                     ||||||||||||||||||||||||||||||||||||||||||||
GDAP1_R310Q        1 ---------TGGAAAGAGACCGAACTTGGAAACCTATTATGAGCGTGTCT     41

GDAP1_wild type  851 TGAAGAGAAAAACATTTAACAAGGTTTTAGGACATGTCAACAATATATTA    900
                     ||||||||||||||||||||||||||||||||||||||||||||||||||||
GDAP1_R310Q       42 TGAAGAGAAAAACATTTAACAAGGTTTTAGGACATGTCAACAATATATTA     91

GDAP1 wild type  901 ATCTCTGCGGTGCTGCCAACAGCATTCCGGGTGGCCAAAAAAAGGGCCCC    950
                     ||||||||||||||||||||||||||||||.||||||||||||||||||||
GDAP1_R310Q       92 ATCTCTGCGGTGCTGCCAACAGCATTCCAGGTGGCCAAAAAAAGGGCCCC    141

GDAP1_wild type  951 AAAAGTTCTTGGCAGCACCCTTGTGGTTGGTTTGCTTGTAGGAATGGGAT   1000
                     ||||||||||||||||||||||||||||||||||||||||||||||||||||
GDAP1 R310Q      142 AAAAGTTCTTGGCAGCACCCTTGTGGTTGGTTTGCTTGTAGGAATGGGAT    191

GDAP1_wild type 1001 ATTTTGCATTTATGCTTTTCAGAAGGAGACTTGGCAGCATGATATTAGCA   1050
                     ||||||||||||||||||||||||||||||||||||||||||||||||||||
GDAP1_R310Q      192 ATTTTGCATTTATGCTTTTCAGAAGGAGACTTGGCAGCATGATATTAGCA    241

GDAP1 wild type 1051 CTTAGACCCAGACCAAATTATTTCTAG   1077
                     ||||||||||||||||||||||||||||
GDAP1_R310Q      242 CTTAGACCCAGACCAAATTATTTCTAG    268


GDAP1 wild type  251 LAVTLHRLKFLGFARRNWGHGKRPNLETYYERVLKRKTFNKVLGHVNNIL    300
                                          ||||||||||||||||||||||||||||||
GDAP1 R310Q        1 --------------------GKRPNLETYYERVLKRKTFNKVLGHVNNIL     30

GDAP1_wild type  301 ISAVLPTAFRVAKKRAPKVLGSTLVVGLLVGMGYFAFMLFRRRLGSMILA    350
                     |||||||||:||||||||||||||||||||||||||||||||||||||||||
GDAP1_R310Q       31 ISAVLPTAFQVAKKRAPKVLGSTLVVGLLVGMGYFAFMLFRRRLGSMILA     80

GDAP1 wild type  351 LRPRPNYF    358
                     ||||||||
GDAP1_R310Q       81 LRPRPNYF     88
```

Supplementary Figure S1: Sequence alignments for verification of the SH-SY5Y R310Q cell line. Displayed is the result of the nucleotide (top) and protein (bottom) sequence alignment for verification of the SH-SY5Y R310Q cell line using the online pairwise sequence alignment tool EMBOSS Needle (http://www.ebi.ac.uk/Tools/psa/emboss_needle/). The sequence of the PCR product from the RT-PCR for verification of R310Q cells was compared with the nucleotide sequence of wild type GDAP1 (CCDS14834.1; http://www.ncbi.nlm.nih.gov/CCDS/CcdsBrowse.cgi) as well as the translated protein sequence was aligned. Noticeable is the point mutation in the nucleotide sequence (.) causing the mutation R310Q on protein level (:).

```
GDAP1_wild type    1 ATGGCTCGGAGGCAGGACGAGGCGCGGGCCGGTGTGCCCCTGAGGGTTGA     50
                     ||||||||||||||||||||||||||||||||||||||||||||||||||||
GDAP1_S34A         1 ATGGCTCGGAGGCAGGACGAGGCGCGGGCCGGTGTGCCCCTGAGGGTTGA     50

GDAP1_wild type   51 AGGCCCGCCGGACAAGGAGGTCCACCTCATTCTGTACCACTGGACGCACT    100
                     ||||||||||||||||||||||||||||||||||||||||||||||||||||.
GDAP1 S34A        51 AGGCCCGCCGGACAAGGAGGTCCACCTCATTCTGTACCACTGGACGCACG    100

GDAP1_wild type  101 CCTTCAGCTCTCAAAAGGTGCGCTTGGTAATTGCTGAAAAGGCACTGAAG    150
                     ||||||||||||||||||||||||||||||||||||||||||||||||||||
GDAP1_S34A       101 CCTTCAGCTCTCAAAAGGTGCGCTTGGTAATTGCTGAAAAGGCACTGAAG    150

GDAP1_wild type  151 TGCGAGGAACACGATGTAAGTCTGCCCCTGAGTGAGCACAATGAGCCTTG    200
                     ||||||||||||||||||||||||||||||||||||||||||||||||||
GDAP1_S34A       151 TGCGAGGAACACGATGTAAGTCTGCCCCTGAGTGAGCACAATGAGCC---    197


GDAP1_wild type    1 MARRQDEARAGVPLRVEGPPDKEVHLILYHWTHSFSSQKVRLVIAEKALK     50
                     ||||||||||||||||||||||||||||||||||:||||||||||||||||
GDAP1_S34A         1 MARRQDEARAGVPLRVEGPPDKEVHLILYHWTHAFSSQKVRLVIAEKALK     50

GDAP1 wild type   51 CEEHDVSLPLSEHNEPWFMRLNSAGEVPVLVHGENIICEATQIIDYLEQT    100
                     ||||||||||||||
GDAP1_S34A        51 CEEHDVSLPLSEHNE-----------------------------------     65
```

Supplementary Figure S2: Sequence alignments for verification of the SH-SY5Y S34AQ cell line. Shown is the result of the nucleotide (top) and protein (bottom) sequence alignment for verification of the SH-SY5Y S34A cell line using the online pairwise sequence alignment tool EMBOSS Needle (http://www.ebi.ac.uk/Tools/psa/emboss_needle/). The nucleotide and translated sequence of the PCR product from the RT-PCR for S34A cells was compared with the corresponding sequences of wild type GDAP1 (CCDS14834.1; http://www.ncbi.nlm.nih.gov/CCDS/CcdsBrowse.cgi). Visible is the point mutation in the nucleotide sequence (.) causing the mutation S34A on protein level (:).

6 REFERENCES

Ahokas, J.T., Nicholls, F.A., Ravenscroft, P.J., and Emmerson, B.T. (1985). Inhibition of purified rat liver glutathione S-transferase isozymes by diuretic drugs. Biochemical pharmacology *34*, 2157-2161.

Alavian, K.N., Li, H., Collis, L., Bonanni, L., Zeng, L., Sacchetti, S., Lazrove, E., Nabili, P., Flaherty, B., Graham, M.*, et al.* (2011). Bcl-xL regulates metabolic efficiency of neurons through interaction with the mitochondrial F1FO ATP synthase. Nature cell biology *13*, 1224-1233.

Albrecht, P., Bouchachia, I., Goebels, N., Henke, N., Hofstetter, H.H., Issberner, A., Kovacs, Z., Lewerenz, J., Lisak, D., Maher, P.*, et al.* (2012). Effects of dimethyl fumarate on neuroprotection and immunomodulation. Journal of neuroinflammation *9*, 163.

Albrecht, P., Lewerenz, J., Dittmer, S., Noack, R., Maher, P., and Methner, A. (2010). Mechanisms of oxidative glutamate toxicity: the glutamate/cystine antiporter system xc- as a neuroprotective drug target. CNS & neurological disorders drug targets *9*, 373-382.

Alexander, C., Votruba, M., Pesch, U.E., Thiselton, D.L., Mayer, S., Moore, A., Rodriguez, M., Kellner, U., Leo-Kottler, B., Auburger, G.*, et al.* (2000). OPA1, encoding a dynamin-related GTPase, is mutated in autosomal dominant optic atrophy linked to chromosome 3q28. Nature genetics *26*, 211-215.

Ambani, L.M., Van Woert, M.H., and Murphy, S. (1975). Brain peroxidase and catalase in Parkinson disease. Archives of neurology *32*, 114-118.

Anastasiou, D., Poulogiannis, G., Asara, J.M., Boxer, M.B., Jiang, J.K., Shen, M., Bellinger, G., Sasaki, A.T., Locasale, J.W., Auld, D.S.*, et al.* (2011). Inhibition of pyruvate kinase M2 by reactive oxygen species contributes to cellular antioxidant responses. Science *334*, 1278-1283.

Andersen, J.K. (2004). Oxidative stress in neurodegeneration: cause or consequence? Nature medicine *10 Suppl*, S18-25.

Anderson, S., Bankier, A.T., Barrell, B.G., de Bruijn, M.H., Coulson, A.R., Drouin, J., Eperon, I.C., Nierlich, D.P., Roe, B.A., Sanger, F.*, et al.* (1981). Sequence and organization of the human mitochondrial genome. Nature *290*, 457-465.

Arbel, N., Ben-Hail, D., and Shoshan-Barmatz, V. (2012). Mediation of the antiapoptotic activity of Bcl-xL protein upon interaction with VDAC1 protein. The Journal of biological chemistry *287*, 23152-23161.

Attardi, G., and Schatz, G. (1988). Biogenesis of mitochondria. Annual review of cell biology *4*, 289-333.

Awasthi, S., Srivastava, S.K., Ahmad, F., Ahmad, H., and Ansari, G.A. (1993). Interactions of glutathione S-transferase-pi with ethacrynic acid and its glutathione conjugate. Biochimica et biophysica acta *1164*, 173-178.

Azzedine, H., Ruberg, M., Ente, D., Gilardeau, C., Perie, S., Wechsler, B., Brice, A., LeGuern, E., and Dubourg, O. (2003). Variability of disease progression in a family with autosomal recessive CMT associated with a S194X and new R310Q mutation in the GDAP1 gene. Neuromuscular disorders : NMD *13*, 341-346.

Bakhshi, A., Jensen, J.P., Goldman, P., Wright, J.J., McBride, O.W., Epstein, A.L., and Korsmeyer, S.J. (1985). Cloning the chromosomal breakpoint of t(14;18) human lymphomas: clustering around JH on chromosome 14 and near a transcriptional unit on 18. Cell *41*, 899-906.

Bannai, S. (1986). Exchange of cystine and glutamate across plasma membrane of human fibroblasts. The Journal of biological chemistry *261*, 2256-2263.

Bannai, S., and Kitamura, E. (1980). Transport interaction of L-cystine and L-glutamate in human diploid fibroblasts in culture. The Journal of biological chemistry *255*, 2372-2376.

Barneo-Munoz, M., Juarez, P., Civera-Tregon, A., Yndriago, L., Pla-Martin, D., Zenker, J., Cuevas-Martin, C., Estela, A., Sanchez-Arago, M., Forteza-Vila, J.*, et al.* (2015). Lack of GDAP1 Induces Neuronal Calcium and Mitochondrial Defects in a Knockout Mouse Model of Charcot-Marie-Tooth Neuropathy. PLoS genetics *11*, e1005115.

Barnham, K.J., Masters, C.L., and Bush, A.I. (2004). Neurodegenerative diseases and oxidative stress. Nature reviews Drug discovery *3*, 205-214.

Bauser, C.A., Elick, T.A., and Fraser, M.J. (1999). Proteins from nuclear extracts of two lepidopteran cell lines recognize the ends of TTAA-specific transposons piggyBac and tagalong. Insect molecular biology *8*, 223-230.

Baxter, R.V., Ben Othmane, K., Rochelle, J.M., Stajich, J.E., Hulette, C., Dew-Knight, S., Hentati, F., Ben Hamida, M., Bel, S., Stenger, J.E.*, et al.* (2002). Ganglioside-induced differentiation-associated protein-1 is mutant in Charcot-Marie-Tooth disease type 4A/8q21. Nature genetics *30*, 21-22.

Ben-Yoseph, O., Boxer, P.A., and Ross, B.D. (1996). Assessment of the role of the glutathione and pentose phosphate pathways in the protection of primary cerebrocortical cultures from oxidative stress. Journal of neurochemistry *66*, 2329-2337.

Benard, G., and Rossignol, R. (2008). Ultrastructure of the mitochondrion and its bearing on function and bioenergetics. Antioxidants & redox signaling *10*, 1313-1342.

Berger, P., Young, P., and Suter, U. (2002). Molecular cell biology of Charcot-Marie-Tooth disease. Neurogenetics *4*, 1-15.

Berman, S.B., Chen, Y.B., Qi, B., McCaffery, J.M., Rucker, E.B., 3rd, Goebbels, S., Nave, K.A., Arnold, B.A., Jonas, E.A., Pineda, F.J.*, et al.* (2009). Bcl-x L increases mitochondrial fission, fusion, and biomass in neurons. The Journal of cell biology *184*, 707-719.

Biedler, J.L., Roffler-Tarlov, S., Schachner, M., and Freedman, L.S. (1978). Multiple neurotransmitter synthesis by human neuroblastoma cell lines and clones. Cancer research *38*, 3751-3757.

Birnboim, H.C., and Doly, J. (1979). A rapid alkaline extraction procedure for screening recombinant plasmid DNA. Nucleic acids research *7*, 1513-1523.

Boise, L.H., Gonzalez-Garcia, M., Postema, C.E., Ding, L., Lindsten, T., Turka, L.A., Mao, X., Nunez, G., and Thompson, C.B. (1993). bcl-x, a bcl-2-related gene that functions as a dominant regulator of apoptotic cell death. Cell *74*, 597-608.

Bolisetty, S., and Jaimes, E.A. (2013). Mitochondria and reactive oxygen species: physiology and pathophysiology. International journal of molecular sciences *14*, 6306-6344.

Bowes, T., and Gupta, R.S. (2008). Novel mitochondrial extensions provide evidence for a link between microtubule-directed movement and mitochondrial fission. Biochemical and biophysical research communications *376*, 40-45.

Bowes, T.J., and Gupta, R.S. (2005). Induction of mitochondrial fusion by cysteine-alkylators ethacrynic acid and N-ethylmaleimide. Journal of cellular physiology *202*, 796-804.

Brunelle, J.K., and Letai, A. (2009). Control of mitochondrial apoptosis by the Bcl-2 family. Journal of cell science *122*, 437-441.

Bucci, C., Bakke, O., and Progida, C. (2012). Charcot-Marie-Tooth disease and intracellular traffic. Progress in neurobiology *99*, 191-225.

Cassereau, J., Chevrollier, A., Bonneau, D., Verny, C., Procaccio, V., Reynier, P., and Ferre, M. (2011a). A locus-specific database for mutations in GDAP1 allows analysis of genotype-phenotype correlations in Charcot-Marie-Tooth diseases type 4A and 2K. Orphanet journal of rare diseases *6*, 87.

Cassereau, J., Chevrollier, A., Gueguen, N., Desquiret, V., Verny, C., Nicolas, G., Dubas, F., Amati-Bonneau, P., Reynier, P., Bonneau, D.*, et al.* (2011b). Mitochondrial dysfunction and pathophysiology of Charcot-Marie-Tooth disease involving GDAP1 mutations. Experimental neurology *227*, 31-41.

Cassereau, J., Chevrollier, A., Gueguen, N., Malinge, M.C., Letournel, F., Nicolas, G., Richard, L., Ferre, M., Verny, C., Dubas, F.*, et al.* (2009). Mitochondrial complex I deficiency in GDAP1-related autosomal dominant Charcot-Marie-Tooth disease (CMT2K). Neurogenetics *10*, 145-150.

Chan, D.C. (2006). Mitochondria: dynamic organelles in disease, aging, and development. Cell *125*, 1241-1252.

Chan, D.C. (2012). Fusion and fission: interlinked processes critical for mitochondrial health. Annual review of genetics *46*, 265-287.

Chen, H., Chomyn, A., and Chan, D.C. (2005). Disruption of fusion results in mitochondrial heterogeneity and dysfunction. The Journal of biological chemistry *280*, 26185-26192.

Chen, H., Detmer, S.A., Ewald, A.J., Griffin, E.E., Fraser, S.E., and Chan, D.C. (2003). Mitofusins Mfn1 and Mfn2 coordinately regulate mitochondrial fusion and are essential for embryonic development. The Journal of cell biology *160*, 189-200.

Chen, Y.B., Aon, M.A., Hsu, Y.T., Soane, L., Teng, X., McCaffery, J.M., Cheng, W.C., Qi, B., Li, H., Alavian, K.N.*, et al.* (2011). Bcl-xL regulates mitochondrial energetics by stabilizing the inner membrane potential. The Journal of cell biology *195*, 263-276.

Chiou, T.J., and Tzeng, W.F. (2000). The roles of glutathione and antioxidant enzymes in menadione-induced oxidative stress. Toxicology *154*, 75-84.

Chipuk, J.E., Moldoveanu, T., Llambi, F., Parsons, M.J., and Green, D.R. (2010). The BCL-2 family reunion. Molecular cell *37*, 299-310.

Choi, D.W. (1988). Glutamate neurotoxicity and diseases of the nervous system. Neuron *1*, 623-634.

Chung, K.W., Kim, S.M., Sunwoo, I.N., Cho, S.Y., Hwang, S.J., Kim, J., Kang, S.H., Park, K.D., Choi, K.G., Choi, I.S.*, et al.* (2008). A novel GDAP1 Q218E mutation in autosomal dominant Charcot-Marie-Tooth disease. Journal of human genetics *53*, 360-364.

Cipolat, S., Martins de Brito, O., Dal Zilio, B., and Scorrano, L. (2004). OPA1 requires mitofusin 1 to promote mitochondrial fusion. Proceedings of the National Academy of Sciences of the United States of America *101*, 15927-15932.

Claramunt, R., Pedrola, L., Sevilla, T., Lopez de Munain, A., Berciano, J., Cuesta, A., Sanchez-Navarro, B., Millan, J.M., Saifi, G.M., Lupski, J.R.*, et al.* (2005). Genetics of Charcot-Marie-Tooth disease type 4A: mutations, inheritance, phenotypic variability, and founder effect. Journal of medical genetics *42*, 358-365.

Cleary, M.L., and Sklar, J. (1985). Nucleotide sequence of a t(14;18) chromosomal breakpoint in follicular lymphoma and demonstration of a breakpoint-cluster region near a transcriptionally active locus on chromosome 18. Proceedings of the National Academy of Sciences of the United States of America *82*, 7439-7443.

Cleland, M.M., Norris, K.L., Karbowski, M., Wang, C., Suen, D.F., Jiao, S., George, N.M., Luo, X., Li, Z., and Youle, R.J. (2011). Bcl-2 family interaction with the mitochondrial morphogenesis machinery. Cell death and differentiation *18*, 235-247.

Cohen, S.N., Chang, A.C., and Hsu, L. (1972). Nonchromosomal antibiotic resistance in bacteria: genetic transformation of Escherichia coli by R-factor DNA. Proceedings of the National Academy of Sciences of the United States of America *69*, 2110-2114.

Collins, T.J., Berridge, M.J., Lipp, P., and Bootman, M.D. (2002). Mitochondria are morphologically and functionally heterogeneous within cells. The EMBO journal *21*, 1616-1627.

Colombini, M. (2012). VDAC structure, selectivity, and dynamics. Biochimica et biophysica acta *1818*, 1457-1465.

Corpet, F. (1988). Multiple sequence alignment with hierarchical clustering. Nucleic acids research *16*, 10881-10890.

Coyle, J.T., and Puttfarcken, P. (1993). Oxidative stress, glutamate, and neurodegenerative disorders. Science *262*, 689-695.

Criddle, D.N., Gillies, S., Baumgartner-Wilson, H.K., Jaffar, M., Chinje, E.C., Passmore, S., Chvanov, M., Barrow, S., Gerasimenko, O.V., Tepikin, A.V.*, et al.* (2006). Menadione-induced reactive oxygen species generation via redox cycling promotes apoptosis of murine pancreatic acinar cells. The Journal of biological chemistry *281*, 40485-40492.

Cuesta, A., Pedrola, L., Sevilla, T., Garcia-Planells, J., Chumillas, M.J., Mayordomo, F., LeGuern, E., Marin, I., Vilchez, J.J., and Palau, F. (2002). The gene encoding ganglioside-induced differentiation-associated protein 1 is mutated in axonal Charcot-Marie-Tooth type 4A disease. Nature genetics *30*, 22-25.

Das, A.M., and Harris, D.A. (1990). Control of mitochondrial ATP synthase in heart cells: inactive to active transitions caused by beating or positive inotropic agents. Cardiovascular research *24*, 411-417.

Davis, J.B., and Maher, P. (1994). Protein kinase C activation inhibits glutamate-induced cytotoxicity in a neuronal cell line. Brain research *652*, 169-173.

Delettre, C., Lenaers, G., Griffoin, J.M., Gigarel, N., Lorenzo, C., Belenguer, P., Pelloquin, L., Grosgeorge, J., Turc-Carel, C., Perret, E.*, et al.* (2000). Nuclear gene OPA1, encoding a mitochondrial dynamin-related protein, is mutated in dominant optic atrophy. Nature genetics *26*, 207-210.

Delivani, P., Adrain, C., Taylor, R.C., Duriez, P.J., and Martin, S.J. (2006). Role for CED-9 and Egl-1 as regulators of mitochondrial fission and fusion dynamics. Molecular cell *21*, 761-773.

Di Monte, D., Ross, D., Bellomo, G., Eklow, L., and Orrenius, S. (1984). Alterations in intracellular thiol homeostasis during the metabolism of menadione by isolated rat hepatocytes. Archives of biochemistry and biophysics *235*, 334-342.

Dittmer, S., Sahin, M., Pantlen, A., Saxena, A., Toutzaris, D., Pina, A.L., Geerts, A., Golz, S., and Methner, A. (2008). The constitutively active orphan G-protein-coupled receptor GPR39 protects from cell death by increasing secretion of pigment epithelium-derived growth factor. The Journal of biological chemistry *283*, 7074-7081.

Drechsel, D.A., and Patel, M. (2010). Respiration-dependent H2O2 removal in brain mitochondria via the thioredoxin/peroxiredoxin system. The Journal of biological chemistry *285*, 27850-27858.

Dringen, R. (2000). Metabolism and functions of glutathione in brain. Progress in neurobiology *62*, 649-671.

Dringen, R., and Hirrlinger, J. (2003). Glutathione pathways in the brain. Biological chemistry *384*, 505-516.

Duvel, K., Yecies, J.L., Menon, S., Raman, P., Lipovsky, A.I., Souza, A.L., Triantafellow, E., Ma, Q., Gorski, R., Cleaver, S.*, et al.* (2010). Activation of a metabolic gene regulatory network downstream of mTOR complex 1. Molecular cell *39*, 171-183.

Elmore, S. (2007). Apoptosis: a review of programmed cell death. Toxicologic pathology *35*, 495-516.

EMBOSS Needle tool: http://www.ebi.ac.uk/Tools/psa/emboss_needle/

Emery, A.E. (1991). Population frequencies of inherited neuromuscular diseases--a world survey. Neuromuscular disorders : NMD *1*, 19-29.

Endo, J., Sano, M., Katayama, T., Hishiki, T., Shinmura, K., Morizane, S., Matsuhashi, T., Katsumata, Y., Zhang, Y., Ito, H.*, et al.* (2009). Metabolic remodeling induced by mitochondrial aldehyde stress stimulates tolerance to oxidative stress in the heart. Circulation research *105*, 1118-1127.

Eno, C.O., Eckenrode, E.F., Olberding, K.E., Zhao, G., White, C., and Li, C. (2012). Distinct roles of mitochondria- and ER-localized Bcl-xL in apoptosis resistance and Ca2+ homeostasis. Molecular biology of the cell *23*, 2605-2618.

Ernster, L., and Schatz, G. (1981). Mitochondria: a historical review. The Journal of cell biology *91*, 227s-255s.

Expasy translation tool: http://www.web.expasy.org/translate/

Finkel, T., and Holbrook, N.J. (2000). Oxidants, oxidative stress and the biology of ageing. Nature *408*, 239-247.

Frank, S., Gaume, B., Bergmann-Leitner, E.S., Leitner, W.W., Robert, E.G., Catez, F., Smith, C.L., and Youle, R.J. (2001). The role of dynamin-related protein 1, a mediator of mitochondrial fission, in apoptosis. Developmental cell *1*, 515-525.

Fraser, M.J., Ciszczon, T., Elick, T., and Bauser, C. (1996). Precise excision of TTAA-specific lepidopteran transposons piggyBac (IFP2) and tagalong (TFP3) from the baculovirus genome in cell lines from two species of Lepidoptera. Insect molecular biology *5*, 141-151.

Frey, T.G., and Mannella, C.A. (2000). The internal structure of mitochondria. Trends in biochemical sciences *25*, 319-324.

Frey, T.G., Renken, C.W., and Perkins, G.A. (2002). Insight into mitochondrial structure and function from electron tomography. Biochimica et biophysica acta *1555*, 196-203.

Garcia-Nogales, P., Almeida, A., and Bolanos, J.P. (2003). Peroxynitrite protects neurons against nitric oxide-mediated apoptosis. A key role for glucose-6-phosphate dehydrogenase activity in neuroprotection. The Journal of biological chemistry *278*, 864-874.

Gerasimenko, J.V., Gerasimenko, O.V., Palejwala, A., Tepikin, A.V., Petersen, O.H., and Watson, A.J. (2002). Menadione-induced apoptosis: roles of cytosolic Ca(2+) elevations and the mitochondrial permeability transition pore. Journal of cell science *115*, 485-497.

Gilkerson, R.W., Selker, J.M., and Capaldi, R.A. (2003). The cristal membrane of mitochondria is the principal site of oxidative phosphorylation. FEBS letters *546*, 355-358.

Giustarini, D., Dalle-Donne, I., Milzani, A., Fanti, P., and Rossi, R. (2013). Analysis of GSH and GSSG after derivatization with N-ethylmaleimide. Nature protocols *8*, 1660-1669.

Gnaiger, E. (2008). Polarographic Oxygen Sensors, the Oxygraph, and High-Resolution Respirometry to Assess Mitochondrial Function. In Drug-Induced Mitochondrial Dysfunction (John Wiley & Sons, Inc.), pp. 325-352.

Gnaiger, E. (2009). Capacity of oxidative phosphorylation in human skeletal muscle: new perspectives of mitochondrial physiology. The international journal of biochemistry & cell biology *41*, 1837-1845.

Gnaiger, E. (2012). Mitochondrial pathways and respiratory control. An introduction to OXPHOS analysis., 3rd edn (Mitochondr Physiol Network 17.18.: OROBOROS MiPNet Publications, Innsbruck).

Gnaiger, E., Kuznetsov, A., Schneeberger, S., Seiler, R., Brandacher, G., Steurer, W., and Margreiter, R. (2000). Mitochondria in the Cold. In Life in the Cold, G. Heldmaier, and M. Klingenspor, eds. (Springer Berlin Heidelberg), pp. 431-442.

Gohil, V.M., Sheth, S.A., Nilsson, R., Wojtovich, A.P., Lee, J.H., Perocchi, F., Chen, W., Clish, C.B., Ayata, C., Brookes, P.S.*, et al.* (2010). Nutrient-sensitized screening for drugs that shift energy metabolism from mitochondrial respiration to glycolysis. Nature biotechnology *28*, 249-255.

Gonzalez-Garcia, M., Perez-Ballestero, R., Ding, L., Duan, L., Boise, L.H., Thompson, C.B., and Nunez, G. (1994). bcl-XL is the major bcl-x mRNA form expressed during murine development and its product localizes to mitochondria. Development *120*, 3033-3042.

Gray, M.W., Burger, G., and Lang, B.F. (1999). Mitochondrial evolution. Science *283*, 1476-1481.

Griffith, O.W. (1999). Biologic and pharmacologic regulation of mammalian glutathione synthesis. Free radical biology & medicine *27*, 922-935.

Griparic, L., van der Wel, N.N., Orozco, I.J., Peters, P.J., and van der Bliek, A.M. (2004). Loss of the intermembrane space protein Mgm1/OPA1 induces swelling and localized constrictions along the lengths of mitochondria. The Journal of biological chemistry *279*, 18792-18798.

Grohm, J., Plesnila, N., and Culmsee, C. (2010). Bid mediates fission, membrane permeabilization and peri-nuclear accumulation of mitochondria as a prerequisite for oxidative neuronal cell death. Brain, behavior, and immunity *24*, 831-838.

Gruning, N.M., Rinnerthaler, M., Bluemlein, K., Mulleder, M., Wamelink, M.M., Lehrach, H., Jakobs, C., Breitenbach, M., and Ralser, M. (2011). Pyruvate kinase triggers a metabolic feedback loop that controls redox metabolism in respiring cells. Cell metabolism *14*, 415-427.

Guillet, V., Gueguen, N., Verny, C., Ferre, M., Homedan, C., Loiseau, D., Procaccio, V., Amati-Bonneau, P., Bonneau, D., Reynier, P.*, et al.* (2010). Adenine nucleotide translocase is involved in a mitochondrial coupling defect in MFN2-related Charcot-Marie-Tooth type 2A disease. Neurogenetics *11*, 127-133.

Habig, W.H., Pabst, M.J., and Jakoby, W.B. (1974). Glutathione S-transferases. The first enzymatic step in mercapturic acid formation. The Journal of biological chemistry *249*, 7130-7139.

Hansford, R.G., and Zorov, D. (1998). Role of mitochondrial calcium transport in the control of substrate oxidation. Molecular and cellular biochemistry *184*, 359-369.

Harding, H.P., Zhang, Y., Zeng, H., Novoa, I., Lu, P.D., Calfon, M., Sadri, N., Yun, C., Popko, B., Paules, R.*, et al.* (2003). An integrated stress response regulates amino acid metabolism and resistance to oxidative stress. Molecular cell *11*, 619-633.

Harel, T., and Lupski, J.R. (2014). Charcot-Marie-Tooth disease and pathways to molecular based therapies. Clinical genetics *86*, 422-431.

Harris, M.H., and Thompson, C.B. (2000). The role of the Bcl-2 family in the regulation of outer mitochondrial membrane permeability. Cell death and differentiation *7*, 1182-1191.

Hartley, J.L., Temple, G.F., and Brasch, M.A. (2000). DNA cloning using in vitro site-specific recombination. Genome research *10*, 1788-1795.

Hayes, J.D., Flanagan, J.U., and Jowsey, I.R. (2005). Glutathione transferases. Annual review of pharmacology and toxicology *45*, 51-88.

Hayes, J.D., and McLellan, L.I. (1999). Glutathione and glutathione-dependent enzymes represent a co-ordinately regulated defence against oxidative stress. Free radical research *31*, 273-300.

He, C.H., Gong, P., Hu, B., Stewart, D., Choi, M.E., Choi, A.M., and Alam, J. (2001). Identification of activating transcription factor 4 (ATF4) as an Nrf2-interacting protein. Implication for heme oxygenase-1 gene regulation. The Journal of biological chemistry *276*, 20858-20865.

Henke, N., Albrecht, P., Bouchachia, I., Ryazantseva, M., Knoll, K., Lewerenz, J., Kaznacheyeva, E., Maher, P., and Methner, A. (2013). The plasma membrane channel ORAI1 mediates detrimental calcium influx caused by endogenous oxidative stress. Cell death & disease *4*, e470.

Herrero, A., and Barja, G. (1997). Sites and mechanisms responsible for the low rate of free radical production of heart mitochondria in the long-lived pigeon. Mechanisms of ageing and development *98*, 95-111.

Hirst, J. (2013). Mitochondrial complex I. Annual review of biochemistry *82*, 551-575.

Hodge, T., and Colombini, M. (1997). Regulation of metabolite flux through voltage-gating of VDAC channels. The Journal of membrane biology *157*, 271-279.

Hoppins, S., Lackner, L., and Nunnari, J. (2007). The machines that divide and fuse mitochondria. Annual review of biochemistry *76*, 751-780.

Hsu, Y.T., Wolter, K.G., and Youle, R.J. (1997). Cytosol-to-membrane redistribution of Bax and Bcl-X(L) during apoptosis. Proceedings of the National Academy of Sciences of the United States of America *94*, 3668-3672.

http://www.ncbi.nlm.nih.gov/gene/54332 (2014).

Huang, H., Hu, X., Eno, C.O., Zhao, G., Li, C., and White, C. (2013). An interaction between Bcl-xL and the voltage-dependent anion channel (VDAC) promotes mitochondrial Ca2+ uptake. The Journal of biological chemistry *288*, 19870-19881.

Huber, N., Guimaraes, S., Schrader, M., Suter, U., and Niemann, A. (2013). Charcot-Marie-Tooth disease-associated mutants of GDAP1 dissociate its roles in peroxisomal and mitochondrial fission. EMBO reports *14*, 545-552.

Igarashi, T., Izumi, H., Uchiumi, T., Nishio, K., Arao, T., Tanabe, M., Uramoto, H., Sugio, K., Yasumoto, K., Sasaguri, Y*., et al.* (2007). Clock and ATF4 transcription system regulates drug resistance in human cancer cell lines. Oncogene *26*, 4749-4760.

ImageJ: http://imagej.nih.gov/ij/

Ishihara, N., Eura, Y., and Mihara, K. (2004). Mitofusin 1 and 2 play distinct roles in mitochondrial fusion reactions via GTPase activity. Journal of cell science *117*, 6535-6546.

Issels, R.D., Bourier, S., Biaglow, J.E., Gerweck, L.E., and Wilmanns, W. (1985). Temperature-dependent influence of thiols upon glutathione levels in Chinese hamster ovary cells at cytotoxic concentrations. Cancer research *45*, 6219-6224.

Issels, R.D., Nagele, A., Eckert, K.G., and Wilmanns, W. (1988). Promotion of cystine uptake and its utilization for glutathione biosynthesis induced by cysteamine and N-acetylcysteine. Biochemical pharmacology *37*, 881-888.

Itoh, K., Nakamura, K., Iijima, M., and Sesaki, H. (2013). Mitochondrial dynamics in neurodegeneration. Trends in cell biology *23*, 64-71.

Iyanagi, T., and Yamazaki, I. (1970). One-electron-transfer reactions in biochemical systems. V. Difference in the mechanism of quinone reduction by the NADH dehydrogenase and the NAD(P)H dehydrogenase (DT-diaphorase). Biochimica et biophysica acta *216*, 282-294.

Jerath, N.U., and Shy, M.E. (2014). Hereditary motor and sensory neuropathies: Understanding molecular pathogenesis could lead to future treatment strategies. Biochimica et biophysica acta.

Kaufmann, T., Schlipf, S., Sanz, J., Neubert, K., Stein, R., and Borner, C. (2003). Characterization of the signal that directs Bcl-x(L), but not Bcl-2, to the mitochondrial outer membrane. The Journal of cell biology *160*, 53-64.

Kazamel, M., and Boes, C.J. (2014). Charcot Marie Tooth disease (CMT): historical perspectives and evolution. Journal of neurology.

Kelly, D.P., and Scarpulla, R.C. (2004). Transcriptional regulatory circuits controlling mitochondrial biogenesis and function. Genes & development *18*, 357-368.

Kim, Y.J., Shin, Y.K., Sohn, D.S., and Lee, C.S. (2014). Menadione induces the formation of reactive oxygen species and depletion of GSH-mediated apoptosis and inhibits the FAK-mediated cell invasion. Naunyn-Schmiedeberg's archives of pharmacology *387*, 799-809.

Kish, S.J., Morito, C., and Hornykiewicz, O. (1985). Glutathione peroxidase activity in Parkinson's disease brain. Neuroscience letters *58*, 343-346.

Koshiba, T., Detmer, S.A., Kaiser, J.T., Chen, H., McCaffery, J.M., and Chan, D.C. (2004). Structural basis of mitochondrial tethering by mitofusin complexes. Science *305*, 858-862.

Kudin, A.P., Augustynek, B., Lehmann, A.K., Kovacs, R., and Kunz, W.S. (2012). The contribution of thioredoxin-2 reductase and glutathione peroxidase to H(2)O(2) detoxification of rat brain mitochondria. Biochimica et biophysica acta *1817*, 1901-1906.

Kumari, S., Mehta, S.L., and Li, P.A. (2012). Glutamate induces mitochondrial dynamic imbalance and autophagy activation: preventive effects of selenium. PloS one *7*, e39382.

Kuznetsov, A.V., Hermann, M., Saks, V., Hengster, P., and Margreiter, R. (2009). The cell-type specificity of mitochondrial dynamics. The international journal of biochemistry & cell biology *41*, 1928-1939.

Laemmli, U.K. (1970). Cleavage of structural proteins during the assembly of the head of bacteriophage T4. Nature *227*, 680-685.

Landshamer, S., Hoehn, M., Barth, N., Duvezin-Caubet, S., Schwake, G., Tobaben, S., Kazhdan, I., Becattini, B., Zahler, S., Vollmar, A.*, et al.* (2008). Bid-induced release of AIF from mitochondria causes immediate neuronal cell death. Cell death and differentiation *15*, 1553-1563.

Landy, A. (1989). Dynamic, structural, and regulatory aspects of lambda site-specific recombination. Annual review of biochemistry *58*, 913-949.

Lardy, H.A., Johnson, D., and Mc, M.W. (1958). Antibiotics as tools for metabolic studies. I. A survey of toxic antibiotics in respiratory, phosphorylative and glycolytic systems. Archives of biochemistry and biophysics *78*, 587-597.

Laux, I., and Nel, A. (2001). Evidence that oxidative stress-induced apoptosis by menadione involves Fas-dependent and Fas-independent pathways. Clinical immunology *101*, 335-344.

Legros, F., Lombes, A., Frachon, P., and Rojo, M. (2002). Mitochondrial fusion in human cells is efficient, requires the inner membrane potential, and is mediated by mitofusins. Molecular biology of the cell *13*, 4343-4354.

Lewerenz, J., Albrecht, P., Tien, M.L., Henke, N., Karumbayaram, S., Kornblum, H.I., Wiedau-Pazos, M., Schubert, D., Maher, P., and Methner, A. (2009). Induction of Nrf2 and xCT are involved in the action of the neuroprotective antibiotic ceftriaxone in vitro. Journal of neurochemistry *111*, 332-343.

Lewerenz, J., Klein, M., and Methner, A. (2006). Cooperative action of glutamate transporters and cystine/glutamate antiporter system Xc- protects from oxidative glutamate toxicity. Journal of neurochemistry *98*, 916-925.

Lewerenz, J., and Maher, P. (2009). Basal levels of eIF2alpha phosphorylation determine cellular antioxidant status by regulating ATF4 and xCT expression. The Journal of biological chemistry *284*, 1106-1115.

Lewerenz, J., and Maher, P. (2011). Control of redox state and redox signaling by neural antioxidant systems. Antioxidants & redox signaling *14*, 1449-1465.

Lewerenz, J., Sato, H., Albrecht, P., Henke, N., Noack, R., Methner, A., and Maher, P. (2012). Mutation of ATF4 mediates resistance of neuronal cell lines against oxidative stress by inducing xCT expression. Cell death and differentiation *19*, 847-858.

Li, C., Wang, X., Vais, H., Thompson, C.B., Foskett, J.K., and White, C. (2007). Apoptosis regulation by Bcl-x(L) modulation of mammalian inositol 1,4,5-trisphosphate receptor channel isoform gating. Proceedings of the National Academy of Sciences of the United States of America *104*, 12565-12570.

Li, H., Chen, Y., Jones, A.F., Sanger, R.H., Collis, L.P., Flannery, R., McNay, E.C., Yu, T., Schwarzenbacher, R., Bossy, B.*, et al.* (2008). Bcl-xL induces Drp1-dependent synapse formation in cultured hippocampal neurons. Proceedings of the National Academy of Sciences of the United States of America *105*, 2169-2174.

Li, Y., Maher, P., and Schubert, D. (1997a). Requirement for cGMP in nerve cell death caused by glutathione depletion. The Journal of cell biology *139*, 1317-1324.

Li, Y., Maher, P., and Schubert, D. (1997b). A role for 12-lipoxygenase in nerve cell death caused by glutathione depletion. Neuron *19*, 453-463.

Lind, C., Hochstein, P., and Ernster, L. (1982). DT-diaphorase as a quinone reductase: a cellular control device against semiquinone and superoxide radical formation. Archives of biochemistry and biophysics *216*, 178-185.

Liu, H., Nakagawa, T., Kanematsu, T., Uchida, T., and Tsuji, S. (1999). Isolation of 10 differentially expressed cDNAs in differentiated Neuro2a cells induced through controlled expression of the GD3 synthase gene. Journal of neurochemistry *72*, 1781-1790.

Loiseau, D., Chevrollier, A., Verny, C., Guillet, V., Gueguen, N., Pou de Crescenzo, M.A., Ferre, M., Malinge, M.C., Guichet, A., Nicolas, G.*, et al.* (2007). Mitochondrial coupling defect in Charcot-Marie-Tooth type 2A disease. Annals of neurology *61*, 315-323.

Loor, G., Kondapalli, J., Schriewer, J.M., Chandel, N.S., Vanden Hoek, T.L., and Schumacker, P.T. (2010). Menadione triggers cell death through ROS-dependent mechanisms involving PARP activation without requiring apoptosis. Free radical biology & medicine *49*, 1925-1936.

Lopez Del Amo, V., Seco-Cervera, M., Garcia-Gimenez, J.L., Whitworth, A.J., Pallardo, F.V., and Galindo, M.I. (2014). Mitochondrial defects and neuromuscular degeneration caused by altered expression of Drosophila Gdap1: implications for the Charcot-Marie-Tooth neuropathy. Human molecular genetics.

MacAskill, A.F., and Kittler, J.T. (2010). Control of mitochondrial transport and localization in neurons. Trends in cell biology *20*, 102-112.

Maher, P. (2005). The effects of stress and aging on glutathione metabolism. Ageing research reviews *4*, 288-314.

Maher, P., and Davis, J.B. (1996). The role of monoamine metabolism in oxidative glutamate toxicity. The Journal of neuroscience : the official journal of the Society for Neuroscience *16*, 6394-6401.

Marco, A., Cuesta, A., Pedrola, L., Palau, F., and Marin, I. (2004). Evolutionary and structural analyses of GDAP1, involved in Charcot-Marie-Tooth disease, characterize a novel class of glutathione transferase-related genes. Molecular biology and evolution *21*, 176-187.

Mariani, E., Polidori, M.C., Cherubini, A., and Mecocci, P. (2005). Oxidative stress in brain aging, neurodegenerative and vascular diseases: an overview. Journal of chromatography B, Analytical technologies in the biomedical and life sciences *827*, 65-75.

Marroquin, L.D., Hynes, J., Dykens, J.A., Jamieson, J.D., and Will, Y. (2007). Circumventing the Crabtree effect: replacing media glucose with galactose increases susceptibility of HepG2 cells to mitochondrial toxicants. Toxicological sciences : an official journal of the Society of Toxicology *97*, 539-547.

McBride, H.M., Neuspiel, M., and Wasiak, S. (2006). Mitochondria: more than just a powerhouse. Current biology : CB *16*, R551-560.

Melo, A., Monteiro, L., Lima, R.M., Oliveira, D.M., Cerqueira, M.D., and El-Bacha, R.S. (2011). Oxidative stress in neurodegenerative diseases: mechanisms and therapeutic perspectives. Oxidative medicine and cellular longevity *2011*, 467180.

Mitsuishi, Y., Taguchi, K., Kawatani, Y., Shibata, T., Nukiwa, T., Aburatani, H., Yamamoto, M., and Motohashi, H. (2012). Nrf2 redirects glucose and glutamine into anabolic pathways in metabolic reprogramming. Cancer cell *22*, 66-79.

Miyamoto, M., Murphy, T.H., Schnaar, R.L., and Coyle, J.T. (1989). Antioxidants protect against glutamate-induced cytotoxicity in a neuronal cell line. The Journal of pharmacology and experimental therapeutics *250*, 1132-1140.

Motoyama, N., Wang, F., Roth, K.A., Sawa, H., Nakayama, K., Nakayama, K., Negishi, I., Senju, S., Zhang, Q., Fujii, S.*, et al.* (1995). Massive cell death of immature hematopoietic cells and neurons in Bcl-x-deficient mice. Science *267*, 1506-1510.

MultAlign: http://multalin.toulouse.inra.fr/multalin/

Murphy, T.H., Miyamoto, M., Sastre, A., Schnaar, R.L., and Coyle, J.T. (1989). Glutamate toxicity in a neuronal cell line involves inhibition of cystine transport leading to oxidative stress. Neuron *2*, 1547-1558.

Murphy, T.H., Schnaar, R.L., and Coyle, J.T. (1990). Immature cortical neurons are uniquely sensitive to glutamate toxicity by inhibition of cystine uptake. FASEB journal : official publication of the Federation of American Societies for Experimental Biology *4*, 1624-1633.

Muyderman, H., Nilsson, M., and Sims, N.R. (2004). Highly selective and prolonged depletion of mitochondrial glutathione in astrocytes markedly increases sensitivity to peroxynitrite. The Journal of neuroscience : the official journal of the Society for Neuroscience *24*, 8019-8028.

Niemann, A., Berger, P., and Suter, U. (2006). Pathomechanisms of mutant proteins in Charcot-Marie-Tooth disease. Neuromolecular medicine *8*, 217-242.

Niemann, A., Huber, N., Wagner, K.M., Somandin, C., Horn, M., Lebrun-Julien, F., Angst, B., Pereira, J.A., Halfter, H., Welzl, H.*, et al.* (2014). The Gdap1 knockout mouse mechanistically links redox control to Charcot-Marie-Tooth disease. Brain : a journal of neurology *137*, 668-682.

Niemann, A., Ruegg, M., La Padula, V., Schenone, A., and Suter, U. (2005). Ganglioside-induced differentiation associated protein 1 is a regulator of the mitochondrial network: new implications for Charcot-Marie-Tooth disease. The Journal of cell biology *170*, 1067-1078.

Niemann, A., Wagner, K.M., Ruegg, M., and Suter, U. (2009). GDAP1 mutations differ in their effects on mitochondrial dynamics and apoptosis depending on the mode of inheritance. Neurobiology of disease *36*, 509-520.

Noack, R. (2011). Resistance against oxidative glutamate toxicity: Functional characterization of amino acid antiporter subunit xCT, purinergic ATP receptor P2X3 and mitochondrial fission factor GDAP1. In Faculty of Mathematics and Natural Sciences (Heinrich-Heine University Düsseldorf), pp. 108.

Noack, R., Frede, S., Albrecht, P., Henke, N., Pfeiffer, A., Knoll, K., Dehmel, T., Meyer Zu Horste, G., Stettner, M., Kieseier, B.C.*, et al.* (2012). Charcot-Marie-Tooth disease CMT4A: GDAP1 increases cellular glutathione and the mitochondrial membrane potential. Human molecular genetics *21*, 150-162.

Novo, E., and Parola, M. (2008). Redox mechanisms in hepatic chronic wound healing and fibrogenesis. Fibrogenesis & tissue repair *1*, 5.

Oka, A., Belliveau, M.J., Rosenberg, P.A., and Volpe, J.J. (1993). Vulnerability of oligodendroglia to glutamate: pharmacology, mechanisms, and prevention. The Journal of neuroscience : the official journal of the Society for Neuroscience *13*, 1441-1453.

Okamoto, K., and Shaw, J.M. (2005). Mitochondrial morphology and dynamics in yeast and multicellular eukaryotes. Annual review of genetics *39*, 503-536.

Olichon, A., Baricault, L., Gas, N., Guillou, E., Valette, A., Belenguer, P., and Lenaers, G. (2003). Loss of OPA1 perturbates the mitochondrial inner membrane structure and integrity, leading to cytochrome c release and apoptosis. The Journal of biological chemistry *278*, 7743-7746.

Olichon, A., Emorine, L.J., Descoins, E., Pelloquin, L., Brichese, L., Gas, N., Guillou, E., Delettre, C., Valette, A., Hamel, C.P.*, et al.* (2002). The human dynamin-related protein OPA1 is anchored to the mitochondrial inner membrane facing the inter-membrane space. FEBS letters *523*, 171-176.

Palade, G.E. (1952). The fine structure of mitochondria. The Anatomical record *114*, 427-451.

Palade, G.E. (1953). An electron microscope study of the mitochondrial structure. The journal of histochemistry and cytochemistry : official journal of the Histochemistry Society *1*, 188-211.

Pallast, S., Arai, K., Wang, X., Lo, E.H., and van Leyen, K. (2009). 12/15-Lipoxygenase targets neuronal mitochondria under oxidative stress. Journal of neurochemistry *111*, 882-889.

Palmer, C.S., Osellame, L.D., Stojanovski, D., and Ryan, M.T. (2011). The regulation of mitochondrial morphology: intricate mechanisms and dynamic machinery. Cellular signalling *23*, 1534-1545.

Pappolla, M.A., Omar, R.A., Kim, K.S., and Robakis, N.K. (1992). Immunohistochemical evidence of oxidative [corrected] stress in Alzheimer's disease. The American journal of pathology *140*, 621-628.

Patra, K.C., and Hay, N. (2014). The pentose phosphate pathway and cancer. Trends in biochemical sciences *39*, 347-354.

Pearce, R.K., Owen, A., Daniel, S., Jenner, P., and Marsden, C.D. (1997). Alterations in the distribution of glutathione in the substantia nigra in Parkinson's disease. Journal of neural transmission *104*, 661-677.

Pedersen, P.L. (2007). Warburg, me and Hexokinase 2: Multiple discoveries of key molecular events underlying one of cancers' most common phenotypes, the "Warburg Effect", i.e., elevated glycolysis in the presence of oxygen. Journal of bioenergetics and biomembranes *39*, 211-222.

Pedrola, L., Espert, A., Valdes-Sanchez, T., Sanchez-Piris, M., Sirkowski, E.E., Scherer, S.S., Farinas, I., and Palau, F. (2008). Cell expression of GDAP1 in the nervous system and pathogenesis of Charcot-Marie-Tooth type 4A disease. Journal of cellular and molecular medicine *12*, 679-689.

Pedrola, L., Espert, A., Wu, X., Claramunt, R., Shy, M.E., and Palau, F. (2005). GDAP1, the protein causing Charcot-Marie-Tooth disease type 4A, is expressed in neurons and is associated with mitochondria. Human molecular genetics *14*, 1087-1094.

Perry, T.L., Godin, D.V., and Hansen, S. (1982). Parkinson's disease: a disorder due to nigral glutathione deficiency? Neuroscience letters *33*, 305-310.

Perry, T.L., and Yong, V.W. (1986). Idiopathic Parkinson's disease, progressive supranuclear palsy and glutathione metabolism in the substantia nigra of patients. Neuroscience letters *67*, 269-274.

Pesta, D., and Gnaiger, E. (2012). High-resolution respirometry: OXPHOS protocols for human cells and permeabilized fibers from small biopsies of human muscle. Methods in molecular biology *810*, 25-58.

Pfeiffer, A., Jaeckel, M., Lewerenz, J., Noack, R., Pouya, A., Schacht, T., Hoffmann, C., Winter, J., Schweiger, S., Schafer, M.K.*, et al.* (2014). Mitochondrial function and energy metabolism in neuronal HT22 cells resistant to oxidative stress. British journal of pharmacology *171*, 2147-2158.

Pich, S., Bach, D., Briones, P., Liesa, M., Camps, M., Testar, X., Palacin, M., and Zorzano, A. (2005). The Charcot-Marie-Tooth type 2A gene product, Mfn2, up-regulates fuel oxidation through expression of OXPHOS system. Human molecular genetics *14*, 1405-1415.

Pla-Martin, D., Rueda, C.B., Estela, A., Sanchez-Piris, M., Gonzalez-Sanchez, P., Traba, J., de la Fuente, S., Scorrano, L., Renau-Piqueras, J., Alvarez, J.*, et al.* (2013). Silencing of the Charcot-Marie-Tooth disease-associated gene GDAP1 induces abnormal mitochondrial distribution and affects Ca2+ homeostasis by reducing store-operated Ca2+ entry. Neurobiology of disease *55*, 140-151.

Ploemen, J.H., van Ommen, B., and van Bladeren, P.J. (1990). Inhibition of rat and human glutathione S-transferase isoenzymes by ethacrynic acid and its glutathione conjugate. Biochemical pharmacology *40*, 1631-1635.

Powis, G., and Appel, P.L. (1980). Relationship of the single-electron reduction potential of quinones to their reduction by flavoproteins. Biochemical pharmacology *29*, 2567-2572.

Pradelli, L.A., Beneteau, M., and Ricci, J.E. (2010). Mitochondrial control of caspase-dependent and -independent cell death. Cellular and molecular life sciences : CMLS *67*, 1589-1597.

Rahman, I., Kode, A., and Biswas, S.K. (2006). Assay for quantitative determination of glutathione and glutathione disulfide levels using enzymatic recycling method. Nature protocols *1*, 3159-3165.

Ralser, M., Wamelink, M.M., Kowald, A., Gerisch, B., Heeren, G., Struys, E.A., Klipp, E., Jakobs, C., Breitenbach, M., Lehrach, H.*, et al.* (2007). Dynamic rerouting of the carbohydrate flux is key to counteracting oxidative stress. Journal of biology *6*, 10.

Ralser, M., Wamelink, M.M., Latkolik, S., Jansen, E.E., Lehrach, H., and Jakobs, C. (2009). Metabolic reconfiguration precedes transcriptional regulation in the antioxidant response. Nature biotechnology *27*, 604-605.

Reitzer, L.J., Wice, B.M., and Kennell, D. (1979). Evidence that glutamine, not sugar, is the major energy source for cultured HeLa cells. The Journal of biological chemistry *254*, 2669-2676.

Richman, P.G., and Meister, A. (1975). Regulation of gamma-glutamyl-cysteine synthetase by nonallosteric feedback inhibition by glutathione. The Journal of biological chemistry *250*, 1422-1426.

Rodriguez-Rodriguez, P., Fernandez, E., Almeida, A., and Bolanos, J.P. (2012). Excitotoxic stimulus stabilizes PFKFB3 causing pentose-phosphate pathway to glycolysis switch and neurodegeneration. Cell death and differentiation *19*, 1582-1589.

Rojo, M., Legros, F., Chateau, D., and Lombes, A. (2002). Membrane topology and mitochondrial targeting of mitofusins, ubiquitous mammalian homologs of the transmembrane GTPase Fzo. Journal of cell science *115*, 1663-1674.

Salvemini, F., Franze, A., Iervolino, A., Filosa, S., Salzano, S., and Ursini, M.V. (1999). Enhanced glutathione levels and oxidoresistance mediated by increased glucose-6-phosphate dehydrogenase expression. The Journal of biological chemistry *274*, 2750-2757.

Santel, A., and Fuller, M.T. (2001). Control of mitochondrial morphology by a human mitofusin. Journal of cell science *114*, 867-874.

Saraste, M. (1999). Oxidative phosphorylation at the fin de siecle. Science *283*, 1488-1493.

Sato, H., Tamba, M., Ishii, T., and Bannai, S. (1999). Cloning and expression of a plasma membrane cystine/glutamate exchange transporter composed of two distinct proteins. The Journal of biological chemistry *274*, 11455-11458.

Satoh, M., Hamamoto, T., Seo, N., Kagawa, Y., and Endo, H. (2003). Differential sublocalization of the dynamin-related protein OPA1 isoforms in mitochondria. Biochemical and biophysical research communications *300*, 482-493.

Schafer, F.Q., and Buettner, G.R. (2001). Redox environment of the cell as viewed through the redox state of the glutathione disulfide/glutathione couple. Free radical biology & medicine *30*, 1191-1212.

Schneider, J. (2014). Effekte des anti-apoptotischen Proteins Bcl-xL auf die mitochondriale Funktion. In Faculty of Biology (Johannes Gutenberg University Mainz), pp. 46.

Schwartz, P.S., Manion, M.K., Emerson, C.B., Fry, J.S., Schulz, C.M., Sweet, I.R., and Hockenbery, D.M. (2007). 2-Methoxy antimycin reveals a unique mechanism for Bcl-x(L) inhibition. Molecular cancer therapeutics *6*, 2073-2080.

Senderek, J., Bergmann, C., Ramaekers, V.T., Nelis, E., Bernert, G., Makowski, A., Zuchner, S., De Jonghe, P., Rudnik-Schoneborn, S., Zerres, K.*, et al.* (2003). Mutations in the ganglioside-induced differentiation-associated protein-1 (GDAP1) gene in intermediate type autosomal recessive Charcot-Marie-Tooth neuropathy. Brain : a journal of neurology *126*, 642-649.

Seyfried, J., Soldner, F., Schulz, J.B., Klockgether, T., Kovar, K.A., and Wullner, U. (1999). Differential effects of L-buthionine sulfoximine and ethacrynic acid on glutathione levels and mitochondrial function in PC12 cells. Neuroscience letters *264*, 1-4.

Sheehan, D., Meade, G., Foley, V.M., and Dowd, C.A. (2001). Structure, function and evolution of glutathione transferases: implications for classification of non-mammalian members of an ancient enzyme superfamily. The Biochemical journal *360*, 1-16.

Shenton, D., and Grant, C.M. (2003). Protein S-thiolation targets glycolysis and protein synthesis in response to oxidative stress in the yeast Saccharomyces cerevisiae. The Biochemical journal *374*, 513-519.

Sheridan, C., Delivani, P., Cullen, S.P., and Martin, S.J. (2008). Bax- or Bak-induced mitochondrial fission can be uncoupled from cytochrome C release. Molecular cell *31*, 570-585.

Shield, A.J., Murray, T.P., and Board, P.G. (2006). Functional characterisation of ganglioside-induced differentiation-associated protein 1 as a glutathione transferase. Biochemical and biophysical research communications *347*, 859-866.

Shih, A.Y., and Murphy, T.H. (2001). xCt cystine transporter expression in HEK293 cells: pharmacology and localization. Biochemical and biophysical research communications *282*, 1132-1137.

Shimizu, S., Narita, M., and Tsujimoto, Y. (1999). Bcl-2 family proteins regulate the release of apoptogenic cytochrome c by the mitochondrial channel VDAC. Nature *399*, 483-487.

Shimizu, S., Shinohara, Y., and Tsujimoto, Y. (2000). Bax and Bcl-xL independently regulate apoptotic changes of yeast mitochondria that require VDAC but not adenine nucleotide translocator. Oncogene *19*, 4309-4318.

Shutt, T., Geoffrion, M., Milne, R., and McBride, H.M. (2012). The intracellular redox state is a core determinant of mitochondrial fusion. EMBO reports *13*, 909-915.

Sian, J., Dexter, D.T., Lees, A.J., Daniel, S., Jenner, P., and Marsden, C.D. (1994). Glutathione-related enzymes in brain in Parkinson's disease. Annals of neurology *36*, 356-361.

Smirnova, E., Griparic, L., Shurland, D.L., and van der Bliek, A.M. (2001). Dynamin-related protein Drp1 is required for mitochondrial division in mammalian cells. Molecular biology of the cell *12*, 2245-2256.

Sofic, E., Lange, K.W., Jellinger, K., and Riederer, P. (1992). Reduced and oxidized glutathione in the substantia nigra of patients with Parkinson's disease. Neuroscience letters *142*, 128-130.

Soltys, B.J., and Gupta, R.S. (1994). Changes in mitochondrial shape and distribution induced by ethacrynic acid and the transient formation of a mitochondrial reticulum. Journal of cellular physiology *159*, 281-294.

Song, Z., Chen, H., Fiket, M., Alexander, C., and Chan, D.C. (2007). OPA1 processing controls mitochondrial fusion and is regulated by mRNA splicing, membrane potential, and Yme1L. The Journal of cell biology *178*, 749-755.

Song, Z., Ghochani, M., McCaffery, J.M., Frey, T.G., and Chan, D.C. (2009). Mitofusins and OPA1 mediate sequential steps in mitochondrial membrane fusion. Molecular biology of the cell *20*, 3525-3532.

Soucek, T., Cumming, R., Dargusch, R., Maher, P., and Schubert, D. (2003). The regulation of glucose metabolism by HIF-1 mediates a neuroprotective response to amyloid beta peptide. Neuron *39*, 43-56.

Stincone, A., Prigione, A., Cramer, T., Wamelink, M.M., Campbell, K., Cheung, E., Olin-Sandoval, V., Gruening, N.M., Krueger, A., Tauqeer Alam, M.*, et al.* (2014). The return of metabolism: biochemistry and physiology of the pentose phosphate pathway. Biological reviews of the Cambridge Philosophical Society.

Suen, D.F., Norris, K.L., and Youle, R.J. (2008). Mitochondrial dynamics and apoptosis. Genes & development *22*, 1577-1590.

Tagami, S., Eguchi, Y., Kinoshita, M., Takeda, M., and Tsujimoto, Y. (2000). A novel protein, RTN-XS, interacts with both Bcl-XL and Bcl-2 on endoplasmic reticulum and reduces their anti-apoptotic activity. Oncogene *19*, 5736-5746.

Tan, S., Sagara, Y., Liu, Y., Maher, P., and Schubert, D. (1998a). The regulation of reactive oxygen species production during programmed cell death. The Journal of cell biology *141*, 1423-1432.

Tan, S., Schubert, D., and Maher, P. (2001). Oxytosis: A novel form of programmed cell death. Current topics in medicinal chemistry *1*, 497-506.

Tan, S., Wood, M., and Maher, P. (1998b). Oxidative stress induces a form of programmed cell death with characteristics of both apoptosis and necrosis in neuronal cells. Journal of neurochemistry *71*, 95-105.

Thor, H., Moldéus, P., and Orrenius, S. (1979). Metabolic activation and hepatotoxicity. Archives of biochemistry and biophysics *192*, 405-413.

Tondera, D., Grandemange, S., Jourdain, A., Karbowski, M., Mattenberger, Y., Herzig, S., Da Cruz, S., Clerc, P., Raschke, I., Merkwirth, C.*, et al.* (2009). SLP-2 is required for stress-induced mitochondrial hyperfusion. The EMBO journal *28*, 1589-1600.

Towbin, H., Staehelin, T., and Gordon, J. (1979). Electrophoretic transfer of proteins from polyacrylamide gels to nitrocellulose sheets: procedure and some applications. Proceedings of the National Academy of Sciences of the United States of America *76*, 4350-4354.

Tsujimoto, Y., Cossman, J., Jaffe, E., and Croce, C.M. (1985). Involvement of the bcl-2 gene in human follicular lymphoma. Science *228*, 1440-1443.

Tsujimoto, Y., Finger, L.R., Yunis, J., Nowell, P.C., and Croce, C.M. (1984). Cloning of the chromosome breakpoint of neoplastic B cells with the t(14;18) chromosome translocation. Science *226*, 1097-1099.

Ursini, M.V., Parrella, A., Rosa, G., Salzano, S., and Martini, G. (1997). Enhanced expression of glucose-6-phosphate dehydrogenase in human cells sustaining oxidative stress. The Biochemical journal *323 (Pt 3)*, 801-806.

Uruno, A., and Motohashi, H. (2011). The Keap1-Nrf2 system as an in vivo sensor for electrophiles. Nitric oxide : biology and chemistry / official journal of the Nitric Oxide Society *25*, 153-160.

Vander Heiden, M.G., Chandel, N.S., Li, X.X., Schumacker, P.T., Colombini, M., and Thompson, C.B. (2000). Outer mitochondrial membrane permeability can regulate coupled respiration and cell survival. Proceedings of the National Academy of Sciences of the United States of America *97*, 4666-4671.

Vander Heiden, M.G., Chandel, N.S., Schumacker, P.T., and Thompson, C.B. (1999). Bcl-xL prevents cell death following growth factor withdrawal by facilitating mitochondrial ATP/ADP exchange. Molecular cell *3*, 159-167.

Vander Heiden, M.G., Chandel, N.S., Williamson, E.K., Schumacker, P.T., and Thompson, C.B. (1997). Bcl-xL regulates the membrane potential and volume homeostasis of mitochondria. Cell *91*, 627-637.

Vander Heiden, M.G., Li, X.X., Gottleib, E., Hill, R.B., Thompson, C.B., and Colombini, M. (2001). Bcl-xL promotes the open configuration of the voltage-dependent anion channel and metabolite passage through the outer mitochondrial membrane. The Journal of biological chemistry *276*, 19414-19419.

Vander Heiden, M.G., and Thompson, C.B. (1999). Bcl-2 proteins: regulators of apoptosis or of mitochondrial homeostasis? Nature cell biology *1*, E209-216.

Vaux, D.L., Cory, S., and Adams, J.M. (1988). Bcl-2 gene promotes haemopoietic cell survival and cooperates with c-myc to immortalize pre-B cells. Nature *335*, 440-442.

Wagner, K.M. (2009). Structural and functional analysis of the neuronal mitochondrial fission factor GDAP1 and its homolog GDAP1L1 (ETH ZÜRICH), pp. 127.

Wagner, K.M., Ruegg, M., Niemann, A., and Suter, U. (2009). Targeting and function of the mitochondrial fission factor GDAP1 are dependent on its tail-anchor. PloS one *4*, e5160.

Wallace, D.C. (1999). Mitochondrial diseases in man and mouse. Science *283*, 1482-1488.

Wang, Y.P., Zhou, L.S., Zhao, Y.Z., Wang, S.W., Chen, L.L., Liu, L.X., Ling, Z.Q., Hu, F.J., Sun, Y.P., Zhang, J.Y.*, et al.* (2014). Regulation of G6PD acetylation by SIRT2 and KAT9 modulates NADPH homeostasis and cell survival during oxidative stress. The EMBO journal *33*, 1304-1320.

Westermann, B. (2010). Mitochondrial fusion and fission in cell life and death. Nature reviews Molecular cell biology *11*, 872-884.

Westermann, B. (2012). Bioenergetic role of mitochondrial fusion and fission. Biochimica et biophysica acta *1817*, 1833-1838.

White, C., Li, C., Yang, J., Petrenko, N.B., Madesh, M., Thompson, C.B., and Foskett, J.K. (2005). The endoplasmic reticulum gateway to apoptosis by Bcl-X(L) modulation of the InsP3R. Nature cell biology *7*, 1021-1028.

Wu, K.C., Cui, J.Y., and Klaassen, C.D. (2011). Beneficial role of Nrf2 in regulating NADPH generation and consumption. Toxicological sciences : an official journal of the Society of Toxicology *123*, 590-600.

Wullner, U., Seyfried, J., Groscurth, P., Beinroth, S., Winter, S., Gleichmann, M., Heneka, M., Loschmann, P., Schulz, J.B., Weller, M.*, et al.* (1999). Glutathione depletion and neuronal cell death: the role of reactive oxygen intermediates and mitochondrial function. Brain research *826*, 53-62.

Yoon, Y., Pitts, K.R., and McNiven, M.A. (2001). Mammalian dynamin-like protein DLP1 tubulates membranes. Molecular biology of the cell *12*, 2894-2905.

Yoon, Y.S., Yoon, D.S., Lim, I.K., Yoon, S.H., Chung, H.Y., Rojo, M., Malka, F., Jou, M.J., Martinou, J.C., and Yoon, G. (2006). Formation of elongated giant mitochondria in DFO-induced cellular senescence: involvement of enhanced fusion process through modulation of Fis1. Journal of cellular physiology *209*, 468-480.

Youle, R.J., and Karbowski, M. (2005). Mitochondrial fission in apoptosis. Nature reviews Molecular cell biology *6*, 657-663.

Youle, R.J., and Strasser, A. (2008). The BCL-2 protein family: opposing activities that mediate cell death. Nature reviews Molecular cell biology *9*, 47-59.

Youle, R.J., and van der Bliek, A.M. (2012). Mitochondrial fission, fusion, and stress. Science *337*, 1062-1065.

Yusa, K., Zhou, L., Li, M.A., Bradley, A., and Craig, N.L. (2011). A hyperactive piggyBac transposase for mammalian applications. Proceedings of the National Academy of Sciences of the United States of America *108*, 1531-1536.

Zemlan, F.P., Thienhaus, O.J., and Bosmann, H.B. (1989). Superoxide dismutase activity in Alzheimer's disease: possible mechanism for paired helical filament formation. Brain research *476*, 160-162.

Zuchner, S., Mersiyanova, I.V., Muglia, M., Bissar-Tadmouri, N., Rochelle, J., Dadali, E.L., Zappia, M., Nelis, E., Patitucci, A., Senderek, J.*, et al.* (2004). Mutations in the mitochondrial GTPase mitofusin 2 cause Charcot-Marie-Tooth neuropathy type 2A. Nature genetics *36*, 449-451.

ACKNOWLEGMENT

For data protection reasons the acknowledgements are not included in the online version.

CURRICULUM VITAE

For data protection reasons the curriculum vitae is not included in the online version.

VERSICHERUNG

Hiermit versichere ich, Annika I. Pfeiffer, dass ich die heute als Dissertation vorgelegte Arbeit mit dem Titel *„ Alterations of mitochondrial form and function caused by resistance against oxidative stress and cytoprotective, mitochondrial proteins”* selbst angefertig und alle benutzten Hilfsmittel (Literatur, Apparaturen, Material) in der Arbeit angegeben habe. Ich habe oder hatte die jetzt als Dissertation vorgelegte Arbeit nicht als Prüfungsarbeit für eine staatliche oder andere wissenschaftliche Prüfung eingereicht. Darüber hinaus hatte ich weder die jetzt als Dissertation vorgelegte Arbeit noch Teile einer Abhandlung bei einer anderen Fakultät bzw. einem anderen Fachbereich als Dissertation eingereicht.

Mainz, den _____ _____

(Annika I. Pfeiffer)